Rocking Response Analysis of Liquid Storage Tanks under Seismic Ground Excitation

by

Yuichi Yoshida

A DISSERTATION SUBMITTED
IN PARTIAL FULFILLMENT OF THE
REQUIRMENTS FOR THE DEGREE OF

Doctor of Engineering

Under the supervision of
Professor Tomoyo Taniguchi

Doctoral Program of Graduate School of Engineering,
Tottori University, Japan

January, 2023

TOTTORI UNIVERSITY

Rocking Response Analysis of Liquid Storage Tanks under Seismic Ground Excitation

by

Yuichi Yoshida

A DISSERTATION SUBMITTED
IN PARTIAL FULFILLMENT OF THE
REQUIRMENTS FOR THE DEGREE OF

Doctor of Engineering

APPROVED, THESIS COMMITTEE:

Tomoyo Taniguchi
Professor
Department of Social Systems and Civil Engineering

Takao Kagawa
Professor
Department of Social Systems and Civil Engineering

Yusuke Ono
Professor
Department of Social Systems and Civil Engineering

Tottori, Japan

January, 2023

Rocking Response Analysis of Liquid Storage Tanks under Seismic Ground Excitation

Yuichi Yoshida

Abstract

This dissertation aims at presenting a method to analyze the time history of rocking response of liquid storage tanks by developing several mechanical models that enable to analytically describe uplift phenomenon of liquid storage tanks from several aspects. The study consists of three parts: the first part confirms a role of rotational inertia force of content liquid and the condition for commencement of uplifting of tank bottom, the second part develops a mechanical model of liquid storage tanks for rocking motion, and the third part validates the proposed method for analyzing the tank rocking motion. The results of this study point out the oversight in conventional calculation methods.

In Chapter 1, the structures of above-ground liquid storage tanks and their typical damage found during the several reconnaissance surveys performed after earthquakes are briefly reviewed. A review is also made on earlier studies on rocking response of liquid storage tanks due to seismic ground excitation. Finally, the objectives of the work are described.

In Chapter 2, preliminary preparations for the development of a method of tank rocking response analysis are conducted, including (1) selection of a suitable method for describing the uplift displacement-width relationship, (2) investigation of contribution of rotational inertia force of content liquid to the tank rocking motion, and (3) investigation of uplift commencement condition. These are conducted to determine the essential conditions and parameters for tank rocking response analysis. In this chapter, significant contribution of the rotational inertia force of the content liquid to the tank

rocking motion is confirmed by comparing the angular acceleration extracted from FE analysis and that calculated from the equilibrium between the overturning moment, the restoring moment and the rotational inertia force, inferred from the equation of motion presented herein. Furthermore, shaking table tests conducted herein highlight the presence of added mass contributing to the uplift commencement condition.

In Chapter 3, equations of motion for the mechanical model of a liquid storage tank in rock are derived based on the analogy between a two-degree-of-freedom model which has the translational and rotational freedoms and the tank in rock. Furthermore, A computational method of the equations of motion for the mechanical model of liquid storage tanks is also described.

In Chapter 4, the accuracy of the proposed method is verified by comparing uplift displacement between the calculation results by the proposed method and those by the dynamic FE analysis as well as observational record. In addition, comparison between the calculation results of uplift displacement by the proposed method and those by the conventional methods reveals that the proposed method gives better approximation compared to the conventional methods.

Finally, the results obtained in this study are summarized in Chapter 5. Although more work remains to be done for improving the proposed method, the purpose of this research, the development of a tank rocking response analysis, has been achieved.

Acknowledgments

The author deeply appreciates the guidance of his thesis advisor, Professor Tomoyo Taniguchi. The author greatly values the experience he has had while working with Professor Taniguchi.

The author thanks Professor Takao Kagawa and Professor Yusuke Ono for serving on the thesis committee and giving helpful comments and suggestions during the course of this work. Thanks are extended to Dr. Ken Hatayama of National Research Institute of Fire and Disaster for his insightful comments. Daily discussions with him help the author improve his research skills. The author also thanks Dr. Teruhiro Nakashima of Nihon Suiko Sekkei Co., Ltd. for giving technical advice on FEM dynamic analysis. His contributions have had good influences on author’s research. The author also tanks Ms. Kaoru Uemura for English proofreading of the dissertation. Her work was prompt and precise, not only in the proofreading, but also in improving the author's English writing skills.

The author would like to thank his parents for their understanding of my decision to enter a doctoral program.

January 2023

Contents

Appendix

Tables

Figures

Symbols

Chapter 1

M_0	=	Impulsive Mass of Content Liquid
h_0	=	Height of Center of Gravity of M_0
M	=	Total Mass of Content Liquid
R	=	Tank Radius
h, H	=	Liquid Height
T_b	=	Fundamental Fluid-Elastic Period
W	=	Total Weight of Content Liquid
g	=	Gravitational Acceleration
E	=	Young's Modulus of Tank Material
$t_{1/3}$	=	Wall Thickness at One Third of Liquid Height H
D	=	Tank Diameter
Ph_0	=	Dynamic Hydraulic Pressure due to Impulsive Response
Ph_1	=	Dynamic Hydraulic Pressure due to Bulging Response
ρ	=	Density of Content Liquid
C_{0i}	=	Coefficient for Calculating Ph_0
C_{1i}	=	Coefficient for Calculating Ph_1
z	=	Arbitrary Height of Content Liquid from Tank Bottom
kh_1	=	Design Horizontal Seismic Coefficient
v_3	=	Amplification Factor of Tank
m	=	Impulsive Mass

u_0	=	Overall Displacement ($= u + \psi\bar{h}$)
c	=	Damping Coefficient for Tank in Its Fixed-Base Condition
k	=	Corresponding Stiffness of Structure
ψ	=	Rotation of Base
$\bar{h}$	=	Height at which Impulsive Mass must be Concentrated to Yield Correct Overturning Base Moment
$M(\psi)$	=	Restoring Moment in Rotational Spring
J	=	Anchorage Ratio
M_{rw}	=	Overturning Moment
w_t	=	Tank and Roof Weight Acting at Base of Shell
A_v	=	Vertical Earthquake Acceleration Parameter
w_a	=	Force Resisting Uplift in Annular Region
F_p	=	Ratio of Normal Operation Pressure to Design Pressure
w_{int}	=	Calculated Design Uplift Force due to Design Pressure per Unit Circumferential Length
W_s	=	Total Weight of Tank Shell and Appurtenances
w_{rs}	=	Roof Load acting on Top of Tank Shell
F_y	=	Minimum Specified Yield Strength of Bottom Annulus
G_e	=	Effective Specific Gravity Including Vertical Seismic Effects
σ_c	=	Maximum Buckling Stress
t_s	=	Thickness of Bottom Shell Course Less Corrosion Allowance
Q_y	=	Maximum Lateral Shear Strength
Q_{dw}	=	Required Maximum Lateral Shear Force
q_y	=	Uplift Resistant Force per Unit Circumferential Length
M_y	=	Restoring Moment obtained by Multiplying Uplift Resistant Force by Moment Arm Length and Integrating It over Circumference

H_G = Height of Centroid of Effective Mass of Content Liquid for Bulging Motion

m_p = Full Plastic Moment at Shell-to-Bottom Connection

t_b = Thickness of Annular Plate

p = Hydrostatic Pressure

σ_y = Yield Stress

ν_1 = Modification Coefficient Depending on Region

ν_2 = Modification Coefficient Depending on Site Condition

ν_3 = Modification Coefficient Depending on Response Magnification Which Depends on Natural Period of Tank

ν_p = Coefficient for Plastic Design ($= 1.5$)

D_s = Structural Coefficient

W_0 = Effective Weight of Content Liquid for Horizontal Direction Motion

Chapter 2

θ = Rocking Angle $(= w/D)$

w = Uplift Displacement

D = Tank Diameter

R = Tank Radius

a = Radius of Circular Contact Region of Tank Bottom Plate

φ = Angle Formed by Horizontal Center Line of Bottom Plate and Line Connecting Center of Bottom Plate and Corner Joint

$L(\varphi)$ = Width of Uplifted Region of Bottom Plate at Arbitrary Point with Respect to φ

L_0 = Width of Uplifted Region of Bottom Plate at $\varphi = 0$

$r(\varphi)$ = Width of Contact Region of Bottom Plate at Arbitrary Point with Respect to φ

$l(\varphi)$ = Length of Moment Arm from Pivot Point to Arbitrary Point with Respect to φ

$Q(\varphi)$	=	Vertical Force at Uplifted End of Bottom Plate at Arbitrary Point with Respect to φ
p	=	Hydraulic Pressure Acting on Beam Model
M_{re}	=	Restoring Moment due to Tank Weight and Liquid Acting on Uplifted Tank Bottom Plate
M_{ov}	=	Overturning Moment due to Dynamic Fluid Pressure Acting on Tank Shell
m_s	=	Sum of Masses of Tank Shell and Appurtenance
g	=	Gravitational Acceleration
$\alpha(t)$	=	Translational Response Acceleration of Tank Which is Equal to Ground Acceleration due to Assumption of Rigid Tank Shell
m_{I}	=	Effective Mass of Content Liquid for Translational Motion
h_{I}	=	Height of Centroid of m_{I} from Base
h, H	=	Liquid Height
m	=	Total Mass of Content Liquid
$\ddot{\theta}(t)$	=	Angular Acceleration of Tank Rocking Motion
$\ddot{z}(t)$	=	Vertical Acceleration at Edge of Tank Bottom
I_{s}	=	Moment of Inertia of Tank Shell
I_{eff}	=	Effective Moment of Inertia of Content Liquid around Pivot Point of Tank Rocking Motion
I_{r}	=	Moment of Inertia of m_r around Centroid
m_{r}	=	Effective Mass of Content Liquid for Rocking Motion
R_{r}	=	Distance between Pivot Point of Tank Rocking Motion and Centroid of m_r
δ	=	Uplift Ratio $(= L_0/D)$
α_r	=	Angle between R_r and Tank Shell
f_r	=	Coefficient for Calculating m_r
$d_{r,x}, d_{r,z}$	=	Coefficients for Calculating R_r
A	=	Amplitude of Horizontal Base Acceleration

T_D = Period of Driving Acceleration of Shaking Table

f_D = Frequency of Driving Acceleration of Shaking Table

α_{req} = Required Acceleration for Uplift (Conventional Method)

α'_{req} = Required Acceleration for Uplift (Method Considering Added Mass)

m_{roof} = Mass of Tank Roof

H_s = Height of Tank Shell

γ = Resistant Moment Correction Factor Which is Ratio of Experimental Value of Acceleration Required for Tank Bottom to Start Uplifting $\alpha_{req,e}$ and Required Acceleration Calculated by Conventional Method of Uplift Commencement Condition α_{req}

Chapter 3

m_1 = Upper Mass of 2DOF System

m_2 = Lower Mass of 2DOF System

x_1 = Translational Response Displacement of m_1 or m_b

c_1 = Damping Coefficient of 2DOF System

k_1 = Spring Constant of 2DOF System

$\ddot{z}_H$ = Horizontal Ground Acceleration

$\mathcal{L}$ = Lagrangian of 2DOF System

T = Kinetic Energy of 2DOF System

V = Potential Energy of 2DOF System

θ = Rocking Angle of 2DOF Model or Mechanical Model of Liquid Storage Tank

g = Gravitational Acceleration

R_1 = Distance between Origin *o* (or *o*') and Centroid of m_1

R_2 = Distance between Origin *o* (or *o*') and Centroid of m_2

α_1 = Angle of Line R_1 with respect to y-Axis

α_2 = Angle of Line R_2 with respect to y-Axis

I_1 = Moment of Inertia around Centroid of m_1

I_2 = Moment of Inertia around Centroid of m_2

λ = Sign function: 1 while 2DOF Model pivots around o, and -1 while It pivots around o'

Q_{x1} = Generalized Force in Translational Direction

Q_θ = Generalized Force in Rotational Direction

OM = Overturning Moment

RM = Resistant Moment

e = Coefficient of Restitution for Rocking Motion

t^+ = Time Immediately after an Impact

t^- = Time Immediately before an Impact

T_1 = Natural Period of 2DOF System

h_1 = Damping Constant of 2DOF System

ρ_{eff} = Nominal Effective Density of Content Liquid for Tank Rocking Motion

r = Distance between Pivot Point and Point of Focus

$p(r,\theta,t)$ = Dynamic Pressure due to Tank Rocking Motion at Point of Focus

$\ddot{\theta}_0(t)$ = Angular Acceleration around Pivot Point

m_b = Effective Mass of Fluid of Bulging System

m_r = Effective Mass of Fluid for Rocking Motion

m_{rb} = Effective Mass of Fluid for Rocking-Bulging Interaction Motion

c_b = Damping Coefficient of Bulging System

k_b = Spring Constant of Bulging System

R_b = Distance between Origin *o* (or *o*') and Centroid of m_b

R_r = Distance between Origin o (or o') and Centroid of m_r

R_{rb} = Distance between Origin o (or o') and Centroid of m_{rb}

α_b = Angle between Line R_b and y-Axis

α_r = Angle between Line R_r and y-Axis

α_{rb} = Angle between Line R_{rb} and y-Axis

I_r = Effective Moment of Inertia of Fluid around Centroid of m_r

m_t = Total Mass of Content Liquid

I = Moment of Inertia around Centroid When Content Rigidly Behaves

D = Tank Diameter

H = Liquid Height

f_r = Ratio of Effective Mass of Content Liquid for Rocking Motion to Total Mass of Fluid Filling Tank

f_{rb} = Ratio of Effective Mass of Content Liquid for Rocking-Bulging Interaction Motion to Total Mass of Fluid Filling Tank

s = Ratio of Effective Moment of Inertia of Content Liquid (around Centroid of m_r) to Moment of Inertia of Rigid Cylinder (around Centroid of m_t)

$d_{r,x}$ = Ratio of Horizontal Distance toward Centroid of Effective Mass of Content Liquid for Rocking Motion to Tank Diameter

$d_{r,z}$ = Ratio of Vertical Distance toward Centroid of Effective Mass of Content Liquid for Rocking Motion to Liquid Height

L = Uplift Width of Tank Bottom Plate

δ = Uplift Ratio ($= L/D$)

m_s = Total Mass of Tank Shell and Roof

ρ_l = Density of Content Liquid

p = Liquid Pressure Acting on Beam Model

p_s = Static Pressure

p_b = Bulging Dynamic Pressure

p_r = Rocking Dynamic Pressure

f_b = Ratio of Effective Mass of Content Liquid for Bulging System to Total Mass of Fluid Filling Tank

$d_{b,z}$ = Ratio of Vertical Distance toward Centroid of m_b to Liquid Height

T_b = Natural Period of Bulging System

W_0 = Total Weight of Content Liquid

E = Young's Modulus of Tank Material

$t_{1/3}$ = Thickness of Tank Shell at One Third of Liquid Height

h_b = Damping Constant of Bulging System

Chapter 4

h_b = Damping Constant of Translational Motion (Bulging System)

h_r = Damping Constant of Rotational Motion

e = Coefficient of Restitution for Rocking Motion

m_b = Effective Mass of Fluid of Bulging System

$v(\theta_b)$ = Additional Uplift Displacement due to Out-of-Round Deformation δ

θ_b = Angle of Line Formed by Arbitrary Point on Tank Shell and Center of Tank Shell Cross Section with Respect to 0°-180° Line

δ = Out-of-Round Deformation of Tank Shell

R = Tank Radius

H = Height of Tank Shell

k_θ = Rotational Spring Stiffness

$\Delta M(\theta)$ = Increment of Restoring Moment

$\Delta\theta$ = Increment of Rocking Angle

Appendix

D	=	Tank Diameter
H	=	Liquid Height
w	=	Uplift Displacement
L	=	Uplift Width
R	=	Tank Radius
a	=	Radius of Circular Contact Region of Tank Bottom Plate
φ	=	Angle Formed by Horizontal Center Line of Bottom Plate and Line Connecting Center of Tank Bottom Plate and Corner Joint
$\phi(\varphi)$	=	Angle Formed by Line a and Line $r(\varphi)$
$r(\varphi)$	=	Contact Width of Tank Bottom Plate
E	=	Young's Modulus of Beam Model
I	=	Geometrical Moment of Inertia
w_1	=	Vertical Displacement of Uplift Part of Beam Model
w_2	=	Vertical Displacement of Contact Part of Beam Model
p	=	Hydraulic Pressure Acting on Beam Model
k	=	Reaction Coefficient of Foundation
Q_0	=	External Force Which is Reaction Force from Tank Shell
M_0	=	Bending Moment Acting on Corner Joint of Tank Bottom
M_x	=	Bending Moment Acting on Arbitrary Cross-Section of Beam Model
Q_x	=	Shear Force Acting on Arbitrary Cross-Section of Beam Model
N	=	Axial Force Acting on Arbitrary Cross-Section of Beam Model
θ	=	Slope of Deflection at Arbitrary Point of Beam Model
θ_s	=	Rotation Angle at Bottom End of Tank Shell
θ_1	=	Rotation Angle at Beam End

u_1	=	Horizontal Displacement at Beam End
M_1	=	Bending Moment at Beam End
$k_{\theta\theta}, k_{\theta u}, k_{uu}$	=	Stiffness Coefficients for Constraints at Uplifted End of Beam Model
$d_{\theta\theta}, d_{\theta u}, d_{uu}$	=	Flexibility Coefficients for Constraints at Uplifted End of Beam Model
t_s	=	Thickness of Tank Shell at Bottom
υ	=	Poisson's Ratio
b	=	Width of Beam Model
$\Delta\theta$	=	Difference between Rotation Angle at Bottom End of Tank Shell θ_s and that at Beam End θ_1
M_y	=	Yield Moment
$\bar{N}$	=	Axial Force Acting on Bottom Corners due to Static Pressure Acting on Tank Shell
$\bar{M}_1$	=	Bending Moment Acting on Bottom Corners due to Static Pressure Acting on Tank Shell
σ_y	=	Yield Stress of Beam Material
h	=	Thickness of Beam Model
A	=	Amplitude of Base Acceleration

Chapter 1

Introduction

Chapter 1

Introduction

1.1 Background

The first part of this chapter gives the structures of above-ground liquid storage tanks and their typical damage found during several reconnaissance surveys performed after earthquakes. The second part of this chapter briefly reviews earlier studies on rocking response of liquid storage tanks due to seismic ground excitation. Finally, objectives of the work are explained.

1.1.1 Liquid Storage Tanks

This study discusses the seismic response of liquid storage tanks. Before examining their responses in detail, the structures of typical liquid storage tanks are introduced. Among several types of liquid storage tanks, only the above-ground flat-bottom cylindrical shell tanks are of interest here. As examples, an oil tank (room temperature) and an LNG tank (cryogenic temperature) are briefly introduced. Figure 1.1 shows a structure of an oil tank and Figure 1.2 shows that of an LNG tank. The main components of both tanks are a bottom plate, a shell plate and a roof. The outer ring-shaped part of the bottom plate is called an annular plate. The annular plate is thicker than the central part of the bottom plate to resist the bending stress transmitted from the tank shell plate. Since internal pressure increases with depth of content liquid, thickness of the tank shell plate increases toward the bottom. In large liquid storage tanks, the depth of the content liquid exceeds 20 m, and in LNG tanks, the thickness of the side shell plate is about 50 mm. Other structural features include the floating roof for large oil tanks and the double shell insulation structure of LNG tanks.

Structure of Oil Tank

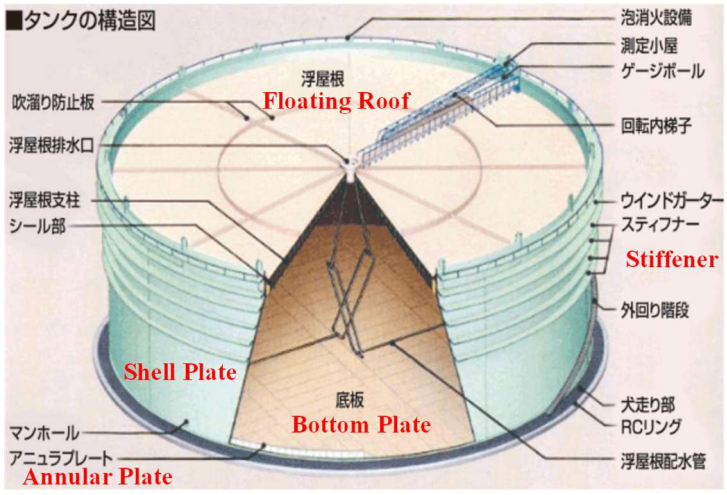

https://www.jogmec.go.jp/content/300054708.gif

Figure 1.1 Structure of Oil Storage Tank (Floating Roof Type, 110,000 kL) [1] (Slightly modified by the author.)

Structure of LNG Tank

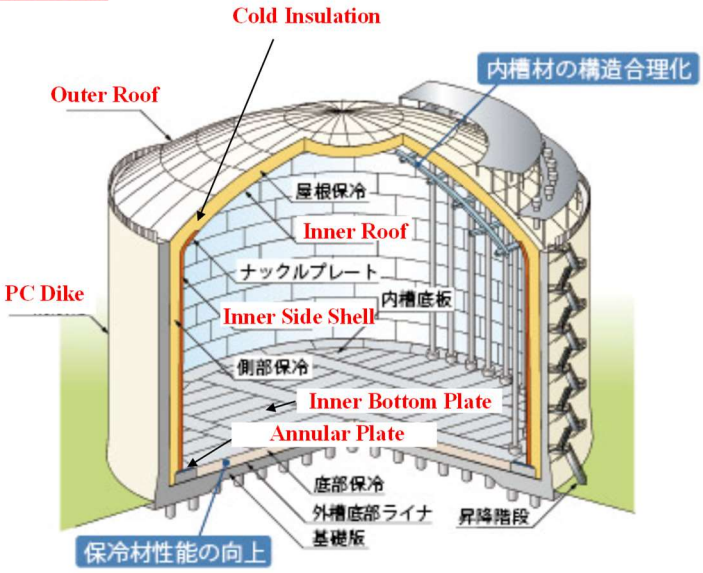

https://www.khi.co.jp/sustainability/earth/green/2020/LNG_Tank.html

Figure 1.2 Structure of LNG Storage Tank (230,000 kL) [2] (Slightly modified by the author.)

1.1.2 Earthquake Damage to Liquid Storage Tanks

This section reviews the typical earthquake damage to liquid storage cylindrical shell tanks. The earthquake damage can be classified as shown in Figure 1.3 [3]. The seismic response of a tank is classified to long-period response and short-period response. In general, the long-period response of a tank is called the sloshing response, and the earthquake damage of types (a) to (e) of Figure 1.3 may occur. On the other hand, the short-period response is called the bulging response [4], and it may cause damage to a tank as shown in (f) to (i) of Figure 1.3.

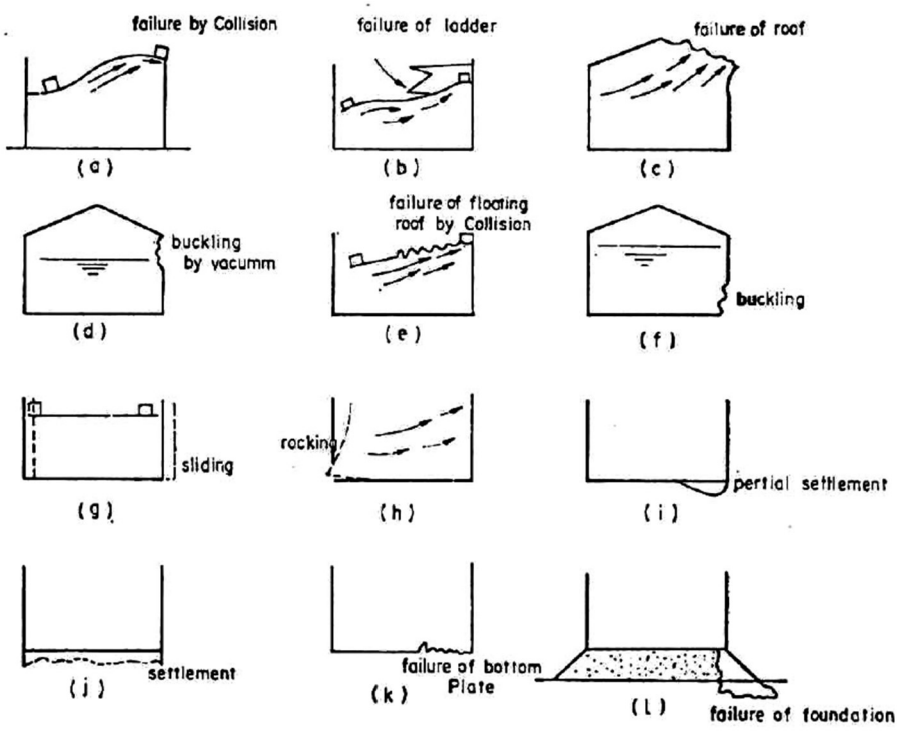

Figure 1.3 Typical Earthquake Damage to Above-Ground Liquid Storage Tanks [3]

Earthquake Damage Due to Long-Period Response

1964 Great Alaska Earthquake, USA (M9.2): This earthquake caused serious damage to fuel storage tanks, and made us aware of the importance of research on earthquake resistance of liquid storage tanks. The earthquake caused both long-period and short-period responses of tanks. Figure 1.4 shows a damaged tank whose roof has fallen off. According to Edwin's report [5], this was due to a large vertical force exerted on the tank bottom by the whirlpool generated in the content liquid. However, the author rather suspects that the cause of the disaster might have been an impact pressure on the roof caused by sloshing. Figure 1.5 shows fire accident of fuel storage tanks. All tanks in the tank yard (Union Oil Co.) were burned and completely destroyed.

Figure 1.4 Damage to Structures in Port Area, Including Petroleum Tank (Lower Right) by Vibration and Ground Fractures (1964 Great Alaska Earthquake) [5]

Figure 1.5 Fire Accident of Fuel Storage Tanks (1964 Great Alaska Earthquake) [6]

1964 Niigata Earthquake, Japan (M7.5): Fire accident on the top of oil storage tanks occurred (see Figure 1.6). The fire accident was caused by collision between the floating roof and the side panels due to sloshing response. The fire lasted 13 days [7].

Figure 1.6 Fire Accident of Oil Storage Tanks due to Sloshing (1964 Niigata Earthquake) [8]

1983 Nihonkai-Chubu Earthquake, Japan (M7.7): This earthquake caused a long-period response of oil storage tanks and caused a fire accident (Figure 1.7) [9]. In addition, other tanks suffered overflow of content liquid, damage to the floating roof, pontoon and rolling ladder, as well as anchor bolt failure. Sloshing damage was more reported in Hokkaido and Niigata compared to Akita which was closer to the epicenter. Sloshing wave heights of 4 m or more have been recorded at oil tanks in Niigata.

Figure 1.7 Fire Accident of 35,000 kL Oil Storage Tank (1983 Nihonkai-Chubu Earthquake) [9]

1999 Chi-Chi Earthquake, Taiwan (M7.6): Several tanks were damaged by sloshing response [10]. Figure 1.8 shows buckling of pontoon of a floating roof. Fire accident did not occur because a rubber seal was installed between the tank shell and the floating roof instead of a steel mechanical seal. In a tank with a fixed roof, connection between the roof and the top of the tank shell was damaged, which was attributed to impact pressure of the liquid acting on the connection due to the sloshing response.

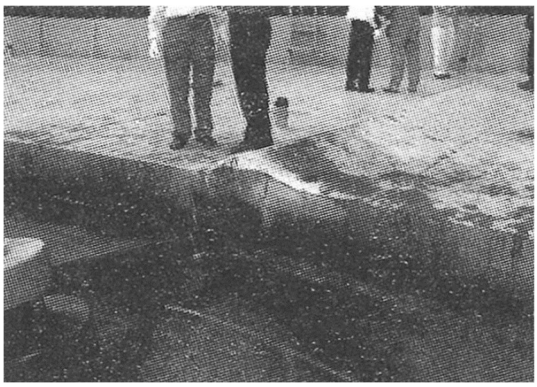

Figure 1.8 Pontoon Buckling of 130,000 kL Oil Storage Tanks due to Sloshing (1999 Chi-Chi Earthquake) [10]

1999 Kocaeli Earthquake, Türkiye (M7.8): Six tanks in the Tupras tank farm collapsed due to fire accident (see Figure 1.9) [11, 12]. All tanks that suffered fire damage were floating roof tanks. The cause of the fire was considered to be the collision between the floating roof and the tank shell due to sloshing response. The fire lasted for about a week until the fuel was completely burned out.

Figure 1.9 Tanks Collapsed due to Fire Accident (1999 Kocaeli Earthquake) [12]

2003 Tokachi-Oki Earthquake, Japan (M7.8): Two tanks caught fire, and floating roof submergence occurred in seven tanks due to sloshing response. Figure 1.10 (a) shows a tank caught in a fire immediately after the earthquake [13]. The cause of the tank fire was thought to be that combustible air-fuel mixture present on the floating roof ignited due to the sparks generated by the collision between the floating roof and the tank upper structure. Figure 1.10 (b) shows a view of a tank collapsed due to full-surface tank fire [14]. This tank fire occurred two days after the earthquake. A possible scenario could be as follows. The floating roof of the tank had sunk, and the surface of the content liquid was sealed with foam to prevent volatilization of oil. However, the foam moved in strong winds, eventually exposing two-thirds of the liquid surface to the atmosphere. At the same time, aqueous solution of the foam settled and acquired electrical charges with time, and the charges accumulated in the isolated floating foam. The electric potential of the foam increased, and discharge occurred between the foam and the tank shell, resulting in a full-surface fire of the tank.

The technical standard for sloshing response of an oil storage tank in the Fire Services Law of Japan originally specified only the maximum design horizontal seismic coefficient with the same level throughout the country, but it was revised after this disaster [13, 15]. The new standard specifies the maximum design horizontal seismic coefficient for sloshing response to be doubled depending on the period and area. In addition, standards for strength of the floating roof were established [15].

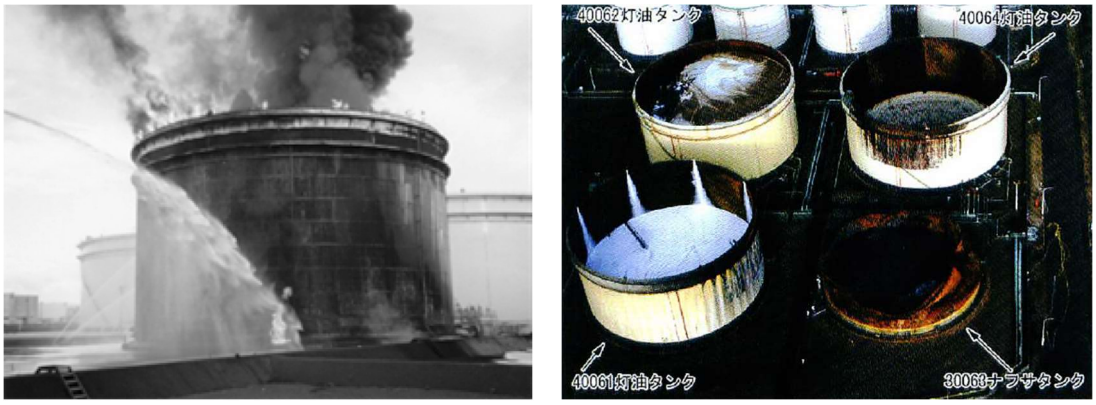

(a) (b)

Figure 1.10 (a) Tank Fire Immediately Following the Earthquake (Photo by Tomakomai Fire Service) [13], and (b) Tank Collapsed due to Tank Fire Occurring Two Days after the Earthquake [14]

Earthquake Damage Due to Short-Period Response

1964 Great Alaska Earthquake, USA (M9.2): A flat-bottom cylindrical shell tank whose diameter and height were 3.2 m and 9.1 m, respectively, slid greatly due to this earthquake (see Figure 1.11) [16]. At the earthquake, the tank held 3.0 m height of product. The sliding displacement was 1.5 m, and this phenomenon has been called “walk” of a tank from the testimony of a witness. A study hypothesized that rocking response would play an important role in the occurrence of tank walk motion [17]. It was also reported that snow was found sucked under the bottom plate as evidence that the tank bottom had uplifted [18].

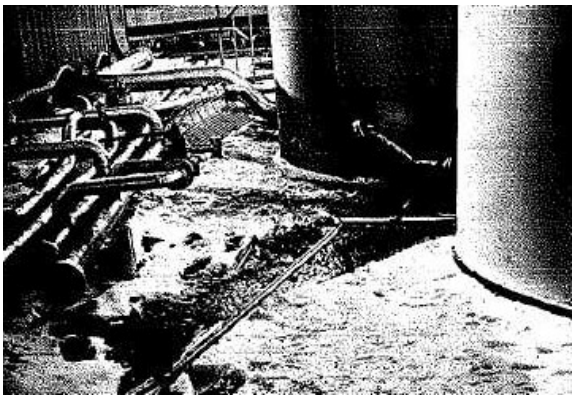

Figure 1.11 “Walk” of Tank [16]

1971 San Fernando Earthquake, USA (M6.6): This earthquake caused great damage to urban facilities. Since oil tanks were far from the epicenter, there was no serious damage. However, water tanks located in various places were considerably damaged. Figure 1.12 shows a water tank that suffered damage in the form of axisymmetric outward bulge of the shell near the bottom. Such buckling is called elephant foot bulging (EFB). In addition, the bottom of the water tank cracked, and all the contents leaked out. Figure 1.13 shows an anchor bolt of a 6,600 kL water tank. This anchor bolt was pulled up 35.5 cm, which was considered to be an evidence of rocking motion of the tank.

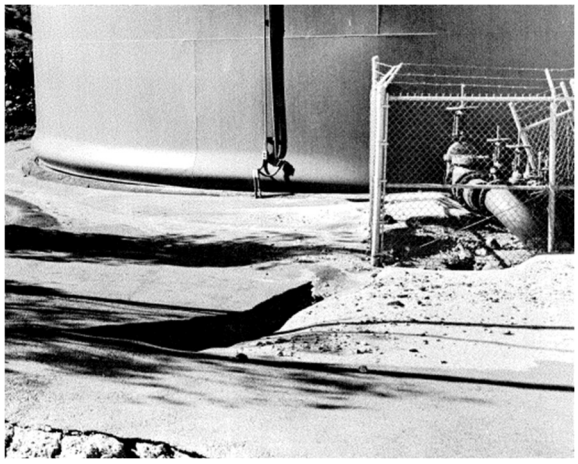

Figure 1.12 Elephant Foot Bulging of 1,000 kL Water Tank [19]

Figure 1.13 Anchor Bolt of 6,600 kL Water Tank (Anchor bolt was pulled up 35.5 cm.) [19]

1978 Miyagiken-Oki Earthquake, Japan (M7.4): The earthquake severely damaged the oil tanks of a refinery in Sendai City. Cracks occurred in the bottom plates of three tanks, and about 68,000 kL of oil leaked out (see Figures 1.14 (a) and (b)) [20, 21]. The cause of this accident has been thought to be the uplifting of the corroded tank bottom plate. Fortunately, there was no fire accident at this refinery. After this accident, there have been no accidents such as oil spills due to cracks in the tank bottom plate in Japan.

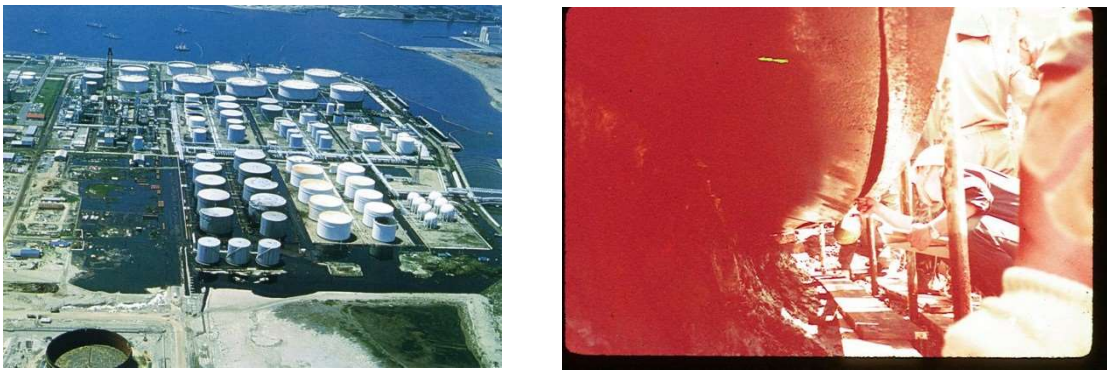

(a) (b)

Figure 1.14 (a) Oil Leak due to Damage to Bottom Plates of Three Oil Tanks (Photo by Kahoku Shimpo Publishing Co.) [20], and (b) Crack in Tank Bottom Plate (Photo by National Research Institute of Fire and Disaster)

1985 Chile Earthquake, Chile (M7.7): Elephant foot buckling occurred as shown in Figures 1.15 (a) and (b) [22]. In addition, there was a tank from which the contents leaked due to cracks in the buckling part.

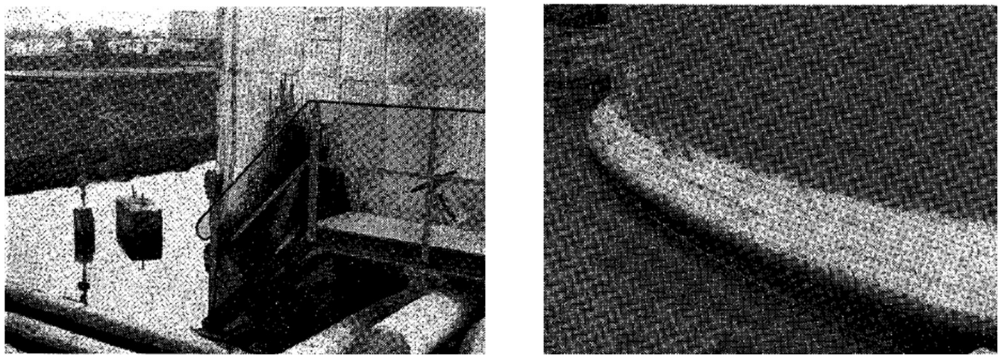

(a) (b)

Figure 1.15 (a) Traces of Leaked Oil [22], and (b) Elephant Foot Bulging of Oil Tank [22]

1995 Kobe Earthquake, Japan (M7.2): This earthquake caused buckling damage to many small tanks [23]. Figure 1.16 (a) shows diamond buckling of a 999 kL oil tank, and Figure 1.16 (b) shows elephant foot bulging of another 999 kL oil tank. Diamond buckling was observed for the first time in Japan. Some tanks had deformation in the upper part. Buckling and pull-out of anchor bolts also occurred in water tanks as shown in Figures 1.17 and 1.18, respectively.

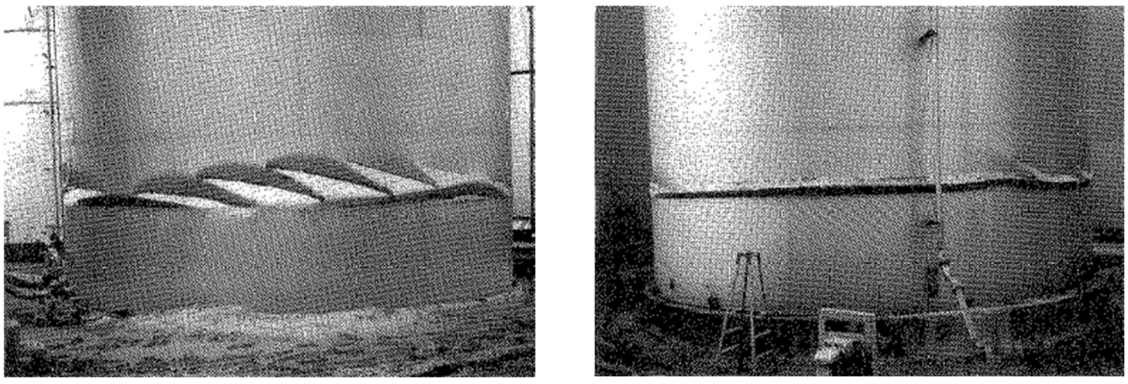

(a) (b)

Figure 1.16 (a) Diamond Buckling of 999 kL Oil Tank [23], and (b) Elephant Foot Bulging of 999 kL Oil Tank [23]

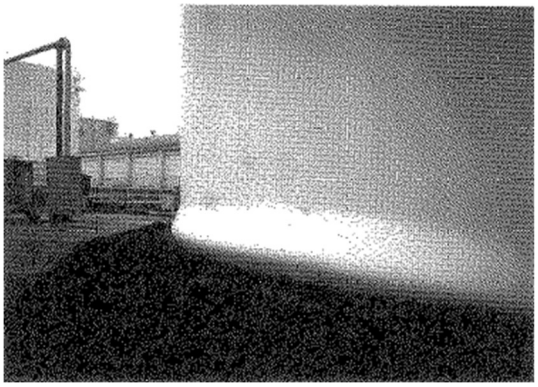

Figure 1.17 Elephant Foot Bulging of Water Tank [23]

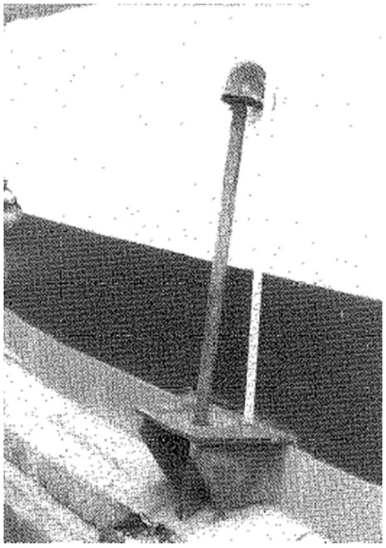

Figure 1.18 Anchor Bolt Pulled out due to Uplift of Tank Bottom [23]

2018 Hokkaido Eastern Iburi Earthquake (M6.7): Buckling damage occurred at the lower end of the shell plate of a 306 kL capacity bunker tank as shown in Figure 1.19. In addition, uplift of a large tank was recorded for the first time in the world by deliberately installed measurement instruments. The capacity of the tank was 115,000 kL, and eight vertical displacement measuring instruments were installed at the bottom part of the tank shell plate at every 45 degrees (see Figure 1.20). According to the observation results, the maximum uplift was 44 mm (see Figure 1.21). The further discussion on this point is provided later.

Figure 1.19 Buckled Shell Plate of 306 kL Capacity Bunker Tank [24]

Figure 1.20 Spring-Operated Displacement Gauge Placed at Bottom Part of Shell Plate of 115,000 kL Capacity Tank [24]

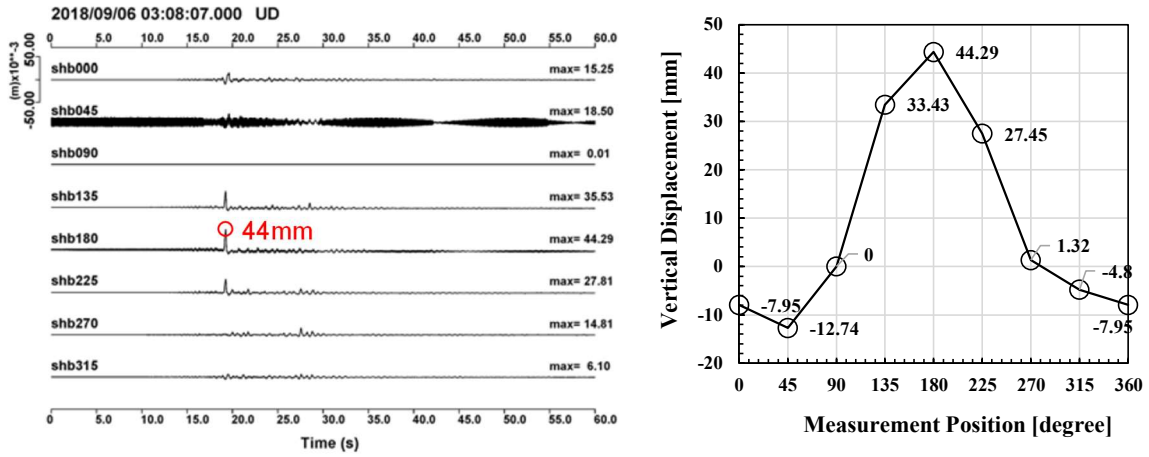

Figure 1.21 Records of Displacement Gauges Placed at Bottom Part of Shell Plate of 115,000 kL Capacity Tank during 2018 Hokkaido Eastern Iburi Earthquake (The maximum uplift displacement was 44 mm at 180° position) [24]

1.1.3 Previous Studies on Seismic Response of Tanks

Seismic response of a tank whose bottom is fixed (anchored tank) is reviewed in brief. Specifically, analytical studies of short-period response of a liquid storage tank are of interest here. Studies of seismic response of unanchored tanks are reviewed in Section 1.2.

Jacobsen (1949) derived effective mass of the fluid in a cylindrical tank with its base experiencing an impulsive horizontal translation, by using the velocity potential theory [25]. Housner (1957) developed a simplified formula of effective mass of content liquid for rectangular and cylindrical tanks in translational motion [26]. This is commonly called the impulsive mass. Both of these analytical solutions of effective mass are formulated for rigid tanks. Housner's simplified formula is used in many seismic standards and guidelines for liquid storage tanks (e.g. [27]). The impulsive mass M_0 and the height of its center of gravity h_0 are expressed by Eqs. (1.1) and (1.2). By using these approximation formulas, the overturning moment and the base shear can be easily estimated.

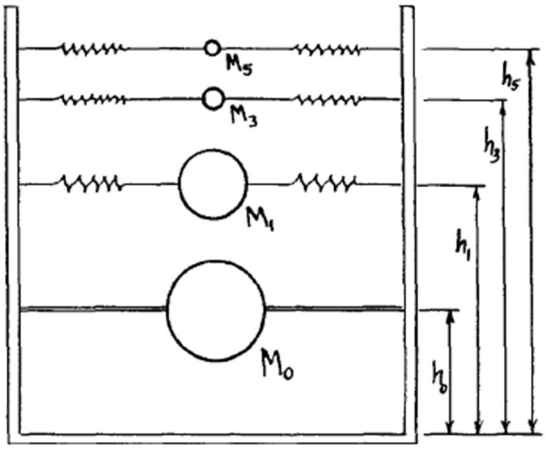

Figure 1.22 Housner's Model [26]

$$M_0 = M\frac{\tanh\sqrt{3}\frac{R}{h}}{\sqrt{3}\frac{R}{h}} \tag{1.1}$$

$$h_0 = \frac{3}{8}h \qquad \left(\frac{h}{R} \leq 1.5\right) \tag{1.2}$$

where, M is the total mass of content liquid, and R is the tank radius and h is the liquid height.

Sakai and Sakoda (1975) rigorously analyzed the fluid-elastic coupled vibration behavior of a cylindrical tank by using FE analysis, and the bulging mode was clarified [4]. Their findings are: (1) the coupled effect between the sloshing response and the bulging response is negligible; (2) hydrodynamic pressure is generated by the bulging response (: fluid-elastic pressure); and (3) the fluid-elastic pressure is not negligible [28, 29].

Sakai and Ogawa (1979) presented a simplified formula to calculate fundamental fluid-elastic period T_b for fixed-based cylindrical tank (Sakai-Ogawa's formula) [30]. Sakai-Ogawa's formula is based on hydroelastic analysis in a beam theory considering cross-sectional deformation. Accuracy of the formula was verified by a comparison with the results of shell theory. Accordingly, the formula has been adopted in the Japanese seismic standards (e.g. [31-34]) and is shown as Eqs. (1.3) and (1.4).

$$T_b = \frac{2}{\lambda}\sqrt{\frac{W}{\pi g E t_{1/3}}} \tag{1.3}$$

$$\lambda = 0.067(H/D)^2 - 0.3(H/D) + 0.46 \qquad (0.15 \leq H/D \leq 2.0) \tag{1.4}$$

where, W is the total weight of content liquid; g is the gravitational acceleration; E is Young's modulus of tank material; H is the liquid height; $t_{1/3}$ is the wall thickness at one third of liquid height H; and D is the tank diameter. As for the dynamic fluid pressure, the following equation is proposed based on the modified seismic coefficient method from the natural period obtained by Eqs. (1.3) and

(1.4), and the acceleration response spectrum.

$$Ph = Ph_0 + Ph_1 \tag{1.5}$$

$$Ph_0 = \frac{9.80665\rho H}{10}\left[\sum_{i=0}^{5} C_{0i}\left(\frac{z}{H}\right)^i\right]\frac{kh_1}{\upsilon_3} \tag{1.6a}$$

$$Ph_1 = \frac{9.80665\rho H}{10}\left[\sum_{i=0}^{5} C_{1i}\left(\frac{z}{H}\right)^i\right]kh_1\left(1-\frac{1}{\upsilon_3}\right) \tag{1.6b}$$

where, Ph_0 is the dynamic hydraulic pressure due to impulsive response and Ph_1 is the dynamic hydraulic pressure due to bulging response. ρ is the density of content liquid. C_{0i} and C_{1i} are the coefficients given by Tables 1.1 and 1.2, respectively. z is an arbitrary height of the content liquid from the tank bottom. kh_1 is the design horizontal seismic coefficient. υ_3 is the amplification factor of a tank. Sakai et al. (e.g. [4, 30]) made the following assumptions for their analysis.

(1) The content liquid is assumed to be inviscid, incompressible, and irrotational.
(2) Deformation of the tank and displacement of the liquid surface are small.
(3) The tank bottom is fully supported on the foundation.

Table 1.1 Values of C_{0i} [32]

		C_{0i}					
		C_{00}	C_{01}	C_{02}	C_{03}	C_{04}	C_{05}
H/D	**0.15**	0.811	-0.130	0.688	-4.21	5.70	-2.85
	0.20	0.824	-0.132	0.688	-4.24	5.71	-2.85
	0.30	0.826	-0.133	0.703	-4.26	5.74	-2.87
	0.40	0.794	-0.129	0.706	-4.11	5.54	-2.79
	0.50	0.724	-0.132	0.811	-4.22	5.65	-2.85
	0.60	0.684	-0.133	0.892	-4.23	5.65	-2.86
	0.70	0.626	-0.131	0.952	-4.21	5.62	-2.86
	0.80	0.572	-0.132	1.03	-4.24	5.66	-2.88
	1.00	0.481	-0.133	1.13	-4.26	5.73	-2.94
	1.20	0.410	-0.134	1.20	-4.33	5.87	-3.02
	1.40	0.356	-0.136	1.26	-4.42	6.06	-3.12
	1.60	0.313	-0.140	1.32	-4.56	6.30	-3.23
	1.80	0.279	-0.144	1.37	-4.71	6.54	-3.34
	2.00	0.252	-0.148	1.43	-4.87	6.79	-3.45

Table 1.2 Values of C_{1i} [32]

		C_{1i}					
		C_{10}	C_{11}	C_{12}	C_{13}	C_{14}	C_{15}
H/D	**0.15**	0.807	0.234	-1.45	0.547	-0.197	0.0626
	0.20	0.813	0.267	-1.48	0.588	-0.217	0.0287
	0.30	0.792	0.277	-1.15	-0.0335	0.418	-0.305
	0.40	0.731	0.241	-0.472	-1.30	1.70	-0.900
	0.50	0.644	0.193	0.265	-2.62	3.05	-1.52
	0.60	0.551	0.133	1.01	-3.98	4.47	-2.17
	0.70	0.462	0.0810	1.61	-5.06	5.63	-2.72
	0.80	0.385	0.0377	2.08	-5.92	6.62	-3.19
	1.00	0.267	-0.0301	2.67	-7.05	8.05	-3.90
	1.20	0.188	-0.0772	2.97	-7.72	9.09	-4.44
	1.40	0.136	-0.112	3.12	-8.18	9.92	-4.88
	1.60	0.100	-0.139	3.19	-8.50	10.6	-5.24
	1.80	0.0753	-0.162	3.23	-8.79	11.2	-5.55
	2.00	0.0580	-0.184	3.27	-9.09	11.8	-5.83

On the other hand, research on the coupled response between the tank and the content liquid is also being conducted in foreign countries (e.g. [35, 36]). Veletsos and Yang (1977) studied response of the tank-fluid combined system and proposed equations for the response of flexible tanks [35]. For a flexible tank with *H*/*R* (aspect ratio of the content liquid) in the range of 0.2 to 1, a solution corresponding to a rigid tank can be obtained by simply applying the pseudo acceleration according to the natural period of the tank-fluid system instead of the ground acceleration. It was shown that the maximum values of impulsive pressure and base shear can be reasonably estimated.

1.2 Previous Studies on Uplift Behavior of Liquid Storage Tanks

Many experimental and analytical studies have been conducted on the uplift of tank bottom due to seismic ground motion. This section briefly reviews previous researches on uplift behavior of liquid storage tanks. According to Isoe (1994) [37], studies on the uplift during earthquakes can be roughly classified into the following studies.

- Experimental studies on the uplift of tank bottom plate
- Analytical studies on the uplift of tank bottom plate
- Studies on the bucking of tank shell plate
- Studies on the strength of uplifted shell-to-annular joint

In this section, some current seismic design standards for the uplift are also explained after the research review.

1.2.1 Experimental Studies on Uplift of Tank Bottom Plate

The following is a brief review of previous experimental studies on the uplift.

Shaking Table Tests

Clough (1977) and Manos et al. (1982): Shaking table tests for a broad tank were conducted by Clough (1977) to investigate the seismic behavior of unanchored tanks [38]. In the experiments, a tank model with a diameter of 3.7 m and a height of 1.8 m was used (see Figure 1.23). The lower part of the tank shell plate and the bottom plate had the same thickness (about 2 mm). A rigid reference frame was used to support the displacement gages. A uniaxial, horizontal base acceleration was input to the shaking table. Figure 1.24 shows a time history of the time-scaled El Centro acceleration record which is used in the experiment. Out-of-round deformation of the tank shell plate, hoop stress and so forth were investigated. In addition, Clough conducted some additional experiments with different parameters such

as with/without the fixed roof, floating roof and anchors. The results of the shaking table tests showed that the deformation and stress of the tank shell plate of an unanchored tank were significantly larger than those of an anchored tank. Based on the test results, Clough proposed a simple model for analyzing the uplift behavior of tanks.

Manos and Clough (1982) conducted additional shaking table tests of a broad tank by using various accelerograms: the 1940 El Centro, the 1971 Pacoima and the 1966 Parkfield earthquakes (PGA: 0.5 G) [41, 42]. It was found that the seismic response of an unanchored tank was strongly influenced by the nonlinearity due to the uplift behavior. In addition, differences in the seismic responses due to stiffness of the foundation were investigated. It was found that the flexible base made the uplift displacement of the tank bottom large.

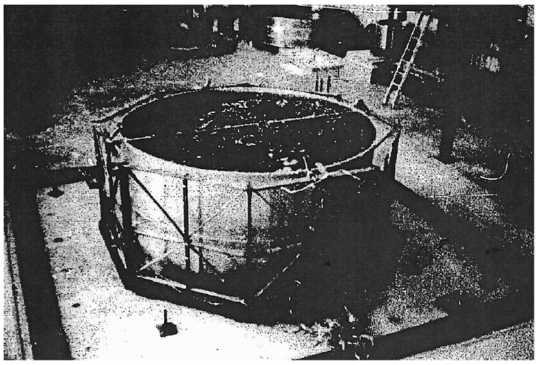

Figure 1.23 Clough's Shaking Table Test for Broad Tank [38]

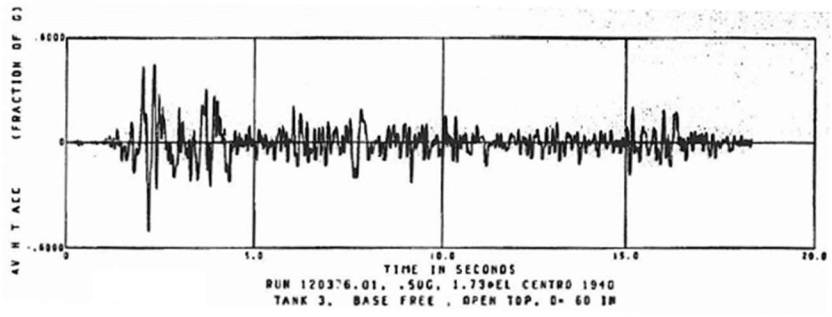

Figure 1.24 Input Acceleration for Unanchored Open Top Tank Model (PGA = 0.5 G) [38]

Niwa (1978): Shaking table tests for a tall tank were conducted by Niwa (1978) who was one of Clough's research groups [39-40, 43-45]. In the experiments, a tank model with a diameter of 2.4 m and a height of 4.6 m was used (see Figure 1.25). The lower part of the tank shell plate and the bottom plate had the same thickness (about 2.3 mm). The uniaxial horizontal acceleration (time-scaled El Centro acceleration record, PGA: 1/8 G) was input to the shaking table, and the responses such as out-of-round deformation of the tank shell plate, hoop stress and so forth were investigated. It was found that out-of-round deformation of the tank shell, in which $\cos(\theta)$ and $\cos(2\theta)$ modes were dominant, occurred when the tank bottom was not fixed (see Figures 1.26 (a) and (b)).

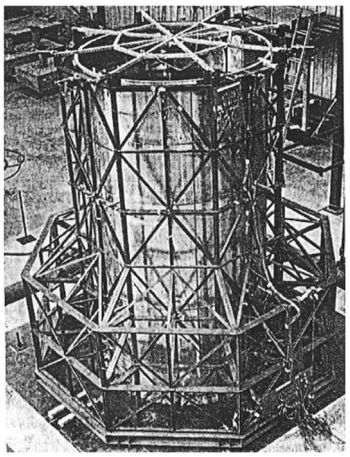

Figure 1.25 Niwa's Shaking Table Test for Tall Tank [43]

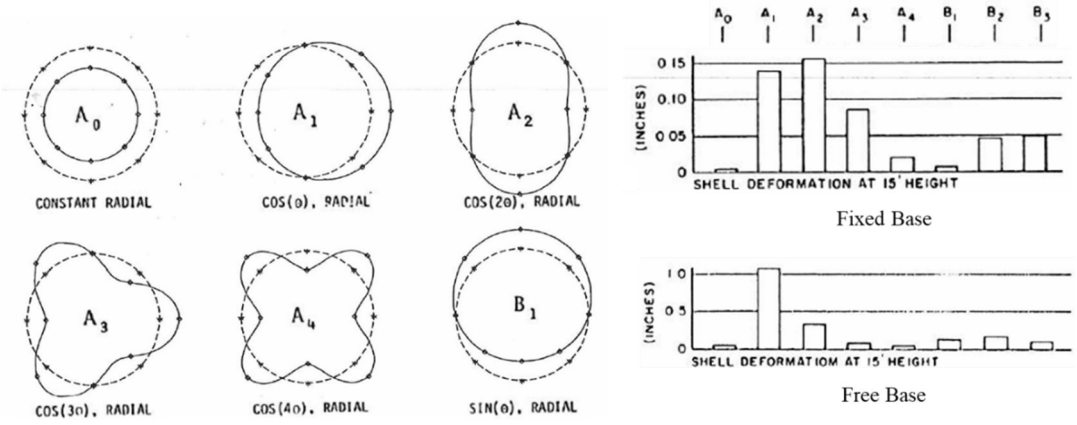

(a) (b)

Figure 1.26 (a) Six Fourier Components of Circumferential Distribution of Responses [43], and (b) Peak Amplitudes of Fourier Response Components (Shell Deformation) [43]

The High Pressure Gas Safety Institute of Japan (KHK) (1982): Shaking table tests of a large tank model were conducted by the High Pressure Gas Safety Institute of Japan (KHK) (1978) [46]. Purpose of this shaking table test was to clarify (1) the stress transferring mechanism between the lower part of the tank shell plate, the tank bottom plate and the foundation, and (2) their ultimate strength. In the experiments, a tank model with a diameter of 10 m and a liquid depth of 6.9 m was used (see Figure 1.27). The bottom of the tank model was fixed with 36 anchor straps (however, uplift was observed in the shaking table test). This tank model was assumed to be 1/5 scale of a 60,000 kL LNG tank (although the model, in the opinion of the author, did not satisfy the similarity requirement). Experiments were conducted with various accelerations such as harmonic ground motion and actual seismic ground motion, and elephant foot bulging was observed. However, the mechanism of EFB was not theoretically investigated, and only an empirical formula was proposed.

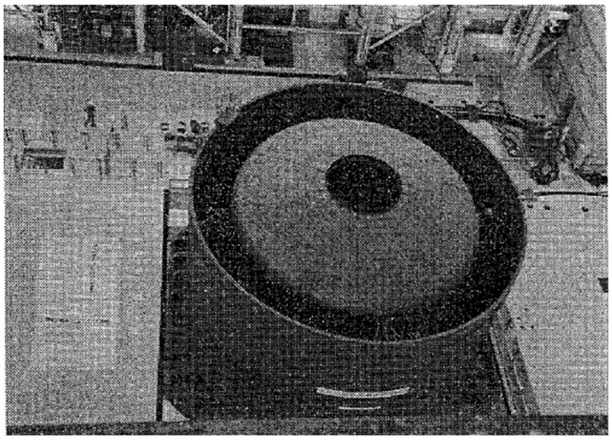

Figure 1.27 KHK's Shaking Table Test [46]

Static Tilt Tests

Niwa (1978): Static tilt test of a tall tank was conducted pioneeringly by Niwa (1978) in order to clarify the uplift behavior of liquid storage tanks. Figure 1.28 (a) shows a view of the static tilt test with a tall tank (2.4 m × 4.6 m) on a rigid steel platform. The experimental results showed that the axial compressive force was concentrated and increased by the uplift (see Figure 1.28 (b)). Shaking table experiments conducted later (Niwa and Clough (1982)) confirmed that the concentration of axial compressive stress would cause the buckling of the tank shell plate [39, 43].

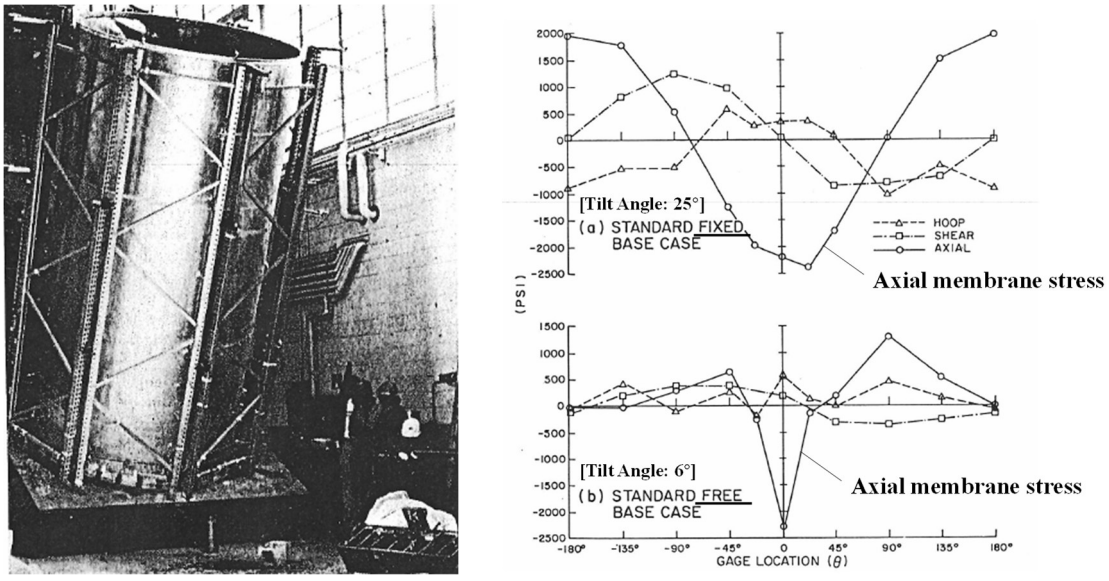

(a) (b)

Figure 1.28 (a) Niwa's Static Tilt Test for Broad Tank [43], and (b) Distribution of Axial Membrane Stress at Bottom Part of Tank Shell (127 mm above Base) in Static Tilt Test [43]

Manos et al. (1982): Static tilt test of a broad tank was conducted by Manos et al. (1982) [41]. In the experiment, a pseudo lateral load was applied to the tank model by tilting the tank, and the uplift behavior of tank was observed in detail. Figure 1.29 shows the tank model (3.6 m × 1.8 m) used in the static tilt test. Based on the experimental results, Manos et al. pointed out that the dominant response mechanism of the uplift behavior was "rocking" of the tank and "ovalling" of the circular cross section

of the tank shell.

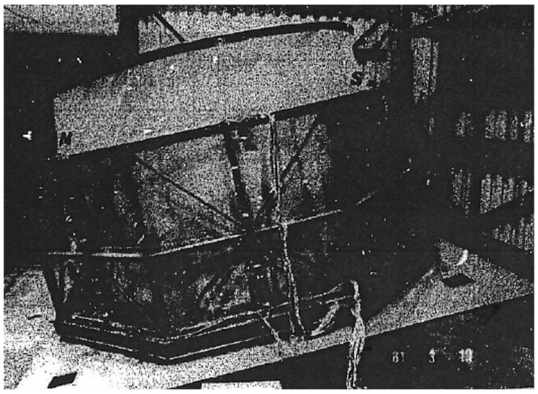

Figure 1.29 Manos's Static Tilt Test for Broad Tank [41]

Sakai et al. (1982): The research group of Sakai et al. (1988-1991) investigated the behavior of uplift for liquid storage tanks through a static tilt test (see Figure 1.30) [47-51]. Their tank model fully satisfied the similitude requirements to large-scaled liquid storage tanks. Sakai et al. (1991) considered a structure with/without a roof and the rigidity of the foundation as experimental conditions, and investigated their effects on the uplift displacement and the stress generated in the tank bottom part (see Figures 1.31 and 1.32). In their researches, a static FE analysis model was also developed, and the results obtained by the FE analysis model were found to agree well with the experimental results (for instance, see Figure 1.32).

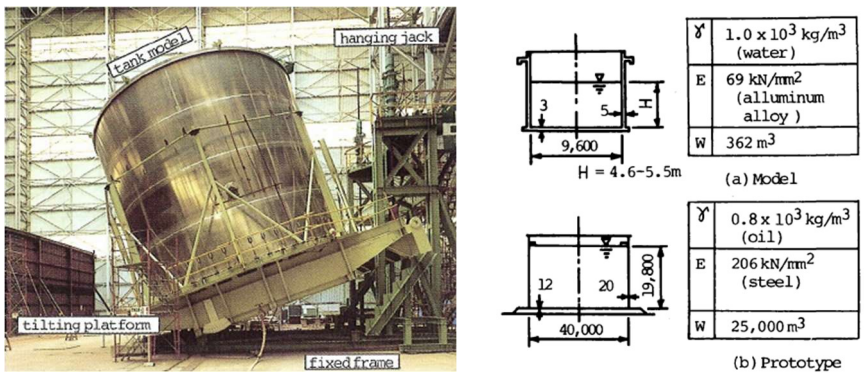

(a) (b)

Figure 1.30(a) Schematic View of Tilt Test [50], and (b) Dimensions [51]

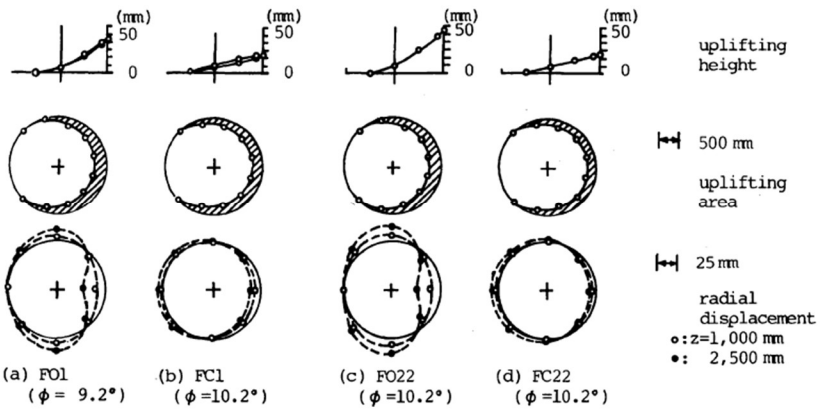

No.	Case	Roof	Foundation	
				Water Depth
1	FC2	exist	r	4.6m
2	FC2D	exist	r	5.5m
3	FO2	no	r	4.6m
4	FO2D	no	r	5.5m
5	FO1	no	p	4.6m
6	FC1	exist	p	4.6m
7	FC22	exist	r	4.6m
8	FC23	exist	r	5.0m
9	FO22	no	r	4.6m
10	FO23	no	r	5.5m
11	FO24	no	r	5.0m
Cf.	RC13	exist	p	4.6m

(p:plywood, r:rubber)

Figure 1.31 Deformation along Circumference [51]

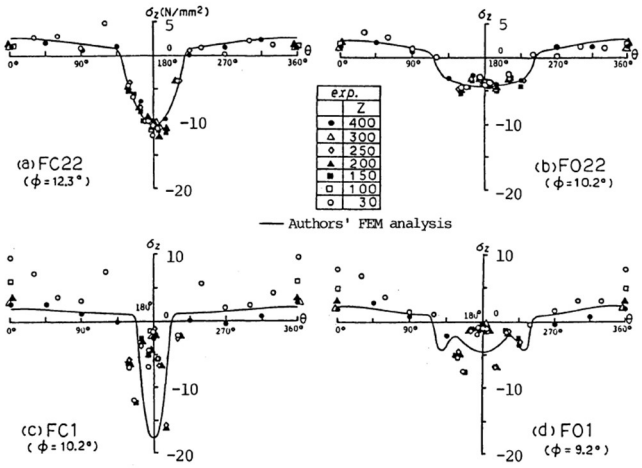

Figure 1.32 Axial Stress Distributions in Shell [51]

1.2.2 Analytical Studies on Uplift of Tank Bottom Plate

The following is a brief review of some typical studies on the rocking response analysis for liquid storage tank.

Ishida and Kobayashi (1984-1988): Ishida and Kobayashi (1984-1988) developed a method for analyzing tank rocking motion [52-54]. They assumed that the axial force distribution at the lower end of the tank shell plate was in the cosine mode in the circumferential direction, and proposed a method to obtain the relationship between the uplift displacement and uplift resistant force from the beam model

which considered large deformation and foundation's stiffness [52]. In addition, Ishida and Kobayashi also developed a method for rocking response analysis using a multi-degree-of-freedom system (see Figure 1.33) [53, 54]. Both analytical models were validated by static tilt and vibration experiments. Rotational inertia force of the content liquid was considered in the mechanical model, and the moment of inertia I_0 was defined by the coupled mass for the translational direction motion.

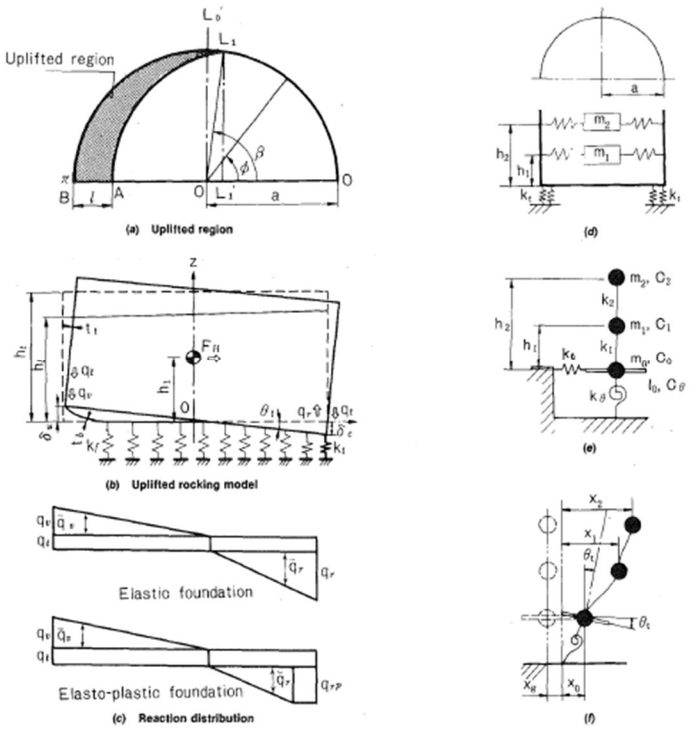

Figure 1.33 Ishida-Kobayashi Model [54]

Malhotra and Veletsos (1994): Malhotra and Veletsos (1994) regarded the tank bottom plate as an assembly of beam models with a unit width, and obtained the rocking resistance of a tank from the sum of vertical reaction forces acting on the connection end of the beam models with the tank shell plate (see Figure 1.34 (a)). Furthermore, the rocking resistance was represented by a rotational spring and introduced into the rocking dynamic analysis model (see Figure 1.34 (b)) [55-57]. In Malhotra's beam model, the membrane force due to geometric nonlinearity and the plasticity of the beam were considered

(see Appendix 3). The equations of Malhotra's model for translational and rotational direction motions are expressed as follows.

Translational Direction:

$$m\ddot{u}_0 + c\left(\dot{u}_0 - \dot{\psi}\bar{h}\right) + k\left(u_0 - \psi\bar{h}\right) = -m\ddot{x}_g \tag{1.7}$$

Rotational Direction:

$$\left[c\left(\dot{u}_0 - \dot{\psi}\bar{h}\right) + k\left(u_0 - \psi\bar{h}\right)\right]\bar{h} = M(\psi) \tag{1.8}$$

where m is the impulsive mass; u_0 is the overall displacement ($u + \psi\bar{h}$); c is the damping coefficient for the tank in its fixed-base condition; k is the corresponding stiffness of the structure; ψ is the rotation of the base; $\bar{h}$ is the height at which the impulsive mass must be concentrated to yield correct overturning base moment; and $M(\psi)$ is the moment in the rotational spring. As can be seen in Eq. (1.8), there is no rotational inertia force term determined by the content liquid. Therefore, this equation only considers the static equilibrium between the overturning moment and the restoring moment induced by the reaction force of the rotational spring proportionally to the rocking angle of the tank. Chapter 4 presents comparison of the calculation by the proposed method in this dissertation to Malhotra's model and also to records of uplift displacement actually observed to verify the necessity of considering the rotational inertia force of the content liquid in tank rocking analysis.

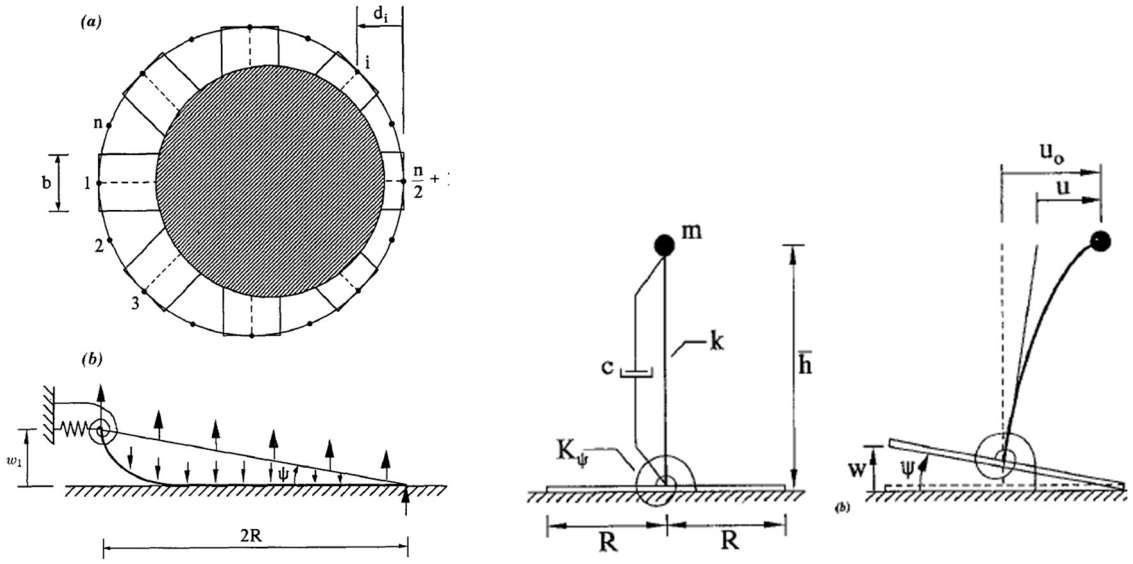

(a) (b)

Figure 1.34 (a) Model of Asymmetrically Uplifted Tank Bottom Plate [56], and (b) Malhotra's Model (Model of Unanchored Tank-Liquid System) [57]

Yuan and Kawano (2004): Yuan and Kawano (2004) developed a more simplified method for rocking response analysis than Malhotra's [58]. The calculation procedure was similar to Malhotra's method, except that (1) a bottom plate was modeled by a beam without considering membrane force, and (2) hydrodynamic pressure acting on the bottom plate was considered without considering its time variation.

Vathi and Karamanos (2015-2017): Vathi and Karamanos (2015-2017) developed a method for rocking response analysis by introducing rotational inertia force into Marhotra's model [59, 60]. However, the moment of inertia considered in their model was simply defined from the effective mass of content liquid in the translational direction (: impulsive mass) without any discussion of its physical background and appropriateness because the impulsive mass was defined by the relationship between the inertia force and the total pressure in the translational direction and regardless of the direction of rotation. In other words, the moment of inertia of content liquid should be defined by considering the balance of forces in the rotational direction.

Taniguchi et al. (2005-): Taniguchi et al. (2005-) are working on the development of a method for analyzing the tank rocking response through a kinematic approach. Taniguchi (2005) clarified the fundamental mechanics of tank rocking motion through the analog of rocking motion of rigid bodies [61]. Taniguchi and Ando (2010) derived a formula for dynamic pressure due to tank rocking motion with uplift of the entire bottom plate [62, 63]. Taniguchi and Segawa (2008) derived a formula for dynamic pressure due to tank rocking motion with partial uplift of the bottom plate [64]. Taniguchi and Segawa (2009) determined the effective mass as well as the effective moment of inertia of content liquid for rocking motion of a rigid rectangular tank whose bottom plate was partially uplifting [65]. Then, Taniguchi (2013) defined the effective mass and the effective moment of inertia of content liquid for the rocking-bulging interaction motion of rectangular tanks [66]. Based on those studies, Taniguchi and Katayama (2016) expanded the definition of the effective mass and the effective moment of inertia of content liquid for tank rocking motion to a cylindrical tank [67]. Taniguchi and Okui (2014) derived equations of motion for cylindrical tanks allowed to rock, based on mechanical analogy between rocking motion of a cylindrical tank and that of a two-degrees-of-freedom (2DOF) system [68]. The mechanical model proposed by them is referred to as Taniguchi model in this dissertation. Then, Taniguchi and Okui (2014) developed a simplified calculation method for translational and rotational responses using the absolute response acceleration spectrum. D'Amico et al. (2017) revised the simplified calculation method by Taniguchi and Okui (2014), and verified the accuracy of the proposed method by comparing it with the results of dynamic FE analysis [69]. However, time history response analysis by Taniguchi model has not yet been conducted due to the difficulty of handling the physical quantities of content liquid according to the uplift width of the tank bottom plate.

The brief reviews provided so far reveal that the mechanical models of a liquid storage tank can be roughly classified into two types: one that does not consider the rotational inertia force, and the other that considers it (see Figure 1.35). Therefore, in this study, by comparing the results of time history

response analysis by each method and the observation record of uplift displacement, the necessity of considering the rotational inertia force of the content liquid in the rocking response analysis of liquid storage tanks is discussed.

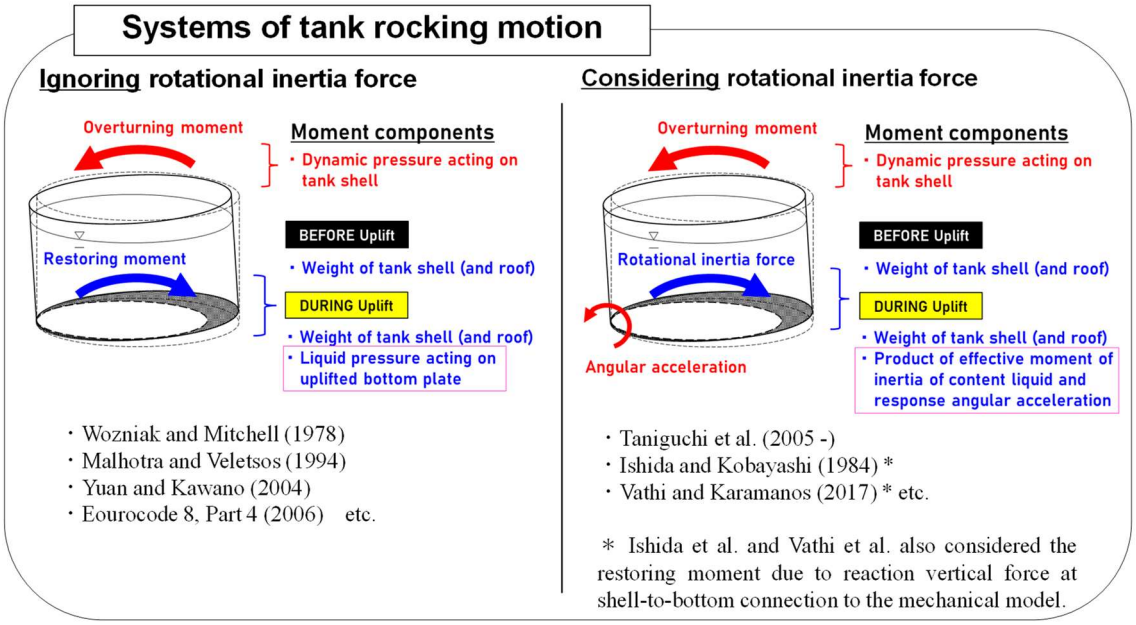

Figure 1.35 Classification of Tank Rocking Models

1.2.3 Seismic Design Standards for Uplift of Liquid Storage Tanks

To show how the uplift problem is considered in the structural design, seismic standards for evaluating the uplift resistance of tank bottom in Japan and foreign countries are briefly reviewed. Basic seismic design has been done so that the stress acting on the members does not exceed the allowable stress determined by the elastic range. Additionally, to prevent breaking of tanks and leakage of content liquid under severe earthquakes, damage to a tank is evaluated considering the limit state of uplift of the tank bottom plate. Foreign seismic design standards evaluate the buckling of the tank shell plate, the background of which is elephant foot bulging accompanying the uplift of tank bottom in severe earthquakes (e.g. [19]). In contrast, seismic design standards in Japan evaluate the strength of the

uplifted part of tank bottom plate, which has a background in massive oil leaks from cracks caused in the uplifted tank bottom plate in severe earthquakes (e.g. [20, 21]).

API 650 (Annex E: Seismic Design of Storage Tanks), U.S.

This design standard specifies the stability of a liquid storage cylindrical tank against overturning moment and the maximum buckling stress of the tank shell [70]. Table 1.3 indicates the criteria of stability against overturning moment. The anchorage ratio J is calculated by Eq. (1.9) and derived based on a balance between the overturning moment and the resistant moment. The resistant moment consists of the weight of the tank shell plate, the reaction force of the bottom end of the tank shell plate due to uplift and the reaction force of the tank foundation. Figure 1.36 shows Wozniak's model [71] which leads the anchorage ratio criteria.

Table 1.3 Anchorage Ratio Criteria (Based on Wozniak's Model) [70]

Anchorage Ratio J	Criteria
$J \leq 0.785$	No calculated uplift under the design seismic overturning moment. The tank is self-anchored.
$0.785 < J \leq 1.54$	Tank is uplifting, but the tank is stable for the design load providing the shell compression requirements are satisfied. Tank is self-anchored.
$J > 1.54$	Tank is not stable and cannot be self-anchored for the design load. Modify the annular ring if $L < 0.035D$ is not controlling or add mechanical anchorage.

$$J = \frac{M_{rw}}{D^2\left[w_t(1 - 0.4A_v) + w_a - F_p w_{int}\right]} \tag{1.9}$$

where D is the tank diameter (m); M_{rw} is the overturning moment (Nm); w_t is the tank and roof weight acting at the base of the shell (N/m) and calculated by Eq. (1.10); A_v is the vertical earthquake acceleration parameter; w_a is the force resisting uplift in the annular region (N/m) and calculated by

Eq. (1.11); F_p is the ratio of normal operation pressure to design pressure, with a minimum value of 0.4; and w_{int} is the calculated design uplift force due to design pressure per unit circumferential length (N/m). w_t and w_a are, respectively,

$$w_t = \frac{W_s}{\pi D} + w_{rs} \tag{1.10}$$

$$w_a = 99\sqrt{F_y H G_e} \qquad (\leq 201.1HDG_e) \tag{1.11}$$

where W_s is the total weight of the tank shell and appurtenances (N) and w_{rs} is the roof load acting on the top of the tank shell; F_y is the minimum specified yield strength of the bottom annulus (MPa); and G_e is the effective specific gravity including vertical seismic effects.

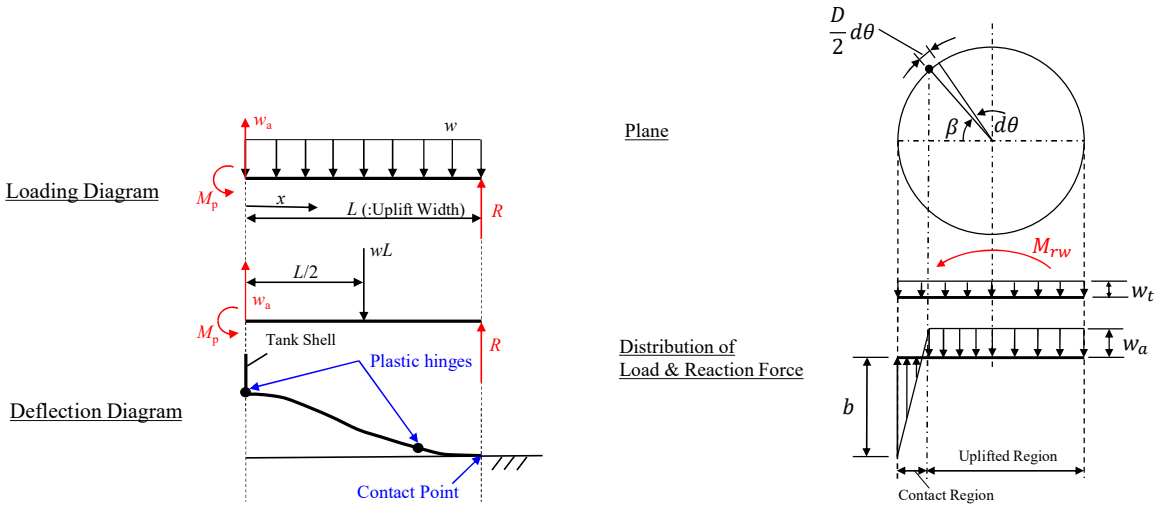

Figure 1.36 Wozniak's Model: (a) Assumed Loading and Deflection [71], and (b) Assumed Load Distribution around Bottom of Tank Shell Plate [71]

The maximum buckling stress σ_c is expressed by the following equations.

When the tank bottom plate does not uplift:

$$\sigma_c = \left(w_t(1 + 0.4A_v) + \frac{1.273M_{rw}}{D^2}\right)\frac{1}{1000t_s} \tag{1.12}$$

When the tank bottom plate uplifts:

$$\sigma_c = \left(\frac{w_t(1 + 0.4A_v) + w_a}{0.607 - 0.18667[J]^{2.3}} - w_a\right)\frac{1}{1000t_s} \tag{1.13}$$

where t_s is the thickness of the bottom shell course less corrosion allowance (mm).

Eurocode 8 (Annex A: Seismic Analysis Procedures for Tanks), EU

Eurocode 8 (BS EN1998-4: 2006) specifies the technical standards for uplift of a tank bottom plate [72]. Some simple diagrams are presented to estimate the uplift displacement and width of the uplift of a tank bottom plate and the vertical compressive membrane force acting on the bottom end of a tank shell plate. The following diagrams (Figures 1.37 (a), (b) and 1.38) are derived from a parametric study with static FE analysis for fixed-roof unanchored tanks. Since these diagrams are obtained by static analysis, the effect of rotational inertia force is implicitly ignored.

Figure 1.37 (a) shows the relationship between nondimensional overturning moment (M/WH, where M is the overturning moment, W is the total weight of content liquid and H is the liquid height) and nondimensional uplift displacement (w_{max}/H, where w_{max} is the maximum uplift displacement). Figure 1.37 (b) shows the relationship between nondimensional overturning moment (M/WH) and nondimensional vertical compressive membrane force (N_u/N_a, where N_u is the vertical membrane force due to uplift and N_a is the vertical membrane force in the anchored case).

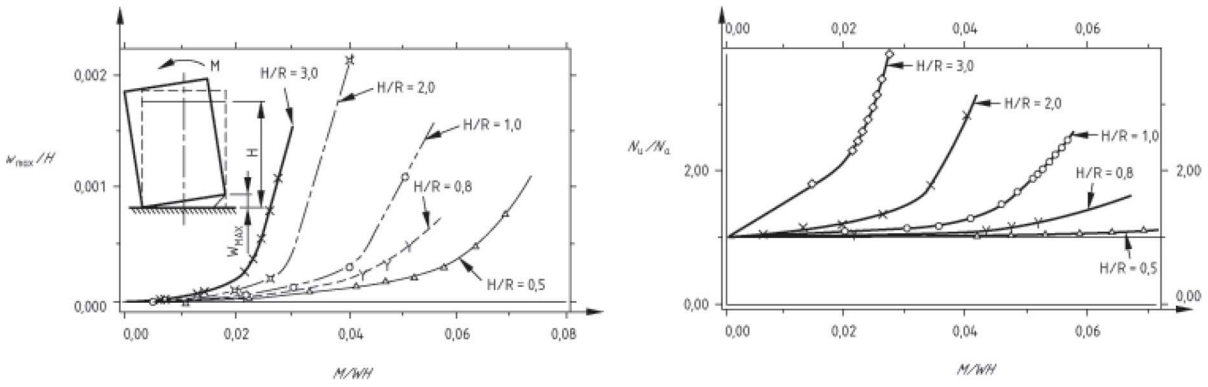

(a) (b)

Figure 1.37 (a) Maximum Vertical Uplift of Fixed-Roof Unanchored Cylindrical Tanks on Ground vs. Overturning Moment M/WH [72], and (b) Ratio of Maximum Axial Compressive Membrane Force for Fixed-Roof Unanchored Cylindrical Tanks on Ground to That for Anchored Tanks vs. Overturning Moment [72]

Figure 1.38 shows the relationship between the uplift displacement w and the uplift width L. The uplift width was likely to increase linearly with the increase of uplift displacement. In this technical standard, the uplift width L is used for calculating radial membrane stress in the tank bottom plate.

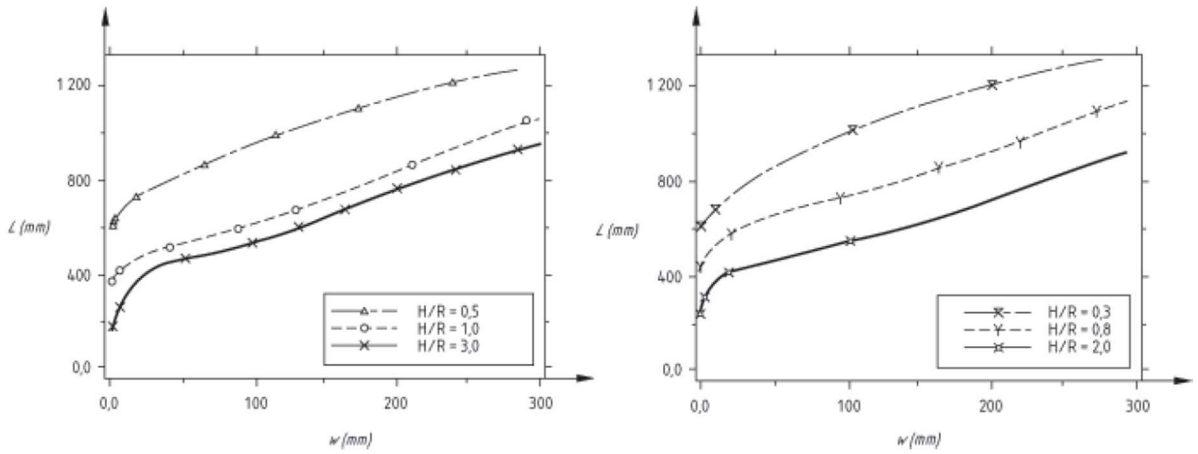

(a) (b)

Figure 1.38 Length of Uplifted Part of Base in Fixed-Roof Unanchored Cylindrical Tanks on Ground as a Function of Vertical Uplift at Edge [72]

Fire Services Law (Notification No. 79), Japan

Japanese Fire Services Law employs the ultimate strength design method as a seismic evaluation for high-level seismic ground motion [73]. This evaluation method was developed by focusing on the strength of the shell-to-bottom connection because cracks in a tank bottom plate could lead to leakage of content liquid which would affect lives and properties seriously. Similar idea is shown in another design guideline [74]. As an evaluation criterion to prevent oil leakage through cracks in a tank bottom plate even with deformation of the tank body during an earthquake, it is stipulated that the maximum lateral shear strength Q_y should be equal to or exceed the required maximum lateral shear force Q_{dw}.

$$Q_y \geq Q_{dw} \tag{1.14}$$

The maximum lateral shear strength Q_y can be calculated by the following equation.

$$Q_y = \frac{2\pi R^2 q_y}{0.44H} \left(= \frac{M_y}{H_G}\right) \tag{1.15}$$

where q_y is the uplift resistant force per unit circumferential length (N/mm); M_y is the restoring moment which is obtained by multiplying the uplift resistant force by the moment arm length and integrating it over the circumference; and H_G is the height of the centroid of effective mass of content liquid for bulging motion. When bending moment of the shell-to-bottom connection reaches the full plastic moment m_p $(= \sigma_y t_b^2/4)$, it is assumed that the tank bottom plate cracks. The mechanical model of the annular plate for limit state of uplift is shown in Figure 1.39, and the uplift resistant force per unit circumferential length q_y is calculated by Eq. (1.16). This model considers only hydrostatic pressure acting on the beam.

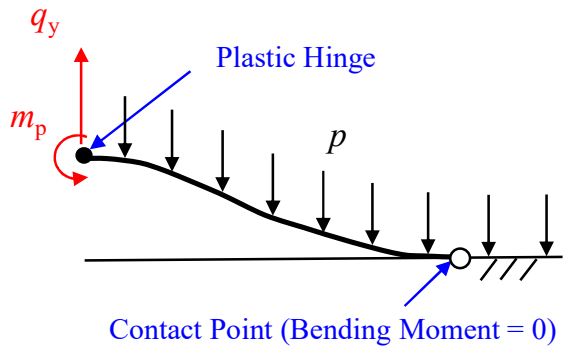

Figure 1.39 Mechanical Model of Annular Plate for Limit State of Uplift (Beams of unit width are considered.)

$$q_y = \frac{2t_b\sqrt{1.5p\sigma_y}}{3} \tag{1.16}$$

where t_b is the thickness of the annular plate (mm); p is the hydrostatic pressure (MPa); and σ_y is the yield stress (N/mm^2). As shown in Eq. (1.15), Q_y is obtained by division of M_y by H_G. Figure 1.40 shows this idea briefly.

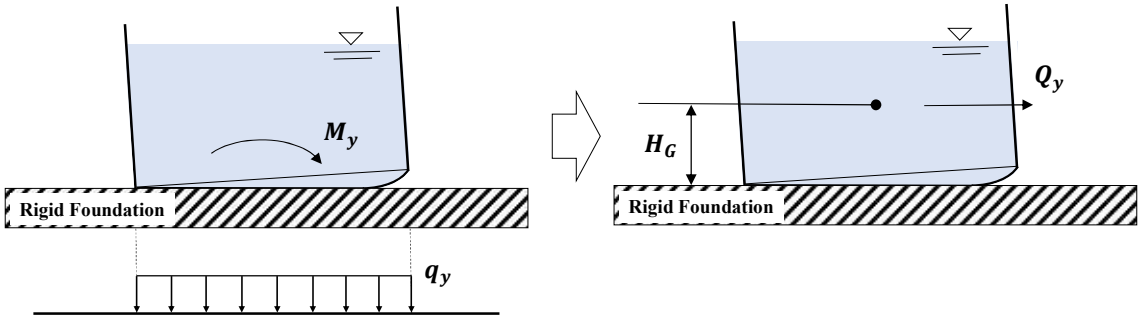

Figure 1.40 Conversion from Restoring Moment M_y to Maximum Lateral Shear Strength Q_y

Whereas, the required maximum lateral shear force Q_{dw} can be calculated by the following equation.

$$Q_{dw} = 0.15\nu_1 \cdot \nu_2 \cdot \nu_3 \cdot \nu_p \cdot D_s \cdot W_0 \quad (1.17)$$

where ν_1 is the modification coefficient depending on region; ν_2 is the modification coefficient depending on site condition; ν_3 is the modification coefficient depending on response magnification which depends on the natural period of the tank; ν_p is the coefficient for plastic design (= 1.5), the value of which is set in accordance with actual damage to the tank; D_s is the structural coefficient; and W_0 is the effective weight of content liquid for horizontal direction motion (N) [75].

1.3 Objectives of Work

The purpose of this study is to develop an analytical method for calculating time history of uplift displacement of liquid storage tanks due to seismic ground motions. This dissertation consists of the following chapters.

In Chapter 2, preliminary preparations for developing a method of tank rocking response analysis are made. To determine the essential conditions and parameters for developing the tank rocking response analysis method, (1) investigation of the relationship between the uplift displacement and the uplift width of the tank bottom plate, (2) investigation of contribution of the rotational inertia force of the content liquid to the tank rocking motion, and (3) experimental study on uplift commencement condition is conducted.

In Chapter 3, equations of motion for a mechanical model of a liquid storage tank are derived based on the 2DOF model and the effective quantities of content liquid for tank rocking motion in the same manner as Taniguchi et al. [68, 69]. Furthermore, in order to conduct time history response analysis, which has not been conducted with Taniguchi model, a computational method is developed for the equations of motion for the mechanical model of a liquid storage tank.

In Chapter 4, time history response analysis of the uplift displacement is conducted by the method developed in Chapter 3 (the proposed method in this dissertation). Accuracy of the proposed method is verified by comparing the computation results of uplift displacement by the proposed method with dynamic FE analysis results and observation record. Additionally, the superiority of the proposed method is verified by comparison with calculation results of uplift displacement by conventional methods.

In Chapter 5, conclusions obtained in this study and future works are described.

In this study, the following conditions are considered.

- Only translational and rotational motions are considered, with sliding motion ignored.
- Foundation is rigid.
- The overturning moment due to sloshing of the content liquid is ignored because sloshing has a very different natural period from those of short-period responses and rarely coincides with them.

The relationship between the previous studies and the current study is summarized in Figure 1.41.

< 2005 >

Clarification of the fundamental mechanics of tank rocking motion through the analogy of rocking motion of rigid bodies

< 2008 – 2010 >

Formulation of the fluid dynamic pressure due to tank rocking motion with partial uplift of the bottom plate

< 2009 – 2016 >

Formulation of the effective mass and the effective moment of inertia of content liquid for tank rocking motion

< 2014 – 2017 >

- Derivation of the equations of motion for tank rocking motion (Taniguchi Model)
- Development of simplified calculation method for tank rocking motion by using response spectrum

< 2020 – 2022 >

- Development of rocking response analysis of liquid storage tanks (Time history analysis)

Current Study

Chapter 1 Introduction

Chapter 2

Preliminary Preparations for Development of Tank Rocking Response Analysis

- Selection of a suitable method for describing the uplift displacement-width relationship
- Investigation of contribution of rotational inertia force of content liquid to the tank rocking motion
- Investigation of uplift commencement condition

Chapter 3

- Re-derivation of the equations of motion for tank rocking motion (Taniguchi Model)
- Development of computational method for rocking response analysis of liquid storage tanks

Chapter 4

- Validation of the computational method for rocking response analysis developed in this study

Chapter 5 Conclusion

Figure 1.41 Summary of Relationship between Previous Studies and Current Study

Bibliography

[1] https://www.jogmec.go.jp/content/300054708.gif

[2] https://www.khi.co.jp/sustainability/earth/green/2020/LNG_Tank.html

[3] Kawano, K. and Yamamoto, S., 1981, "Earthquake Damages of Cylindrical Storage Tanks," Journal of High Pressure Institute of Japan, Vol. 19, Issue 1, pp. 48-51. (in Japanese)

[4] Sakai, F. and Sakoda, H., 1975, "A Study on Earthquake Response of Large-Sized Liquid-Filled Tanks," Proc. 4th Japan Earthq. Engng. Symp., pp. 623-629 (in Japanese)

[5] Eckel, E.B., 1967, "Effects of The Earthquake of March 27, 1964, on Air and Water Transport, Communications, and Utilities Systems in South-Central Alaska," US Government Printing Office, Vol. 545.

[6] Kachadoorian, R., 1965, "Effects of The Earthquake of March 27, 1964, at Whittier, Alaska," U.S. Geological Survey Professional Paper, Vol. 542.

[7] Wakazono, Y. and Ando, N., 1965, "Report on The Industrial by Earthquake at Niigata," Disaster Prevention Research Institute Annuals 8, pp. 177-191. (in Japanese)

[8] Fire and Disaster Management Agency, 1977, "Examples of Disasters at Hazardous Materials Facilities due to Earthquakes (photo collection) - 1964 Niigata Earthquake -," p. 36. (Japanese, Title translated by the author of this dissertation.)

[9] Japan Society of Civil Engineers, 1986, "1983 Nihonkai-Chubu Earthquake Damage Survey Report," Chapter 12, pp. 867-905. (in Japanese, Title translated by the author of this dissertation.)

[10] Yoshida, S., Zama, S., Yamada, M., Ishida, K. and Tahara, T., 2000, "Report on Damage and Failure of Oil Storage Tanks due to The 1999 Chi-Chi Earthquake in Taiwan," Journal of High Pressure Institute of Japan, Vol. 38, Issue 6, pp. 363-374. (in Japanese)

[11] Zama, S., 2003, "Damage and Failure of Oil Storage Tanks due to The 1999 Kocaeli Earthquake in Turkey and Chi-Chi Earthquake in Taiwan," Journal of High Pressure Institute of Japan, Vol. 41, Issue 2, pp. 33-40. (in Japanese)

[12] Sezen, H. and Whittaker, A, S., 2004, "Performance of Industrial Facilities during The 1999, Kocaeli, Turkey Earthquake," 13th World Conference on Earthquake Engineering.

[13] Zama, S., 2006, "Damage of Oil Storage Tanks due to The 2003 Tokachi-Oki Earthquake and Revision of Design Spectra for Liquid Sloshing," BUTSURI-TANSA (Geophysical Exploration), Vol. 59, Issue 4, pp. 353-362. (in Japanese)

[14] Nishi, H. and Yokomizo, T., 2006, "Report on The Investigation of The Tank Fires at The Idemitsu Kosan Hokkaido Refinery (Final Report)," Report of National Research Institute of Fire and

Disaster, Vol. 100, pp. 59-63. (in Japanese)

[15] MIC Notification No. 30, Issued Jan. 14, 2005. (in Japanese)

[16] Rinne, J, E., 1967, Oil Storage Tanks, The Prince William Sound, Alaska, Earthquake of 1964 and Aftershocks, U.S. Department of Commerce Environmental Science Service Administration, pp. 245-252.

[17] Taniguchi, T. and Segawa, T., 2013, "Fundamental Mechanics of Walking of Unanchored Flat-Bottom Cylindrical Shell Model Tanks Subjected to Horizontal Harmonic Base Excitation," Journal of Pressure Vessel Technologies, ASME, Vol. 135, Issue 2.

[18] Shibata, H., 1974, "Survey Report on Earthquake Damage of Industrial Facilities in The World – Spherical Vessels and Cylindrical Vessels," SEISAN KENKYU, Vol. 26, Issue 7, pp. 259-264. (in Japanese)

[19] Jennings, P, C. et al., 1971, "Engineering Features of The San Fernando Earthquake of February 9, 1971," EERL71-02, Cal. Tech.

[20] Ministry of Home Affairs, Fire and Disaster Management Agency, 1979, "Disaster Report for The 1978 Miyagiken-Oki Earthquake," pp. 93-100. (Japanese, Title translated by the author of this dissertation.)

[21] Ministry of Home Affairs, Fire and Disaster Management Agency, 1979, "Collection of Disaster Case Studies of Hazardous Materials Facilities Caused by The Miyagiken-Oki Earthquake," pp. 51-64. (in Japanese, Title translated by the author of this dissertation.)

[22] Watanabe, H. and Takeuchi, M., 1985, "Report for Field Investigation of The Chile Earthquake of March 3, 1985," JSCE Magazine, Vol. 70, No. 9, September, pp. 17-27. (in Japanese, Title translated by the author of this dissertation.)

[23] Yamada, H. and Kamei, A., 1995, "Damage to Storage Tanks in The Great Hanshin-Awaji Earthquake," Journal of Japan Society for Safety Engineering, Vol. 34, Issue 6, pp. 459-465. (in Japanese, Title translated by the author of this dissertation.)

[24] Hatayama, K., Nishi, H., Hayashi, M. and Tokutake, K., 2020, "Damage to Oil Tanks Caused by Severe Strong Ground Motion due to The 2018 Hokkaido, Japan Iburi-Tobu Earthquake (Mw6.6)," Proc. ASME PVP Conference, Seismic Engineering, Paper No. PVP2020-21447.

[25] Jacobsen, S., 1949, "Impulsive Hydrodynamics of Fluid Inside A Cylindrical Tank and of A Fluid Surrounding A Cylindrical Pier," Bulletin of the Seismological Society of America, Vol. 39, pp. 189-204.

[26] Housner, G. W., 1957, "Dynamic Pressure on Accelerated Fluid Containers," Bulletin of The

Seismological Society of America, Vol. 47, Issue 1, pp. 15-35.

[27] API Standard 620, 2008, “Design and Construction of Large, Welded, Low-Pressure Storage Tanks, Appendix L: Seismic Design of Storage Tanks,” Eleventh Edition.

[28] Okada, M., Sakai, F. and Sakoda, H., 1975, “Earthquake Response Analysis of Large Tanks Containing Liquid by Finite Element Method,” Tech. Review of Kawasaki Heavy Ind. Ltd., No. 59 (in Japanese)

[29] Okada, M., Sakai, F., Sakoda, H. and Tada, B., 1976, “Earthquake Response Analysis of Large Tanks Containing Liquid by Finite Element Method (Continuation),” Tech. Review of Kawasaki Heavy Ind. Ltd., No. 61 (in Japanese)

[30] Sakai, F. and Ogawa, H., 1979, “On a Simplified Theory for the Vibration Analysis of Circular Cylindrical Liquid Storage Tanks,” Proc. 13th National Symp. Matrix Meth. Analysis, Japanese Society of Steel Construction, (in Japanese)

[31] Fire Services Law (Notification No. 4 (20)), “Effect of earthquakes”. (in Japanese, Title translated by the author of this dissertation.)

[32] FDMA Notification No. 44, Issued Apr. 28, 1983.

[33] METI Notification No. 515, Issued Oct. 26, 1981.

[34] Sakai, F. and Ogawa, H., 1982, “Seismic Resistant Design of Liquid Storage Tanks in Japan,” Proc. of Sino-American Symposium on Bridge and Structural Engineering, Beijing, China.

[35] Veletsos, A.S. and Yang, J.Y., 1977, “Earthquake Response of Liquid-Storage Tanks,” Proc. of Advances in Civil Engineering Through Engineering Mechanics.

[36] Haroun, M.A., 1980, “Dynamic Analysis of Liquid Storage Tanks,” EERL Report, 80-04. California Institute of Technology, Pasadena, CA.

[37] Isoe, A., 1994, “A Study on Uplift and Sliding Behavior of An Above-Ground Flat-Bottom Cylindrical Tank due to Seismic Ground Motion,” PhD. Dissertation, Tokyo University. (in Japanese, Title translated by the author of this dissertation.)

[38] Clough, D.P., 1977, “Experimental Evaluation of Seismic Design Methods for Broad Cylindrical Tanks,” Univ. of California, EERC Rep., UCB/EERC-77/10.

[39] Niwa, A., 1978, “Seismic Behavior of Tall Liquid Storage Tanks,” Univ. of California, EERC Rep., UCB/EERC-78/04.

[40] Clough, R.W. and Niwa, A., 1979, “Static Tilt Tests of A Tall Cylindrical Liquid Storage Tank,” Univ. of California, EERC Rep., UCB/EERC-79/06.

[41] Manos, G.C. and Clough, R.W., 1982, “Further Study of The Earthquake Response of A Broad

Cylindrical Liquid-Storage Tank Model," Univ. of California, EERC Rep., UCB/EERC-82/07.

[42] Manos, G.C., 1986, "Dynamic Response of A Broad Storage Tank Model under A Variety of Simulated Earthquake Motions," Proc. of the third U.S. National Conference on Earthquake Engineering by Earthquake Engineering Research Institute, pp. 2131-2142.

[43] Clough, R.W., Niwa, A. and Clough, D.W., 1979, "Experimental Seismic Study of Cylindrical Tanks," J. Struct. Div. ASCE, Vol.105, Issue 12, pp. 2565–2590.

[44] Niwa, A. and Clough, R.W., 1981, "Earthquake Damage and Shaking Table Test of Thin Cylindrical Shell Tank," Proc. of The JSCE Earthquake Engineering Symposium, Vol. 16, pp. 249-252. (in Japanese, Title translated by the author of this dissertation.)

[45] Niwa, A. and Clough, R.W., 1982, "Buckling of Cylindrical Liquid Storage Tanks under Earthquake Loading," Earthquake Engineering and Structural Dynamics, Vol. 10, pp. 107-122.

[46] The High Pressure Gas Safety Institute of Japan (KHK), 1982, "Report on Shaking Table Test of Steel Cylindrical Storage Tank (1-3)," Journal of the Institution for Safety of High Pressure Gas Engineering, Vol. 21, No.7-9.

[47] Sakai, F., Isoe, A., Hirakawa, H. and Mentani, Y., 1988, "Experimental Study on Uplifting Behavior of Flat-Based Liquid Storage Tanks Without Anchors," Proc. of the Ninth World Conference on Earthquake Engineering, Tokyo/Kyoto, Japan.

[48] Sakai, F. and Isoe, A., 1988, "An Experimental Verification on Seismic Behavior of Large-Scaled Liquid Storage Tanks," Proc. of the Ninth World Conference on Earthquake Engineering, Tokyo/Kyoto, Japan.

[49] Sakai, F., 1988, "Static Tilt Tests of A Full-Sized Cylindrical Liquid Storage Tank Model," Conference: On site experimental verification of the seismic behavior of nuclear reactor structures and components, pp.117-125, Italy.

[50] Sakai, F., Isoe, A., Hirakawa, H. and Mentani, Y., 1989, "Static Tilt Test Using A Large Model of Exact Similitude With Flat-Based Cylindrical Liquid Storage Tanks," Doboku Gakkai Ronbunshu 1989 Vol. 404, pp. 229-238, Japan Society of Civil Engineers. (in Japanese)

[51] Sakai, F. and Isoe, A., 1991, "Seismic Study on Uplift Behavior of Cylindrical Liquid Storage Tanks by Static Tilt Tests with A Full Scale Model, " Doboku Gakkai Ronbunshu 1991 Vol. 432, pp. 175-184, Japan Society of Civil Engineers. (in Japanese)

[52] Kobayashi, N. and Ishida, K., 1984, "Nonlinear Rocking Analysis of Unanchored Cylindrical Tanks: 1st Report, Uplift Deformation of Bottom Plate Subjected by Overturning Moment," Transactions of The Japan Society of Mechanical Engineers Series A, Vol. 50, Issue 451, pp. 514-519.

(in Japanese)

[53] Ishida, K. and Kobayashi, N., 1984, “Nonlinear Rocking Analysis of Unanchored Cylindrical Tanks: 2nd Report, Dynamic Response with Consideration of Uplift of Bottom Plates,” Transactions of the Japan Society of Mechanical Engineers Series A, Vol. 50, Issue 453, pp. 1042-1048. (in Japanese)

[54] Ishida, K. and Kobayashi, N., 1988, “An Effective Method of Analyzing Rocking Motion for Unanchored Cylindrical Tanks Including Uplift,” Journal of Pressure Vessel Technologies, ASME, Vol. 110, Issue 1, pp. 76-87.

[55] Malhotra, P.K. and Veletsos, A.S., 1994, “Beam Model for Base Uplifting Analysis of Cylindrical Tanks,” J. Struct. Div. ASCE, Vol. 120, Issue 12, pp. 3471-3488.

[56] Malhotra, P.K. and Veletsos, A.S., 1994, “Uplifting Analysis of Base Plates in Cylindrical Tanks,” J. Struct. Div. ASCE, Vol. 120, Issue 12, pp. 3489-3505.

[57] Malhotra, P.K. and Veletsos, A.S., 1994, “Uplifting Response of Unanchored Liquid-Storage Tanks,” J. Struct. Div. ASCE, Vol. 120, Issue 12, pp. 3525-3547.

[58] Yuan, H., Kawano, K. and Yoshida, S., 2004, “Study on Restoring Force Models of Nonlinear Uplift Behavior of Unanchored Oil Storage Tank Under Strong Seismic Excitation,” Proc. ASME PVP Conference, Seismic Engineering, Paper No. PVP2004-3070.

[59] Vathi, M. and Karamanos, S.A., 2015, “Simplified Model for The Seismic Performance of Unanchored Liquid Storage Tanks,” Proc. ASME PVP Conference, Seismic Engineering, Paper No. PVP2015-45695.

[60] Vathi, M. and Karamanos, S.A., 2017, “A Simple and Efficient Model for Seismic Response and Low-Cycle Fatigue Assessment of Uplifting Liquid Storage Tanks,” Journal of Loss Prevention in The Process Industries, Vol. 53, pp. 29-44.

[61] Taniguchi, T., 2005, “Rocking Dynamics of Unanchored Model Flat-Bottom Cylindrical Shell Tanks subjected to Harmonic Excitation,” Journal of Pressure Vessel Technologies, ASME, Vol. 127, Issue 4, pp. 373-386.

[62] Taniguchi, T. and Ando, Y., 2010, “Fluid Pressures on Unanchored Rigid Rectangular Tanks Under Action of Uplifting Acceleration,” Journal of Pressure Vessel Technologies, ASME, Vol. 132, Issue 1, 011801.

[63] Taniguchi, T. and Ando, Y., 2010, “Fluid Pressures on Unanchored Rigid Flat-Bottom Cylindrical Tanks Under Action of Uplifting Acceleration,” Journal of Pressure Vessel Technologies, ASME, Vol. 132, Issue 1, 011802.

[64] Taniguchi, T. and Segawa, T., 2008, “Fluid Pressures on Rectangular Tank Consisting of Rigid

Side Walls and Rectilinearly Deforming Bottom Plate due to Uplift Motion," Proc. ASME PVP Conference, Seismic Engineering, Paper No. PVP2008-61166.

[65] Taniguchi, T. and Segawa, T., 2009, "Effective Mass of Fluid for Rocking Motion of Flat-Bottom Cylindrical Tanks," Proc. ASME PVP Conference, Seismic Engineering, Paper No. PVP2009-77580.

[66] Taniguchi, T., 2013, "Contributions of Fluid to Rocking–Bulging Interaction of Rectangular Tanks whose Walls are Rigid and Bottom Plate Rectilinearly Uplifts," Journal of Pressure Vessel Technologies, ASME, Vol. 135, Issue 1, 011304.

[67] Taniguchi, T. and Katayama, Y., 2016, "Masses of Fluid for Cylindrical Tanks in Rock with Partial Uplift of Bottom Plate," Journal of Pressure Vessel Technologies, ASME, Vol. 138, Issue 5, 051301.

[68] Taniguchi, T. and Okui, D., 2014, "A Case Study of Evaluation of Tank Rock Motion with Simplified Analysis Procedure," Proc. ASME PVP Conference, Seismic Engineering, Paper No. PVP2014-28635.

[69] D'Amico, M., Taniguchi, T. and Nakashima, T., 2017, "Simplified Analysis of The Rocking Motion of A Cylindrical Tank Focusing on The Role of Dynamical Forces Involved in Rocking-Bulging Interaction," Proc. ASME PVP Conference, Seismic Engineering, Paper No. PVP2017-65442.

[70] API Standard 650, 2020, "Welded Tanks for Oil Storage, Annex E: Seismic Design of Storage Tanks," Thirteenth Edition.

[71] Wozniak, R.S. and Mitchell, W.W., 1978, "Basis of Seismic Design Provisions for Welded Steel Oil Storage Tanks," API Refining Dept., 43rd Midyear meeting, Toronto.

[72] European Committee for Standardization, 2006, "Silos, Tanks and Pipelines," Eurocode 8, part 4, CEN/TC 250, EN 1998-4, Brussels.

[73] Fire Services Law (Notification No. 79), "Calculation Method of Maximum Lateral Shear Strength etc." (in Japanese, Title translated by the author of this dissertation.)

[74] Architectural Institute of Japan, 2010, "Design Recommendation for Storage Tanks and Their Supports." (in Japanese)

[75] Fire Services Law (Notice of Hazardous Material Regulations No. 44), 1983. (in Japanese)

Chapter 2

Preliminary Preparations for Development of Tank Rocking Response Analysis

Chapter 2

Preliminary Preparations for Development of Tank Rocking Response Analysis

2.1 Introduction

In this chapter, to determine the essential conditions and parameters for tank rocking response analysis, the following unknown subjects are clarified before developing a mechanical model for analyzing tank rocking motion.

- Selection of a suitable method for describing the uplift displacement-width relationship
- Investigation of contribution of rotational inertia force of content liquid to the tank rocking motion
- Investigation of uplift commencement condition

2.2 Selection of A Suitable Method for Describing Uplift Displacement-Width Relationship

According to Taniguchi and Katayama (2016), estimation of the physical quantities of content liquid related to the tank rocking motion requires to know the value of the uplift width L [9]. In contrast, the rocking angle θ (= uplift displacement w/tank diameter D) will be obtained directly from the time history response analysis of the tank rocking motion. Therefore, it would be convenient if the uplift width of the tank bottom plate could be straightforwardly obtained from the calculated rocking angle. The uplift displacement-width relationship can be easily obtained from beam models which represent

the tank bottom plate, and several beam models have been proposed so far (e.g. [1, 8]).

This section confirms the accuracy of two representative beam models to select the most suitable one for calculating the uplift displacement-width relationship which is applied to Taniguchi model. One is a beam model based on the small deformation theory, which does not consider the plastic yielding at the bottom edge, and is supported by elastic foundation (the simple beam model, see Figure 2.1 (a)). The other is a beam model that considers geometric nonlinearity and also considers the plastic yielding at the bottom edge, and is supported by rigid foundation (Malhotra's beam model, see Figure 2.1 (b)). Detailed description of these models is given in Appendix 3.

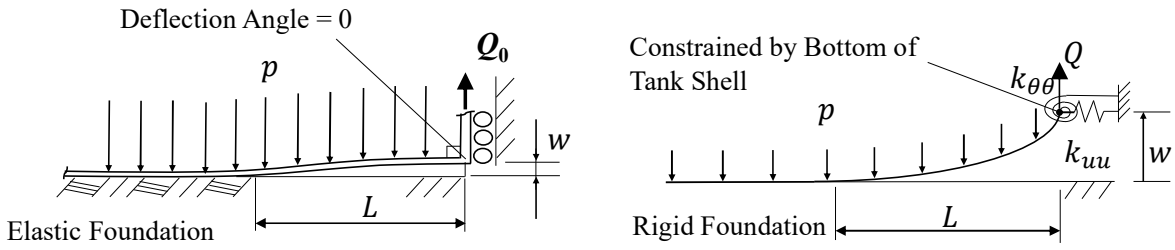

(a) Simple Beam Model [1] (b) Malhotora's Beam Model [8]

Figure 2.1 Beam Models Examined in This Study

In this verification, the uplift displacement-width relationship obtained by each beam model is compared with that obtained from dynamic FE analysis [1, 2]. The tank model in dynamic FE analysis is a 60,000 kL LNG tank with a diameter of 51.5 m and a liquid depth of 28.8 m, which is on a concrete foundation (see Figure 2.2). Detailed description of the dynamic FE analysis is given in Appendix 1.

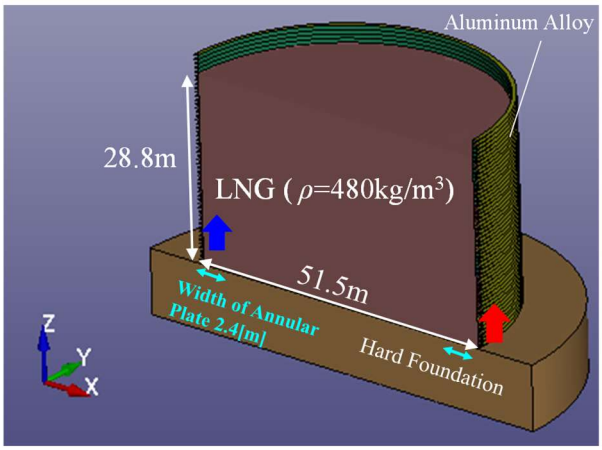

Figure 2.2 Numerical Model Used in This Study [1]

Accuracy determined in the same manner as the numerical analysis used herein has been validated by Nakashima et al. (2008) by comparing it with free rocking experiments of a small tank model [3]. Figures 2.3 (a) to (c) show the experimental model, the FE analysis model, and the time history of the vertical displacement at the tank bottom, respectively. The content liquid was water, and the tank shell was made of polypropylene. As seen in Figure 2.3 (c), the results of the dynamic FE analysis agreed well with the experimental results. Therefore, it can be considered that the dynamic FE analysis adopted in both studies well approximates behaviors of tank rocking motion. Except for the mechanical properties of a tank model and content liquid, the analysis conditions of the tank model used in the current study were basically the same as those of the tank model validated by Nakashima et al. (2008).

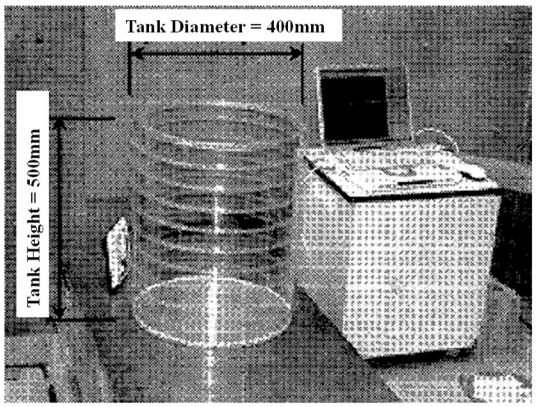

(a) Experimental Model

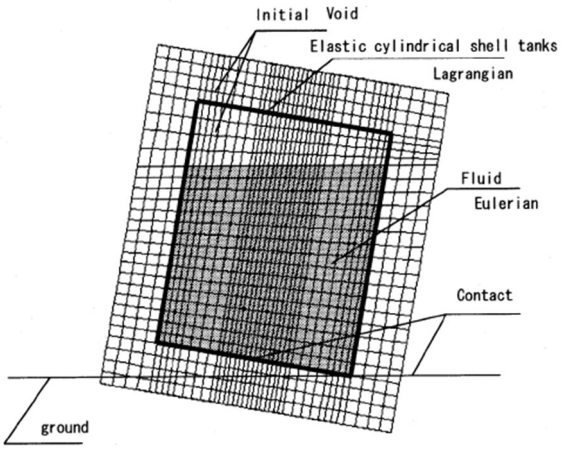

(b) FE Analysis Model

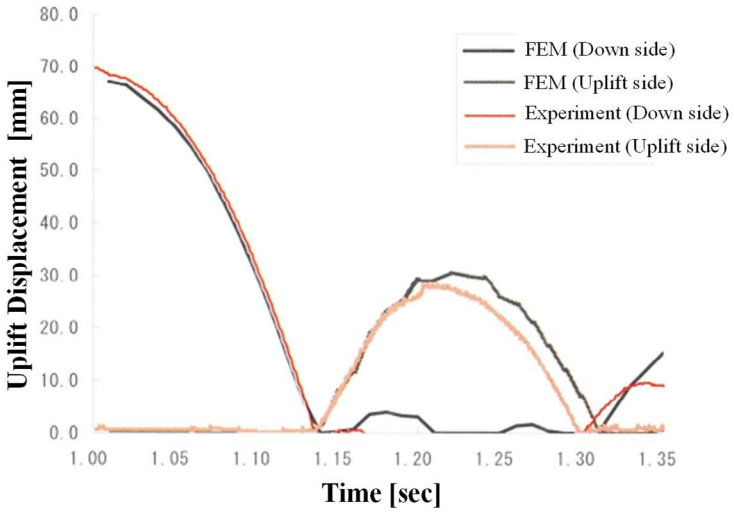

(c) Time History of Vertical Displacement of Tank Bottom

Figure 2.3 Validation of FE Analysis Conducted by Nakashima et al. (2008) [3]

Figure 2.4 (a) shows the time histories of the uplift displacement at both left and right sides of the tank bottom and the base acceleration. The driving period of the horizontal sinusoidal base acceleration was identical with the first natural period of tank bulging motion, and the amplitude was set to 1000 Gal. As a result of inputting the acceleration to the tank base, the bottom of the tank uplifted alternately to the left and right. Using these results, the uplift displacement-width relationship was plotted by nondimensional displacement as shown in Figure 2.4 (b). This relationship was used to verify the accuracy of the beam models.

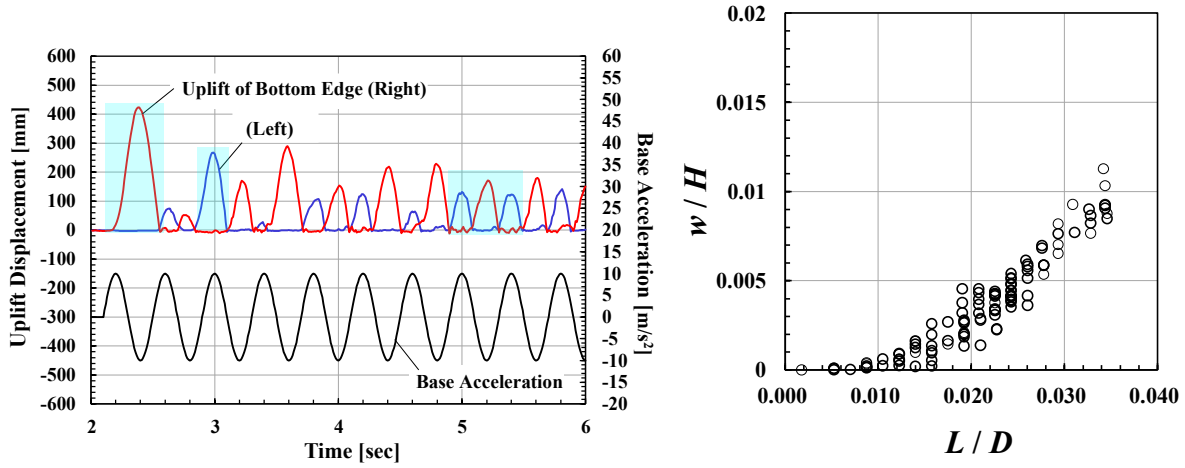

(a) (b)

Figure 2.4 Results of Dynamic FE Analysis: (a) Uplift Displacement and Base Acceleration [1], and (b) Uplift Displacement-Width Relationship* [1]

* Time histories of uplift displacement-width relationship (Range highlighted with ■ in Figure 2.4 (a)) are plotted. Where, ***w*** is the uplift displacement; ***H*** is the liquid height; ***L*** is the uplift width; and ***D*** is the tank diameter.

Finally, the uplift displacement-width relationship calculated by dynamic FE analysis and those by the two different beam models are compared in Figures 2.5 (a) and (b). From the comparisons, the followings were obtained.

- When the uplift displacement was small, the results from the simple beam model generally agreed with the results of dynamic FE analysis. However, when w/H exceeded about 0.005, the simple beam model could not reproduce the FE analysis results.
- When the uplift displacement was small, the results from Malhotra's beam model also generally agreed with the results of dynamic FE analysis. Furthermore, the shapes of the curves calculated by Malhotra's beam model agreed with those by the FE analysis even after w/H exceeded about 0.005. This was because the membrane force in the axial direction and the uplift width increased with the increase of uplift displacement. In addition, the model showed better agreement when the reduction in the hydraulic pressure was considered assuming the hydrodynamic pressure due to the bulging response (see the dotted curve in Figure 2.5 (b)).

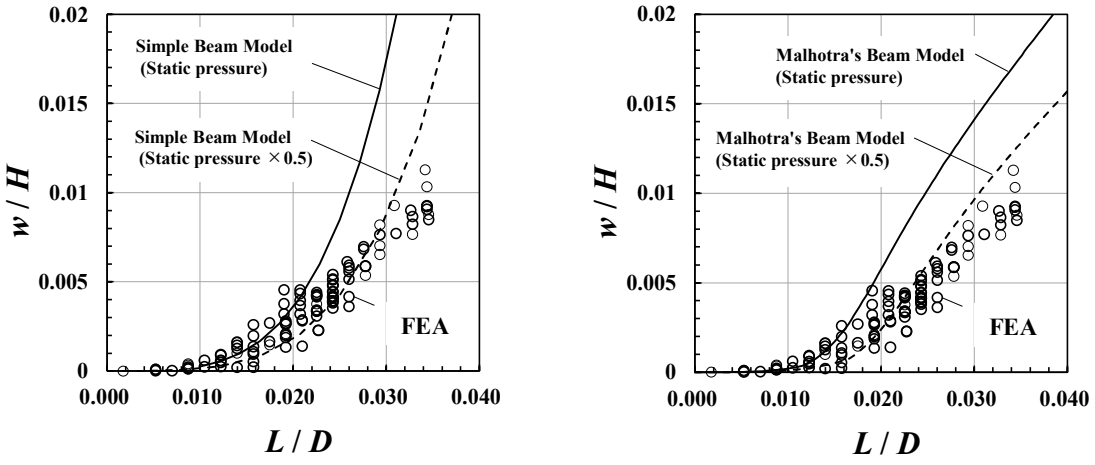

(a) Simple Beam Model vs. FE Analysis (b) Malhotra's Beam Model vs. FE Analysis

Figure 2.5 Comparison of Uplift Displacement-Width Relationships Calculated by Dynamic FE Analysis and Beam Models

Consequently, Malhotra's beam model was selected for the development of rocking response analysis in the present study, because the model was found to be superior to other methods in ease of calculating the uplift displacement-width relationship considering the membrane force.

2.3 Rotational Inertia Force of Content Liquid

The equation of motion for tank rocking motion may be mainly composed of a moment of inertia term, a restoring moment term, and an overturning moment term (see Figure 2.6). However, the earlier investigators have not taken into account the rotational inertia force (e.g. [4-6]).

In this section, contribution of moment of inertia of content liquid moving in unison with the tank rocking motion to the rocking response of a liquid storage tank is investigated using the results of dynamic FE analysis [7]. Appendix 1 gives details of the dynamic FE analysis used in the current study. However, since it was impossible to obtain the value of the rotational inertia force of content liquid directly from the dynamic FE analysis, the validation was carried out with angular acceleration of the tank in rock.

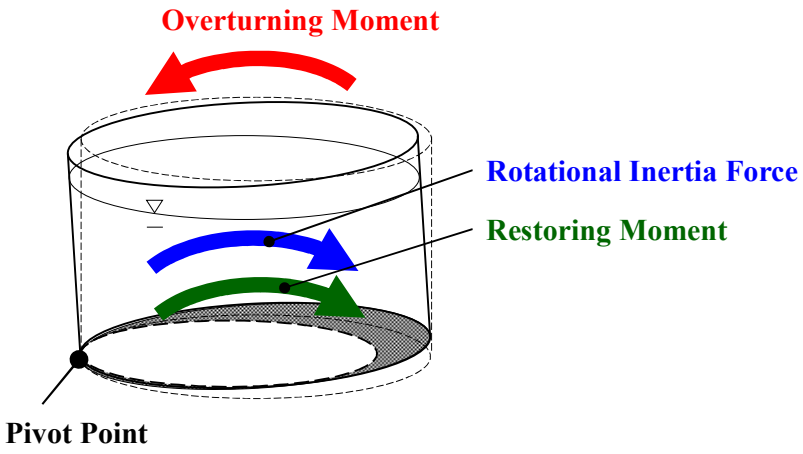

Figure 2.6 Main Components of Tank Rocking Motion Considered

As a preparation for this investigation, a method to estimate the restoring moment indirectly using the uplift width obtained by the dynamic FE analysis is developed in the first subsection.

2.3.1 Method to Estimate Restoring Moment Generated by Uplifting of Bottom Plate

The restoring moment may be determined by the areal extent of uplift of the bottom plate and the hydraulic pressure acting on it. In order to obtain the restoring moment analytically, it is convenient to assume the uplifting area to have a crescent shape as shown in Figure 2.7. This assumption leads the distributions of uplift and contact widths in the circumferential direction. Equations of the width of the uplifted region of the bottom plate $L(\varphi)$ at an arbitrary point with respect to φ (uplift width), the width of the contact region of the bottom plate $r(\varphi)$ at an arbitrary point with respect to φ (contact width) and the length of the moment arm $l(\varphi)$ from the pivot point to an arbitrary point with respect to φ are as follows:

$$L(\varphi) = R - r(\varphi) \qquad (\varphi \neq 0, \pi) \tag{2.1}$$

$$r(\varphi) = \frac{a}{\sin\varphi} \sin\left[\varphi - \sin^{-1}\left\{\frac{(R-a)\sin\varphi}{a}\right\}\right] \quad (\varphi \neq 0, \pi) \tag{2.2}$$

$$l(\varphi) = (1 + \cos\varphi)R \tag{2.3}$$

where R is the tank radius; a is the radius of the circular contact region of the tank bottom plate; and φ is the angle formed by the horizontal center line of the bottom plate and the line connecting the center of the bottom plate and the corner joint. Appendix 2 gives its derivation process. When $\varphi = 0$ or $\varphi = \pi$, the uplift width $L(\varphi)$ and the contact width $r(\varphi)$ in Eqs. (2.1) and (2.2) are the indeterminate form. The limit of this indeterminate form is obtained by using L'Hôpital's rule as follows.

$$r(0) = 2a - R, \quad L(0) = 2(R - a) \tag{2.4a}$$

$$r(\pi) = R, \qquad L(\pi) = 0 \tag{2.4b}$$

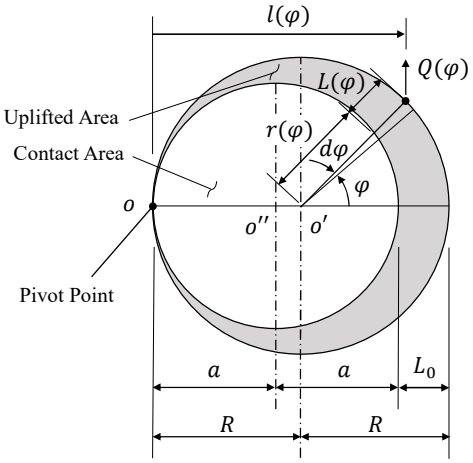

Figure 2.7 Assumed Shape of Uplifted Area of Bottom Plate

The distribution of the uplift width $L(\varphi)$ can be converted to the distribution of the vertical force $Q(\varphi)$ at the uplifted end of the bottom plate at an arbitrary point with respect to φ (uplift resistant force) by using the relationship between resistant force and uplift width shown in Figure 2.8 (b). The resistant force-uplift width relationship was calculated by Malhotra's beam model (see Figure 2.8 (a) and Appendix 3) [8]. By giving the hydraulic pressure p acting on the beam model and the mechanical properties of the beam to the beam model, the relationship between the uplift width $L(\varphi)$ and the uplift resistant force $Q(\varphi)$ are uniquely determined.

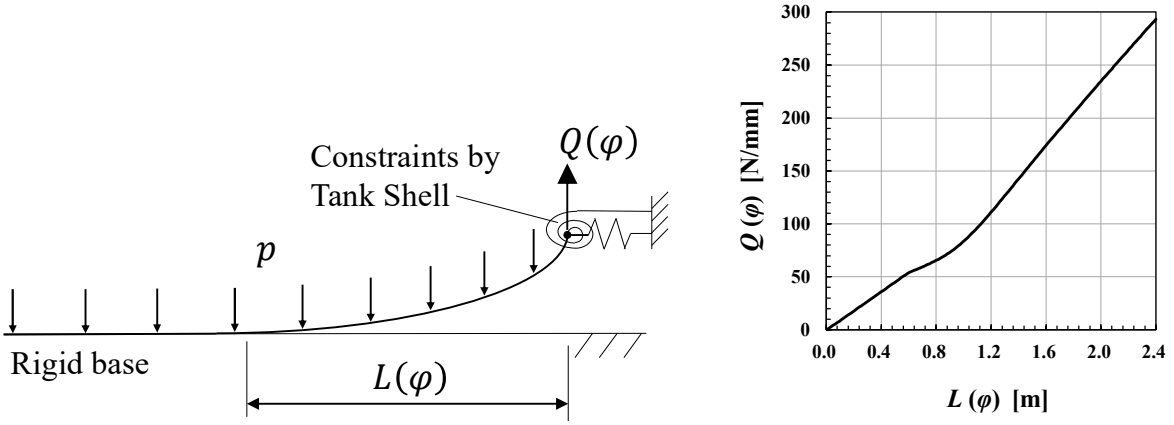

(a) (b)

Figure 2.8 (a) Beam Model (Malhotra and Veletsos, 1994) [8], and (b) Example of Relationship between Resistant Force and Uplift Width Calculated by Malhotra's Beam Model (Static pressure is considered.)

The relationship between the uplift width $L(\varphi)$ and the resistant force $Q(\varphi)$ cannot be obtained as an explicit closed form solution. To simplify the integration and other complexities, an approximate expression (6th order) obtained by the least squares method is used herein (see Figure 2.9).

$$Q(\varphi) = C_6[L(\varphi)]^6 + C_5[L(\varphi)]^5 + C_4[L(\varphi)]^4 + C_3[L(\varphi)]^3 + C_2[L(\varphi)]^2 + C_1[L(\varphi)] \tag{2.5a}$$

$$\begin{aligned} C_1 &= \ \ 8.8175 \times 10^1 \\ C_2 &= \ \ 6.3522 \times 10^1 \\ C_3 &= -2.4765 \times 10^2 \\ C_4 &= \ \ 2.9150 \times 10^2 \\ C_5 &= -1.2960 \times 10^2 \\ C_6 &= \ \ 1.9835 \times 10^1 \end{aligned} \tag{2.5b}$$

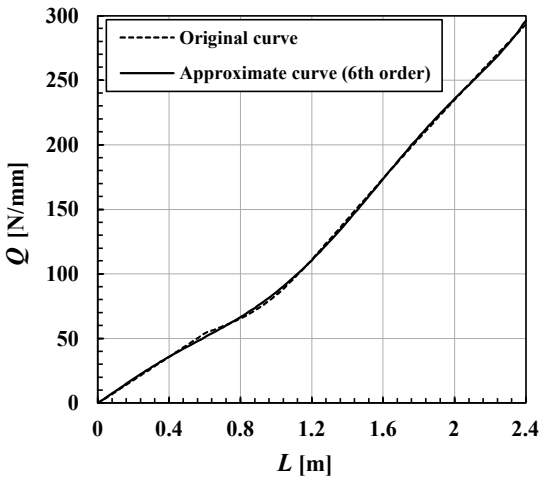

Figure 2.9 Approximate Curve of Uplift Force-Width Relationship Shown in Figure 2.8 (b)

Based on the above, the restoring moment M_{re} is obtained as

$$M_{\mathrm{re}} = 2\int_0^{\pi} Q(\varphi) l(\varphi) R d\varphi + m_s g R \tag{2.6}$$

where m_s is the sum of the masses of the tank shell and the appurtenance, and g is the gravitational acceleration, respectively. The first term of Eq. (2.6) is the restoring moment due to the distribution of the uplift resistant force, while the second term is the restoring moment due to the mass of the tank.

The procedure for estimating the restoring moment M_{re} is summarized in Figure 2.10. By extracting the uplift width L_0 from the result of dynamic FE analysis, the restoring moment M_{re} can be easily estimated by the proposed calculation procedure.

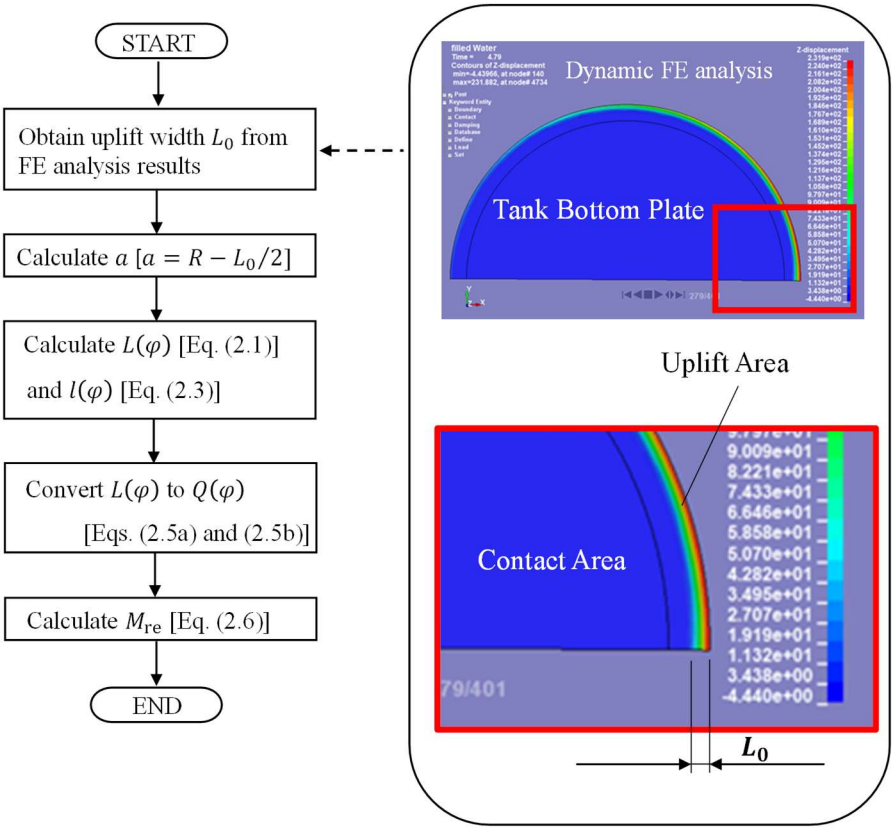

Figure 2.10 Calculation Procedure of Restoring Moment M_{re}

2.3.2 Comparison of Restoring Moment and Overturning Moment

The overturning moment M_{ov} and the restoring moment M_{re} estimated from the results of dynamic FE analysis were compared to examine the balance of rotational forces. The overturning moment M_{ov} is calculated by Housner's theory as follows.

$$M_{\mathrm{ov}} = \alpha(t)\, m_{\mathrm{I}}\, h_{\mathrm{I}} \tag{2.7}$$

$$m_{\mathrm{I}} = \frac{\tanh\sqrt{3}\frac{R}{h}}{\sqrt{3}\frac{R}{h}}\, m \qquad (\text{when } D/H \leq 0.75) \tag{2.8a}$$

$$h_{\mathrm{I}} = \frac{3}{8}\, h \qquad (\text{when } D/H \leq 0.75) \tag{2.8b}$$

where $\alpha(t)$ is the translational response acceleration of the tank which is equal to the ground acceleration due to the assumption of a rigid tank shell; m_{I} is the effective mass of content liquid for translational motion; m is the total mass of content liquid; h_{I} is the height of the centroid of m_{I} from the base; and h is the liquid height. Since the overturning moment due to the sloshing response is considered to be sufficiently smaller than that due to the impulsive response, the overturning moment due to sloshing is ignored. Since the shell of the tank model of the FE analysis is modeled as a rigid body, it is assumed that $\alpha(t)$ is equal to the ground acceleration.

The overturning moment and restoring moment during the first uplift of the tank bottom were calculated and compared with each other. Figure 2.11 shows the time histories of the uplift displacement of the right edge of the tank bottom plate and the ground acceleration. Table 2.1 compares the overturning moment M_{ov} and the restoring moment M_{re}. At 2.20 seconds, the ground acceleration was at its peak, and the tank bottom was in a state immediately after the start of uplift. Since the ratio of the restoring moment to the overturning moment was only about 0.151, the restoring moment conventionally considered by Eq. (2.6) was clearly insufficient to resist the rotation. In addition, the uplift displacement continued to increase even after the direction of ground acceleration was reversed

at around 2.28 seconds. These results suggest that rotational inertia works in the tank rocking motion.

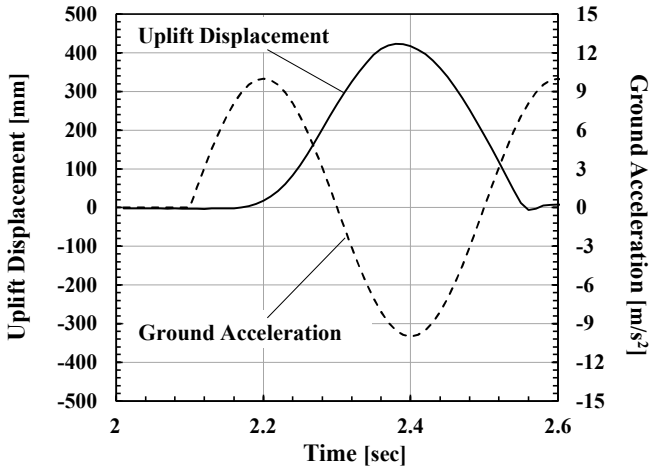

Figure 2.11 Time Histories of Uplift Displacement and Ground Acceleration Computed by Dynamic FE Analysis [Appendix 1]

Table 2.1 Comparison between Restoring Moment and Overturning Moment

t [sec]	Ground Acc. [m/s]	L_0[m]	M_{re} [$\times 10^9$ N·m]	M_{ov}[$\times 10^9$N·m]	M_{re} / M_{ov}
2.20	10.0	0.63	0.278	1.839	0.151

2.3.3 Confirmation of Effectiveness of Rotational Inertia Force of Content Liquid

A comparison was made between the angular acceleration of the tank rocking motion obtained from the dynamic FE analysis and that obtained from the simplified equation of motion in the rotational direction considering the effective moment of inertia of content liquid. Since time history of the angular acceleration $\ddot{\theta}(t)$ of tank rocking motion could not be directly extracted from the results of the dynamic FE analysis, it was obtained indirectly as a quotient of the time history of the vertical acceleration $\ddot{z}(t)$ at the edge of the tank bottom by the tank diameter D.

$$\ddot{\theta}(t) = \ddot{z}(t)/D \tag{2.9}$$

Meanwhile, the angular acceleration of tank rocking motion obtained from the equation of motion was evaluated by Eq. (2.10a) or (2.10b). The direction of the action of the restoring moment M_{re} changes depending on the position of the pivot of tank rocking motion. Therefore, the evaluation formula of the angular acceleration was divided according to the position of the pivot of rocking motion as follows.

i) When the right edge of the tank bottom is uplifting:

$$\ddot{\theta} = (M_{\mathrm{ov}} - M_{\mathrm{re}})/(I_{\mathrm{eff}} + I_{\mathrm{s}}) \tag{2.10a}$$

ii) When the left edge of the tank bottom is uplifting:

$$\ddot{\theta} = (M_{\mathrm{ov}} + M_{\mathrm{re}})/(I_{\mathrm{eff}} + I_{\mathrm{s}}) \tag{2.10b}$$

where I_{s} is the moment of inertia of the tank shell, and I_{eff} represents the effective moment of inertia of content liquid around the pivot point of tank rocking motion, respectively. I_{eff} is evaluated by the following equation.

$$I_{\mathrm{eff}} = I_r + m_r R_r^2 \tag{2.11}$$

in which

$$I_r = s \cdot I \tag{2.12a}$$

$$m_r = f_r \cdot m \tag{2.12b}$$

$$R_r = \sqrt{\left(d_{r,x} \cdot D\right)^2 + \left(d_{r,\mathrm{z}} \cdot H\right)^2} \tag{2.12c}$$

where I_{r} is the moment of inertia of m_r around the centroid; m_{r} is the effective mass of content liquid for rocking motion; R_{r} is the distance between the pivot point of tank rocking motion and the centroid of m_r; I is the moment of inertia around the centroid when the content liquid is regarded as

a rigid cylinder; m is the total mass of content liquid; D is the tank diameter; and H is the liquid height. Each coefficient for obtaining these physical quantities has been studied and the curves which decide the coefficients depicted by Taniguchi and Katayama (2016) [9] (see Figures 2.12 (a) to (d)). The coefficients in the current study were obtained by using their diagram. These coefficients change according to the uplift ratio δ (= uplift width L_0/tank diameter D).

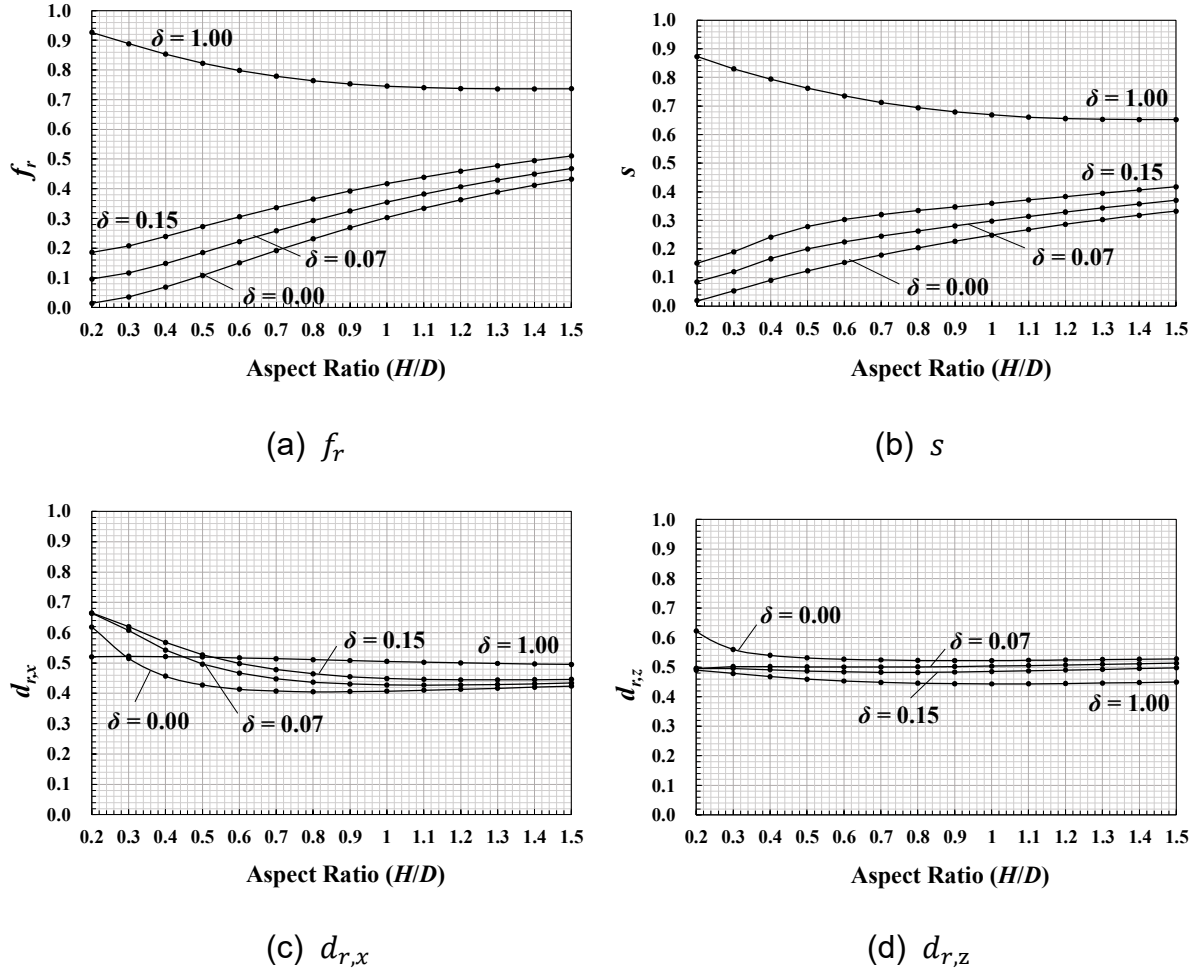

Figure 2.12 Coefficients for Determining Physical Quantities for Tank Rocking Motion [9]

Simplified Equation of Motion

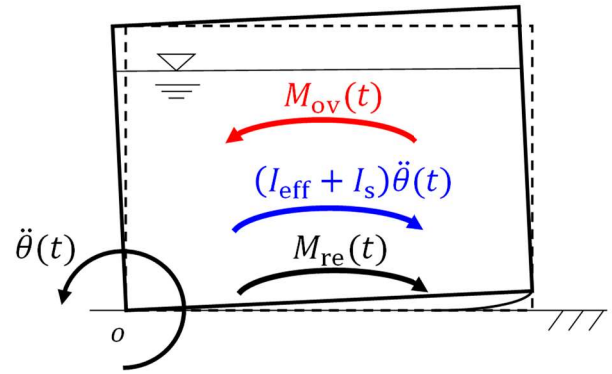

Overturning Moment $M_{ov}(t)$

− Restoring Moment $M_{re}(t)$

= Moment required for equilibrium

It is assumed that the moment required for equilibrium is rotational inertia force of content liquid.

Angular acceleration required for equilibrium $\ddot{\theta}(t)$

$$\ddot{\theta}(t) = (M_{ov}(t) - M_{re}(t))/(I_{eff} + I_s) \qquad (2.10a)$$

Dynamic FE Analysis

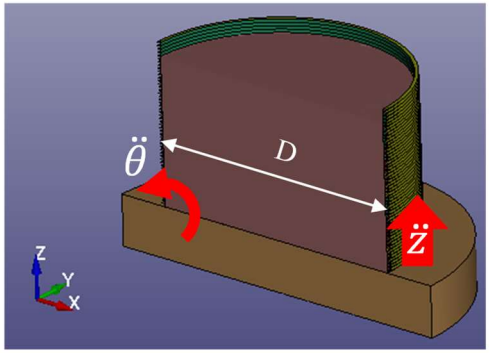

Angular acceleration converted from vertical acceleration

$$\ddot{\theta}(t) = \ddot{z}(t)/D \qquad (2.9)$$

Comparison

Figure 2.13 Outline of Comparison of Angular Acceleration between Equation of Motion and Dynamic FE Analysis

The comparison of the angular acceleration calculated by the simplified equation of motion and that obtained from the dynamic FE analysis is schematically shown in Figure 2.13. The angular acceleration examined in this study is that of the tank in rock at five selected time points as shown in Table 2.2.

Table 2.2 Selected Time Points for Examination of Angular Acceleration

t [sec]	Remarks
2.20	Ground acceleration is maximum on the positive side.
2.30	Ground acceleration is zero.
2.38	Uplift displacement is maximum.
2.40	Ground acceleration is maximum on the negative side.
2.50	Ground acceleration is zero.

The result of the comparison is shown in Figure 2.14. From this figure, it can be seen that the results of calculation by the two methods agree well.

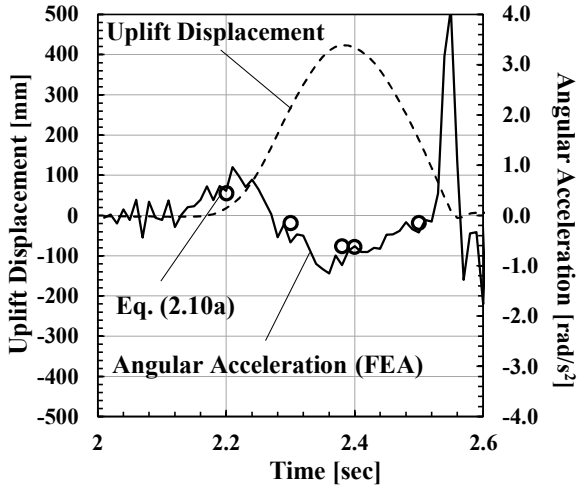

Figure 2.14 Result of Comparison of Angular Accelerations Calculated by Simplified Equation of Motion and Dynamic FE Analysis

Moreover, to confirm the effectiveness of the rotational inertia force of content liquid on tank rocking motion, three case studies were conducted. In Case 1, the restoring moment M_{re} is ignored in the calculation of the angular acceleration by Eq. (2.10a). Case 2 ignores the moment of inertia I_{s}, in addition to the condition of Case 1. Meanwhile, in Case 3, I_{eff} is ignored in the calculation of the angular acceleration by Eq. (2.10a).

Figures 2.15 (a) to (c) show the results of the case studies. Case 1 showed almost the same results as those of the original case, indicating that the restoring moment M_{re} had little effect as rotational resistance. The results of Case 2 showed that the rotational inertia of the tank body was also negligible, which was likely because the mass of tank shell was sufficiently small relative to the total mass of content liquid. On the other hand, the results of Case 3 was significantly different from those of the original case, showing a significant influence of the rotational inertia force of content liquid on the tank rocking response. Consequently, it is concluded that the rotational inertia force of content liquid should not be ignored in the rocking response analysis of a liquid storage tank.

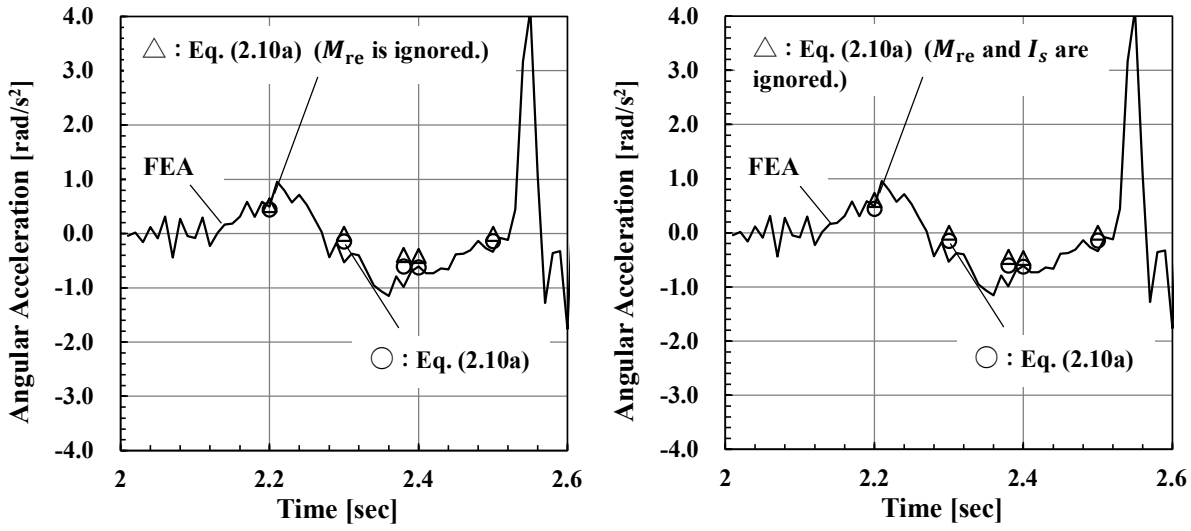

(a) Case 1: M_{re} is ignored

(b) Case 2: M_{re} and I_s are ignored

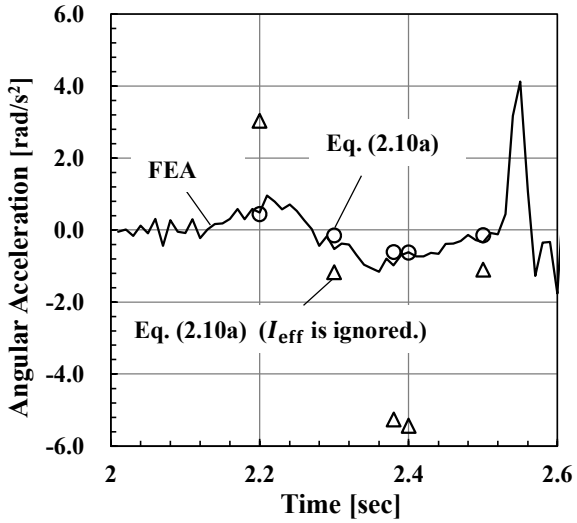

(c) Case 3: I_{eff} is ignored

Figure 2.15 Case Studies for Confirmation of Effectiveness of Rotational Inertia Force of Content Liquid on Tank Rocking Motion

2.4 Experimental Study on Liquid Mass Contributing to Resistance of Uplift Commencement

2.4.1 Objective of The Work

The conventional analytical models assume that the tank bottom plate uplifts when the overturning moment overcomes the resistant moment consisting of dead weight of a side shell (including the fixed roof and the appurtenances) as shown in Figure 2.16 (a). In other words, the conventional uplifting resistance system in tanks does not implicitly expect any contribution of the content liquid to it.

Meanwhile, this study hypothesized that the effective mass of content liquid in the rotational direction would contribute to the resistance of uplift commencement as shown in Figure 2.16 (b). The resistant moment considering the added mass due to content liquid M_{re} is expressed as:

$$M_{\mathrm{re}} = (m_s + m_{\mathrm{roof}}) \cdot g \cdot R + m_r \cdot g \sin\alpha_r \cdot R_r \tag{2.13}$$

in which

$$m_r = f_r \cdot m \tag{2.14a}$$

$$R_r = \sqrt{\left(d_{r,x} \cdot D\right)^2 + \left(d_{r,\mathrm{z}} \cdot H\right)^2} \tag{2.14b}$$

where m_s and m_{roof} are the mass of the tank shell and that of the tank roof, respectively; g is the gravitational acceleration; R is the tank radius; m_r is the effective mass of content liquid in the direction of rotation; α_r is the angle between R_r and the tank shell; R_r is the moment arm of m_r around the pivot point; m is the total mass of content liquid; D is the tank diameter; and H is the height of content liquid. f_r, $d_{r,x}$ and $d_{r,z}$ are the coefficients for calculating m_r and R_r, and these are determined by Figures 2.17 (a) to (c), respectively [9]. Since literature [9] does not describe the effective mass at $\delta(=$ uplift width $L_0/$ tank diameter $D) = 0$, values of the effective mass and its centroid are recalculated herein. In the current study, some shaking table tests were conducted to investigate contribution of content liquid to the resistance of uplift commencement. In addition, accuracy

of the hypothesis of this study was examined.

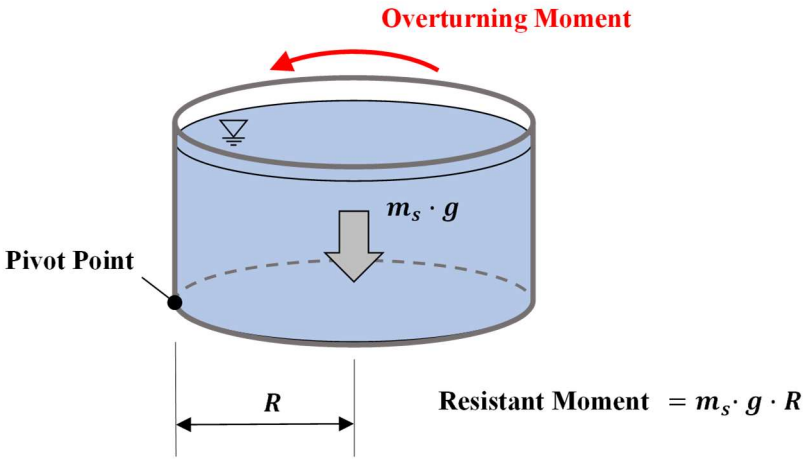

(a) Conventional Idea

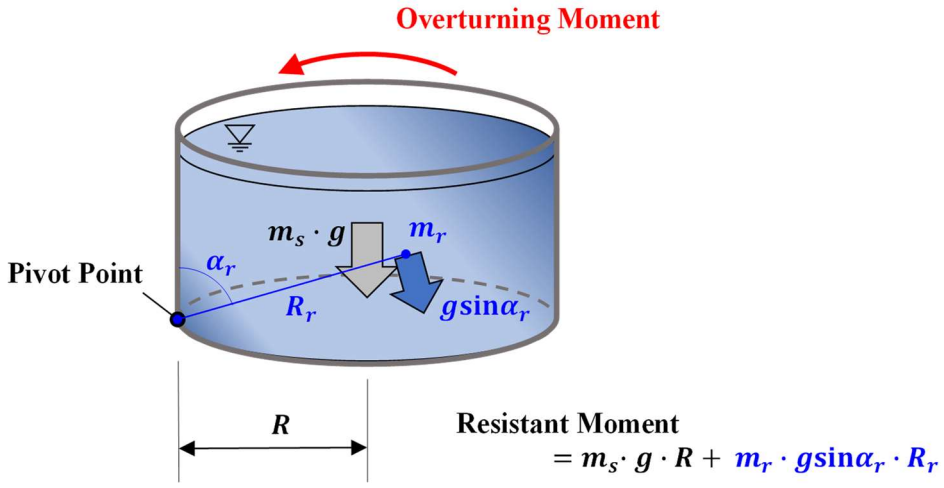

(b) Hypothesis in This Study (Added mass is considered.)

Figure 2.16 Ideas for Liquid Mass Contribution to Uplift Resistance

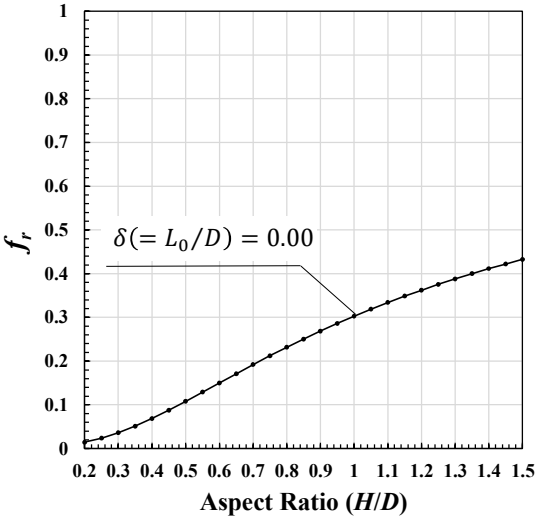

(a)

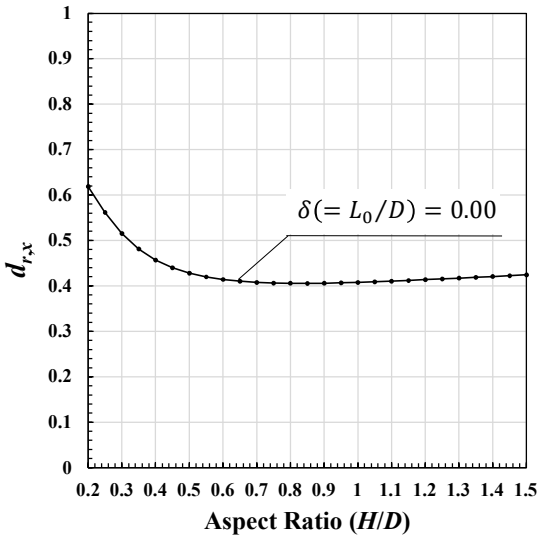

(b)

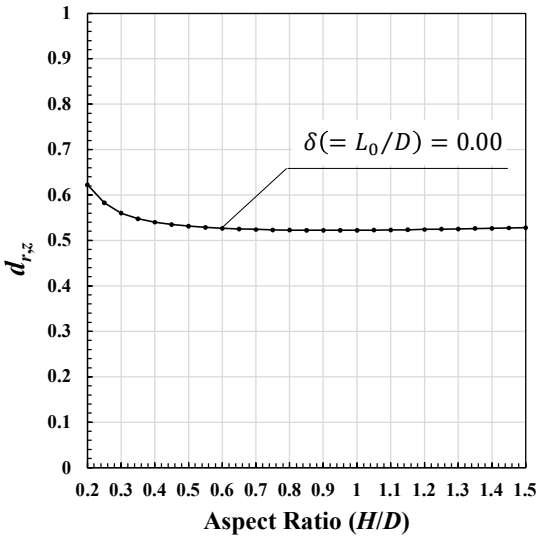

(c)

Figure 2.17 (a) Ratio of Effective Mass of Content Liquid for Rocking Motion to Total Mass of Content Liquid, (b) Ratio of Horizontal Distance toward Centroid of m_r to Diameter of Tank, and (c) Ratio of Vertical Distance toward Centroid of m_r to Height of Content Liquid

2.4.2 Description of Shaking Table Tests

Some shaking table tests were conducted by using a tank model made of polyvinyl chloride (PVC) plate on a shaking table in Tottori University. The physical quantities of the tank model for the shaking table test are shown in Table 2.3, and the specifications of the shaking table are shown in Table 2.4. Water (with an assumed density of 1000 kg/m^3) was used as the content liquid in this experimental test.

Table 2.3 Physical Quantities of Tank Model for Shaking Table Test

Diameter of Tank Model [cm]	85
Height of Tank Model [cm]	40
Depth of Content Liquid [cm]	21.3, 25.5, 29.8, 34.0
Thickness of Tank Shell [mm]	0.5
Thickness of Bottom Plate [mm]	0.5
Thickness of Stiffeners [mm]	0.5
Width of Stiffeners [mm]	30
Number of Stiffeners	12
Mass of Tank Model (Shell and Stiffeners (PVC*)) [kg]	1.5
Mass of Cover Plate [kg]	0.870

* PVC: polyvinyl chloride

Table 2.4 Specifications of Shaking Table

Manufacturer	San-Esu Co., Ltd.
Model Number	SPTD-12K-85L-30T
Installation Location	Tottori University
Table Size [m × m]	1.2 × 1.2
Maximum Displacement [mm$^{p\text{-}p}$]	400
Maximum Mass of Load [kg]	3000
Direction of Excitation, Number	Horizontal, One

Figure 2.18 shows a view of the shaking table test. The tank is equipped with multi-stage stiffeners to prevent out-of-round deformation of the tank shell and a cover plate at the top of the tank shell to prevent splash of content liquid (see Figure 2.19). A stand is installed between the tank model and the shaking table to install laser displacement transducers beneath the tank bottom plate. The laser displacement transducers measure vertical displacement of the tank bottom plate.

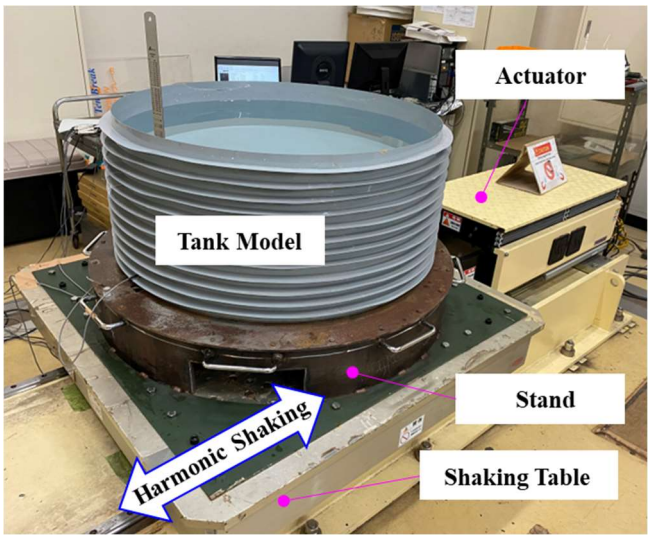

Figure 2.18 View of Shaking Table Test

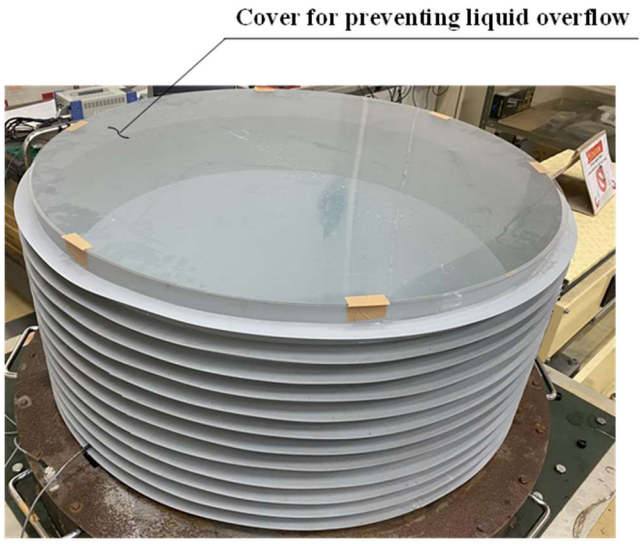

Figure 2.19 Cover Plate for Preventing Liquid Overflow

Furthermore, two accelerometers are installed to measure the uplift of the tank bottom, the other accelerometer is placed to measure the movement of the shaking table, and three laser displacement transducers are also attached for the measurement. The locations of these sensors are shown in Figure 2.20, and their additional information is shown in Table 2.5. The sampling frequency of all sensors is 1000 Hz.

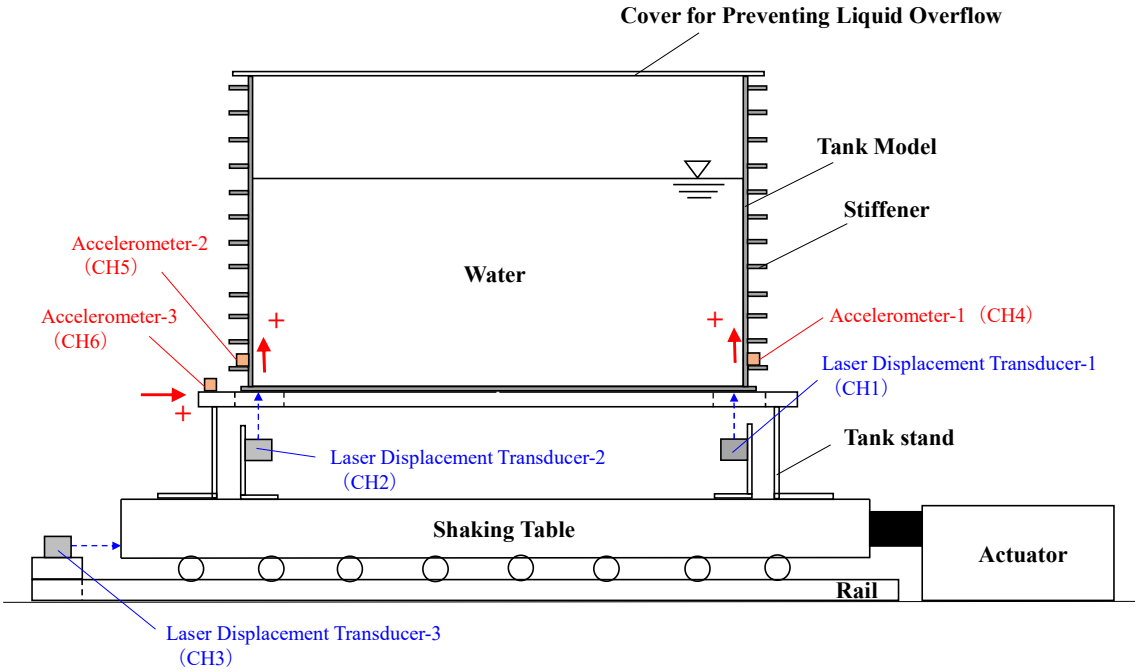

Figure 2.20 Locations of Accelerometers and Laser Displacement Transducers

Table 2.5 Additional Information of Sensors

CH	Sensor	Remarks
1	Laser Displacement Transducer-1	Uplift Displacement of Right Bottom Edge
2	Laser Displacement Transducer-2	Uplift Displacement of Left Bottom Edge
3	Laser Displacement Transducer-3	Horizontal Displacement of Shaking Table
4	Accelerometer-1	Uplift Acceleration of Right Bottom Edge
5	Accelerometer-2	Uplift Acceleration of Left Bottom Edge
6	Accelerometer-3	Horizontal Acceleration of Shaking Table

In the shaking table test, a series of sinusoidal waves as shown in Figure 2.21 were input as the base acceleration. Its driving frequency f_D was set to 6.0 Hz ($T_D = 0.167$ sec) not to excite sloshing response (a range of the sloshing fundamental natural frequency under the experimental conditions: 0.9 to 1.0 Hz) and the amplitude of the driving acceleration A was 0.1 G to 0.6 G. The amplitude of the driving acceleration was increased step by step until uplift of the tank bottom was observed.

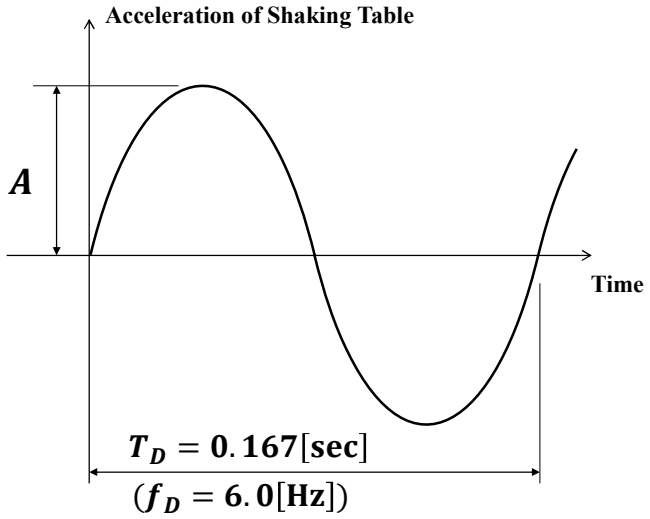

Figure 2.21 Driving Harmonic Acceleration for Shaking Table Test

Unfortunately, the commencement of tank bottom uplift cannot be determined with the laser displacement transducers alone. Since the initial downward deflection of the bottom plate occurs at the slits for the sensors made in the tank stand (see Figure 2.22), an upward displacement recorded by the sensors does not necessarily indicate an uplift of the tank bottom plate. Therefore, impact from landing of the tank bottom is used to judge uplift of the tank bottom. As shown in Figure 2.23, the landing impact can be identified from the time history of the accelerometers. The horizontal base acceleration required for the tank bottom to start uplifting was determined from the records of the vertical displacement and horizontal acceleration of the shaking table. The detailed method is shown in the latter part of Appendix 4.

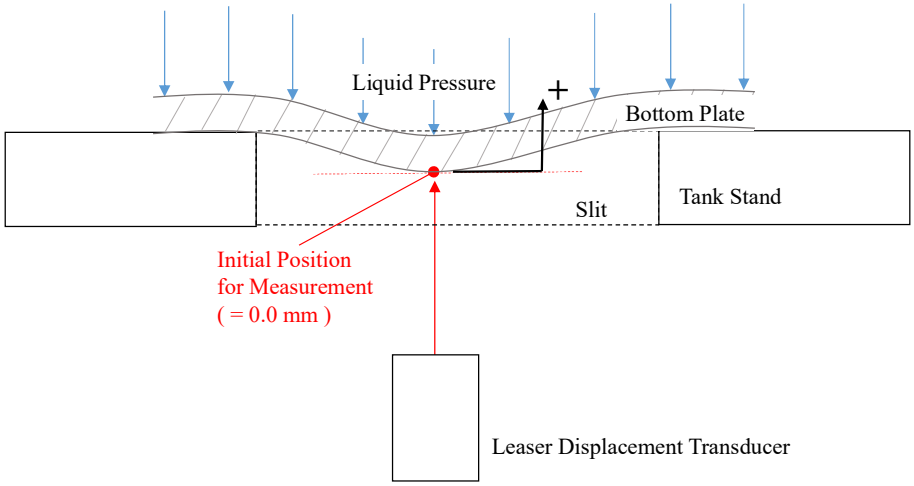

Figure 2.22 Situation of Initial Downward Deflection due to Slit

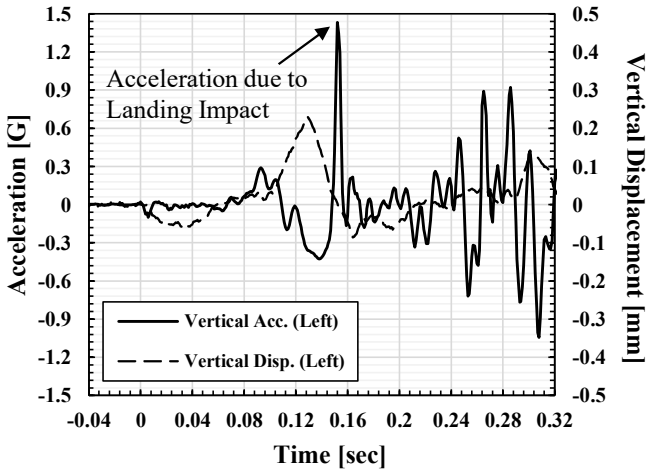

Figure 2.23 Typical Time History of Uplift Displacement and Vertical Acceleration with Tank Model Uplifting (e.g., $H/D = 0.35,\ A = 0.4$ G)

2.4.3 Results and Discussion

Experimental results are summarized in Table 2.6. The results of the shaking table tests for each experimental condition are shown in Appendix 4.

Table 2.6 Required Acceleration for Uplifting (Results of Shaking Table Tests) [G]

		Aspect ratio H/D			
		0.25	**0.30**	**0.35**	**0.40**
Amplitude of Base Acceleration A [G]	**0.1**	Not Conducted	Not Conducted	Not Conducted	No Uplift
	0.2	No Uplift	No Uplift	No Uplift	No Uplift
	0.3	No Uplift	No Uplift	0.242	0.214
	0.4	No Uplift	0.365	0.350	0.268
	0.5	0.436	0.307	0.243	0.294
	0.6	0.421	0.317	0.284	Not Conducted
Average		**0.43**	**0.33**	**0.28**	**0.26**

From the conventional idea of the uplift resistance and the hypothesis of the added mass to that (see Eq. (2.13)), the horizontal accelerations required for the tank bottom to start uplifting α_{req} and α'_{req} are expressed as follows, respectively.

From the conventional idea:

$$\alpha_{req} = \frac{(m_s + m_{\mathrm{roof}}) \cdot g \cdot R}{m_I h_I + m_s \cdot \frac{H_s}{2} + m_{\mathrm{roof}} \cdot H_s} \tag{2.15}$$

From the hypothesis in this study (with the added mass considered):

$$\alpha'_{req} = \frac{(m_s + m_{\mathrm{roof}}) \cdot g \cdot R + m_r \cdot g \sin\alpha_r \cdot R_r}{m_I h_I + m_s \cdot \frac{H_s}{2} + m_{\mathrm{roof}} \cdot H_s} \tag{2.16}$$

where H_s is the height of the tank shell.

Finally, Figure 2.24 compares the results of the experimental test and those by the estimation formulas. The comparison results showed the followings.

- The comparison between the experimental results and the results from Eq. (2.15) confirmed the presence of the additional mass of content liquid contributing to the uplift resistance. In addition, the ratio of the added mass to the total uplift resistance increased with the increase of the aspect ratio.

- The comparison between the experimental results and the results from Eq. (2.16) showed that Eq. (2.16) overestimated the required horizontal acceleration to almost two times experimental results. The entire effective rocking mass of content liquid may not contribute to the resistance of uplift commencement. Further research is necessary to correctly estimate the uplift commencement condition.

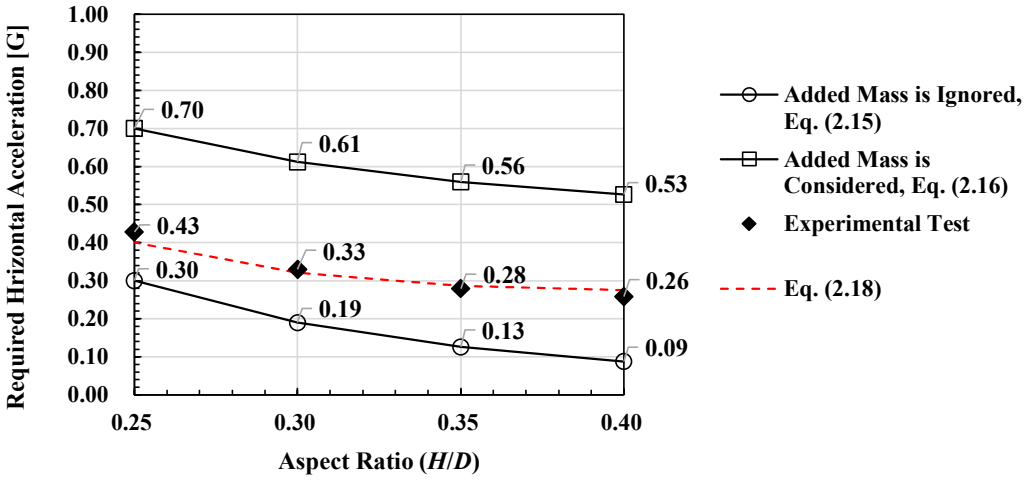

Figure 2.24 Comparison between Experimental Results and Results from Estimation Formulas

Based on the aforementioned discussion, the rest of this subsection tries to modify Eqs. (2.15) and (2.16). First, find a correction factor for the conventional idea given by Eq. (2.15) to fit the experimental results. This way implicitly assumes existence of the mass of content liquid contributing

to the uplift commencement condition, but it does not try to quantify it. The revised uplift commencement condition can be expressed as follows.

$$M_{\mathrm{OV}} > \gamma(m_s + m_{\mathrm{roof}}) \cdot g \cdot R \tag{2.17}$$

where M_{OV} is the overturning moment; and γ is the resistant moment correction factor which is the ratio of the experimental value of the acceleration required for the tank bottom to start uplifting $\alpha_{req,e}$ and the required acceleration calculated by the conventional method of the uplift commencement condition α_{req}, as summarized in Table 2.7.

Table 2.7 Correction Factor for Resistant Moment

	Aspect Ratio *H*/*D*			
	0.25	0.30	0.35	0.40
$\alpha_{req,e}$	0.43	0.33	0.28	0.26
α_{req}	0.30	0.19	0.13	0.09
$\gamma = \alpha_{req,e}/\alpha_{req}$	1.43	1.74	2.15	2.89

The following way explicitly assumes the values of the mass of content liquid contributing to the uplift commencement condition. However, to fit it to the experimental results, its extent of contribution to the uplift commencement condition is modified by multiplying $\cos\alpha_r$ without consideration of mechanical background (see the red dotted line of Figure 2.24 and Eq. (2.18)). The revised uplift commencement condition is expressed as Eq. (2.19).

$$\alpha'_{req} = \frac{(m_s + m_{\mathrm{roof}}) \cdot g \cdot R + m_r \cos\alpha_r \cdot g \sin\alpha_r \cdot R_r}{m_l h_l + m_s \cdot \frac{H_s}{2} + m_{\mathrm{roof}} \cdot H_s} \tag{2.18}$$

$$M_{\mathrm{OV}} > (m_s + m_{\mathrm{roof}}) \cdot g \cdot R + m_r \cos\alpha_r \cdot g \sin\alpha_r \cdot R_r \tag{2.19}$$

2.5 Conclusions

The research results introduced in Chapter 2 are summarized below.

Selection of A Suitable Method for Describing Uplift Displacement-Width Relationship

By comparing the uplift displacement and the uplift width obtained from the results of the dynamic FE analysis and those obtained by several beam models, it was shown that the simple beam model could be used to calculate the uplift displacement-width relationship when the uplift displacement was small (e.g., $w/H \leq 0.005$). However, when the uplift displacement was large (e.g., $w/H > 0.005$), accurate determination of its relationship with the uplift width could be made by considering the geometric nonlinearity of the beam and the reduction of fluid pressure acting on the tank bottom plate due to dynamic pressure.

Rotational Inertia Force of Content Liquid

From the results of the dynamic FE analysis, significant contribution of the rotational inertia force of the content liquid to the tank rocking motion was confirmed. On the other hand, the restoring moment composed by the circumferential distribution of vertical reaction force at the shell-to-bottom connection could not adequately resist the overturning moment.

Experimental Study on Uplift Commencement Condition

Using a scaled model tank made of PVC on a shaking table, the horizontal base acceleration required for the commencement of tank uplift was examined. The test results revealed the presence of added mass as a contributing factor to the uplift commencement condition. Further study is needed to quantify the mass mathematically.

Bibliography

[1] Yoshida, Y., Taniguchi, T. and Nakashima, T., 2020, “Uplift Deformation of The Bottom Plate of The Cylindrical Shell Tanks Under Steady-State Response of Tank Rocking Motion,” Proc. ASME PVP Conference, Seismic Engineering, Paper No. PVP2020-21418.

[2] Yoshida, Y., Taniguchi, T. and Nakashima, T., 2021, “Verification of Accuracy of The Beam Model and Resistant Moment Generated by Base Uplifting of Flat-Bottom Cylindrical Shell Tanks,” Proc. ASME PVP Conference, Seismic Engineering, Paper No. PVP2021-61319.

[3] Nakashima, T., Ando, Y. and Taniguchi, T., 2008, “A Basic Study of Applicability of Explicit FE-Analyses to Uplift Motion of Flat-Bottom Cylindrical Shell Tanks,” Journal of Applied Mechanics, Vol. 11, pp. 1047-1054.

[4] Clough, D. P., 1977, “Experimental Evaluation of Seismic Design Methods for Broad Cylindrical Tanks,” Univ. of California, EERC Rep., UCB/EERC-77/10.

[5] Malhotra, P. K. and Veletsos, A. S., 1994, “Uplifting Response of Unanchored Liquid-Storage Tanks,” J. Struct. Div., ASCE, Vol. 120, Issue 12, pp. 3525–3547.

[6] European Committee for Standardization (2006), “Silos, Tanks and Pipelines,” Eurocode 8, Part 4, CEN/TC 250, EN 1998-4, Brussels.

[7] Yoshida, Y., Taniguchi, T. and Nakashima, T., 2021, “A Study on Restoration Mechanism in Rocking Behavior of Flat-Bottom Cylindrical Storage Tank During Earthquake,” Proc. Dynamics and Design Conference, JSME, Paper No. 222. (in Japanese)

[8] Malhotra, P. K. and Veletsos, A. S., 1994, “Beam Model for Base Uplifting Analysis of Cylindrical Tanks,” J. Struct. Div., ASCE, Vol.120, Issue12, pp. 3471-3488.

[9] Taniguchi, T. and Katayama, Y., 2016, “Masses of Fluid for Cylindrical Tanks in Rock with Partial Uplift of Bottom Plate,” Journal of Pressure Vessel Technologies, ASME, doi: 10.1115/1.4032784.

Chapter 3

Dynamic Response Analysis of Tank Rocking Motion

Chapter 3

Dynamic Response Analysis of Tank Rocking Motion

3.1 Introduction

The purpose of this chapter is to develop the method of time history analysis of tank rocking motion. Chapter 2 reveals that several physical quantities that have not been considered in earlier investigations contribute to the tank rocking motion. This implies the necessity of developing a new mechanical model which includes their actions adequately. The equations of motion of the mechanical model of a liquid storage tank are derived in the same way as for Taniguchi model [1].

First, equations of motion for a two-degree-of-freedom (2DOF) system with degrees of freedom in the translational and rotational directions are derived. The reason for considering the 2DOF model is to introduce physical quantities of tank rocking motion into a conventionally used SDOF system by modeling the translational response of a liquid storage tank. Next, the computational method of the equations of motion for the 2DOF model is described, and the accuracy of the method is verified by comparison with experimental test results. Finally, equations of motion for a mechanical model of a liquid storage tank are derived based on the analogy between the 2DOF model and the tank in rock. The quantities of the 2DOF model are replaced with the effective quantities of content liquid for tank rocking motion in the same way as in Taniguchi model. Then the computational method of the equations of motion for the mechanical model of liquid storage tank is explained.

Due to the difficulty of evaluating the physical quantities related to tank rocking motion which changes according to the extent of uplift width of the tank bottom plate, the time history analysis has not been conducted with Taniguchi model. This study attempts to solve the equations of motion by using the uplift displacement-width relationship obtained from Malhotra's beam model verified in chapter 2. For convenience, the uplift displacement-width relationship is converted to a rocking angle-uplift ratio

relationship in this study. The rocking angle θ is defined as a quotient of the uplift displacement w and the tank diameter D, and the uplift ratio δ is defined as a quotient of the uplift width L and the tank diameter D. By using this relationship, the uplift ratio δ is evaluated from the response of rocking angle θ, and the physical quantities related to the tank rocking motion (i.e. effective mass for rocking motion) are evaluated by using the uplift ratio δ and the diagrams proposed by Taniguchi and Katayama [6].

3.2 Definition of 2DOF Model and Its Validation

3.2.1 Equations of Motion for 2DOF Model

In preparation for deriving the equations of motion of tank rocking motion, a 2DOF system with degrees of freedom in the translational and rotational directions as shown in Figure 3.1 is considered in this section. It was assumed that the 2DOF model was subjected to the uniaxial horizontal ground motion. The equations of motion of this model have already been derived from Lagrange's equation of motion by D'Amico et al. [1]. However, since the equations of motion for the pivot point o' at the right bottom edge of the 2DOF model did not follow the right-handed system, they were re-derived in this work. The re-derived equations of motion allow to unify the sign of the rocking angle and the moments. In the 2DOF model, the counterclockwise rotation is positive. Before a tank starts rocking, equation of motion for the translational motion is conventionally written as

$$m_1\ddot{x}_1 + c_1\dot{x}_1 + k_1x_1 = -m_1\ddot{z}_H \tag{3.1}$$

where m_1, c_1 and k_1 are the upper mass, damping coefficient and spring constant of the 2DOF model, respectively; x_1 is the translational response displacement of m_1; and $\ddot{z}_H$ is the horizontal ground acceleration.

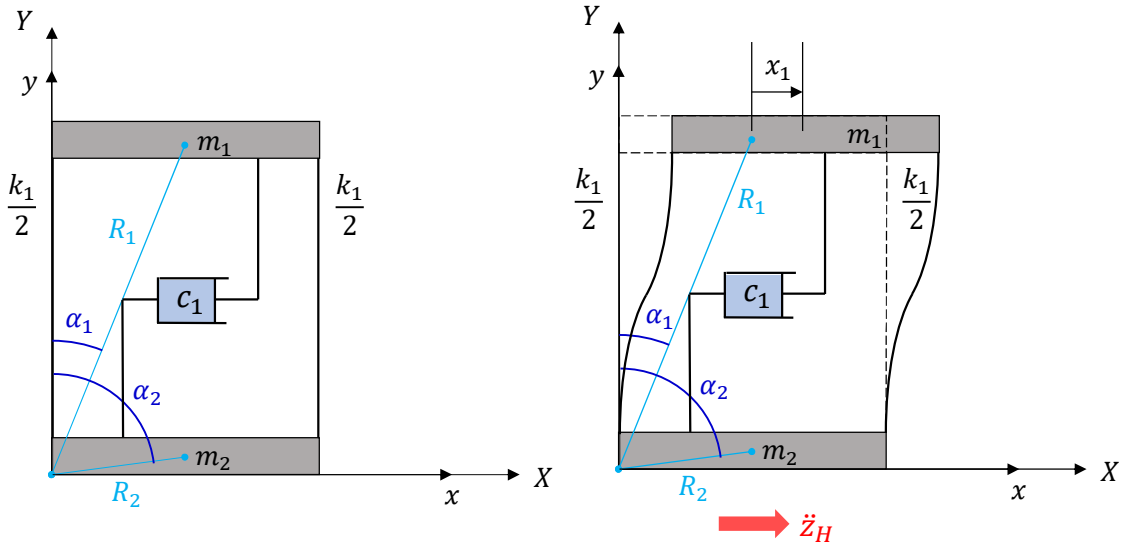

(a) Rest

(b) Translational Motion

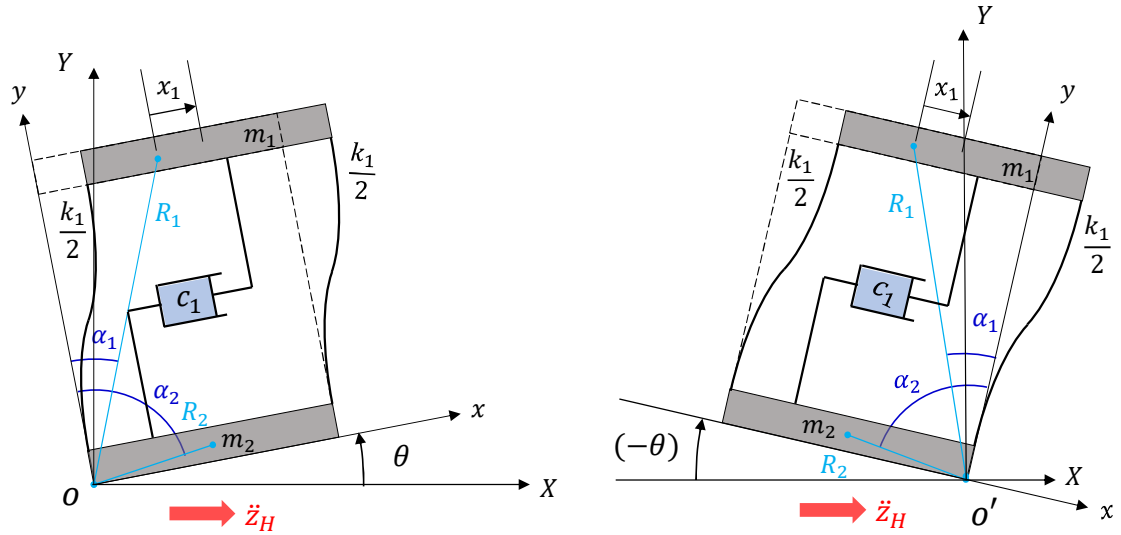

(c) Rocking-Translation Interaction Motion

Figure 3.1 2DOF Model Considered

Equation (3.2a) gives Lagrangian $\mathcal{L}$ of the 2DOF model, while Eqs. (3.3a) and (3.3b) are re-derived as equations of motion in the translational and rocking directions that include the rocking-translation interaction motion.

$$\mathcal{L} = T - V \tag{3.2a}$$

in which

$$\begin{aligned} T = {} & \frac{1}{2}m_1\left(\dot{x}_1^2 + x_1^2\dot{\theta}^2 - 2R_1\dot{x}_1\dot{\theta}\cos\alpha_1 + 2\lambda R_1 x_1\dot{\theta}^2\sin\alpha_1\right) + \frac{1}{2}(I_1 + m_1R_1^2)\dot{\theta}^2 \\ & + \frac{1}{2}(I_2 + m_2R_2^2)\dot{\theta}^2 \end{aligned} \tag{3.2b}$$

$$\begin{aligned} V = {} & -m_1g[R_1\cos(\alpha_1 - \lambda\theta) + x_1\sin\theta - R_1\cos\alpha_1] \\ & -m_2g[R_2\cos(\alpha_2 - \lambda\theta) - R_2\cos\alpha_2] \\ & -\frac{1}{2}k_1x_1^2 \end{aligned} \tag{3.2c}$$

where T and V are the kinetic energy and potential energy of the 2DOF system, respectively; θ is the rocking angle; m_2 is the lower mass of the 2DOF model; I_1 and I_2 are the moments of inertia around the centroid of m_1 and m_2, respectively; R_1 and R_2 are the distances between the origin o (or o') and the centroid of m_1 and m_2, respectively; α_1 and α_2 are the angles of lines R_1 and R_2 with respect to the y-axis, respectively; and the value of λ is 1 while the 2DOF model pivots around o, and is -1 while it pivots around o'.

Generalized forces in the translational and rotational directions Q_{x1} and Q_θ are given by the following equations, respectively:

$$Q_{x1} = -m_1\ddot{z}_H\cos\theta \tag{3.2d}$$

$$Q_\theta = m_1\ddot{z}_H[R_1\cos(\alpha_1 - \lambda\theta) + x_1 sin\theta] + m_2\ddot{z}_H R_2\cos(\alpha_2 - \lambda\theta) \tag{3.2e}$$

The equations of motion of the 2DOF model are derived by solving Lagrange's equation shown below.

In the translational direction:

$$\frac{d}{dt}\left(\frac{\partial L}{\partial \dot{x}_1}\right) - \frac{\partial L}{\partial x_1} = Q_{x1} \tag{3.2f}$$

In the rotational direction:

$$\frac{d}{dt}\left(\frac{\partial L}{\partial \dot{\theta}}\right) - \frac{\partial L}{\partial \theta} = Q_{\theta} \tag{3.2g}$$

As a result, the equations of motion of the 2DOF model are obtained as shown in Eqs. (3.3a) and (3.3b). Here, the position of λ in the terms of equations of motion is different from D'Amico's one. Furthermore, the damping force term $c_1\dot{x}_1$ which is proportional to the translational velocity is introduced in the 2DOF model.

The equation of motion of the 2DOF model in the translational direction is:

$$\begin{aligned} &m_1\ddot{x}_1 - m_1R_1\cos\alpha_1\ddot{\theta} + c_1\dot{x}_1 + k_1x_1 + m_1g\sin\theta \\ &\qquad -m_1(x_1 + \lambda R_1\sin\alpha_1)\dot{\theta}^2 = -m_1\ddot{z}_H\cos\theta \end{aligned} \tag{3.3a}$$

Whereas the equation of motion of 2DOF model in the rotational direction is:

$$\begin{aligned} &m_1R_1\cos\alpha_1\ddot{x}_1 - \{(I_1 + m_1R_1^2) + (I_2 + m_2R_2^2) + m_1(x_1^2 + 2\lambda x_1R_1\sin\alpha_1)\}\ddot{\theta} \\ &-2m_1(x_1 + \lambda R_1\sin\alpha_1)\dot{x}_1\dot{\theta} \\ &-\lambda[m_1g\{R_1\sin(\alpha_1 - \lambda\theta) + \lambda x_1\cos\theta\} + m_2gR_2\sin(\alpha_2 - \lambda\theta)] \\ &\qquad = -[m_1\{R_1\cos(\alpha_1 - \lambda\theta) + x_1\sin\theta\} + m_2R_2\cos(\alpha_2 - \lambda\theta)]\ddot{z}_H \end{aligned} \tag{3.3b}$$

In this model, uplift commencement and restitution conditions are defined for switching the equations of motion. The uplift commencement condition of the 2DOF model subjected to horizontal

ground accelerations is expressed by a balance between the overturning moment (OM) and the resistant moment (RM) around a pivoting edge.

$$|RM| < |OM| \tag{3.4}$$

where

$$OM = m_1(\ddot{x}_1 + \ddot{z}_H)R_1\cos\alpha_1 + m_2\ddot{z}_H R_2\cos\alpha_2 \tag{3.5}$$

When $OM \geq 0$, then

$$RM = -\{m_1 g(R_1\sin\alpha_1 - x_1) + m_2 g R_2\sin\alpha_2\} \tag{3.6a}$$

$$\lambda = 1 \tag{3.6b}$$

When $OM < 0$, then

$$RM = m_1 g(R_1\sin\alpha_1 - x_1) + m_2 g R_2\sin\alpha_2 \tag{3.7a}$$

$$\lambda = -1 \tag{3.7b}$$

It is necessary to define restitution condition because an impact accompanies when the pivoting edge changes sides. The associated loss of energy is considered by reducing the angular velocity of the system after the impact. This may be expressed as:

$$\dot{\theta}(t^+) = e\dot{\theta}(t^-) \qquad (0 \leq e \leq 1) \tag{3.8}$$

where t^+ is the time immediately after an impact; t^- is the time immediately before the impact; and e is the coefficient of restitution for rocking motion. Changes in angular velocity are considered to occur instantaneously. Since there is no method to determine the exact value of the coefficient of

restitution e, it can only be estimated appropriately at present.

3.2.2 Computational Method of 2DOF Model

Matrix representation of Eqs. (3.3a) and (3.3b) can be expressed as Eq. (3.9). To solve the nonlinear equations explicitly, response values of the previous time step (at $t = t_n$) shown in Eqs. (3.10a) to (3.10j) are used in the coefficient matrix $[C]$, and the vectors $\{q\}$ and $\{f\}$. Then, values of responses (at $t = t_{n+1}$) shown in Eq. (3.10k) are obtained. The logic of the calculation program is shown in Figure 3.2.

$$[M]\{\ddot{x}\} + [C]\{\dot{x}\} + [K]\{x\} + \{q\} = \{f\} \tag{3.9}$$

where

$$[M] = \begin{bmatrix} m_1 & -m_1 R_1 \cos\alpha_1 \\ m_1 R_1 \cos\alpha_1 & -I_0 \end{bmatrix} \tag{3.10a}$$

$$[C] = \begin{bmatrix} c_1 & 0 \\ 0 & -2m_1(x_1 + \lambda R_1 \sin\alpha_1)\dot{x}_1 \end{bmatrix} \tag{3.10b}$$

$$[K] = \begin{bmatrix} k_1 & 0 \\ 0 & 0 \end{bmatrix} \tag{3.10c}$$

$$\{q\} = \begin{Bmatrix} q_1 \\ q_2 \end{Bmatrix} \tag{3.10d}$$

$$\{f\} = \begin{Bmatrix} f_1 \\ f_2 \end{Bmatrix} \tag{3.10e}$$

$$I_0 = (I_1 + m_1 R_1^2) + (I_2 + m_2 R_2^2) + m_1(x_1^2 + 2\lambda x_1 R_1 \sin\alpha_1) \tag{3.10f}$$

$$q_1 = m_1 g \sin\theta - m_1(x_1 + \lambda R_1 \sin\alpha_1)\dot{\theta}^2 \tag{3.10g}$$

$$q_2 = -\lambda[m_1 g\{R_1 \sin(\alpha_1 - \lambda\theta) + \lambda x_1 \cos\theta\} + m_2 g R_2 \sin(\alpha_2 - \lambda\theta)] \tag{3.10h}$$

$$f_1 = -m_1 \ddot{z}_H \cos\theta \tag{3.10i}$$

$$f_2 = -[m_1\{R_1 \cos(\alpha_1 - \lambda\theta) + x_1 sin\theta\} + m_2 R_2 \cos(\alpha_2 - \lambda\theta)]\ddot{z}_H \tag{3.10j}$$

$$\{x\} = \begin{Bmatrix} x_1 \\ \theta \end{Bmatrix} \tag{3.10k}$$

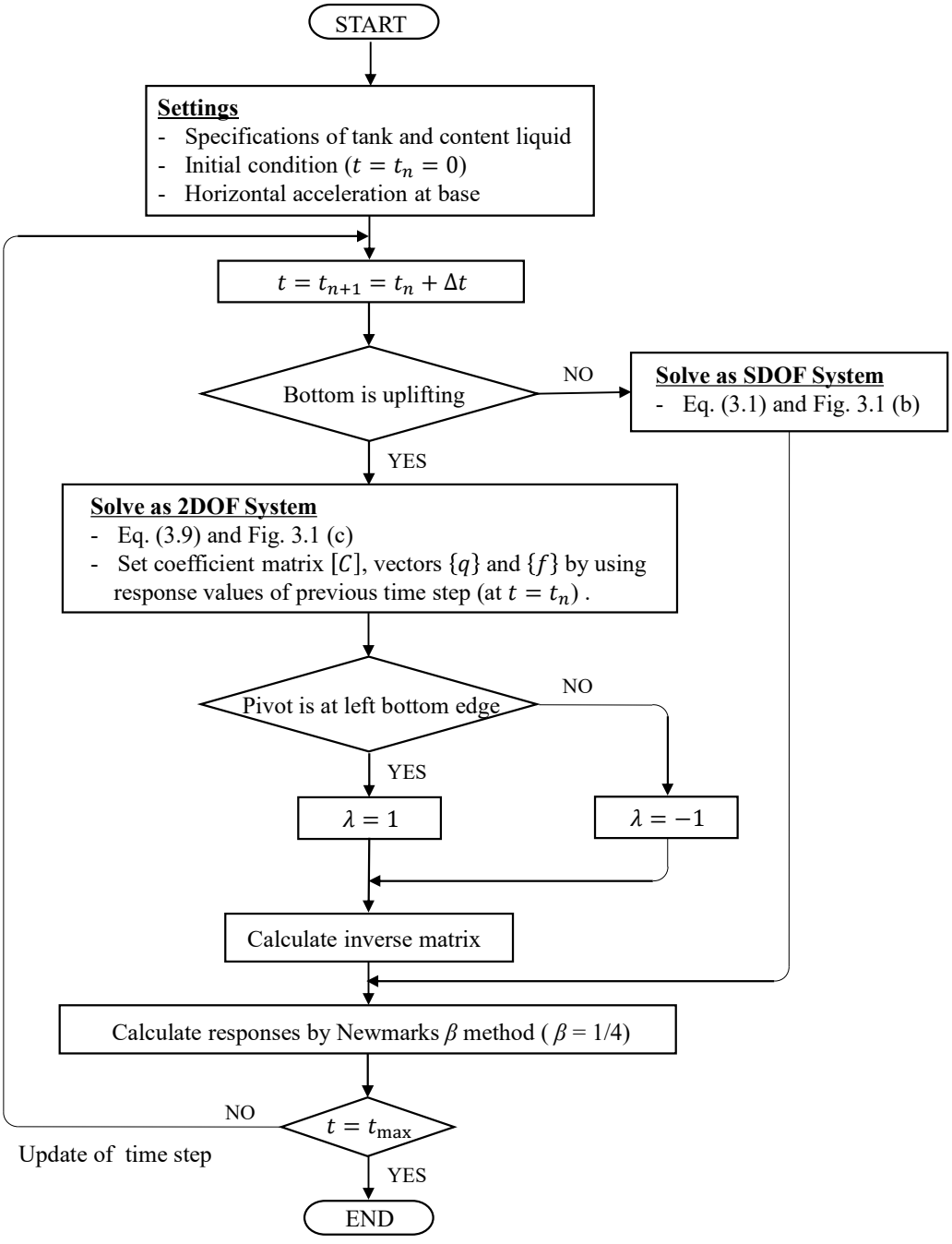

Figure 3.2 Calculation Flow of 2DOF Model

3.2.3 Verification of Accuracy of 2DOF Model

To verify the accuracy of the 2DOF model, the calculation results by the model were compared with the results of the free-rocking test conducted by D'Amico et al. (2017) [1]. Main phases of the free-rocking test are shown in Figure 3.3 [3]. The mechanical properties of the 2DOF model are shown in Table 3.1. The values of the damping constant h_1 and the coefficient of restitution for rocking motion e are based on assumption. The spring constant k_1 of the 2DOF system can be calculated by using the natural period T_1 of the 2DOF model ($k_1 = 4\pi^2 m_1 / T_1^2$). In this calculation, Newmark's β method ($\beta = 1/4$) is used. Solving nonlinear equations as linear equations requires the time step to be very small. In this calculation, the time step is set as $\Delta t = 0.0001$[sec]. In Figures 3.4 (a) and (b) the results of the 2DOF model are in general agreement with the free rocking test's results, which confirms the accuracy of the 2DOF model. Furthermore, it was shown that nonlinear equations could be analyzed by the simple method proposed here.

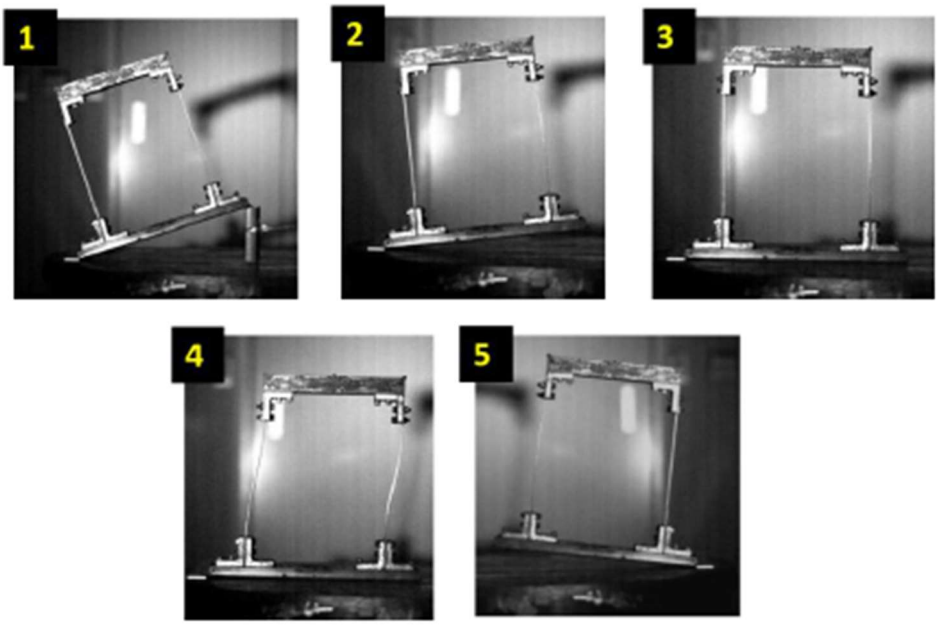

Figure 3.3 Main Phases of Free-Rocking Test Conducted by D'Amico et al. [1, 3]

Table 3.1 Mechanical Properties of 2DOF Model for Free-Rocking Test

m_1 [kg]	m_2 [kg]	R_1 [m]	R_2 [m]	α_1 [rad]	α_1 [rad]	T_1 [sec]	h_1 [-] (Assumed)	e [-] (Assumed)
3.33	2.34	0.299	0.101	0.341	1.446	0.25	0.02	0.85

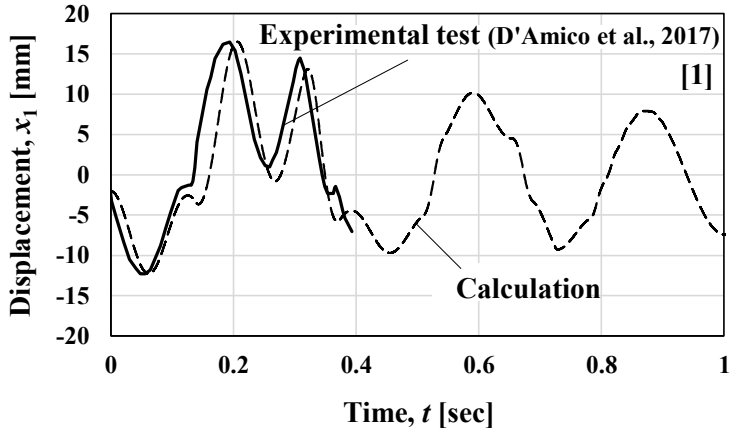

(a) Translational Displacement of Upper Mass

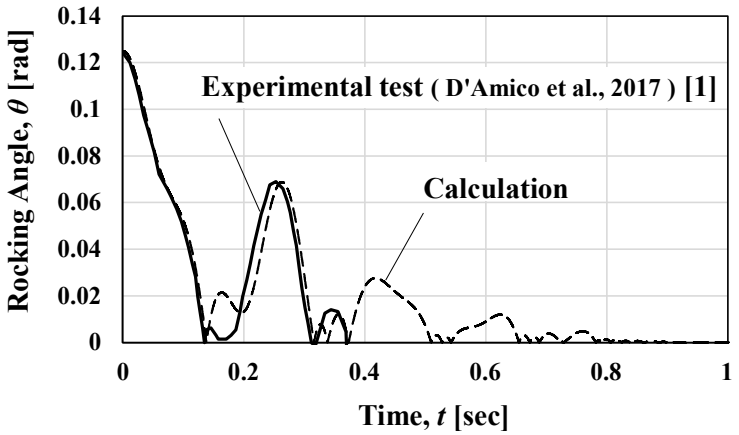

(b) Rotational Angle of 2DOF Model (Initial Angle: $\theta = 0.125$ [rad])

Figure 3.4 Comparison between Calculation and Experimental Results

3.3 Derivation of Mechanical Model of Liquid Storage Tank

3.3.1 Mass of Content Liquid that Works Effectively along with Tank Rocking Motion

As the results in Section 2.3 show, rotational inertia force must be taken in to account in order to solve the tank rocking motion. However, since the content is fluid, the moment of inertia of content liquid cannot be straightforwardly defined like that of a rigid body. As mentioned in Chapter 1, the moment of inertia of content liquid for tank rocking motion has already been derived in previous studies [4 - 6]. In this study, such a moment of inertia is referred to as the effective moment of inertia of content liquid.

Taniguchi and Segawa (2009) determined the effective mass as well as the effective moment of inertia of content liquid for rocking motion of a rigid rectangular tank whose bottom plate uplifted partially [4]. According to Taniguchi and Segawa (2009), the nominal effective density of content liquid for tank rocking motion can be quantified in accordance with hydraulic pressure gradient in the rotational direction (see Figures 3.5(a) and (b)). The distribution of the nominal effective density that determines the effective mass of content liquid for tank rocking motion can be calculated by Eq. (3.11). In addition, Taniguchi (2013) defined the effective mass of content liquid for interaction between bulging and rocking motions as a product of the nominal effective densities of fluid for rocking and bulging motions [5]. Based on these ideas, Taniguchi and Katayama (2016) expanded the definition of the effective mass and the effective moment of inertia of content liquid for tank rocking motion to a cylindrical tank [6]. A model that considers rotational inertia force of content liquid has also been proposed by other researchers, but the definition of moment of inertia of content liquid is ambiguous (e.g. [7]). Therefore, the definition of the effective mass and the effective moment of inertia of content liquid for tank rocking motion proposed by Taniguchi and Segawa (2009) is a breakthrough idea.

The theory of Taniguchi and Katayama (2016) is used in this study to estimate the effective mass and the moment of inertia of content liquid for tank rocking motion. The values related to tank rocking motion were re-evaluated as depicted in Figures 3.6 to 3.10. The reason for the re-evaluation was that the figure depicted by Taniguchi and Katayama (2016) did not show the values for immediately

before the commencement of the tank bottom uplift (when uplift width = 0) and for tanks with a small aspect ratio (liquid height H/ tank diameter $D < 0.3$). The specific values are summarized in Tables in Appendix 5.

$$\rho_{eff} = -\frac{1}{r^2\ddot{\theta}_0(t)}\frac{\partial p(r,\theta,t)}{\partial \theta} \tag{3.11}$$

where ρ_{eff} is the nominal effective density of content liquid for tank rocking motion; r is the distance between the pivot point and the point of focus; $p(r,\theta,t)$ is the dynamic pressure due to the tank rocking motion at the point of focus; θ is the rocking angle; and $\ddot{\theta}_0(t)$ is the angular acceleration around the pivot point.

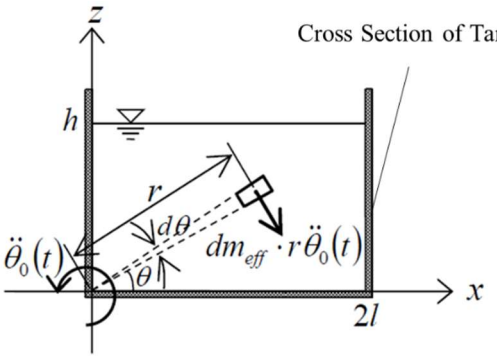

(a) Inertia Force Acting on Small Volume

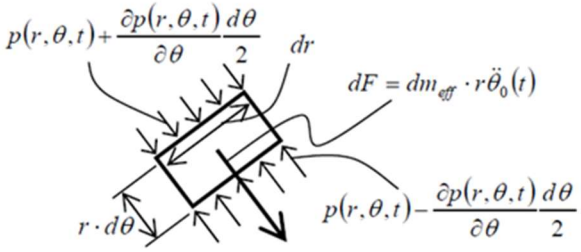

(b) Equilibrium of Forces on Small Volume

Figure 3.5 Definition of Nominal Effective Density of Content Liquid for Tank Rocking Motion [4]

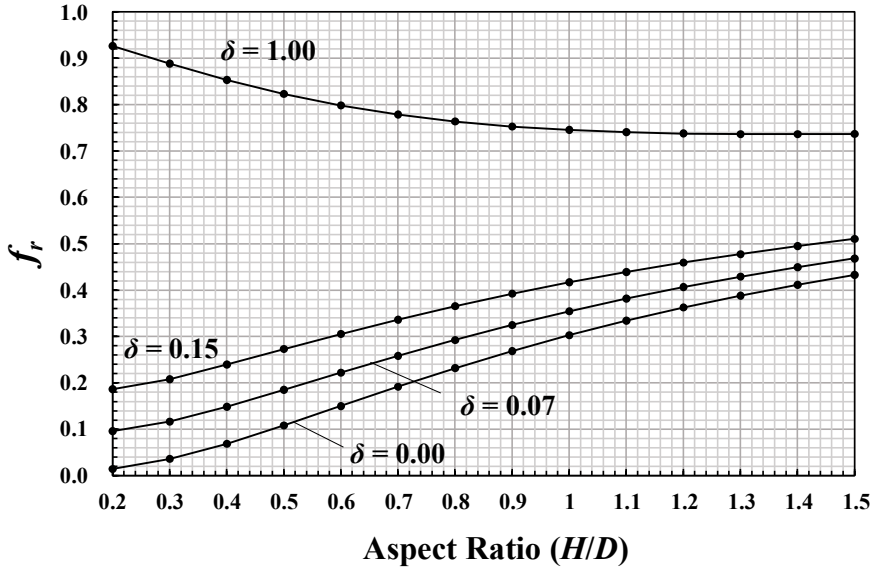

Figure 3.6 Values of Ratio of Effective Mass of Content Liquid for Rocking Motion to Total Mass of Fluid Filling Tank: f_r [6]

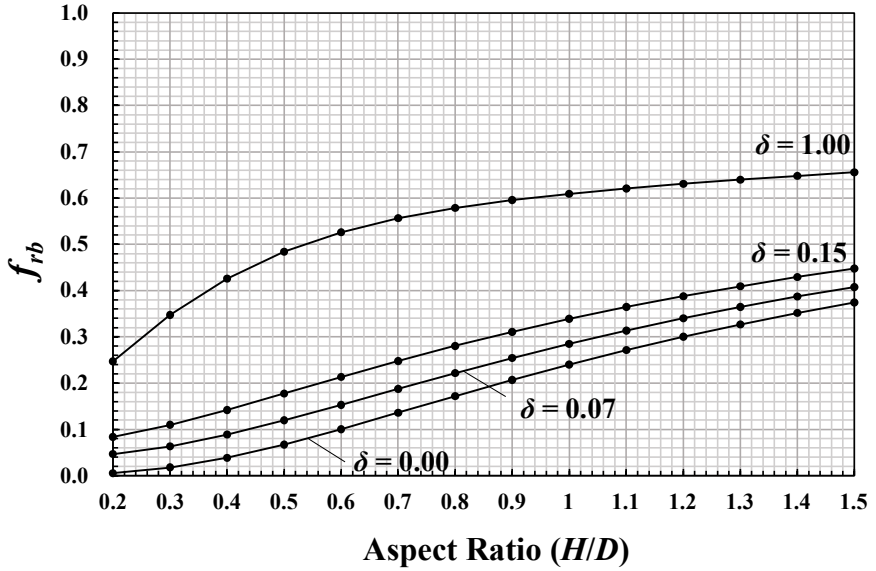

Figure 3.7 Values of Ratio of Effective Mass of Content Liquid for Rocking-Bulging Interaction Motion to Total Mass of Fluid Filling Tank: f_{rb} [6]

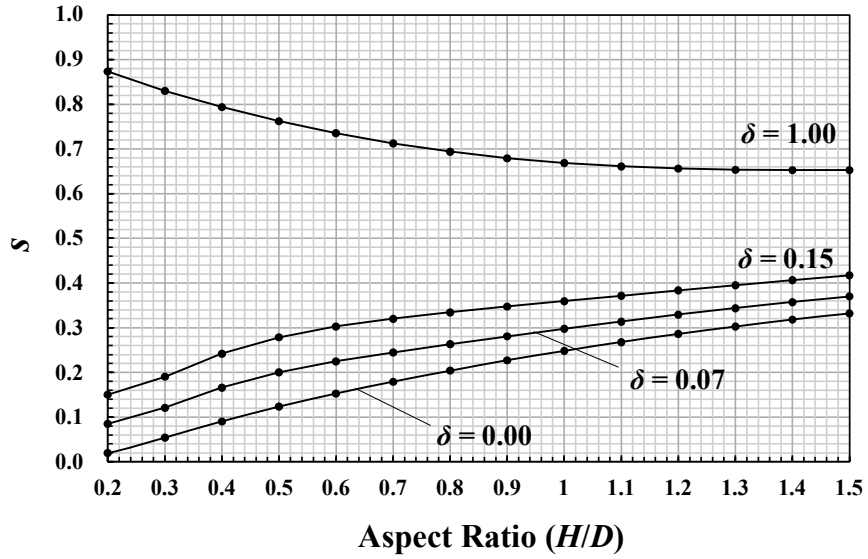

Figure 3.8 Values of Ratio of Effective Moment of Inertia of Content Liquid (around Centroid of m_r) to Moment of Inertia of Rigid Cylinder (around Centroid of m_t): s [6]

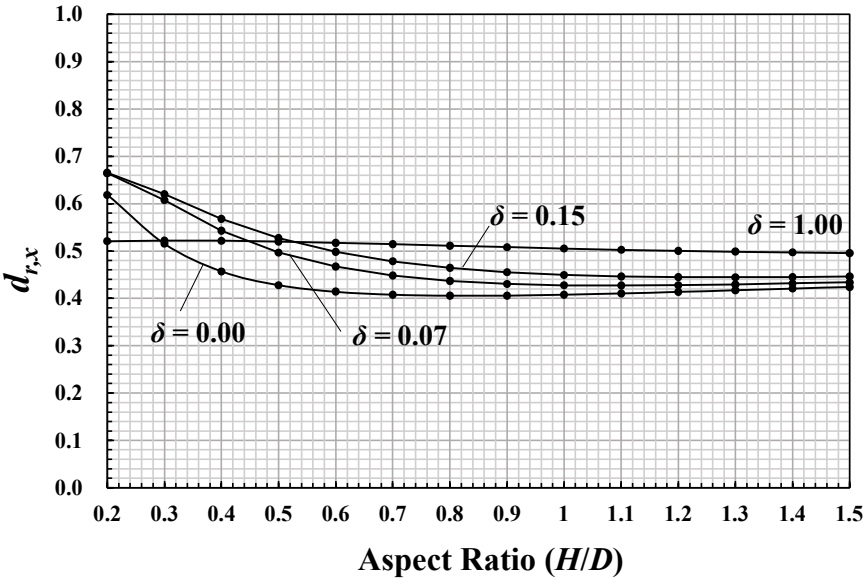

Figure 3.9 Values of Ratio of Horizontal Distance toward Centroid of Effective Mass of Content Liquid for Rocking Motion to Tank Diameter: $d_{r,x}$ [6]

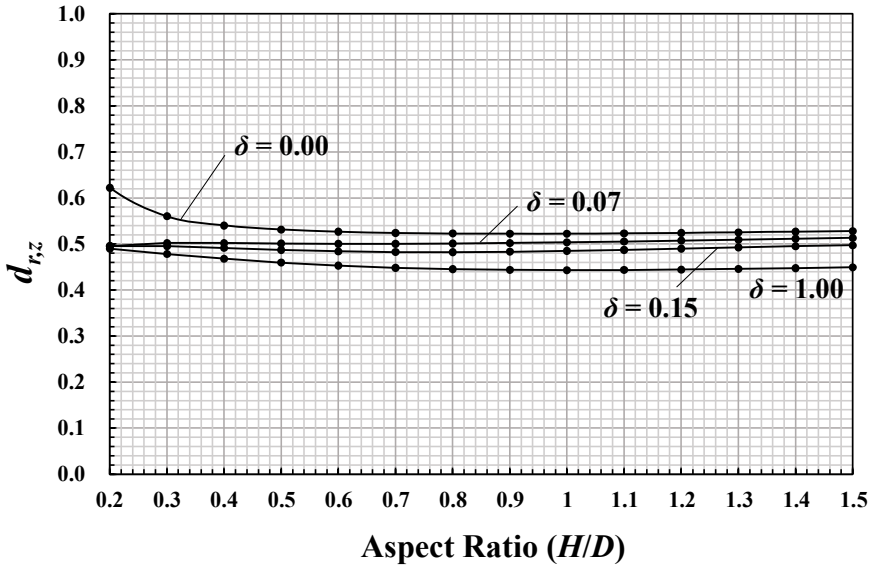

Figure 3.10 Values of Ratio of Vertical Distance toward Centroid of Effective Mass of Content Liquid for Rocking Motion to Liquid Height: $d_{r,z}$ [6]

3.3.2 Derivation of Equations of Motion for Tank Rocking Motion

The mechanical model for analyzing the rocking motion of a liquid storage tank is depicted in Figure 3.11. The equations of motion for the mechanical model of a liquid storage tank are derived based on the analogy between the 2DOF model and the tank in rock.

Here, m_1 of the 2DOF model is replaced with the effective mass of fluid for bulging motion m_b in the terms related to the translational motion, then m_1 is also replaced with the effective mass of fluid for rocking-bulging interaction motion m_{rb} in the terms related to the rotational and translational motions. Meanwhile, m_2 and I_2 of the 2DOF model are replaced with the effective mass of fluid for rocking motion m_r and the effective moment of inertia of fluid around m_r's centroid I_r in the terms related to the rotational motion, respectively. The centroids of masses are also replaced in the same manner. With the physical quantities replaced as detailed in Tables 3.2 and 3.3, the equation of motion for the bulging motion can be written as Eq. (3.12). Additionally, the equations of motion for the tank

rocking motion that include the rocking-bulging interaction motion are expressed in Eqs. (3.13a) and (3.13b). The mass of a tank is significantly smaller than that of content liquid and thus ignored in this study. Figure 2.15 (b) also corroborates why the mass of a tank can be ignored.

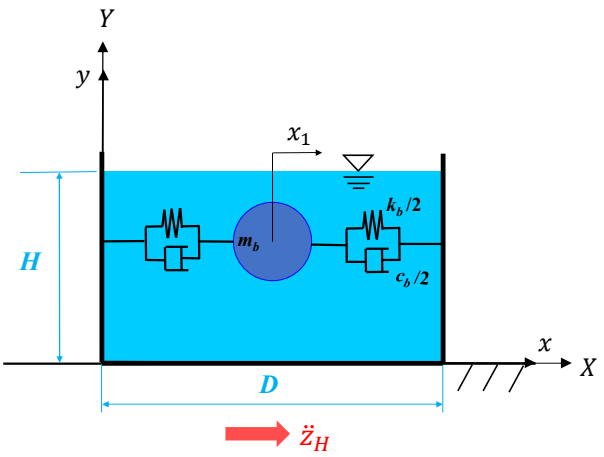

(a) Rest or Bulging Motion

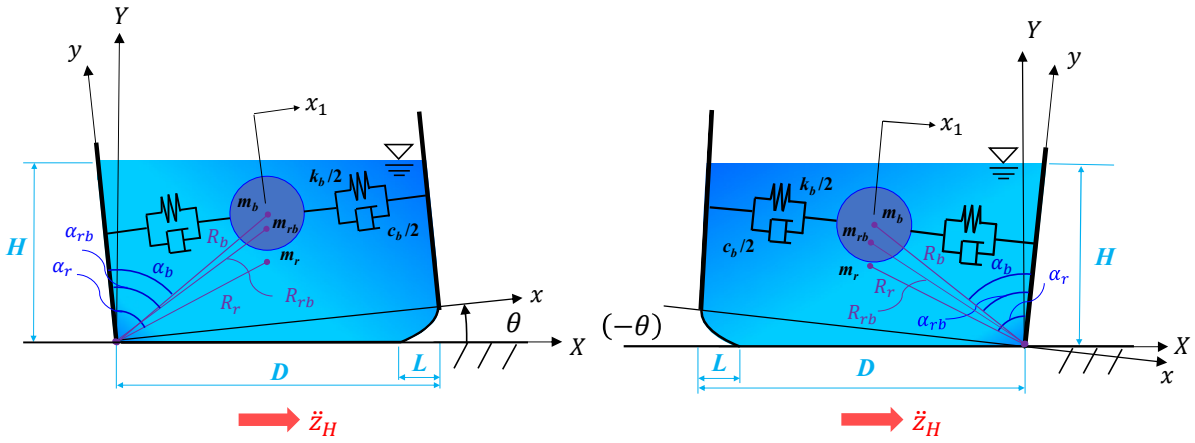

(b) Rocking-Bulging Interaction Motion

Figure 3.11 Mechanical Model of Liquid Storage Tank Considered

Table 3.2 Replacement of Physical Quantities between 2DOF and Mechanical Models of Liquid Storage Tank (Translational Motion)

No.	2DOF Model	Mechanical Model (Tank)	Remarks
1	$m_1\ddot{x}_1$	$m_b\ddot{x}_1$	Translational Inertia Force
2	$-m_1R_1\cos\alpha_1\ddot{\theta}$	$-m_{rb}R_{rb}\cos\alpha_{rb}\ddot{\theta}$	Translational Component of Rotational Inertia Force
3	$c_1\dot{x}_1$	$c_b\dot{x}_1$	Damping Force
4	k_1x_1	k_bx_1	Restoring Force
5	$m_1g\sin\theta$	$m_bg\sin\theta$	Translational Component of Gravity
6	$-m_1(x_1+\lambda R_1\sin\alpha_1)\dot{\theta}^2$	$-m_{rb}(x_1+\lambda R_{rb}\sin\alpha_{rb})\dot{\theta}^2$	Translational Component of Centrifugal Force
7	$-m_1\ddot{z}_H\cos\theta$	$-m_b\ddot{z}_H\cos\theta$	Translational Component of Seismic Inertia Force

Table 3.3 Replacement of Physical Quantities between 2DOF and Mechanical Models of Liquid Storage Tank (Rotational Motion)

No.	2DOF Model	Mechanical Model (Tank)	Remarks
1	$m_1R_1\cos\alpha_1\ddot{x}_1$	$m_bR_b\cos\alpha_b\ddot{x}_1$	Moment generated by Translational Inertia Force
2	$-(I_1+m_1R_1^2)\ddot{\theta}$	0	Rotational Inertia Force
3	$-(I_2+m_2R_2^2)\ddot{\theta}$	$-(I_r+m_rR_r^2)\ddot{\theta}$	Rotational Inertia Force
4	$-m_1(x_1^2+2\lambda x_1R_1\sin\alpha_1)\ddot{\theta}$	$-m_{rb}(x_1^2+2\lambda x_1R_{rb}\sin\alpha_{rb})\ddot{\theta}$	Rotational Inertia Force
5	$-2m_1(x_1+\lambda R_1\sin\alpha_1)\dot{x}_1\dot{\theta}$	$-2m_{rb}(x_1+\lambda R_{rb}\sin\alpha_{rb})\dot{x}_1\dot{\theta}$	Coriolis Force
6	$-\lambda m_1g\{R_1\sin(\alpha_1-\lambda\theta)+\lambda x_1\cos\theta\}$	0	Moment generated by Gravity
7	$-\lambda m_2gR_2\sin(\alpha_2-\lambda\theta)$	$-\lambda m_rgR_r\sin(\alpha_r-\lambda\theta)$	Moment generated by Gravity
8	$-m_1\{R_1\cos(\alpha_1-\lambda\theta)+x_1\sin\theta\}\ddot{z}_H$	$-m_b\{R_b\cos(\alpha_b-\lambda\theta)+x_1\sin\theta\}\ddot{z}_H$	Moment generated by Seismic Inertia Force
9	$-m_2R_2\cos(\alpha_2-\lambda\theta)\ddot{z}_H$	0	Moment generated by Seismic Inertia Force

The equation of motion for the tank bulging motion:

$$m_b\ddot{x}_1 + c_b\dot{x}_1 + k_b x_1 = -m_b\ddot{z}_H \tag{3.12}$$

where m_b, c_b and k_b are the effective mass of fluid, damping coefficient and spring constant of the bulging system, respectively; x_1 is the translational response displacement of the bulging system; and $\ddot{z}_H$ is the horizontal ground acceleration.

The equation of motion for the tank rocking motion in the translational direction:

$$\begin{aligned} m_b\ddot{x}_1 - m_{rb}R_{rb}\cos\alpha_{rb}\ddot{\theta} + c_b\dot{x}_1 + k_b x_1 + m_b g\sin\theta \\ -m_{rb}(x_1 + \lambda R_{rb}\sin\alpha_{rb})\dot{\theta}^2 = -m_b\ddot{z}_H\cos\theta \end{aligned} \tag{3.13a}$$

where m_{rb}, R_{rb} and α_{rb} are the effective mass of fluid for rocking-bulging interaction motion, the distance between the pivot point and the centroid of m_{rb}, and the angle between the line R_{rb} and the y-axis, respectively; θ is the rocking angle; g is the gravitational acceleration; and the value of λ is 1 while the mechanical model pivots around o, and is -1 while it pivots around o'.

The equation of motion for the tank rocking motion in the rotational direction:

$$\begin{aligned} & m_b R_b\cos\alpha_b\ddot{x}_1 - \{(I_r + m_r R_r^2) + m_{rb}(x_1^2 + 2\lambda x_1 R_{rb}\sin\alpha_{rb})\}\ddot{\theta} \\ & -2m_{rb}(x_1 + \lambda R_{rb}\sin\alpha_{rb})\dot{x}_1\dot{\theta} - \lambda m_r g R_r\sin(\alpha_r - \lambda\theta) \\ & \qquad = -m_b\{R_b\cos(\alpha_b - \lambda\theta) + x_1\sin\theta\}\ddot{z}_H \end{aligned} \tag{3.13b}$$

where R_b and α_b are the distance between the pivot point and the centroid of m_b and the angle between the line R_b and the y-axis, respectively; m_r, R_r and α_r are the effective mass of fluid for rocking motion, the distance between the pivot point and the centroid of m_r, and the angle between the

line R_r and the y-axis, respectively; and I_r is the effective moment of inertia of fluid around the centroid of m_r.

Same as with the 2DOF model, uplift commencement and restitution conditions are defined for switching the equations of motion. The uplift commencement condition of the mechanical model of a liquid storage tank subjected to horizontal ground acceleration is derived from a balance between the overturning moment (OM) and the resistant moment (RM) around a pivoting edge. For the resistant moment (RM), the added mass of content liquid to the tank shell $m_r g R_r \sin\alpha_r$ is considered (See Eq. (2.13)).

$$|RM| < |OM| \tag{3.14}$$

where

$$OM = m_b(\ddot{x}_1 + \ddot{z}_H)R_b\cos\alpha_b \tag{3.15}$$

When $OM \geq 0$, then

$$RM = -(m_s g R + m_r g R_r \sin\alpha_r) \tag{3.16a}$$

$$\lambda = 1 \tag{3.16b}$$

When $OM < 0$, then

$$RM = m_s g R + m_r g R_r \sin\alpha_r \tag{3.17a}$$

$$\lambda = -1 \tag{3.17b}$$

where m_s is the total mass of the tank shell and the roof.

The mechanical model of a liquid storage tank considers restitution condition because an impact accompanies when the pivoting edge changes sides. The associated loss of energy is considered by reducing the angular velocity of the system after the impact. Similar to the 2DOF model, this may be expressed in Eq. (3.18).

$$\dot{\theta}(t^+) = e\dot{\theta}(t^-) \qquad (0 \leq e \leq 1) \tag{3.18}$$

where t^+ is the time immediately after an impact; t^- is the time immediately before the impact; and e is the coefficient of restitution for tank rocking motion. Changes in angular velocity are considered to occur instantaneously. Since there is no method to determine the exact value of the coefficient of restitution e, it can only be estimated appropriately at present in the same manner with the 2DOF model.

3.3.3 Computational Method of Mechanical Model of Liquid Storage Tank

Matrix representation of Eqs. (3.13a) and (3.13b) can be expressed as Eq. (3.19). To solve the nonlinear equations explicitly, response values of the previous time step (at $t = t_n$) shown in Eqs. (3.20a) to (3.20j) are used in the coefficient matrix $[C]$, and the vectors $\{q\}$ and $\{f\}$. Then, values of responses (at $t = t_{n+1}$) shown in Eq. (3.20k) are obtained. The logic of the calculation program is shown in Figure 3.12.

$$[M]\{\ddot{x}\} + [C]\{\dot{x}\} + [K]\{x\} + \{q\} = \{f\} \tag{3.19}$$

where

$$[M] = \begin{bmatrix} m_b & -m_{rb}R_{rb}\cos\alpha_{rb} \\ m_bR_b\cos\alpha_b & -I_0 \end{bmatrix} \tag{3.20a}$$

$$[C] = \begin{bmatrix} c_b & 0 \\ 0 & -2m_{rb}(x_1 + \lambda R_{rb}\sin\alpha_{rb})\dot{x}_1 \end{bmatrix} \tag{3.20b}$$

$$[K] = \begin{bmatrix} k_b & 0 \\ 0 & 0 \end{bmatrix} \tag{3.20c}$$

$$\{q\} = \begin{Bmatrix} q_1 \\ q_2 \end{Bmatrix} \tag{3.20d}$$

$$\{f\} = \begin{Bmatrix} f_1 \\ f_2 \end{Bmatrix} \tag{3.20e}$$

$$I_0 = (I_r + m_rR_r^2) + m_{rb}(x_1^2 + 2\lambda x_1 R_{rb}\sin\alpha_{rb}) \tag{3.20f}$$

$$q_1 = m_b g\sin\theta - m_{rb}(x_1 + \lambda R_{rb}\sin\alpha_{rb})\dot{\theta}^2 \tag{3.20g}$$

$$q_2 = -\lambda m_r g R_r \sin(\alpha_r - \lambda\theta) \tag{3.20h}$$

$$f_1 = -m_b\ddot{z}_H\cos\theta \tag{3.20i}$$

$$f_2 = -m_b\{R_b\cos(\alpha_b - \lambda\theta) + x_1 sin\theta\}\ddot{z}_H \tag{3.20j}$$

$$\{x\} = \begin{Bmatrix} x_1 \\ \theta \end{Bmatrix} \tag{3.20k}$$

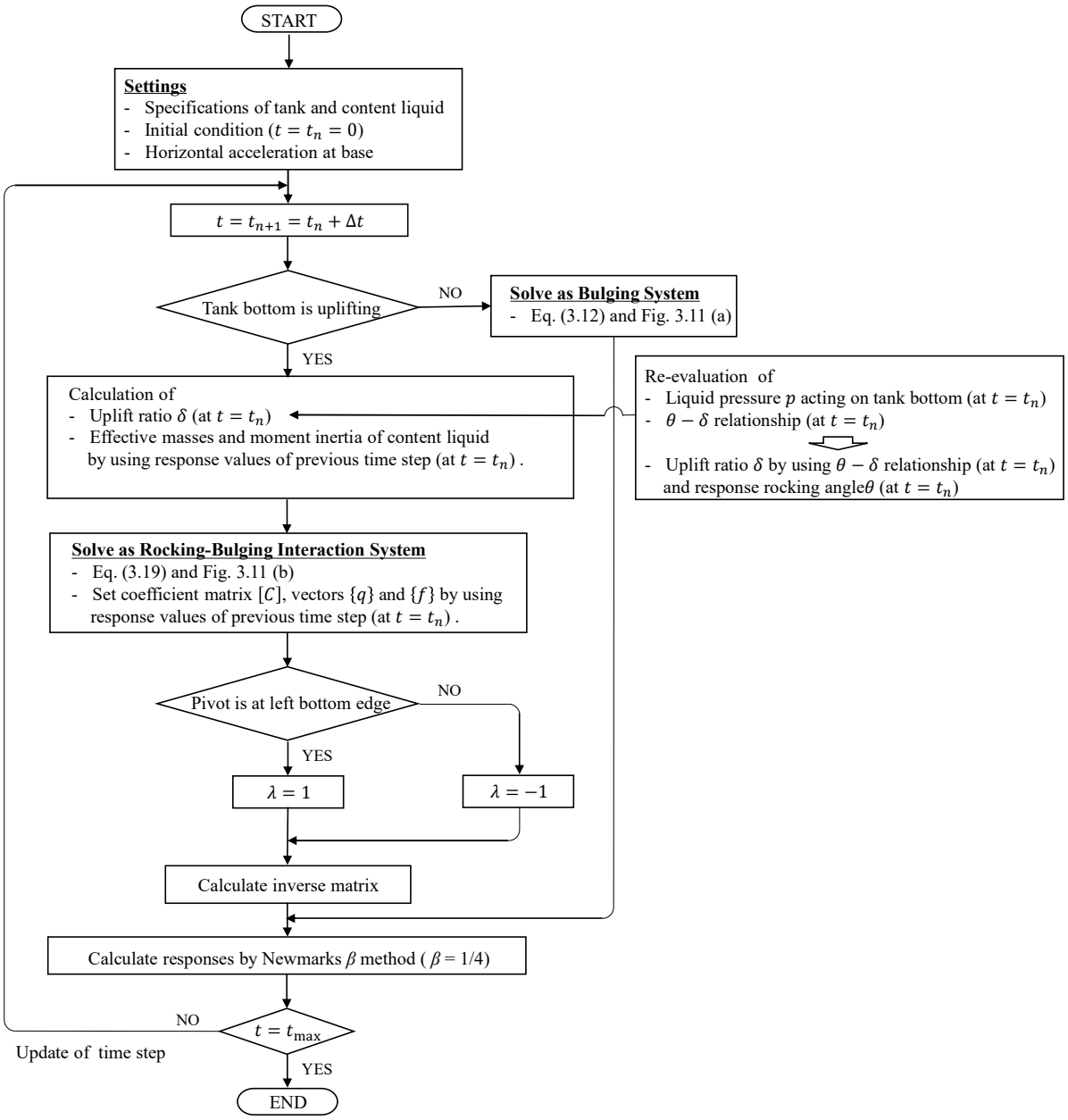

Figure 3.12 Calculation Flow of Mechanical Model of Liquid Storage Tank

The effective masses of fluid are calculated by Eqs. (3.21a) to (3.21d), respectively. Where, m_t and I are the total mass of content liquid and the moment of inertia around the centroid when the content rigidly behaves ($m_t = \rho_l \pi R^2 H,\ I = m_t\left(\frac{R^2}{4} + \frac{H^2}{12}\right)$). The distances between the pivot point and the centroid of each effective mass are calculated by Eqs. (3.21e) to (3.21g), respectively.

$$m_b = f_b m_t \tag{3.21a}$$

$$m_r = f_r m_t \tag{3.21b}$$

$$m_{rb} = f_{rb} m_t \tag{3.21c}$$

$$I_r = sI \tag{3.21d}$$

$$R_b = \sqrt{H_b^2 + R^2}\ ,\quad \left(H_b = d_{b,z} H\right) \tag{3.21e}$$

$$R_r = \sqrt{H_r^2 + D_r^2}\ ,\ \left(H_r = d_{r,z} H,\ D_r = d_{r,x} D\right) \tag{3.21f}$$

$$R_{rb} = R_b \tag{3.21g}$$

where each coefficient for calculating these quantities is obtained from Figures 3.6 to 3.10. The values of effective masses of fluid for rocking motion and rocking-bulging interaction are defined as a function of a ratio of the uplift width L to the tank diameter D, which is referred to as the uplift ratio δ herein. In this calculation, therefore, the uplift ratio $\delta\ (= L/D)$ is required to obtain these coefficients.

The uplift ratio δ is determined by applying the response rocking angle θ of the previous time step to the relationship between the rocking angle θ and the uplift ratio δ (see Figure 3.13(b)). That relationship is obtained from Malhotra's beam model (see Figure 3.13(a)) [8]. Eq. (3.22) gives the total pressure p acting on Malhotra's beam model. The total pressure consists of static pressure p_s, bulging dynamic pressure p_b, and rocking dynamic pressure p_r (Eqs. (3.23a) to (3.23c)). Here, the total pressure is assumed to be constant in the radial direction because the uplift width L is about a few percent of the diameter D. Therefore, its distribution along the diameter is negligible. Since the $\theta - \delta$ relationship changes with the change in the pressure acting on the beam model as shown in Figure

3.13(c), the computational method proposed in this study re-evaluates the $\theta - \delta$ relationship at every time step of the calculation.

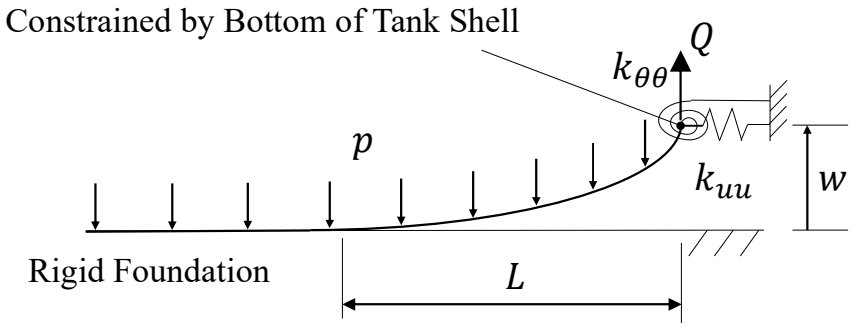

(a) Beam Model (Malhotra and Veletsos, 1994) [8]

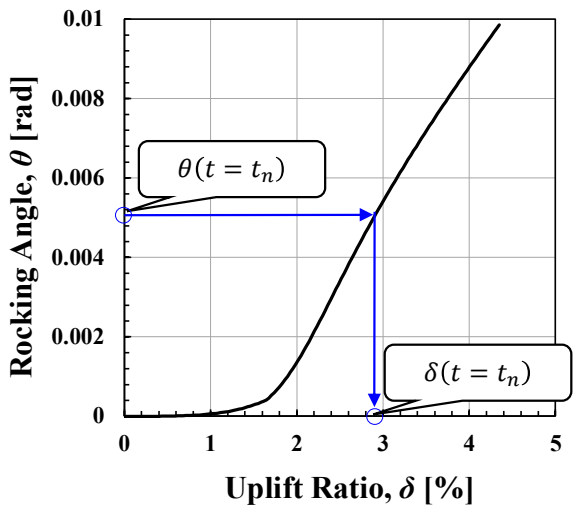

(b) $\theta - \delta$ Relationship (e.g., Tank in Appendix 1)

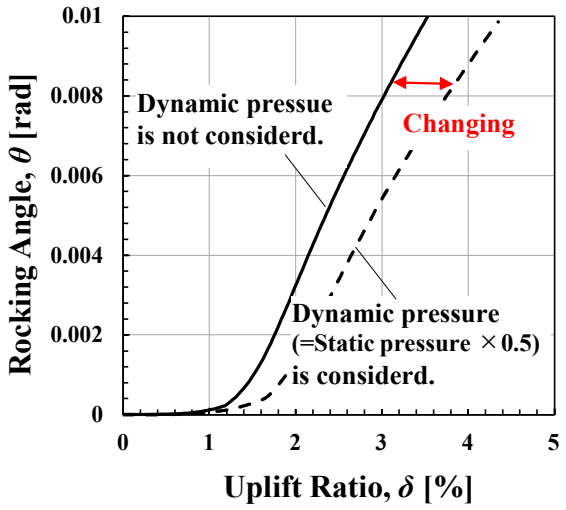

(c) Effect of Dynamic Pressure

Figure 3.13 Relationship between Uplift Ratio and Rocking Angle Calculated by Malhotra's Beam Model

$$p = p_s + p_b + p_r \tag{3.22}$$

in which

static pressure, p_s:

$$p_s = \rho_l g H \tag{3.23a}$$

where ρ_l is the density of content liquid; g is the gravitational acceleration; and H is the liquid height;

dynamic pressure due to bulging motion, p_b:

$$p_b = \frac{8\rho_l R}{\pi^2}(\ddot{x}_1 + \ddot{z}_H \cos\theta) \sum_{n=1,3,\cdots}^{\infty} \frac{1}{n^2}\left(\frac{1}{\cosh\frac{n\pi H}{2R}} - 1\right) \tag{3.23b}$$

and dynamic pressure due to rocking motion, p_r:

$$\begin{aligned} p_r = -\rho_l \ddot{\theta}\Bigg[& -H\left(R - \frac{D-L}{2}\right) \\ & + \frac{4R}{\pi^2}\sum_{n=1}^{\infty}\left(\left\{(-1)^n - \cos\frac{n\pi(D-L)}{2R}\right\}\frac{2R}{n^3\pi}\cdot\frac{2R}{2R-(D-L)}\cdot\left(-\tanh\frac{n\pi H}{2R}\right)\right. \\ & \left. + \{1-(-1)^n\}\frac{1}{n^2}\left(\frac{2R}{n\pi}\tanh\frac{n\pi H}{2R} - \frac{H}{\cosh\frac{n\pi H}{2R}}\right)\right)(-1)^n\Bigg] \end{aligned} \tag{3.23c}$$

The quantities related to the tank bulging motion in this computation method are determined as follows.

- The values of the ratio of the effective mass of content liquid for the bulging system to the total mass of fluid filling the tank f_b as well as the value of the ratio of vertical distance toward the centroid of m_b to the liquid height $d_{b,z}$ are obtained by Eqs. (3.24a) and (3.24b) or Figure

3.14 [9, 10]. These formulas are originally derived by Housner [11].

- The spring constant for tank bulging motion k_b is set to meet the natural period of the tank bulging motion, and calculated as $k_b = m_b(2\pi/T_b)^2$. T_b is the natural period of the bulging system, and can be obtained from Eqs. (3.25) and (3.26) [12,13].
- The damping coefficient for tank bulging motion c_b is calculated as $c_b = 2h_b\sqrt{k_b m_b}$. h_b is the damping constant of the bulging system, and set as $h_b = 0.05$ in this study.

$$f_b = \frac{\tanh(0.866\,D/H)}{0.866\,D/H} \quad (\text{when } D/H \le 0.75) \qquad (3.24a)$$
$$f_b = 1.0 - 0.218\,D/H \quad (\text{when } D/H > 0.75)$$

$$d_{b,z} = 0.375 \quad (\text{when } D/H \le 0.75) \qquad (3.24b)$$
$$d_{b,z} = 0.5 - 0.094\,D/H \quad (\text{when } D/H > 0.75)$$

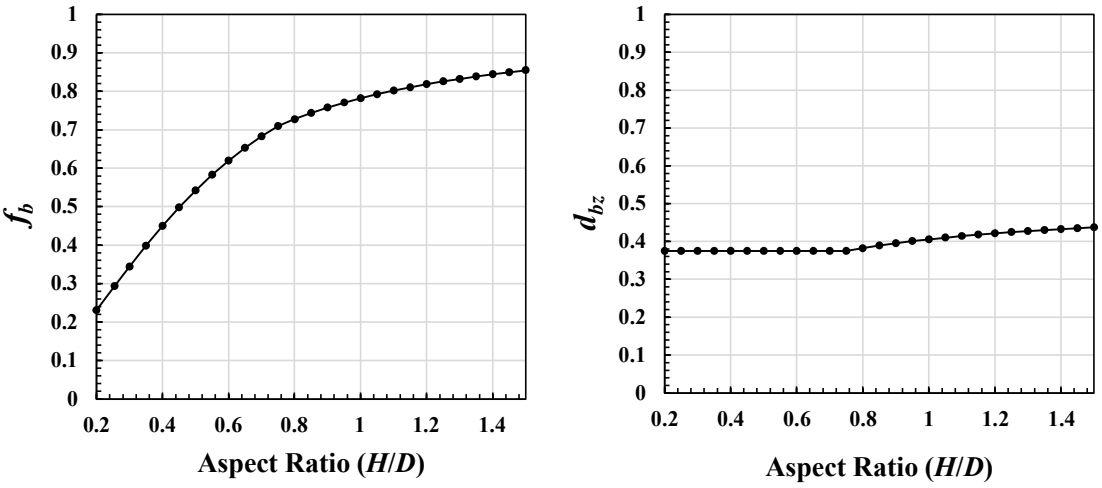

(a) f_b (b) $d_{b,z}$

Figure 3.14 Ratio of Effective Mass of Content Liquid for Bulging Motion to Total Mass of Fluid Filling Tank f_b, and Ratio of Vertical Distance toward Centroid of m_b to Liquid Height $d_{b,z}$ [9, 10]

$$T_b = \frac{2}{\lambda}\sqrt{\frac{W_0}{\pi g E t_{1/3}}} \tag{3.25}$$

$$\lambda = 0.067(H/D)^2 - 0.30(H/D) + 0.46 \qquad (\text{For } 0.15 \leq H/D \leq 2.0) \tag{3.26}$$

where W_0 is the total weight of the content liquid; E is the Young's modulus of the tank material; and $t_{1/3}$ is the thickness of the tank shell at one third of the liquid height H.

3.4 Conclusions

In this chapter, derivation process of the mechanical model of a liquid storage tank and the method of time history analysis for tank rocking motion were presented. The principal conclusions of this chapter are summarized as follows:

- Equations of motion for the 2DOF system with freedom in the translational and rotational directions were derived. Then computational method of the equations of motion for the 2DOF model was explained. Accuracy of the computational method was verified by comparison with the results of experimental test.

- Based on the analogy between the 2DOF model and the tank in rock, equations of motion for the mechanical model of a liquid storage tank were derived. The computational method of the equations of motion for the mechanical model of a liquid storage tank was then developed by introducing the rocking angle-uplift ratio relationship calculated by Malhotra's beam model to the computational method. Accuracy of the computational method of the mechanical model of a liquid storage tank is verified in the next chapter.

Bibliography

[1] D'Amico, M., Taniguchi, T. and Nakashima, T., 2017, "Simplified Analysis of The Rocking Motion of A Cylindrical Tank Focusing on The Role of Dynamical Forces Involved in Rocking-Bulging Interaction," Proc. ASME PVP Conference, Seismic Engineering, Paper No. PVP2017-65442.

[2] Yoshida, Y., Taniguchi, T. and Nakashima, T., 2022, "Rocking Response Analysis of Flat-Bottom Cylindrical Tanks Considering Rotational Inertia of Content Liquid," Proc. ASME PVP Conference, Seismic Engineering, Paper No. PVP2022-84909.

[3] D'Amico, M., 2018, "Seismic Fragility and Dynamic Behavior of Atmospheric Cylindrical Steel Tanks," Ph.D. Dissertation, University of Bologna, Italy.

[4] Taniguchi, T. and Segawa, T., 2009, "Effective Mass of Fluid for Rocking Motion of Flat-Bottom Cylindrical Tanks," Proc. ASME PVP Conference, Seismic Engineering, Paper No. PVP2009-77580.

[5] Taniguchi, T., 2013, "Contributions of Fluid to Rocking-Bulging Interaction of Rectangular Tanks Whose Walls Are Rigid and Bottom Plate Rectilinearly Uplifts," Journal of Pressure Vessel Technologies, ASME, doi:10.1115/1.4007286.

[6] Taniguchi, T. and Katayama, Y., 2016, "Masses of Fluid for Cylindrical Tanks in Rock with Partial Uplift of Bottom Plate," Journal of Pressure Vessel Technologies, ASME, doi:10.1115/1.4032784.

[7] Vathi, M. and Karamanos, S.A., 2017, "A Simple and Efficient Model for Seismic Response and Low-Cycle Fatigue Assessment of Uplifting Liquid Storage Tanks," Journal of Loss Prevention in The Process Industries, Vol. 53, pp. 29-44.

[8] Malhotra, P.K. and Veletsos, A.S., 1994, "Beam Model for Base Uplifting Analysis of Cylindrical Tanks," J. Struct. Div., ASCE, Vol. 120 Issue 12, pp. 3471–3488.

[9] METI Notification No. 515, issued Oct. 26, 1981. (in Japanese)

[10] API Standard 650, 2020, "Welded Tanks for Oil Storage, Annex E: Seismic Design of Storage Tanks," Thirteenth Edition.

[11] Housner, G.W., 1957, "Dynamic Pressure on Accelerated Fluid Containers," Bulletin of the Seismological Society of America, Vol. 47, Issue 1, pp. 15-35.

[12] Sakai, F. and Ogawa, H., 1979, "On A Simplified Theory for The Vibration Analysis of Circular Cylindrical Liquid Storage Tanks," Proc. 13th National Symp. Matrix Meth. Analysis, Japanese Society of Steel Construction, (in Japanese)

[13] Sakai, F. and Ogawa, H., 1982, "Seismic Resistant Design of Liquid Storage Tanks in Japan," Sino-American Symp. on Bridge and Str. Engng.

Chapter 4

Validation of Mechanical Model of Liquid Storage Tank

Chapter 4

Validation of Mechanical Model of Liquid Storage Tank

4.1 Introduction

This chapter verifies the accuracy of the mechanical model of a liquid storage tank developed for analyzing the tank rocking response (hereinafter referred to as the proposed method), through the following case studies.

- A comparison is conducted between the calculation results of uplift displacement by the proposed method and those by the dynamic FE analysis. The horizontal harmonic ground acceleration is input to the bottom of a 60,000 kL LNG storage tank.
- A comparison of uplift displacement is also conducted between the calculation results by the proposed method and an observational record. Further comparison is made between the calculation results of uplift displacement by the proposed method and those by the conventional methods. The tank used in the validation is a 114,800 kL oil storage tank.

4.2 Comparison of Uplift Displacement Calculation Results between Mechanical Model and Dynamic FE Analysis

The tank rocking response due to harmonic excitation calculated by the proposed method is compared with that computed by the dynamic FE analysis. The details of the dynamic FE analysis are shown in Appendix 1. The tank shell is assumed to be rigid in the tank model of the dynamic FE analysis, and thus that in the proposed method is also assumed to be rigid.

The calculation results of uplift displacement by the dynamic FE analysis and those by the proposed method are compared with each other as shown in Figures 4.1 (a) and (b), where, except for

the magnitude of the initial ones, the uplift responses show a good agreement with a reasonable accuracy.

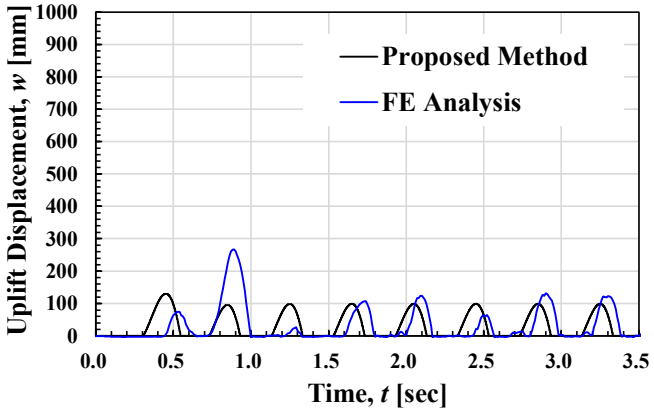

(a) Left Bottom Edge

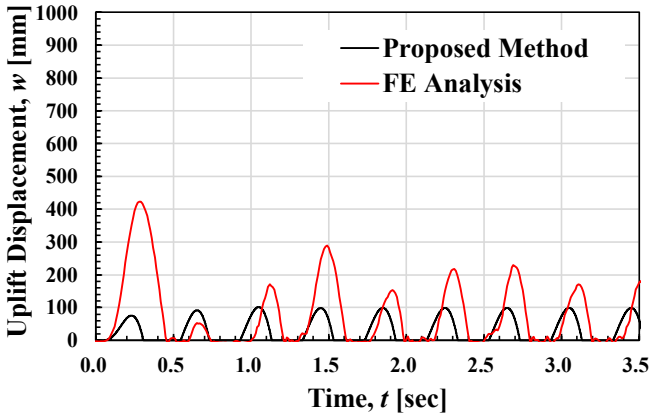

(b) Right Bottom Edge

Figure 4.1 Calculation Results of Uplift Displacement by Proposed Method and Dynamic FE Analysis [60,000 kL LNG Storage Tank]

Additional dynamic FE analysis was also conducted with the property of the tank shell changed from rigidity to elasticity, using horizontal harmonic ground acceleration with a maximum amplitude of 300 gal (see Figure 4.2). The damping constant h_b and the coefficient of restitution e were set to 0.05 and 0.2, respectively. A conventional value was used for h_b, and the value of e was determined appropriately.

The calculation results of uplift displacement by the additional dynamic FE analysis and those by the proposed method are compared with each other as shown in Figures 4.3(a) and (b). The calculation results by the method of Malhotra and Veletsos (1994) [1] are also shown for further comparison. The comparison results are as follows.

- The calculation results of uplift displacement by the proposed method are about two times larger than those by the additional dynamic FE analysis. Meanwhile, the maximum uplift displacement in the calculation by Malhotra's method is about three times larger than that by the additional dynamic FE analysis. The main reason for the difference may be the rotational inertia term of liquid mass which is included in the proposed method as a factor contributing to the tank rocking motion.
- In the results calculated by Malhotra's method, only one bottom edge is uplifted, and the number of times of uplift is significantly different from the results of the additional dynamic FE analysis. This is likely because the translational spring is combined in series with the rotational spring, which acts as the main uplift resistance and increases the natural period of the mechanical model of Malhotra's method.

These show that Malhotra’s and similar methods cannot well explain the dynamic rocking response of tanks, while the proposed method, which considers the rotational inertia force of the content liquid, yields more accurate results.

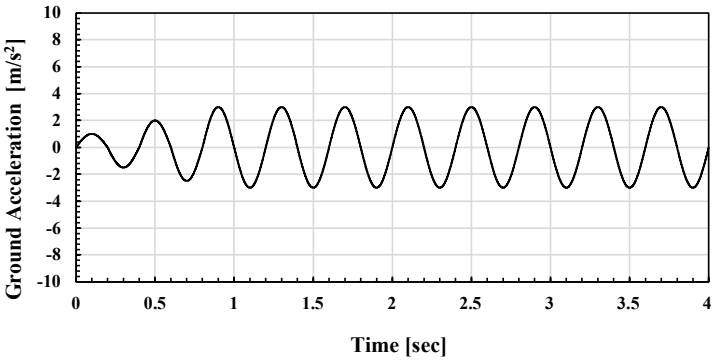

Figure 4.2 Ground Acceleration for Further Examination

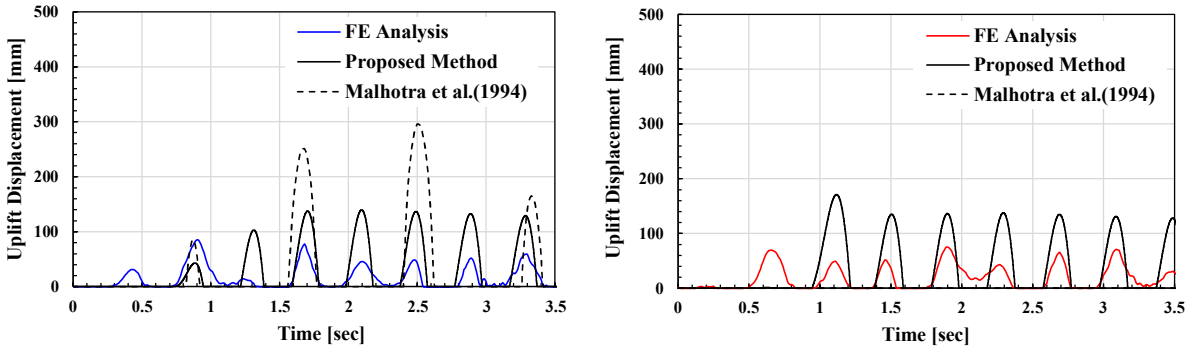

(a) Left Bottom Edge (b) Right Bottom Edge

Figure 4.3 Further Examination (Elastic Tank Shell, $h = 0.05$)

4.3 Comparison of Uplift Displacement between Calculation Results by Mechanical Model and Observational Record during 2018 Hokkaido Eastern Iburi Earthquake

In this section, the accuracy of the proposed method is verified by comparing the calculation results of uplift displacement by the proposed method to an observational record at the site. The Hokkaido Eastern Iburi earthquake of September 6, 2018 gave a unique opportunity to understand the uplift behavior of unanchored oil storage tanks under strong motion earthquakes. There was a petroleum stockpiling base near the epicenter. A seismometer installed near tank-A successfully recorded seismic ground motion near the tank (see Figure 4.4). Displacement gauges were attached to the bottom of tank-A (see Figure 1.20), and uplift of a large tank was recorded for the first time in the world by the deliberately installed measurement instruments [2]. The maximum uplift displacement recorded was 44 mm (see Figure 4.5). The mechanical properties of tank-A and content liquid are tabulated in Tables 4.1 and 4.2, respectively.

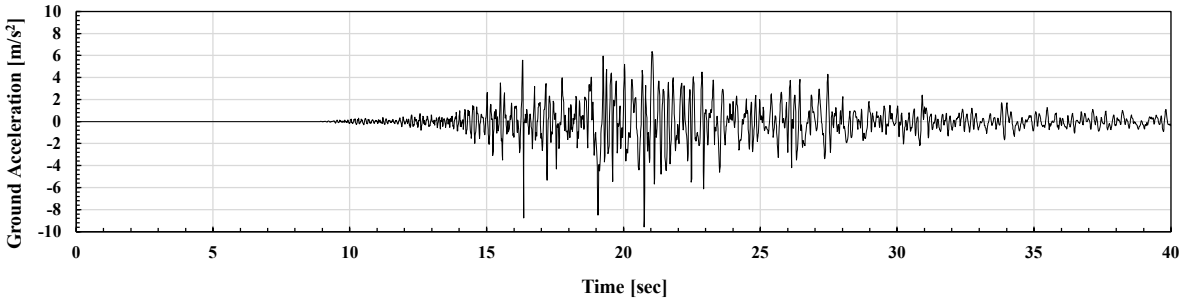

Figure 4.4 Ground Acceleration Observed in Tank-A Yard (in CN0°-CN180° Direction)

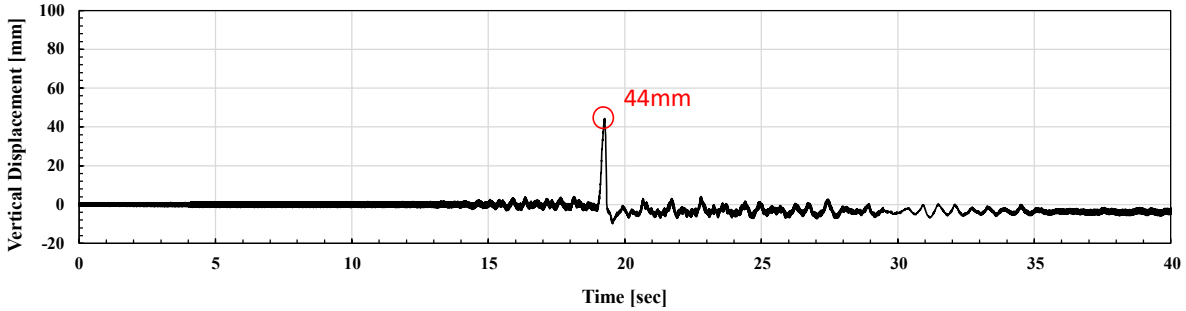

Figure 4.5 Record of Uplift Displacement of Tank-A, CN180°

Table 4.1 Mechanical Properties of Tank-A (114,800 kL)

Diameter of Tank [m]		82.0
Height of Tank [m]		24.5
Thickness of Tank Shell [mm]		12.0 to 37.0
Thickness of Bottom Plate [mm]	General Part	12.0
	Annular Part	26.0
Young's Modulus of Material [GPa]		206
Poisson's Ratio of Material [-]		0.3
Density of Material [kg/m^3]		7850

Table 4.2 Mechanical Properties of Content Liquid (Oil)

Depth of Content Liquid [m]	20.865
Density of Content Liquid [kg/m^3]	865.1

The response analysis results by the proposed method are shown in Figures 4.6 (a) to (d) and 4.7 (a) to (d). Figure 4.7 (d) shows the calculation results of uplift displacement, where multiple uplift events can be seen. The overturning moment was large during 19 to 25 seconds, and uplift was likely to have occurred accordingly. Since the peak of each uplift event is slightly behind that of an overturning moment as shown in Figure 4.8, the magnitude of uplift displacement may depend on the overturning moment slightly before that. Not only the magnitude of the overturning moment but also the duration over which the overturning moment exceeds the restoring moment ($m_r g R_r \sin\alpha_r$) may affect the amount of uplift.

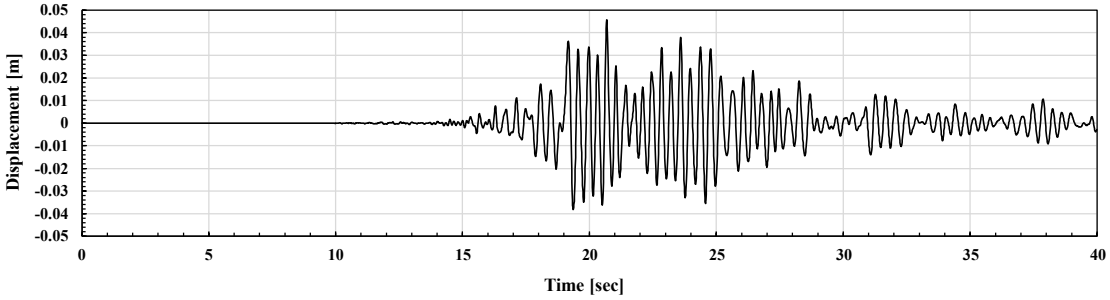

(a) Translational Displacement of m_b

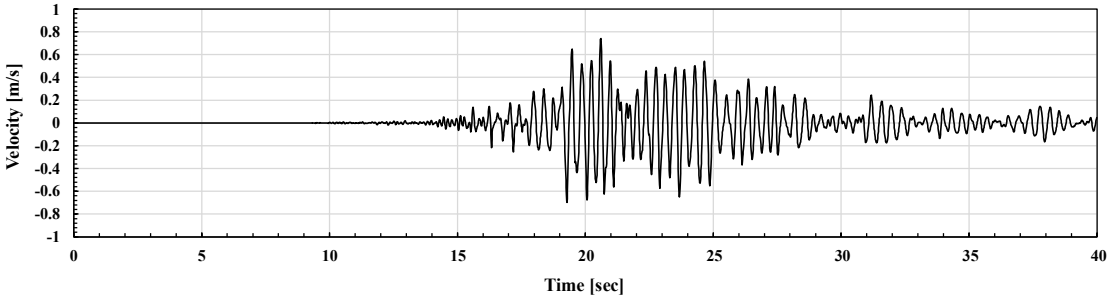

(b) Translational Velocity of m_b

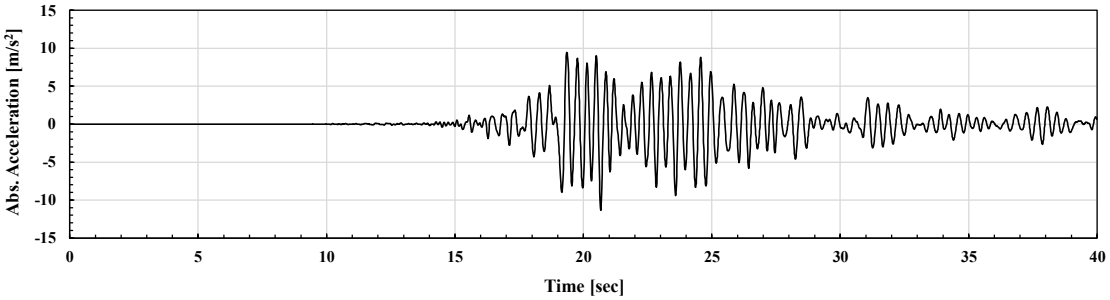

(c) Translational Absolute Acceleration of m_b

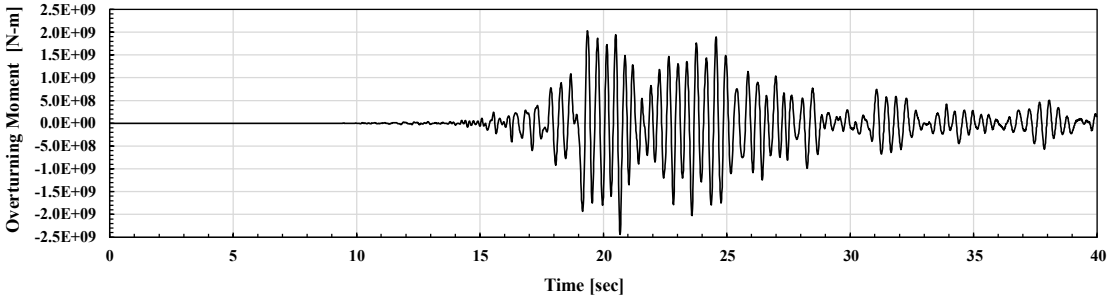

(d) Overturning Moment

Figure 4.6 Time Histories of Responses of Mechanical Model Developed (1)

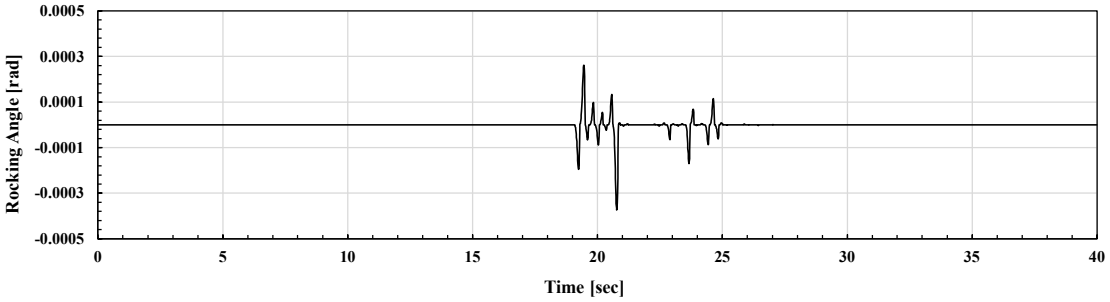

(a) Rocking Angle of Mechanical Model

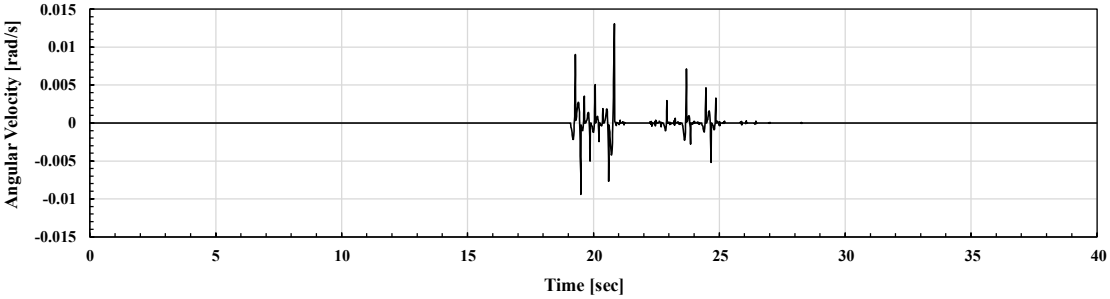

(b) Angular Velocity of Mechanical Model

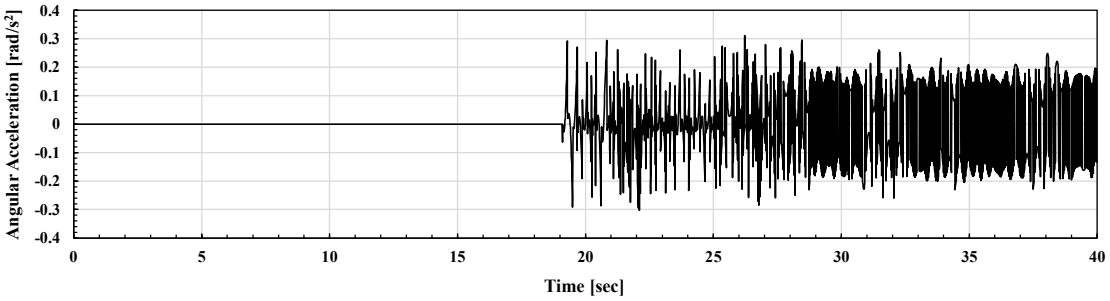

(c) Angular Acceleration of Mechanical Model

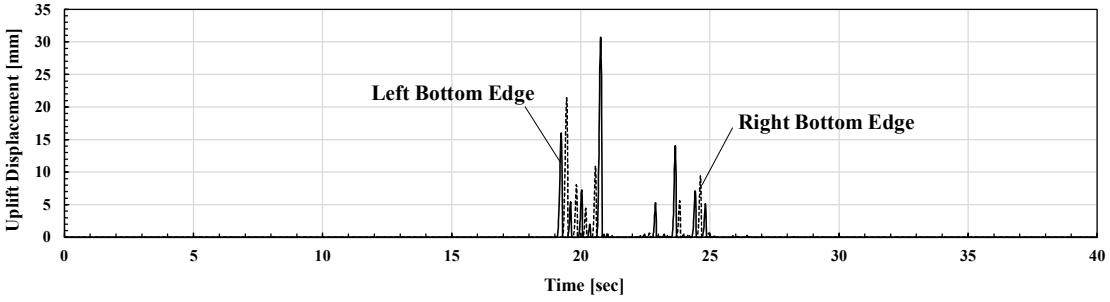

(d) Uplift Displacement of Mechanical Model

Figure 4.7 Time Histories of Responses of Mechanical Model Developed (2)

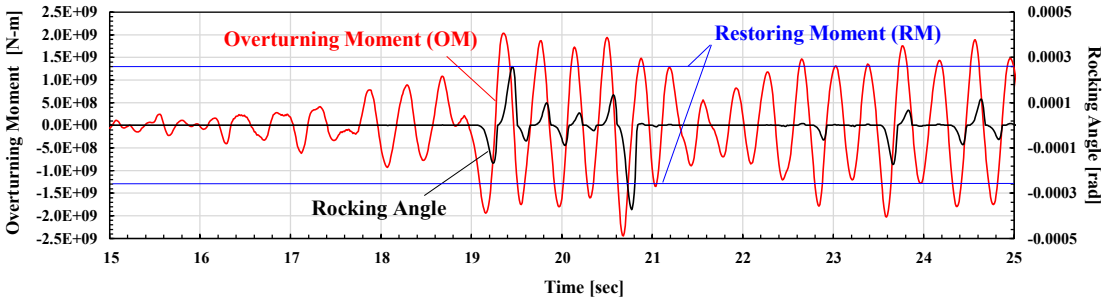

Figure 4.8 Time Histories of Overturning Moment and Rocking Angle

Figure 4.9 shows the time history of the liquid pressure acting on the uplifted bottom plate during the tank rocking motion. These results are calculated by the proposed method. The liquid pressure in the graph is shifted to the uplift side as appropriate. As shown in this graph, the liquid pressure acting on the uplifted bottom plate is smaller than the static liquid pressure due to the bulging dynamic pressure. In the beam models verified in Chapter 2 (see Figures 2.5 (a) and (b)), it has been shown that the accuracy is higher when the reduction of the liquid pressure acting on the tank bottom plate due to the dynamic pressure is taken into account.

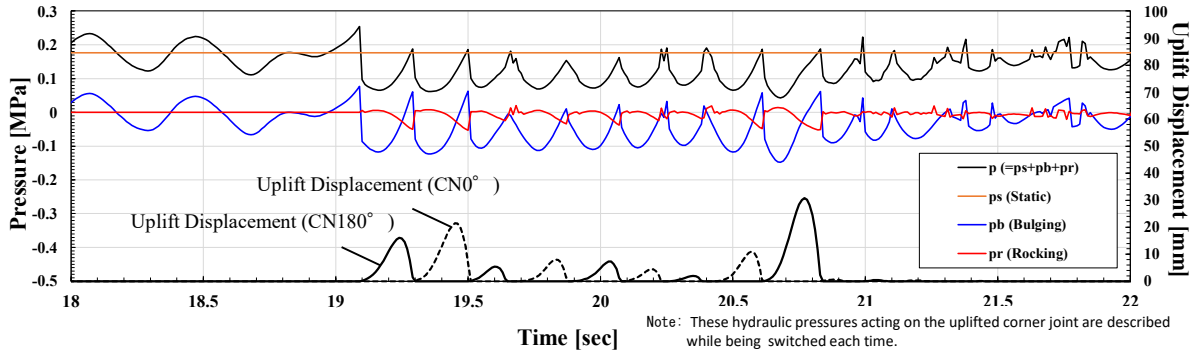

Figure 4.9 Liquid Pressure Acting on Uplifted Bottom Plate under Tank Rocking Motion

Figure 4.10 shows a comparison between the calculation results of uplift displacement by the proposed method ($h_b = 0.05,\ e = 0.01$) and the observational record. The comparison results are as follows.

- The calculated and recorded initial uplifts are almost at the same time. However, the uplift displacement calculated by the proposed method is about half the recorded data. The reasons for this may be the additional uplift due to the out-of-round deformation of the tank shell and that from the elasticity of the base which are implicitly included in the recorded uplift.
- The observational record of uplift displacement shows almost no uplift events after the main uplift, whereas the time history of the uplift displacement calculated by the proposed method has several uplifts. The reason for the multiple uplifts occurring in the calculation is the balance of moment as described in Figure 4.8. In reality, however, there was only one large uplift. This suggests that damping induced by landing on a soft base is quite effective against the tank rocking response due to the reduced ease of rotation.

Nevertheless, the proposed computational method can be considered to have a reasonable degree of accuracy, given that the uplift of a tank is a natural phenomenon that may have conditions that are not taken into account in such simple calculations. Further study is necessary to improve the accuracy.

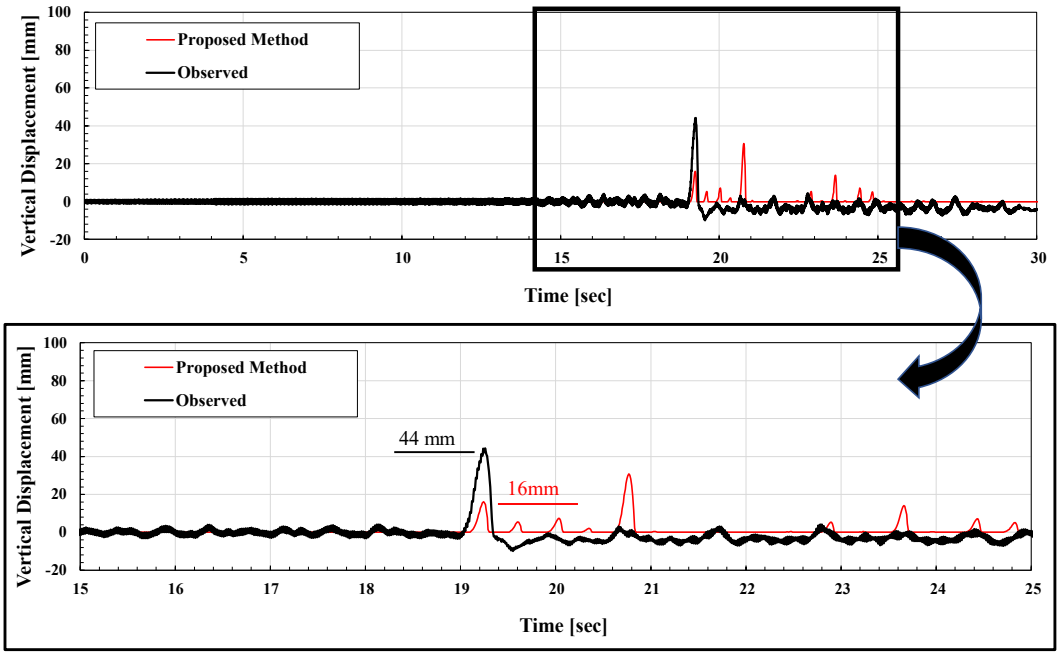

Figure 4.10 Uplift Displacement of Tank-A, CN180° (Observed vs. Proposed Method)

Comparison of uplift displacement was also made between the calculation results by the method of Malhotra and Veletsos (1994) [1], the estimation by the Eurocode 8 method [3], and the observational record. As shown in Figure 4.11, the uplift displacement calculated by Malhotra's method is about ten times larger than the recorded value. On the other hand, the uplift displacement estimated by the Eurocode 8 method is about six times larger than the recorded value. This indicates that the proposed method yields more accurate results compared to the conventional methods.

Figure 4.12 shows a comparison between the overturning moment calculated by the proposed method and that by Malhotra's method. Since there is no major difference in the magnitude of overturning moment between the two methods, the significant difference found in the uplift displacement is considered to have been caused by the rotational inertia term of liquid mass which is included in the proposed method as a factor contributing to the tank rocking motion.

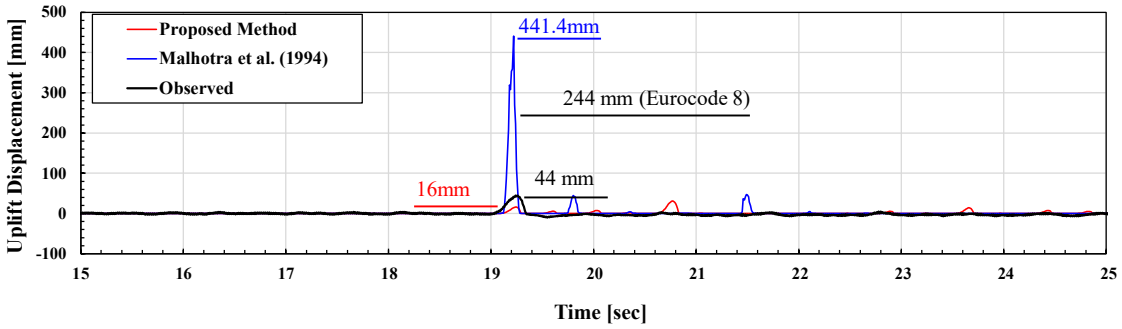

Figure 4.11 Uplift Displacement of Tank-A, CN180° (Observed vs. Proposed Method vs. Malhotra's Method)

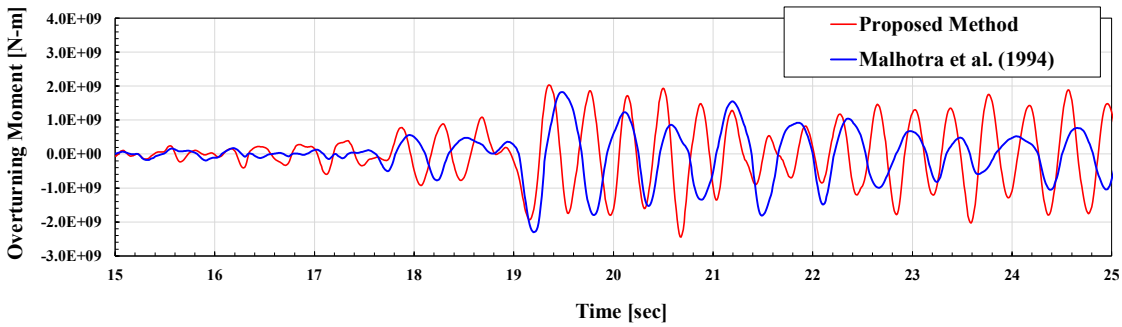

Figure 4.12 Overturning Moment of Tank-A (Proposed Method vs. Malhotra's Method)

4.4 Further Investigations

4.4.1 Effect of Difference in Uplift Commencement Condition on Tank Rocking Response Calculation

This part of the study investigates the effect of difference in uplift commencement condition on tank rocking response calculation. Figure 4.13 (a) compares the calculation results of uplift displacement by the proposed method for different uplift commencement conditions. The black curve represents the calculation under uplift commencement condition that takes into account the additional mass due to the content liquid, and the red curve represents the calculation under uplift commencement condition that takes into account only the tank mass (conventional condition). The figure shows a slight difference in the uplift displacement calculation results depending on the difference in the uplift commencement condition. This is because the difference in the uplift commencement condition causes a difference in the angular velocity at the time of the main uplift.

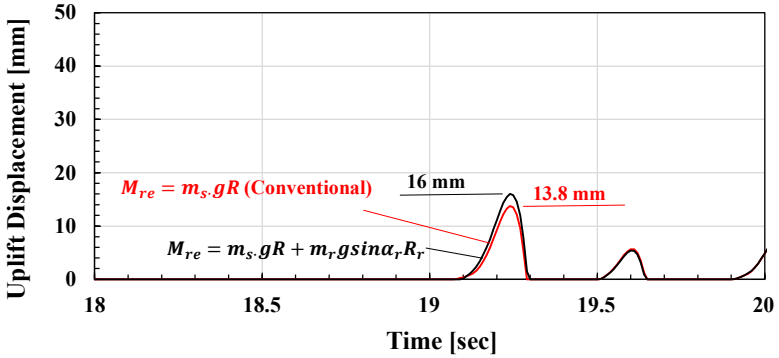

(a) Time Histories of Uplift Displacement

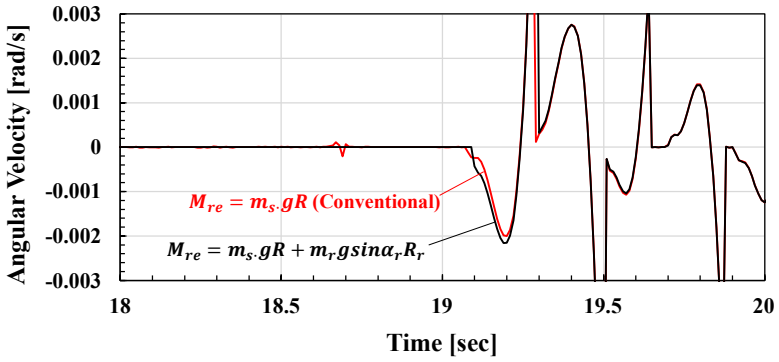

(b) Time Histories of Angular Velocity

Figure 4.13 Examination of Uplift Commencement Condition [Tank-A]

4.4.2 Estimation of Uplift due to Out-of-Round Deformation of Tank Shell

The additional uplift due to the out-of-round deformation of the tank shell is examined. An analytical model developed by Hayashi (2019) is used herein [4], and the formula to estimate the additional uplift displacement $v(\theta_b)$ due to the out-of-round deformation δ of the tank shell is shown in Eq. (4.1). In this model, a simple elliptical deformation is considered as Figure 4.14 shows. In Hayashi's model, the additional uplift displacement $v(\theta_b)$ can be estimated by giving the out-of-round deformation δ, but the response of the out-of-round deformation δ cannot be obtained by Hayashi's model. Therefore, the out-of-round deformation δ should be estimated.

It can be considered that the uplift due to the out-of-round deformation of the tank shell is independent of the tank rocking response. In other words, the total uplift displacement can be obtained by simply adding the uplift displacement due to the tank rocking response to the uplift displacement due to the out-of-round deformation of the tank shell. Because, even if the tank shell shows out-of-round deformation, it does not affect the rotational motion of the tank. However, it is quite conceivable that the distribution of liquid pressure caused by the dynamic response of the tank affects the out-of-round deformation of the tank shell.

Considering Tank-A, the relationship between the additional uplift and the out-of-round deformation of the tank shell is obtained as shown in Figure 4.15. The maximum uplift displacement recorded is 44 mm, while that calculated by the proposed method is 16 mm, with a difference of 28 mm. Their difference is likely to be attributable to out-of-round deformation of the tank shell. It is highly possible for a tank with a large diameter of 82 m to experience out-of-round deformation on the order of 17 mm. For further investigation, development of a response analysis method for out-of-round deformation of the tank shell is necessary.

$$v(\theta_b) = \frac{2RH}{\delta}\left[1 - \cos\left\{\tan^{-1}\left(\frac{\delta}{2H}(1-\cos\theta_b)\right)\right\}\right] \tag{4.1}$$

where θ_b is an angle of a line formed by an arbitrary point on the tank shell and the center of the tank shell cross section with respect to the 0°-180° line; R is the tank radius; and H is the height of the tank shell.

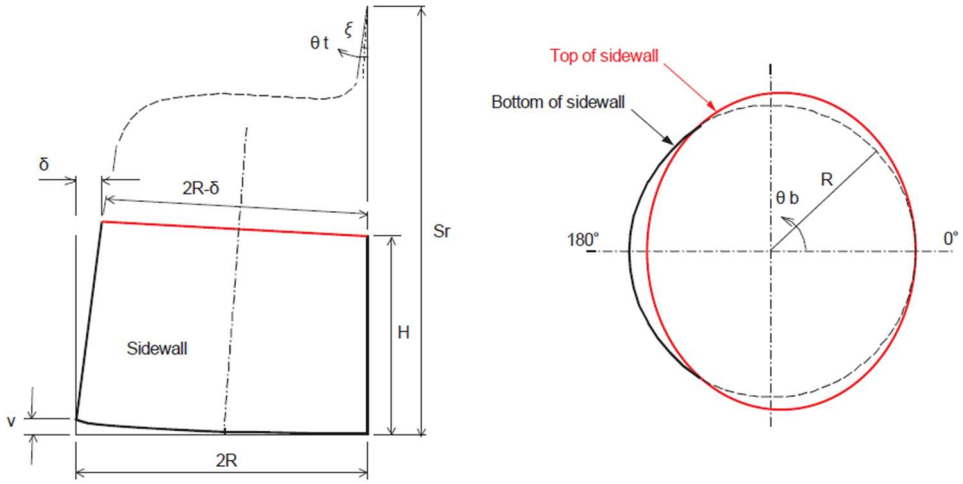

Figure 4.14 Analytical Model of Uplift due to Out-of-Round Deformation of Tank Shell [4]

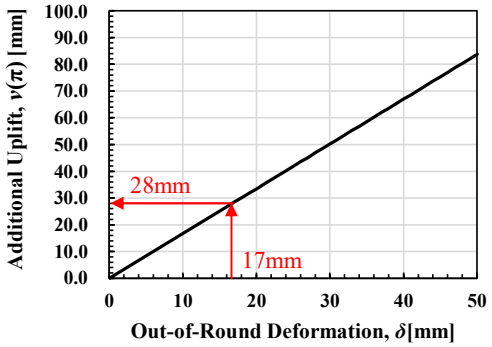

Figure 4.15 Relationship between Additional Uplift and Out-of-Round Deformation of Tank Shell [Tank-A]

4.4.3 Effect of Restoring Moment due to Pulling Down of Uplifted Part of Bottom Plate on Tank Rocking Response

Most conventional methods only consider the static equilibrium between the overturning and restoring moments. However, as the investigation in Chapter 2 revealed that the rotational inertia force of content liquid dominates the tank rocking response, while the restoring moment due to pulling down of the uplifted part of bottom plate has less influence on the tank rocking response. This subsection examines its effects on the time history of the uplift displacement.

To examine the effect of the restoring moment on tank rocking response, (1) define the rotational spring stiffness k_θ from the relationship between the rocking angle θ and the restoring moment $M(\theta)$, (2) substitute it into the proposed method, and (3) conduct the time history response analysis. Equation (4.2) shows the stiffness matrix used in the proposed method that includes k_θ (see also Eq. (3.20c)). Under the static liquid pressure, the relationship between the rocking angle θ and the restoring moment $M(\theta)$ is calculated by Malhotra's method [7]. Figure 4.16 shows its results. As Equation (4.3) shows, the rotational spring stiffness k_θ is defined from the ratio of increment of the restoring moment $\Delta M(\theta)$ to increment of the rocking angle $\Delta\theta$ (see also Figure 4.16).

$$[K] = \begin{bmatrix} k_b & 0 \\ 0 & -k_\theta \end{bmatrix} \tag{4.2}$$

$$k_\theta = \Delta M(\theta)/\Delta\theta \tag{4.3}$$

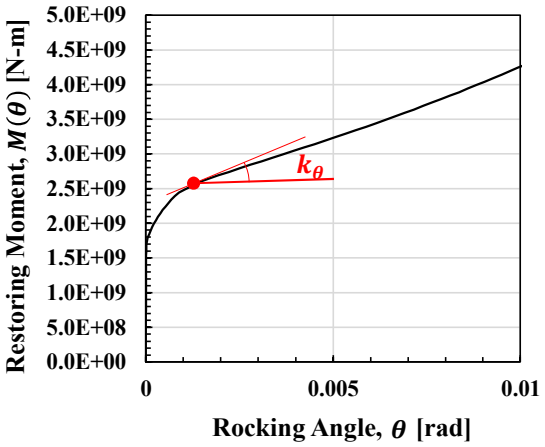

Figure 4.16 Relationship between Rocking Angle and Restoring Moment [Tank-A]

Figure 4.17 overplots the results of the time history that considers the rotational spring. It can be seen that the rotational spring reduces the response of the uplift displacement of tank bottom by about 6% to 9%. In other words, effect of the restoring moment on the tank uplift is negligible within practical range.

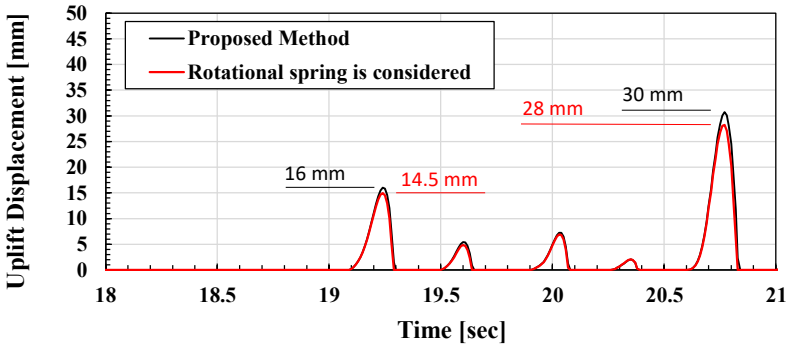

Figure 4.17 Examination of Effect of Rotational Spring on Tank Rocking Response

4.4.4 Time History Response Analyses of Uplift Displacement by Other Methods

Time history response analyses are conducted by methods of Yuan et al. (2004) and Vathi et al. (2017) in the same manner as the case study introduced earlier (refer to literature for the theory of each method). The results are summarized in a table at the end of this subsection, along with the maximum uplift displacement estimated by the Eurocode 8 method.

Yuan, Kawano and Yoshida (2004) [5]: The results of time history response analysis by Yuan's method are shown here. Figures 4.19 (a) and (b) show the results of time history response analysis of a 60,000 kL LNG storage tank. The damping constant h_b is set to 0.05. A ground acceleration of 300-gal amplitude was input (see Figure 4.2). The relationship between restoring force and translational displacement is shown in Figure 4.18 (see the red line). For simplicity, the second stiffness was assumed to be zero in this calculation. In this model, it is assumed that when the uplifted end of the bottom plate

becomes plastic, the stiffness of the system transitions to the second stiffness (see Reference [5] for details). Comparing the results of Yuan's method and the dynamic FE analysis, the maximum value differs by about two times. This may be caused by changes in the restoring force characteristics due to time history of dynamic hydraulic pressure acting on the bottom plate and lack of consideration of the rotational inertia force.

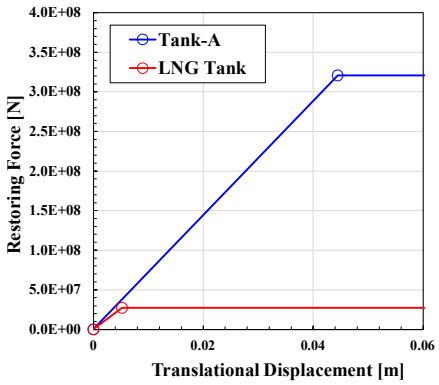

Figure 4.18 Relationship between Restoring Force and Translational Displacement (Bilinear Approximation)

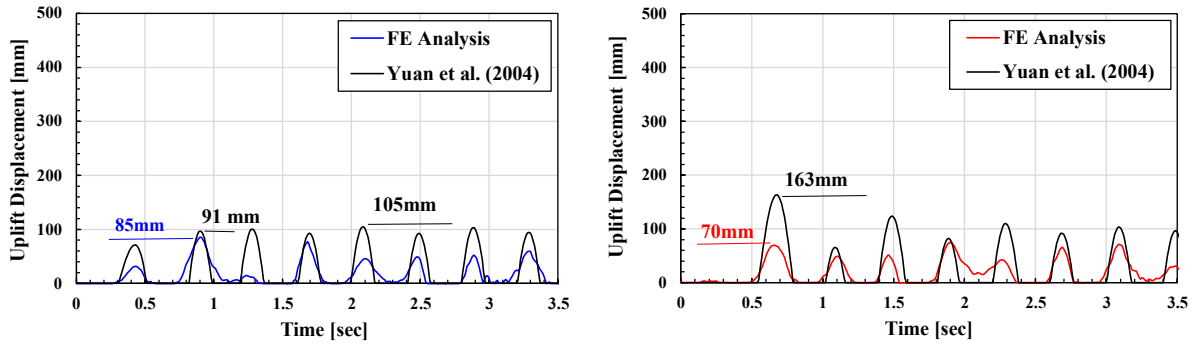

(a) Left Bottom Edge (b) Right Bottom Edge

Figure 4.19 Calculation Results of Uplift Displacement by Yuan's Method and Dynamic FE Analysis [60,000 kL LNG Storage Tank]

Figure 4.20 shows the results of time history response analysis of Tank-A. The damping constant h_b is set to 0.05. The ground acceleration observed in the Tank-A yard (CN0°- CN180° direction) was input (see Figure 4.4). The relationship between restoring force and horizontal displacement is shown in Figure 4.18 (see the blue line). Comparing the results of Yuan's method and the observational record, these maximum uplift displacements are in good agreement, though at different times.

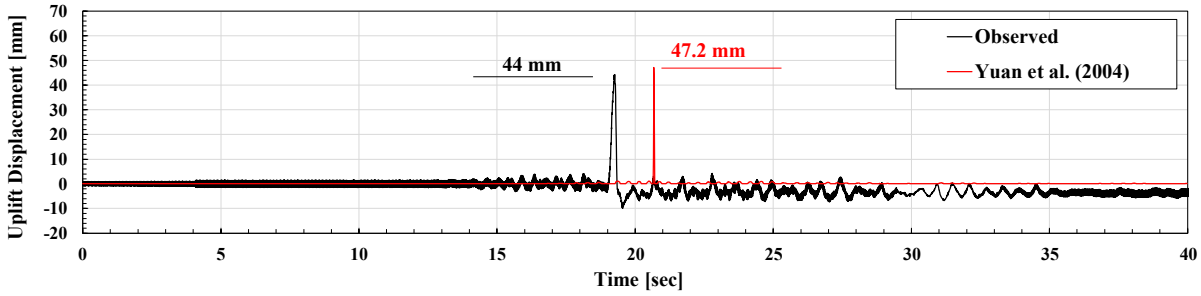

Figure 4.20 Calculation Result of Uplift Displacement by Yuan's Method and Observational Record [Tank-A, 114,800 kL Oil Storage Tank]

Vathi and Karamanos (2017) [6]: Figures 4.22 (a) and (b) show the results of time history response analysis of a 60,000 kL LNG storage tank under the ground acceleration of 300-gal amplitude. The damping constants for the translational motion h_b and for the rotational motion h_r are set to 0.05 and 0.10, respectively. The relationship between restoring moment and rotational angle of the system is shown in Figure 4.21 (see the red line). This relationship was obtained by Malhotra's method [7], and approximated by bilinear characteristics of the restoring force. When calculating this relationship, the gradual decrease in the hydraulic pressure acting on the bottom plate due to the gradual increase in overturning moment was considered. Comparing the results of Vathi's method and the dynamic FE analysis, although the initial uplifts do not match, the later uplifts are in good agreement.

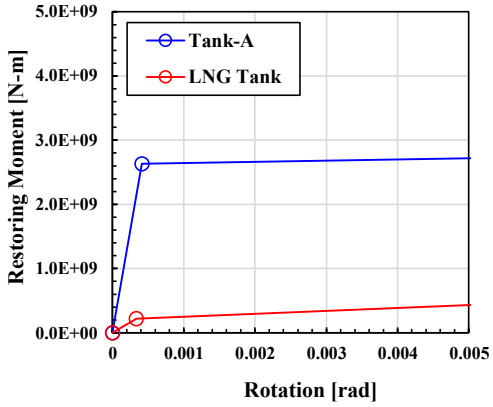

Figure 4.21 Relationship between Restoring Moment and Rotational Angle (Bilinear Approximation)

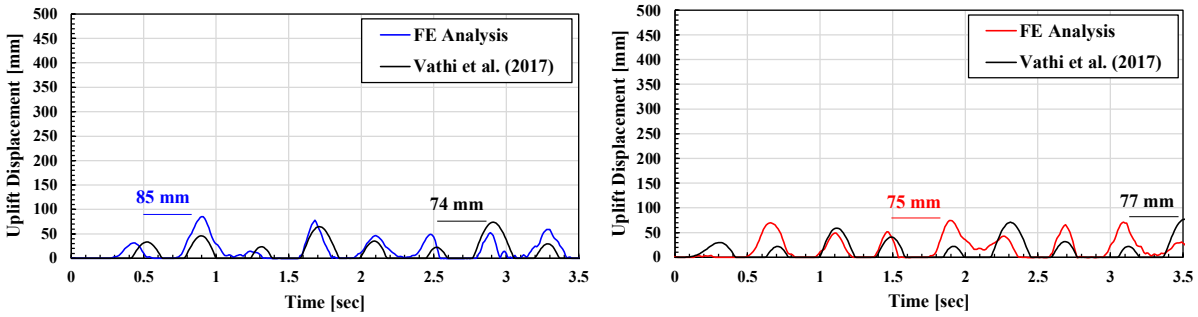

(a) Left Bottom Edge (b) Right Bottom Edge

Figure 4.22 Calculation Results of Uplift Displacement by Vathi's Method and Dynamic FE Analysis [60,000 kL LNG Storage Tank]

Whereas Figure 4.23 shows the results of time history response analysis of Tank-A under the ground acceleration observed in the Tank-A yard. The damping constants for the translational motion h_b and for the rotational motion h_r are set to 0.05 and 0.10, respectively. The relationship between restoring moment and rotational angle is shown in Figure 4.21 (see the blue line). This relationship was obtained by the same method as that used for the case of an LNG tank. Comparing the results of Vathi's method and the observational record, the maximum values differ by about 4.4 times and do not coincide in time. Furthermore, rotation continues even after the seismic motion has weakened. This may be

because the system has a natural period in the direction of rotation due to the moment of inertia and the rotating spring.

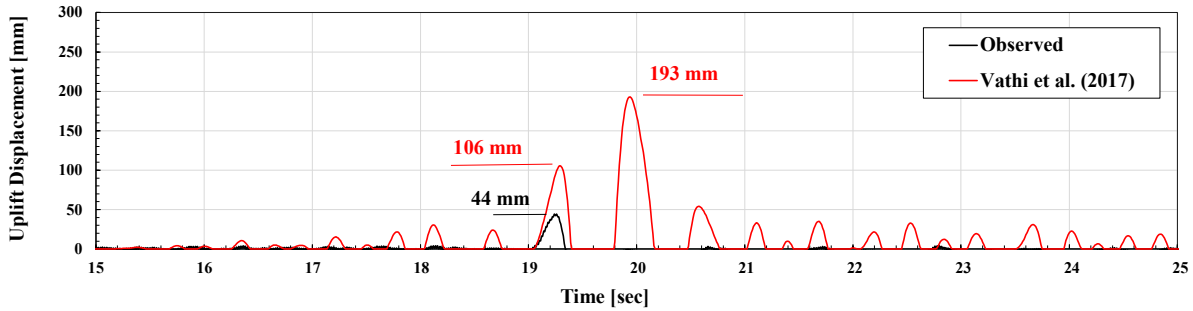

Figure 4.23 Calculation Result of Uplift Displacement by Vathi's Method and Observational Record [Tank-A 114,800 kL Oil Storage Tank]

Finally, the results of case studies are summarized in Table 4.3. The results by the Eurocode 8 method are also added to the table, but they are much larger than the dynamic FE analysis results or the recorded data. This is because the overturning moment is estimated based on the translational response only, ignoring the coupled rotational motion. The method developed in this study may have a higher accuracy than other methods, but there is still room for improvement.

Table 4.3 Summary of Case Studies (Uplift Displacement [mm])

Methods	LNG Tank ① Rigid Shell 1000-gal harmonic ground excitation	LNG Tank ② Elastic Shell 300-gal harmonic ground excitation	Tank-A Elastic Shell Seismic ground excitation	Remarks
Observational record	-	-	**44** (at 19.26 sec)	2018 Hokkaido Eastern Iburi Earthquake [2]
FE Analysis	**114** (at 2.93 sec): Left **148** (at 3.14 sec): Right	**85** (Max)	-	Solver: LS-Dyna
Yoshida et al. (2022)	98 (at 2.86 sec): Left 97 (at 3.06 sec): Right	171 (Max)	16 (at 19.24 sec) (Max: 31)	Translational damping constant = 0.05
Malhotra et al. (1994)	-	296 (Max)	441 (at 19.22 sec) (Max: 441)	Translational damping constant = 0.05
Yuan et al. (2004)	-	163 (Max)	46.2 (at 20.68 sec) (Max: 46)	Translational damping constant = 0.05 Bilinear restoring force characteristics
Vathi et al. (2017)	-	77 (Max)	106 (at 19.29 sec) (Max: 193)	Translational damping constant = 0.05 Rotational damping constant = 0.10
Eurocode 8	514 (Max)	2186 (Max)	244 (Max)	

4.5 Conclusions

In this chapter, the accuracy of the proposed method developed for analyzing a time history of tank rocking motion was verified through a comparative approach. The principal conclusions of this chapter are summarized as follows:

- To verify the accuracy of the proposed method, a comparison was conducted between the calculation results of uplift displacement by the proposed method and those by the dynamic FE analysis. The findings show that the uplift responses calculated by the two methods agree well with a reasonable accuracy, except for the initial uplifts. Since the reason for the discrepancy in the initial uplifts is unclear, more should be studied to identify the exact cause, thereby improving the accuracy of the proposed method. It has been also found through further investigation that the proposed method is more accurate than the conventional method.

- To verify the accuracy of the proposed method, comparison of uplift displacement was also conducted between the calculations by the proposed method, Malhotra's method and the Eurocode 8 method as well as the observational record. The findings show that the proposed method has a higher accuracy than the conventional calculation methods used for the tank bottom uplift displacement.

- In order to prevent damage to the tank bottom plate and tank shell due to the uplift of the tank bottom plate, it is necessary to accurately predict the maximum uplift displacement and the number of times of uplift caused by a scenario earthquake. Therefore, further research is necessary to improve the accuracy of the proposed method, including the followings.

  (1) Investigation of the effects of the impact immediately after landing (changing of the pivoting edge) on responses in the translational and rotational directions

(2) Investigation of the factors that determine the maximum uplift displacement

- Investigation of the effect of foundation elasticity on the tank rocking response

- Development of a response analysis method for out-of-round deformation of the tank shell

(3) Validation of the definition of the effective mass of the content liquid related to the rocking motion

(4) Shaking table tests using a large-scale tank model

(5) Formulation of the reasonable uplift commencement condition

- It is also necessary to develop a simplified method for calculating the maximum uplift displacement using the response spectrum for practical purpose.

Bibliography

[1] Malhotra, P.K. and Veletsos, A.S., 1994, “Uplifting Response of Unanchored Liquid-Storage Tanks,” J. Struct. Div., ASCE, Vol. 120, Issue 12, pp. 3525–3547.

[2] Hatayama, K., Nishi, H., Hayashi, M. and Tokutake, K., 2020, “Damage to Oil Tanks caused by Severe Strong Ground Motion due to The 2018 Hokkaido, Japan Iburi-Tobu Earthquake (Mw6.6),” Proc. ASME PVP Conference, Seismic Engineering, Paper No. PVP2020-21447.

[3] European Committee for Standardization, 2006, “Silos, Tanks and Pipelines,” Eurocode 8, Part 4, CEN/TC 250, EN 1998-4, Brussels.

[4] Hayashi, S., 2019, “Seismic Design Procedure for The Bottom Plate Corner Connection of Flat-Bottom Cylindrical Tanks due to Uplift Response of The Bottom Plate During Earthquakes,” Ph.D. Dissertation, Tottori University, Japan.

[5] Yuan, H., Kawano, K. and Yoshida, S., 2004, “Study on Restoring Force Models of Nonlinear Uplift Behavior of Unanchored Oil Storage Tank Under Strong Seismic Excitation,” Proc. ASME PVP Conference, Seismic Engineering, Paper No. PVP2004-3070, pp. 195-200.

[6] Vathi, M. and Karamanos, S.A., 2017, “A Simple and Efficient Model for Seismic Response and Low-Cycle Fatigue Assessment of Uplifting Liquid Storage Tanks,” Journal of Loss Prevention in The Process Industries, Vol. 53, pp. 29-44.

[7] Malhotra, P.K. and Veletsos, A.S., 1994, “Uplifting Analysis of Base Plates in Cylindrical Tanks,” J. Struct. Div., ASCE, Vol. 120, Issue 12, pp. 3489-3505.

Chapter 5

Conclusions

Chapter 5

Conclusions

Chapter 5 concludes this study. This dissertation aims at presenting a method to analyze the time history of rocking response of liquid storage tanks by developing several mechanical models that enable to analytically describe uplift phenomenon of liquid storage tanks from several aspects. First, the effect of the rotational inertia force of the content liquid on the rocking motion of a liquid storage tank is examined, and a beam model that has been proposed and is considered to be correctly modeled is selected. Next, the derivation of the mechanical model of the tank rocking motion that takes into account the rotational inertia force of the content liquid is explained. Finally, the accuracy of the proposed method is verified by comparing the calculation results of the proposed method with those of the dynamic FE analysis and conventional methods as well as observational record.

In Chapter 1, the structures of above-ground liquid storage tanks and their typical damage found during reconnaissance surveys performed after earthquakes were briefly reviewed. A review was also made on the earlier studies on rocking response of liquid storage tanks due to seismic ground excitation. Finally, the objectives of the work were described.

In Chapter 2, preliminary preparations for the development of a method of tank rocking response analysis were conducted, including (1) selection of a suitable method for describing the uplift displacement-width relationship, (2) investigation of contribution of rotational inertia force of content liquid to the tank rocking motion, and (3) investigation of uplift commencement condition. These were conducted to determine the essential conditions and parameters for tank rocking response analysis, and following findings were obtained.

- **Relationship between Uplift Displacement and Uplift Width of Bottom Plate:** By comparing the uplift displacement and the uplift width obtained from the results of the dynamic FE analysis and those obtained by several beam models, it was shown that the simple beam model could be used to calculate the uplift displacement-width relationship when the uplift displacement was small (e.g., $w/H \leq 0.005$). However, when the uplift displacement was large (e.g., $w/H > 0.005$), accurate determination of its relationship with the uplift width could be made by considering the geometric nonlinearity of the beam and the reduction of fluid pressure acting on the tank bottom plate due to dynamic pressure.
- **Rotational Inertia Force of Content Liquid:** From the results of the dynamic FE analysis, significant contribution of the rotational inertia force of the content liquid to the tank rocking motion was confirmed. On the other hand, the restoring moment composed by the circumferential distribution of vertical reaction force at the shell-to-bottom connection could not adequately resist the overturning moment.
- **Experimental Study on Uplift Commencement Condition:** Using a scaled model tank made of PVC on a shaking table, the horizontal base acceleration required for the commencement of tank uplift was examined. The test results revealed the presence of added mass as a contributing factor to the uplift commencement condition. Further study is needed to quantify the mass mathematically.

In Chapter 3, equations of motion for the mechanical model of a liquid storage tank in rock are derived based on the analogy between the 2DOF model and the tank in rock. The computational method of the derived equations of motion was then explained. The principal conclusions of this chapter are summarized as follows:

- Equations of motion for the 2DOF system with freedom in the translational and rotational directions were derived. Then computational method of the equations of motion for the 2DOF

model was explained. Accuracy of the computational method was verified by comparison with the results of experimental test.

- Based on the analogy between the 2DOF model and the tank in rock, equations of motion for the mechanical model of a liquid storage tank were derived. Then the computational method of the equations of motion for the mechanical model of a liquid storage tank was developed by introducing the rocking angle-uplift ratio relationship calculated by Malhotra's beam model to the computational method.

In Chapter 4, the accuracy of the proposed method developed for analyzing the tank rocking response was verified by comparing the uplift displacement between the calculation results by the proposed method and those by the dynamic FE analysis as well as observational record. Comparison of uplift displacement was also made between the calculation results by the proposed method and those by the conventional methods. The findings show that the proposed method yields more accurate results compared to the conventional methods. The principal conclusions of this chapter are summarized as follows.

- To verify the accuracy of the proposed method, a comparison was conducted between the calculation results of uplift displacement by the proposed method and those by the dynamic FE analysis. The findings show that the uplift responses calculated by the two methods agree well with a reasonable accuracy, except for the initial uplifts. Since the reason for the discrepancy in the initial uplifts is unclear, more should be studied to identify the exact cause, thereby improving the accuracy of the proposed method. It has been also found through further investigation that the proposed method is more accurate than the conventional method.
- To verify the accuracy of the proposed method, comparison of uplift displacement was conducted between the calculation results by the proposed method, Malhotra's method and the

Eurocode 8 method as well as the observational record. The findings show that the proposed method has a higher accuracy than the conventional calculation methods used for the tank bottom uplift displacement.

- In order to prevent damage to the tank bottom plate and tank shell due to the uplift of the tank bottom plate, it is necessary to accurately predict the maximum uplift displacement and the number of times of uplift due to a scenario earthquake. Therefore, further research is necessary to improve the accuracy of the proposed method, including the followings.

  (1) Investigation of the effects of the impact immediately after landing (changing of the pivoting edge) on responses in the translational and rotational directions

  (2) Investigation of the factors that determine the maximum uplift displacement

  - Investigation of the effect of foundation elasticity on the tank rocking response
  - Development of a response analysis method for out-of-round deformation of the tank shell

  (3) Validation of the definition of the effective mass of the content liquid related to the rocking motion

  (4) Shaking table tests using a large-scale tank model

  (5) Formulation of the reasonable uplift commencement condition

- It is also necessary to develop a simplified method for calculating the maximum uplift displacement using the response spectrum for practical purpose.

Although more work remains to be done for improving the proposed method as shown above, the purpose of this research, the development of a tank rocking response analysis, has been achieved.

Publications of Author &

Awards for Publications of Author

Publications of Author

Refereed Papers

1. Yoshida, Y., Taniguchi, T. and Nakashima, T., 2020, “Uplift Deformation of The Bottom Plate of The Cylindrical Shell Tanks Under Steady-State Response of Tank Rocking Motion,” Proc. ASME PVP Conference, Seismic Engineering, Paper No. PVP2020-21418.

2. Yoshida, Y., Taniguchi, T. and Nakashima, T., 2021, “Verification of Accuracy of The Beam Model and Resistant Moment Generated by Base Uplifting of Flat-Bottom Cylindrical Shell Tanks,” Proc. ASME PVP Conference, Seismic Engineering, Paper No. PVP2021-61319.

3. Yoshida, Y., Taniguchi, T. and Nakashima, T., 2022, “Rocking Response Analysis of Flat-Bottom Cylindrical Tanks Considering Rotational Inertia of Content Liquid,” Proc. ASME PVP Conference, Seismic Engineering, Paper No. PVP2022-84909.

Presentations

1. Yoshida, Y., Taniguchi, T. and Nakashima, T., 2020, “Characteristics of Uplift Force at Uplifted End of The Bottom Plate of The Cylindrical Shell Tanks under Steady-State Response of Tank Rocking Motion,” Proc. JSCE, Paper No. I-442. (in Japanese)

2. Yoshida, Y., Taniguchi, T. and Nakashima, T., 2021, “A Study on Restoration Mechanism in Rocking Behavior of Flat-Bottom Cylindrical Storage Tank During Earthquake,” Proc. Dynamics and Design Conference 2021, JSME, Paper No. 222. (in Japanese)

Awards for Publications of Author

1. Excellent Paper Award (November 1, 2020)

Japan Society of Civil Engineers 2020 Annual Meeting, Online, Japan, September 9-11, 2020

Title:

Yoshida, Y., Taniguchi, T. and Nakashima, T., 2020, “Characteristics of Uplift Force at Uplifted End of The Bottom Plate of The Cylindrical Shell Tanks under Steady-State Response of Tank Rocking Motion,” Proc. JSCE, Paper No. I-442. (in Japanese)

2. Outstanding Student Paper, PhD Category (July 20, 2022)

Rudy Scavuzzo Student Paper Competition at the PVP2022, Las Vegas, USA, July 17-22, 2022

Title:

Yoshida, Y., Taniguchi, T. and Nakashima, T., 2022, “Rocking Response Analysis of Flat-Bottom Cylindrical Tanks Considering Rotational Inertia of Content Liquid,” Proc. ASME PVP Conference, Seismic Engineering, Paper No. PVP2022-84909.

Appendix

Appendix

Appendix 1　Dynamic FE Analysis Used in This Study

Outline of the dynamic FE analysis used in this paper is briefly described here. This analysis was originally conducted in Bib. [1]. The calculation was conducted by LS-DYNA (ver.7.1.1). The analysis conditions for the tank model are as follows.

(1) Tank Model

- The tank model consists of a cylindrical shell and a flat bottom, but without a roof.
- The tank is unanchored with respect to a foundation.
- The mechanical properties of the tank are described in Table A1.1.
- To prevent effects of out-of-round deformation of the sidewall, the tank model has the multistage rigid stiffeners that are modeled by rigid elements spaced at intervals of 600.5 mm (see Figure A1.1 (e)). Therefore, the tank shell behaves rigidly.
- Symmetry in the behavior of the tank with respect to the x-z plane enables to use a half-part of the tank model (see Figures A1.1(a) and (b)).
- The sidewall and the bottom plate are modelled by shell elements consisting of 21,639 nodes and 21,640 elements.
- The sizes of the finite elements of the connection part are shown in Figure A1.1 (f).
- The numerical model of the tank is assumed to have a structural damping ratio of 5%.
- Plastic deformation is not considered.

Table A1.1 Mechanical Properties of Tank Model

Tank Diameter, *D* [m]		51.5
Height of Tank [m]		31.44
Thickness of Sidewall [mm]		16.0 to 54.5
Thickness of Bottom Plate [mm]	General Part	6.0
	Annular Part	16.0
Young's Modulus of Aluminum Alloy [GPa]		70
Poisson's Ratio of Aluminum Alloy [-]		0.3
Density of Aluminum Alloy [kg/m^3]		2670

(2) Content Liquid

- The liquid surface is free surface.
- The mechanical properties of the content liquid are described in Table A1.2.
- The Arbitrary Lagrangian Eulerian (ALE) approach is employed for modeling the fluid-structure interaction.
- A fluid part is modelled by Eulerian elements consisting of 301,168 nodes and 301,400 elements (see Figure A1.1 (c)).

Table A1.2 Mechanical Properties of Content Liquid (LNG)

Liquid Height, *H* [m]	28.824
Density of Content Liquid [kg/m^3]	480
Viscosity of Content Liquid [MPa·sec]	1.0x10^{-20}

(3) Foundation

- The tank is supported by a foundation, which is modelled by solid elements consisting of 15,651 nodes and 10,640 elements (see Figure A1.1 (d)).
- The mechanical properties of the foundation are shown in Table A1.3.
- The tank bottom plate is in contact with the foundation. The static and dynamic friction coefficients between them are both set as 1.0×10^5 to prevent slip motions.

Table A1.3 Mechanical Properties of Foundation

Diameter of Foundation [m]	71.50
Thickness of Foundation [m]	10
Density of Foundation [kg/m^3]	7700
Young's Modulus of Foundation [GPa]	30
Poisson's Ratio of Foundation [-]	0.3

The first natural period of the tank bulging motion is 0.38 seconds (if the tank model does not have the multistage rigid stiffeners). Therefore, the driving period of horizontal sinusoidal base acceleration is set as 0.4 seconds and amplitude is set as 10 m/s^2. The time history response analysis of this tank model was carried out by inputting this harmonic ground acceleration to the bottom of foundation. Some examples of the dynamic FE analysis results are shown below.

- Figure A1.2 shows the time histories of uplift displacement for each bottom edge.
- Figure A1.3 depicts a shape of the uplifted area.
- Figures A1.4 and A1.5 show changes in the uplift width with changes in the uplift displacement.
- Figures A1.6 shows the relationship between dimensionless uplift width and dimensionless uplift displacement.

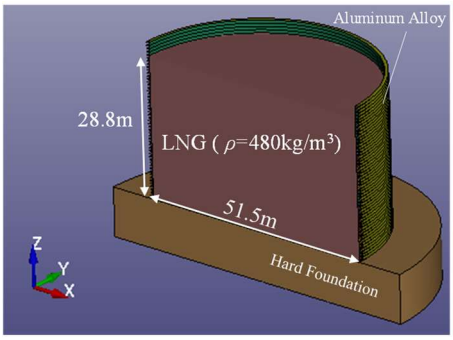

(a) General View

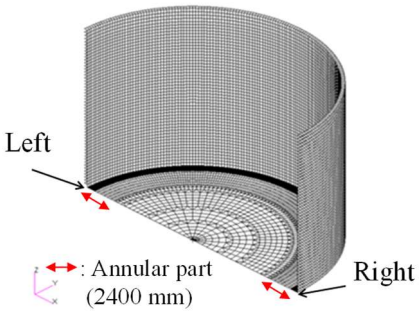

(b) Tank Shell and Bottom Plate

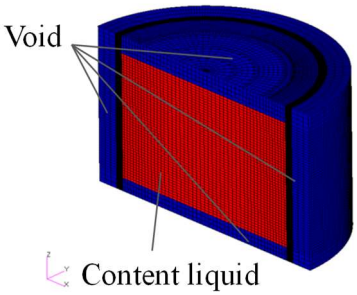

(c) Content Liquid

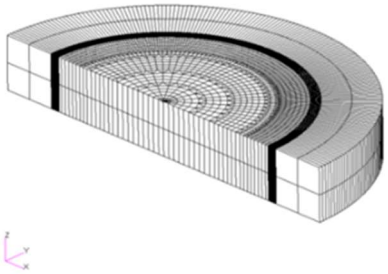

(d) Foundation

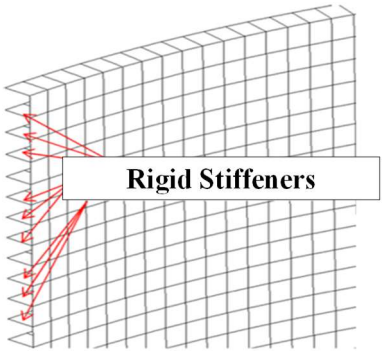

(e) Multistage Stiffeners

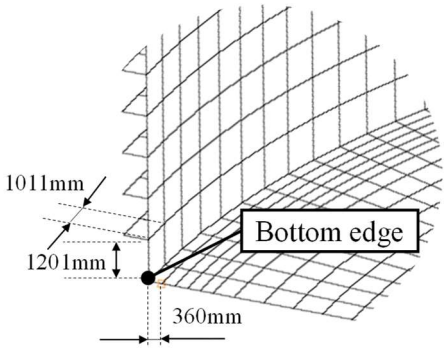

(f) Mesh Sizes

Figure A1.1 Numerical Model

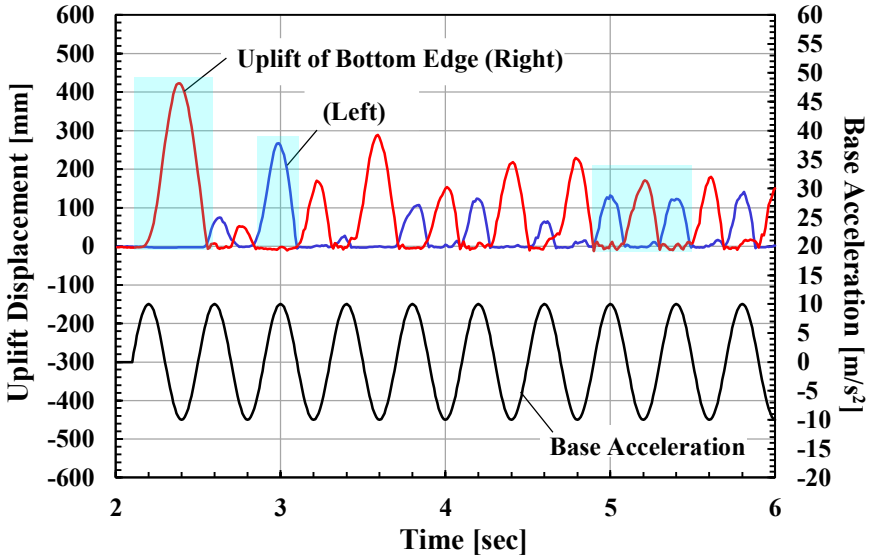

Figure A1.2 Time Histories of Uplift Displacement Computed by Dynamic FE Analysis

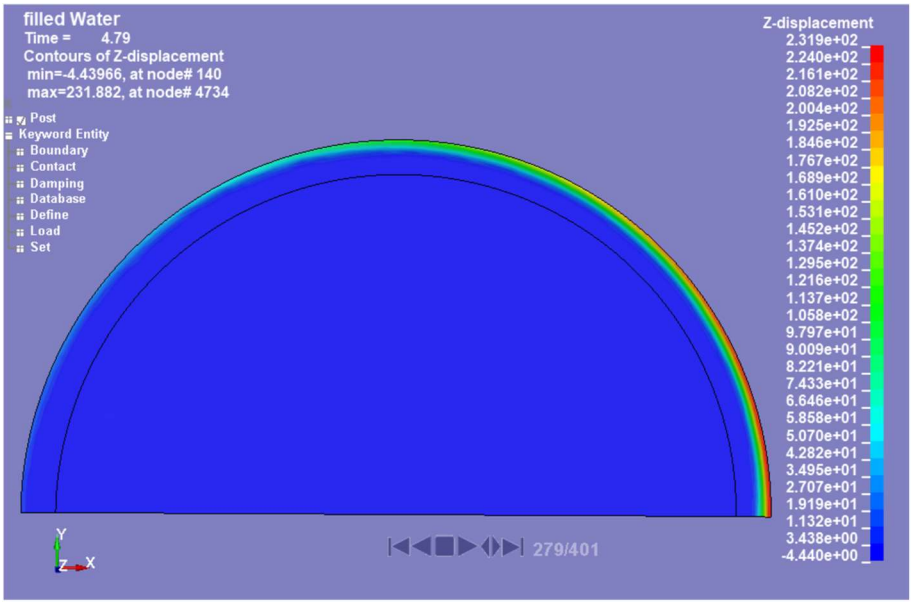

Figure A1.3 Uplifted Area Computed by Dynamic FE Analysis

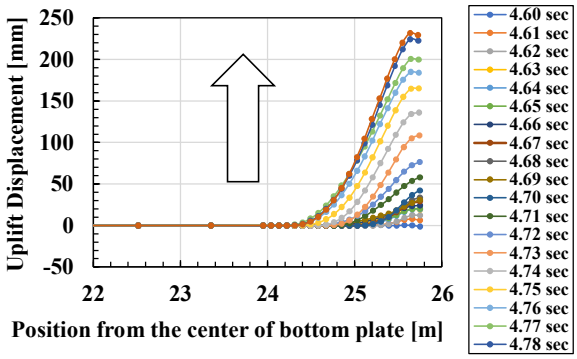

(a) Tracking of Uplifting

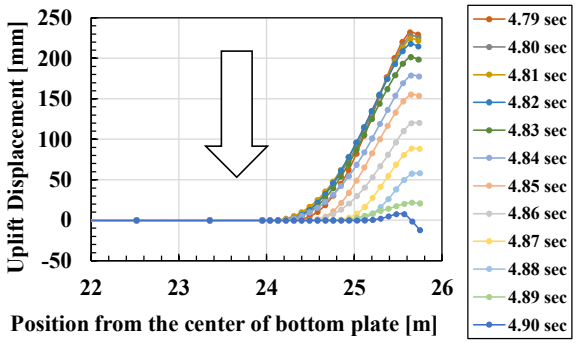

(b) Tracking of Landing

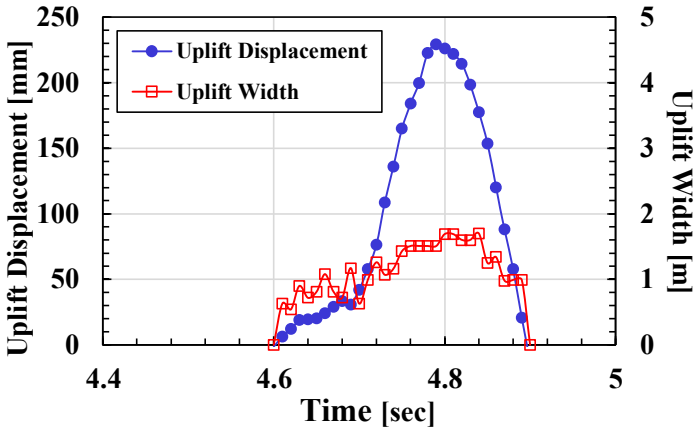

(c) Time Histories of Uplift Width and Displacement

Figure A1.4 Calculated Uplift Deformation (at Right Bottom Edge)

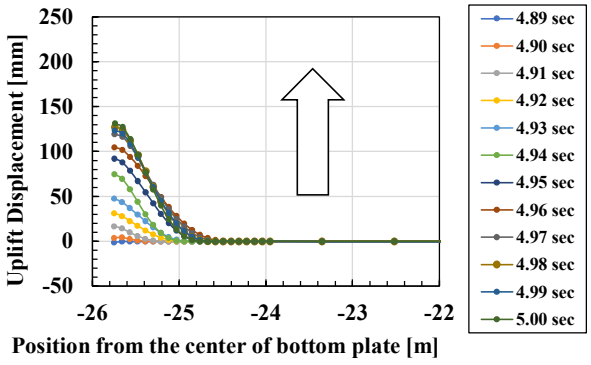

(a) Tracking of Uplifting

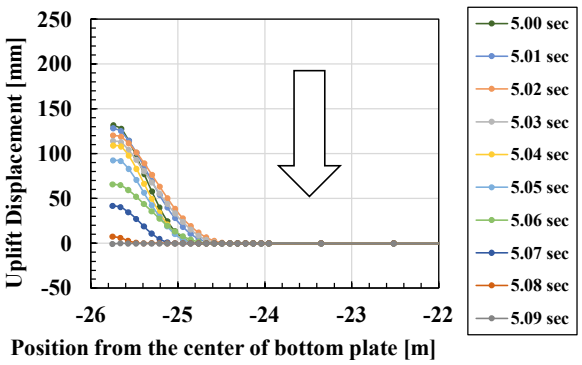

(b) Tracking of Landing

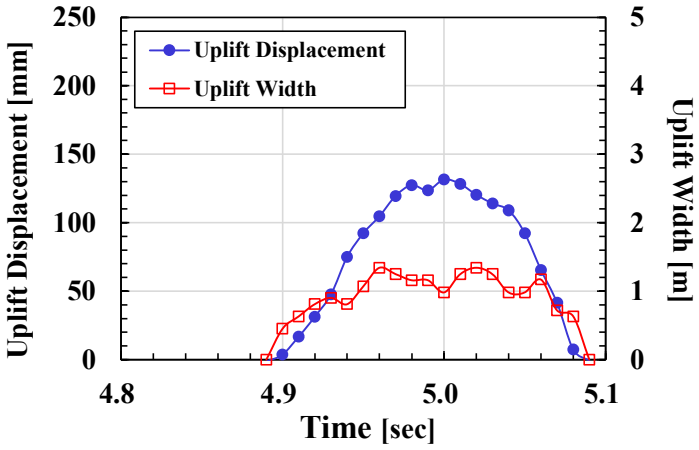

(c) Time Histories of Uplift Width and Displacement

Figure A1.5 Calculated Uplift Deformation (at Left Bottom Edge)

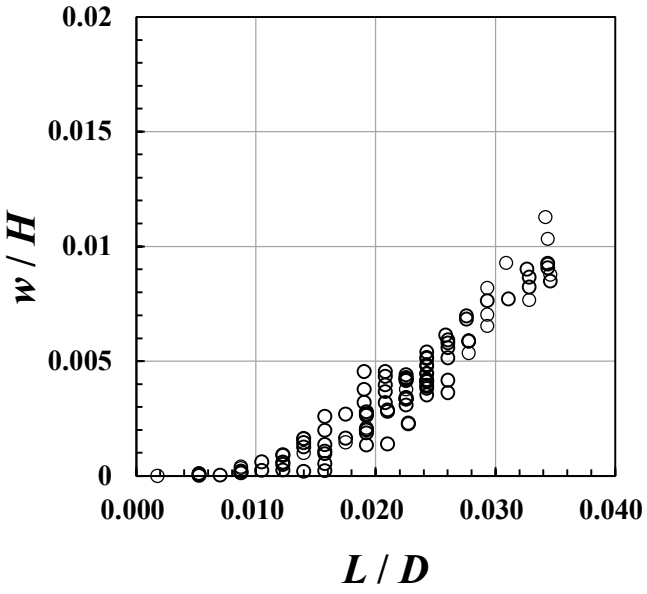

Figure A1.6 Relationship between Dimensionless Uplift Width and Dimensionless Uplift Displacement Plotted from Time Histories by Dynamic FE Analysis*

* Time histories of uplift displacement-width relationship (Range highlighted with ■ in Figure A 1.2) are plotted. Where, w is the uplift displacement; H is the liquid height; L is the uplift width; and D is the tank diameter.

Appendix 2 Derivation of Formulas for Calculating Uplift and Contact Areas

Formulas for calculating the uplift area and the contact area are derived in this section. The shape of the area where the bottom plate uplifted is assumed to be a crescent moon. Using the law of sines for the triangle shown in Figure A2.1, the following equations are obtained.

$$\frac{R-a}{\sin\{\phi(\varphi)\}} = \frac{a}{\sin(\pi-\varphi)} \tag{A2.1}$$

$$\frac{a}{\sin(\pi-\varphi)} = \frac{r(\varphi)}{\sin\{\varphi-\phi(\varphi)\}} \tag{A2.2}$$

where R is the tank radius; a is the radius of the circular contact region of the tank bottom plate; φ is the angle formed by the horizontal center line of the bottom plate and the line connecting the center of the tank bottom plate and the corner joint; $\phi(\varphi)$ is the angle formed by the lines a and $r(\varphi)$; and $r(\varphi)$ is the contact width of the tank bottom plate. Arranging Eq. (A2.1) with respect to $\phi(\varphi)$ gives the following formula.

$$\phi(\varphi) = \sin^{-1}\left\{(R-a)\frac{\sin(\pi-\varphi)}{a}\right\} \tag{A2.3}$$

Similarly, arranging Eq. (A2.2) with respect to $r(\varphi)$ gives the following formula.

$$r(\varphi) = \frac{a}{\sin(\pi-\varphi)}\sin\{\varphi-\phi(\varphi)\} \tag{A2.4}$$

Substituting Eq. (A2.3) into Eq. (A2.4) yields the following equation.

$$r(\varphi) = \frac{a}{\sin(\pi-\varphi)}\sin\left[\varphi-\sin^{-1}\left\{(R-a)\frac{\sin(\pi-\varphi)}{a}\right\}\right] \tag{A2.5}$$

Integrating Eq. (A2.5) in the circumferential direction gives the contact range of the tank bottom plate. Finally, the uplift width is expressed by the following formula. Integrating Eq. (A2.6) in the circumferential direction gives the uplift area of the tank bottom plate.

$$L(\varphi) = R - r(\varphi) = R - \frac{a}{\sin(\pi - \varphi)} \sin\left[\varphi - \sin^{-1}\left\{(R-a)\frac{\sin(\pi-\varphi)}{a}\right\}\right] \tag{A2.6}$$

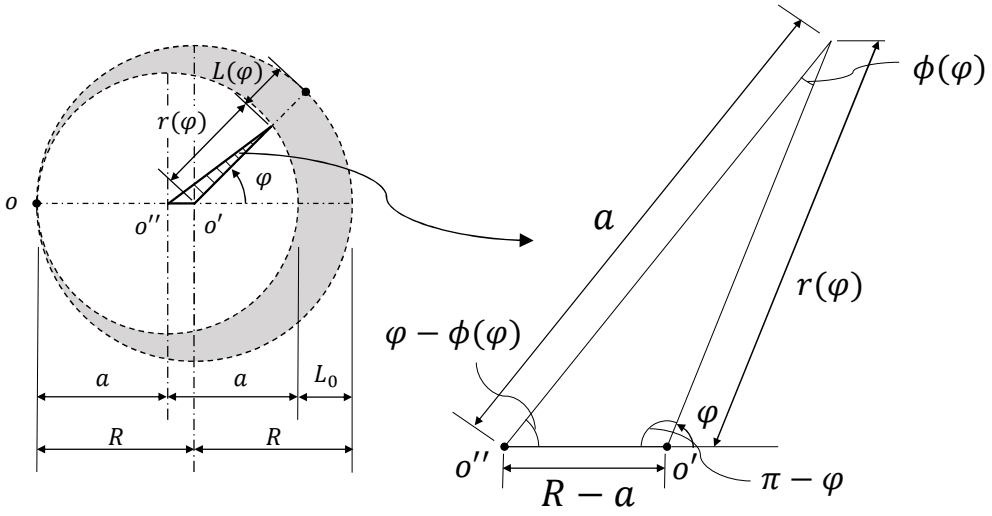

Figure A2.1 Geometric Relationship Diagram of Assumed Uplift Region

Appendix 3 Brief Review of Beam Models

In order to analyze the uplift of the tank bottom plate, some analytical methods have been proposed. In general, the tank bottom plate is modeled as a beam. This section provides a brief review on the following two beam models.

Beam model without geometric nonlinearity but with foundation elasticity

The first model introduced here is the Euler-Bernoulli beam under the condition where it is in contact with an elastic foundation as shown in Figures A3.1(a) and (b). The original model of this was developed by Hayashi et al. (2012) [2], and Yoshida et al. (2020) simplified the Hayashi's model by introducing the assumption that the deflection angle of the uplifted end of the beam would be zero [3]. The method of Yoshida et al. (2020) is described below.

The fundamental equations of the beam of the uplift part and that of the contact part are given as Eqs. (A3.1) and (A3.2), respectively.

$$EI\frac{d^4w_1}{dx^4} = -p \tag{A3.1}$$

$$EI\frac{d^4w_2}{dx^4} = -p - kw_2 \tag{A3.2}$$

where E is the Young's modulus of the beam model; I is the geometrical moment of inertia; w_1 is the vertical displacement of the uplift part of the beam model; w_2 is the vertical displacement of the contact part of the beam model; p is the hydraulic pressure acting on the beam model; and k is the reaction coefficient of the foundation.

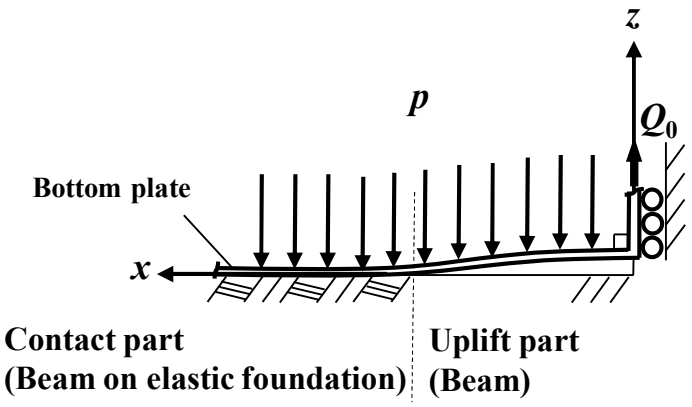

(a) System Considered

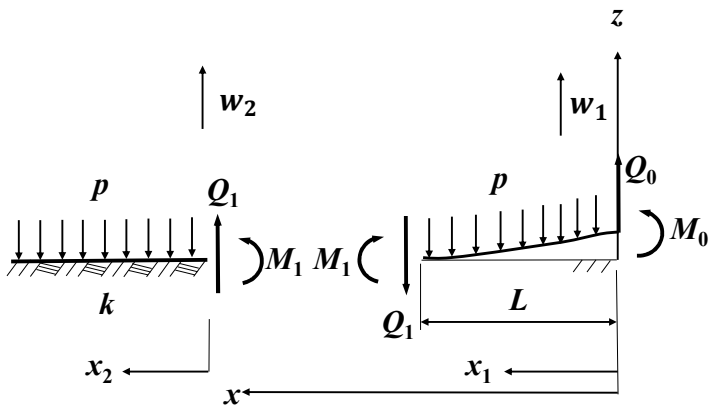

(b) Boundary Conditions

Figure A3.1 Analytical Model of Tank Bottom Plate [3]

Boundary conditions at the uplifted end and at the connection between the uplift and contact parts of the beam model are given as Eqs. (A3.3a) to (A3.3g).

$$EI\left[\frac{d^2w_1}{dx_1^2}\right]_{x_1=0} = M_0 \tag{A3.3a}$$

$$EI\left[\frac{d^3w_1}{dx_1^3}\right]_{x_1=0} = Q_0 \tag{A3.3b}$$

$$[w_1]_{x_1=L} = [w_2]_{x_2=0} = 0 \tag{A3.3c}$$

$$\left[\frac{dw_1}{dx_1}\right]_{x_1=L} = \left[\frac{dw_2}{dx_2}\right]_{x_2=0} \tag{A3.3d}$$

$$\left[\frac{d^2w_1}{dx_1^2}\right]_{x_1=L} = \left[\frac{d^2w_2}{dx_2^2}\right]_{x_2=0} \tag{A3.3e}$$

$$\left[\frac{d^3w_1}{dx_1^3}\right]_{x_1=L} = \left[\frac{d^3w_2}{dx_2^3}\right]_{x_2=0} \tag{A3.3f}$$

$$[w_2]_{x_2=\infty} = \left[\frac{dw_2}{dx_2}\right]_{x_2=\infty} = 0 \tag{A3.3g}$$

where, Q_0 is an external force which is the reaction force from the tank shell. As a result of the uplift, a bending moment M_0 acts on the corner joint of the tank bottom (see Figure A3.1(b)).

Employing the boundary conditions to the fundamental equations of the beam model, analytical solutions of the uplift displacement of the uplift part and the contact part are derived as follows:

$$w_1 = -\frac{1}{EI}\left(\frac{1}{24}px_1^4 - \frac{1}{6}Q_0x_1^3 - \frac{1}{2}M_0x_1^2 + C_{13}x_1 + C_{14}\right) \tag{A3.4}$$

$$\begin{aligned} w_2 = {} & e^{-\beta x_2}(C_{23}\cos\beta x_2 + C_{24}\sin\beta x_2) \\ & -\frac{p}{8\beta^4 EI}\left[-e^{-\beta(L+x_2)}\cos\beta(L+x_2) + e^{-\beta L}\cos\beta L\right. \\ & \left.-e^{-\beta(2R-L-x_2)}\cos\beta(2R-L-x_2) + 1\right] \end{aligned} \tag{A3.5}$$

in which

$$C_{13} = -\left(\frac{1}{6}pL^3 - \frac{1}{2}Q_0L^2 - M_0L\right) - \frac{1}{2\beta}\left(\frac{1}{2}pL^2 - Q_0L - M_0\right) - \frac{p}{4\beta^3} \quad \text{(A3.6a)}$$

$$C_{14} = \frac{1}{8}pL^4 - \frac{1}{3}Q_0L^3 - \frac{1}{2}M_0L^2 + \frac{L}{2\beta}\left(\frac{1}{2}pL^2 - Q_0L - M_0\right) + \frac{p}{4\beta^3} \quad \text{(A3.6b)}$$

$$C_{23} = \frac{p}{8\beta^4 EI}\left\{-e^{-\beta(2R-L)}\cos\beta(2R-L) + 1\right\} \quad \text{(A3.6c)}$$

$$C_{24} = \frac{1}{2\beta^2 EI}\left(\frac{1}{2}pL^2 - Q_0L - M_0\right) + \frac{p}{8\beta^4 EI}e^{-\beta(2R-L)}\sin\beta(2R-L) \quad \text{(A3.6d)}$$

where β is calculated as $\beta = \sqrt[4]{k/(4EI)}$. The uplift width L can be obtained by solving the following quadratic equation.

$$\frac{1}{2}\beta pL^2 + (p - \beta Q_0)L - \beta M_0 - Q_0 = 0 \qquad (L \geq 0) \quad \text{(A3.7)}$$

Assuming that the angle of deflection at the connection between the bottom plate and the sidewall is zero, the bending moment at the uplifted end of the bottom plate is obtained as

$$M_0 = \frac{2\beta}{2\beta L + 1}\left\{\frac{1}{6}pL^3 - \frac{1}{2}Q_0L^2 + \frac{1}{2\beta}\left(\frac{1}{2}pL^2 - Q_0L\right) + \frac{p}{4\beta^3}\right\} \quad \text{(A3.8)}$$

A calculation example is shown in Figure A3.2. The calculation conditions are same as the dynamic FE analysis in Appendix 1. In this calculation, only static pressure is considered for pressure acting on the bottom plate. When the uplift displacement is small (e.g., $w/H \leq 0.005$), the beam model and the FE analysis results are in good agreement. However, when w/H exceeds about 0.005, the simple beam model cannot reproduce the FE analysis results. This is because the bending moment is the

dominant parameter when the uplift displacement is small, while the axial force, which is not considered in this model, becomes the dominant parameter when the uplift displacement is large.

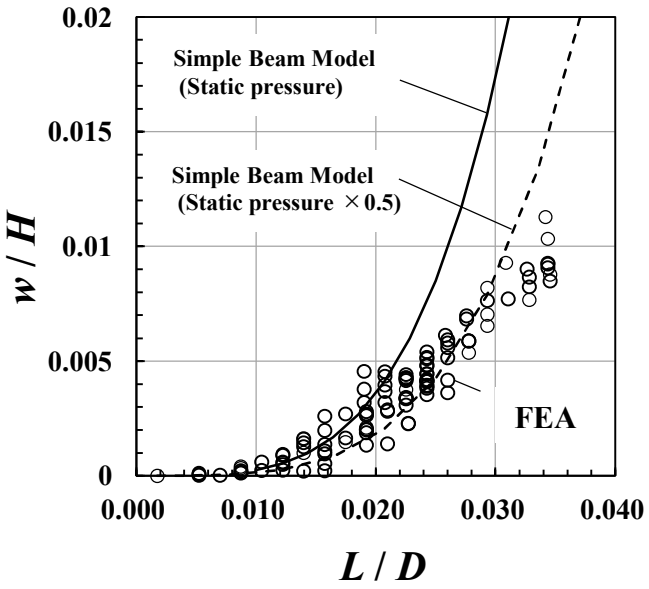

Figure A3.2 Calculation Example of Relationship between Uplift Width and Displacement [Simple Beam Model]

Beam model considering geometric nonlinearity (Malhotra et al. (1994))

The second model introduced here is the beam under the condition where it is in contact with a rigid foundation as shown in Figure A3.3. This model was developed by Malhotra et al. (1994) [4].

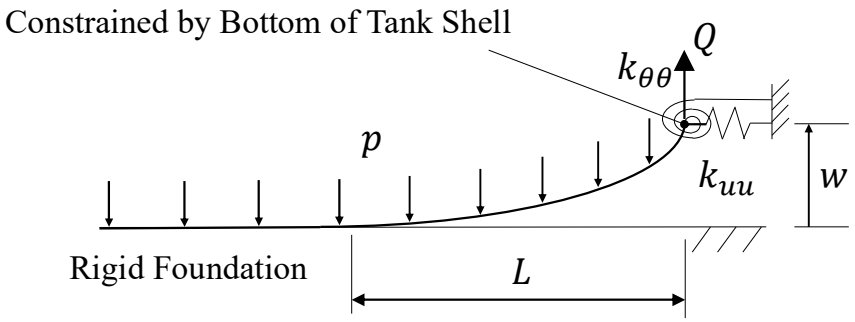

Figure A3.3 Beam Model Developed by Malhotra et al. (1994) [4]

The derivation process of the equation for this model is shown below. First, forces acting on a differential element are considered as shown in Figure A3.4.

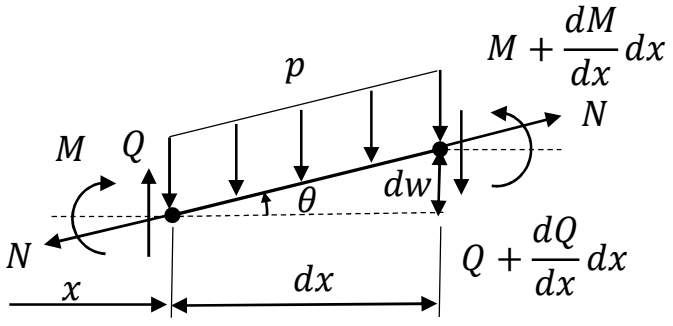

Figure A3.4 Forces Acting on Differential Element

Considering the equilibrium of moments at the x-position of the small beam element, the following equation is obtained.

$$-M_x + \left(M_x + \frac{dM_x}{dx}dx\right) - \left(Q_x + \frac{dQ_x}{dx}dx\right)dx - N\cos\theta dw - p\frac{dx}{\cos\theta}\frac{dx}{2} = 0 \tag{A3.9}$$

where M_x is the bending moment acting on an arbitrary cross-section of the beam model; Q_x is the shear force acting on an arbitrary cross-section of the beam model; N is the axial force acting on an arbitrary cross-section of the beam model; and θ is the slope of deflection at an arbitrary point of the beam model. Considering $\cos\theta \approx 1$ and $(dx)^2 \approx 0$ to Eq. (A3.9) leads to

$$\frac{dM_x}{dx}dx - Q_x dx - N dw = 0 \tag{A3.10}$$

Dividing both sides of Eq. (A3.10) by dx and then differentiating this equation by x gives,

$$\frac{d^2M_x}{dx^2} - \frac{dQ_x}{dx} - N\frac{d^2w}{dx^2} = 0 \tag{A3.11}$$

Substituting the following equations

$$\frac{d^2w}{dx^2} = \frac{M_x}{EI} \tag{A3.12a}$$

$$\frac{dQ_x}{dx} = -p \tag{A3.12b}$$

into Eq. (A3.11), the differential equation for an elastic beam in the presence of an axial force N is obtained.

$$\frac{d^2M_x}{dx^2} - \frac{N}{EI}M_x = -p \tag{A3.13}$$

Furthermore, considering $\xi = x/L$ to Eq. (A3.13) leads to

$$\frac{d^2M_x}{d\xi^2} - \frac{NL^2}{EI}M_x = -pL^2 \tag{A3.14}$$

The end of the beam is restrained by the bottom of the tank shell, and the strength of constraint is represented by the springs based on the stiffness of the tank shell (see Figure A3.3). The force-displacement relationships of the end constraints are expressed as

$$\begin{Bmatrix} M_1 \\ N \end{Bmatrix} = -\begin{bmatrix} k_{\theta\theta} & k_{\theta u} \\ k_{\theta u} & k_{uu} \end{bmatrix} \begin{Bmatrix} \theta_s \\ u_1 \end{Bmatrix} \tag{A3.15}$$

where θ_s is the rotation angle at the bottom end of the tank shell, u_1 is the horizontal displacement at the beam end and M_1 is bending moment at the beam end, respectively. The stiffness coefficients for constraints at the uplifted end of the beam model in Eq. (A3.15) are given as

$$k_{\theta\theta} = \frac{Ebt_s^2(t_s/R)^{1/2}}{2[3(1-\nu^2)]^{3/4}} \tag{A3.16a}$$

$$k_{\theta u} = -\frac{Ebt_s(t_s/R)}{2[3(1-\nu^2)]^{1/2}} \tag{A3.16b}$$

$$k_{uu} = \frac{Eb(t_s/R)^{3/2}}{[3(1-\nu^2)]^{1/4}} \tag{A3.16c}$$

where t_s is the thickness of the tank shell at the bottom; ν is Poisson's ratio; and b is the width of the beam model. Then, the inverse matrix of Eq. (A3.15) is

$$\begin{Bmatrix}\theta_s\\ u_1\end{Bmatrix} = -\begin{bmatrix}d_{\theta\theta} & d_{\theta u}\\ d_{\theta u} & d_{uu}\end{bmatrix}\begin{Bmatrix}M_1\\ N\end{Bmatrix} \tag{A3.17}$$

The flexibility coefficients for constraints at the uplifted end of the beam model in Eq. (A3.17) are given as

$$d_{\theta\theta} = \frac{k_{uu}}{k_{\theta\theta}k_{uu} - k_{\theta u}^2} \tag{A3.18a}$$

$$d_{\theta u} = -\frac{k_{\theta u}}{k_{\theta\theta}k_{uu} - k_{\theta u}^2} \tag{A3.18b}$$

$$d_{uu} = \frac{k_{\theta\theta}}{k_{\theta\theta}k_{uu} - k_{\theta u}^2} \tag{A3.18c}$$

The solution of Eq. (A3.14) is described in detail in Malhotra's paper. The representative formulas are shown here. The uplift displacement w_1 at the beam end is expressed as

$$w_1 = \frac{M_1}{N}\left(1 - \frac{\lambda}{\sinh\lambda}\right) + \frac{pL^2}{2N}\left(1 - \frac{2}{\lambda}\tanh\frac{2}{\lambda}\right) \tag{A3.19}$$

where

$$\lambda = \sqrt{\frac{NL^2}{EI}} \tag{A3.20}$$

$$N = -\left(k_{uu} - \frac{k_{\theta u}^2}{k_{\theta\theta}}\right)u_1 + \frac{k_{\theta u}}{k_{\theta\theta}}M_1 \tag{A3.21}$$

The horizontal displacement u_1 at the beam end is calculated by the following equation.

$$u_1 = \frac{NL}{bt_bE} - \frac{D^2L}{2\lambda^2}\left(-\frac{1}{2} + \frac{\lambda^2}{3} + \frac{2\sinh\lambda}{\lambda} + \frac{\sinh 2\lambda}{4\lambda} - 2\cosh\lambda\right) \tag{A3.22}$$

$$-\frac{C^2L}{2\lambda^2}\left(\frac{3}{2}-\frac{2\sinh\lambda}{\lambda}+\frac{\sinh 2\lambda}{4\lambda}\right)$$
$$-\frac{CDL}{2\lambda^2}\left(\lambda-\frac{1}{2\lambda}-2\sinh\lambda+\frac{\cosh 2\lambda}{2\lambda}\right)$$

where

$$C=\frac{M_1L}{EI}\frac{1}{\sinh\lambda}+\frac{pL}{N}\tanh\frac{\lambda}{2}\quad,\quad D=-\frac{pL}{N} \tag{A3.23}$$

The bending moment M_1 at the beam end is calculated by the following equation.

$$M_1=-\frac{\frac{pL}{N}\left(1-\frac{2}{\lambda}\tanh\frac{\lambda}{2}\right)+d_{\theta u}N-\Delta\theta}{\frac{L}{EI\lambda}\tanh\frac{\lambda}{2}+d_{\theta\theta}} \tag{A3.24}$$

where $\Delta\theta$ is a difference between rotation angle at the bottom end of the tank shell θ_s and that at the beam end θ_1. For elastic response, $\theta_s=\theta_1$. When the bending moment at the beam end reaches the yield moment $M_y(=\sigma_y bh^2/4)$, the beam end yields. Here, σ_y and h are the yield stress of the beam material and the thickness of the beam model, respectively. Since the beam end may yield earlier than the tank shell, a difference in rotation angle between the side plate and the beam can be generated. This difference in rotation angle represents the angle of plastic rotation.

$$\Delta\theta=\theta_1-\theta_s \tag{A3.25}$$

The rotation angle at the beam end θ_1 is calculated by the following equation.

$$\theta_1=\frac{M_1L}{EI}\frac{1}{\lambda}\tanh\frac{\lambda}{2}+\frac{pL}{N}\left(1-\frac{2}{\lambda}\tanh\frac{\lambda}{2}\right) \tag{A3.26}$$

The uplift force Q_1 is calculated by the following equation.

$$Q_1 = pL - \frac{\lambda EIC}{L^2} \tag{A3.27}$$

The basis of the theory of Malhotra's beam model is as described above. In addition, Malhotra et al. (1994) also considers the axial force $\bar{N}$ and bending moment $\bar{M}_1$ acting on the bottom corners due to the static pressure acting on the tank shell [5]. These external forces are expressed as:

$$\bar{N} \approx -\frac{\sqrt{Rt_s}p}{[3(1-\nu^2)]^{1/4}} \tag{A3.28}$$

$$\bar{M}_1 \approx -\frac{Rt_s p}{2[3(1-\nu^2)]^{1/2}} \tag{A3.29}$$

Therefore, Eqs. (A3.21) and (A3.24) are modified as follows:

$$N = -\left(k_{uu} - \frac{k_{\theta u}^2}{k_{\theta\theta}}\right)u_1 + \frac{k_{\theta u}}{k_{\theta\theta}}(M_1 - \bar{M}_1) + \bar{N} \tag{A3.30}$$

$$M_1 = -\frac{\frac{pL}{N}\left(1 - \frac{2}{\lambda}\tanh\frac{\lambda}{2}\right) + d_{\theta u}(N - \bar{N}) - \Delta\theta - \bar{M}_1 d_{\theta\theta}}{\frac{L}{EI\lambda}\tanh\frac{\lambda}{2} + d_{\theta\theta}} \tag{A3.31}$$

These equations are arranged by the author of this dissertation, and obtained from

$$\begin{Bmatrix} M_1 - \bar{M}_1 \\ N - \bar{N} \end{Bmatrix} = -\begin{bmatrix} k_{\theta\theta} & k_{\theta u} \\ k_{\theta u} & k_{uu} \end{bmatrix}\begin{Bmatrix} \theta_s \\ u_1 \end{Bmatrix} \tag{A3.32}$$

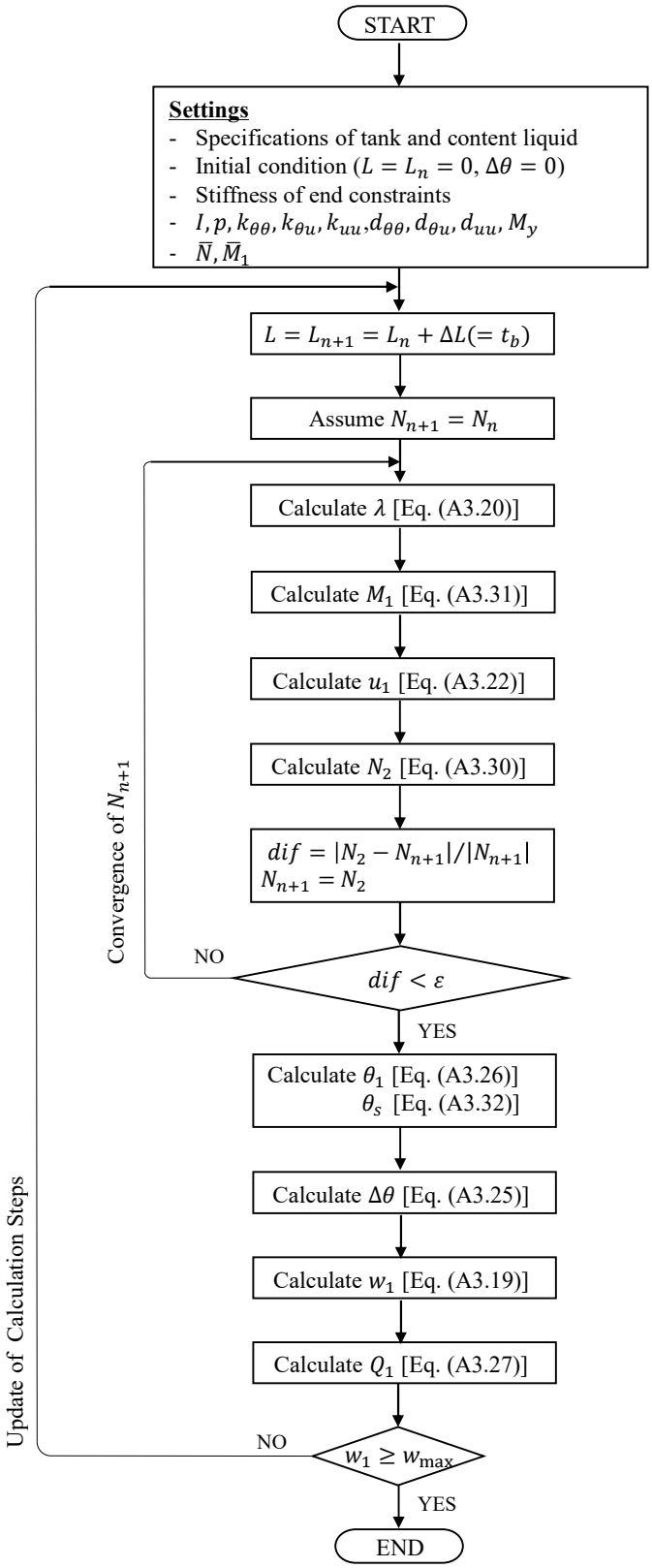

Figure A3.5 Calculation Flow of Malhotra's Beam Model

Finally, the calculation flow of Malhotra's beam model is shown in Figure A3.5. In this calculation, a fixed value of the uplift width L is considered in each step. Further assumptions about the value of N determine all the other values. At the same time, the new value of N can be obtained from Eq. (A3.30), so it is necessary to perform convergence calculations the value of N. ε is a value for judgment of convergence and is set as 0.0001 in this study. Two curves are shown in Figure A3.6 as examples of the calculation. It can be seen that the shapes of the curves calculated by Malhotra's beam model agree with the results of FE analysis even after w/H exceeds about 0.005.

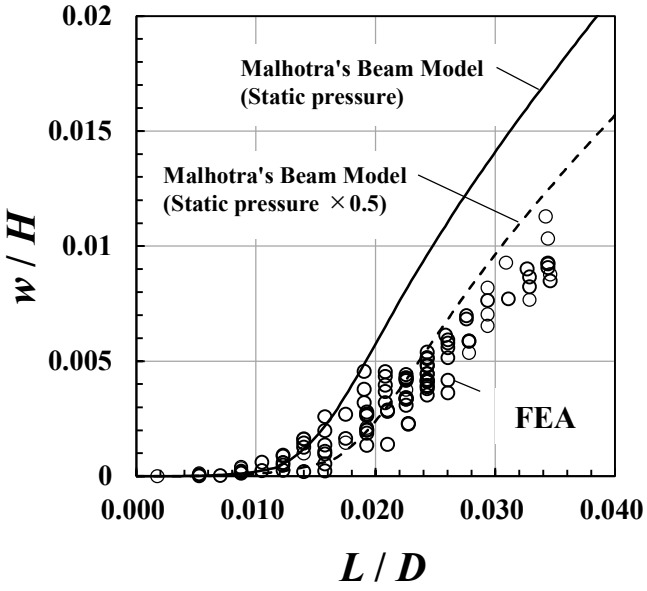

Figure A3.6 Calculation Example of Relationship between Uplift Width and Displacement [Malhotra's Beam Model]

Appendix 4　Results of Shaking Table Test

To understand the resistance to commencement of uplift of tank bottom accurately, the shaking table tests were conducted. Summary of the shaking table test is shown in Chapter 2. Here, the results of shaking table tests for each experimental condition are shown. The experimental conditions are shown in Table A4.1. Appendix 4 is intended to estimate the required horizontal acceleration for uplifting the tank bottom by using the experimental results.

Table A4.1 Cases for Shaking Table Test

		Aspect Ratio *H*/*D* (Depth of Content Liquid [cm])			
		0.25 (21.3)	**0.30 (25.5)**	**0.35 (29.8)**	**0.40 (34.0)**
Amplitude of Base Acceleration *A* [G]	**0.1**	-	-	-	○
	0.2	○	○	○	○
	0.3	○	○	○	○
	0.4	○	○	○	○
	0.5	○	○	○	○
	0.6	○	○	○	-

○: Test was conducted

The shaking table tests were conducted by the method shown in Chapter 2, and the results shown in Figures A4.1 to A4.20 were obtained.

With Aspect Ratio = 0.25 (H = 21.3 cm)

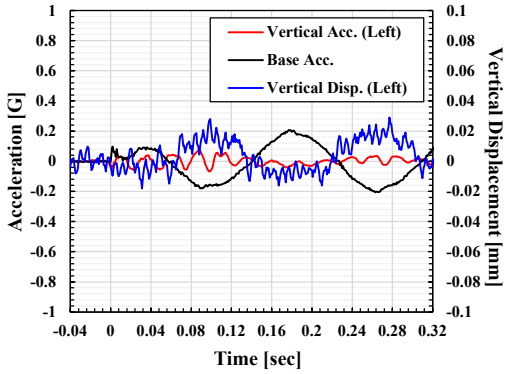

(a) Left Bottom Edge

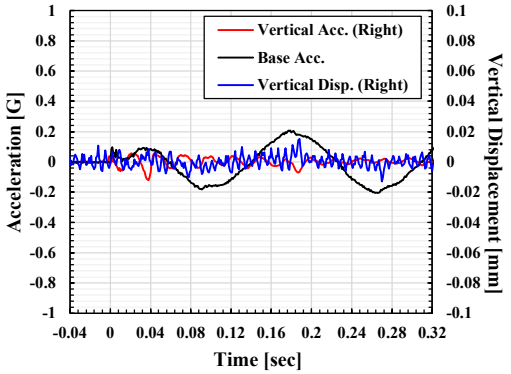

(b) Right Bottom Edge

Figure A4.1 Results of Shaking Table Test ($H/D = 0.25,\ A = 0.2$ G)

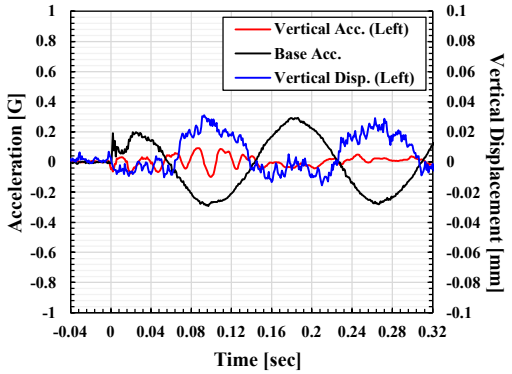

(a) Left Bottom Edge

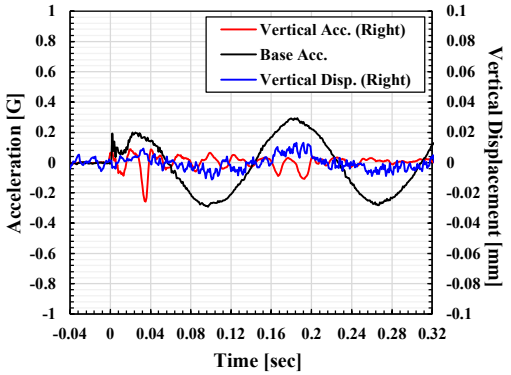

(b) Right Bottom Edge

Figure A4.2 Results of Shaking Table Test ($H/D = 0.25,\ A = 0.3$ G)

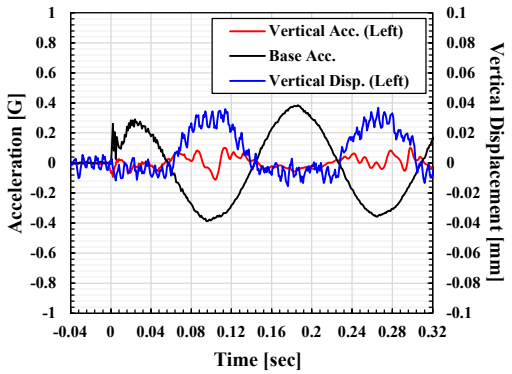

(a) Left Bottom Edge

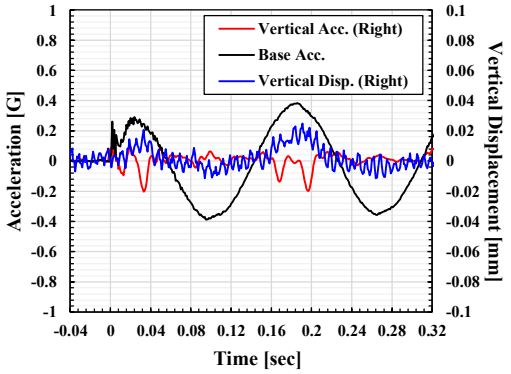

(b) Right Bottom Edge

Figure A4.3 Results of Shaking Table Test ($H/D = 0.25,\ A = 0.4$ G)

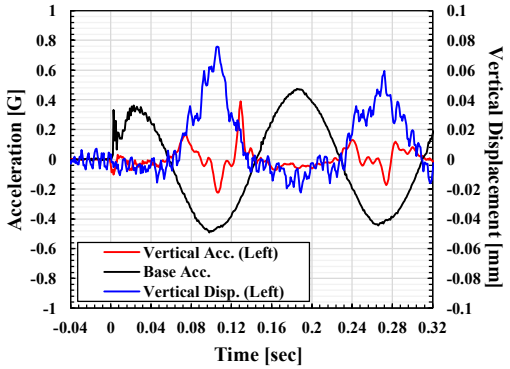

(a) Left Bottom Edge

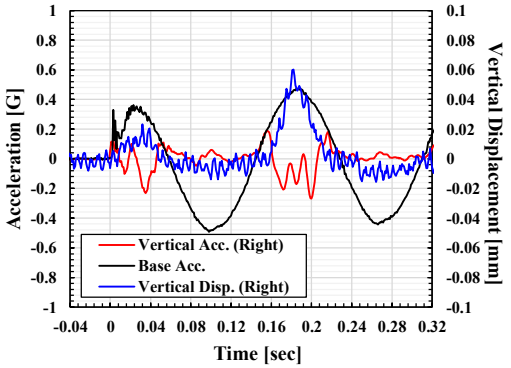

(b) Right Bottom Edge

Figure A4.4 Results of Shaking Table Test ($H/D = 0.25,\ A = 0.5$ G)

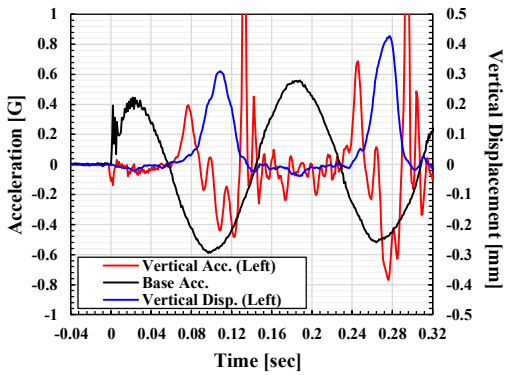

(a) Left Bottom Edge

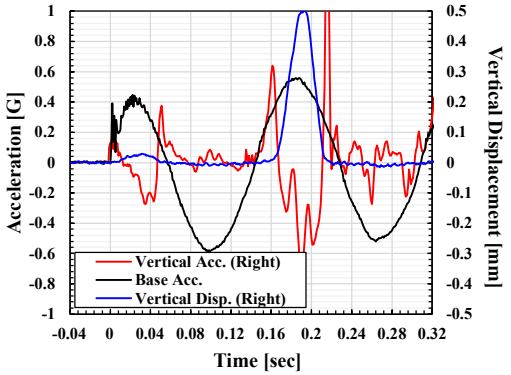

(b) Right Bottom Edge

Figure A4.5 Results of Shaking Table Test ($H/D = 0.25,\ A = 0.6$ G)

With Aspect Ratio = 0.30 (H = 25.5 cm)

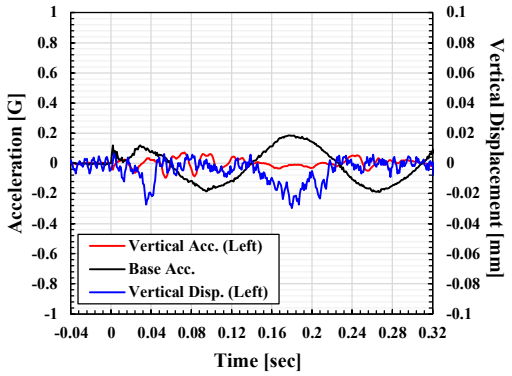

(a) Left Bottom Edge

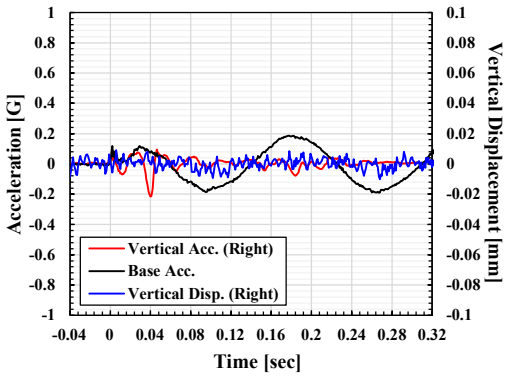

(b) Right Bottom Edge

Figure A4.6 Results of Shaking Table Test ($H/D = 0.30,\ A = 0.2$ G)

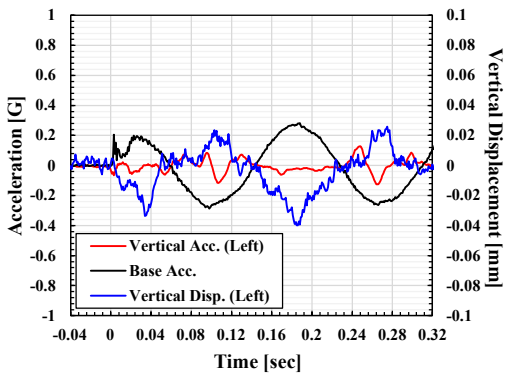

(a) Left Bottom Edge

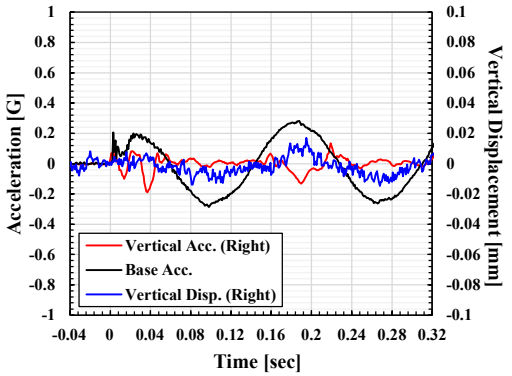

(b) Right Bottom Edge

Figure A4.7 Results of Shaking Table Test ($H/D = 0.30,\ A = 0.3$ G)

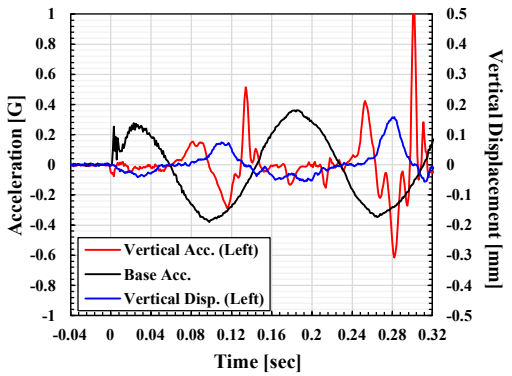

(a) Left Bottom Edge

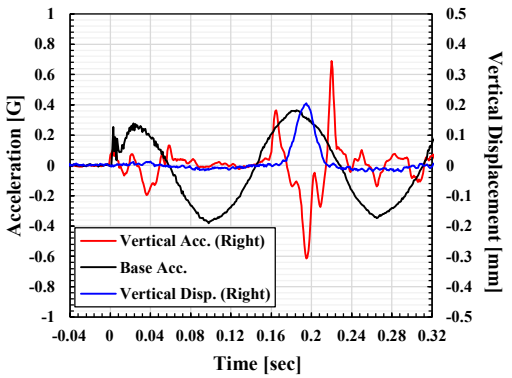

(b) Right Bottom Edge

Figure A4.8 Results of Shaking Table Test ($H/D = 0.30,\ A = 0.4$ G)

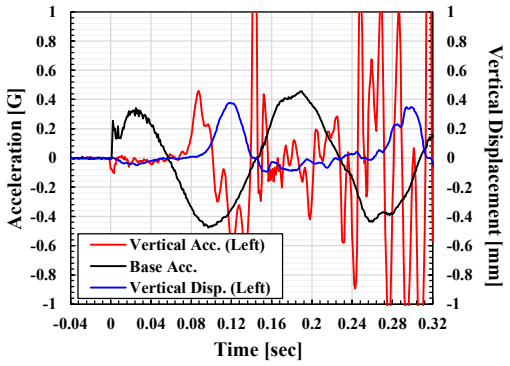

(a) Left Bottom Edge

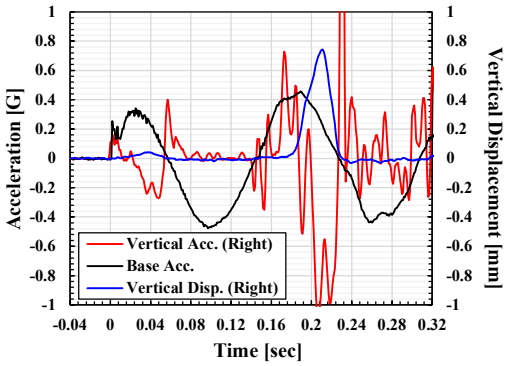

(b) Right Bottom Edge

Figure A4.9 Results of Shaking Table Test ($H/D = 0.30,\ A = 0.5$ G)

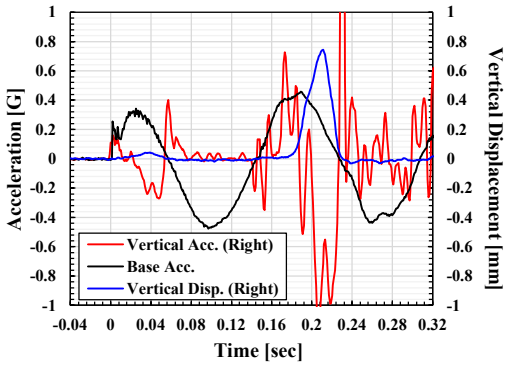

(a) Left Bottom Edge

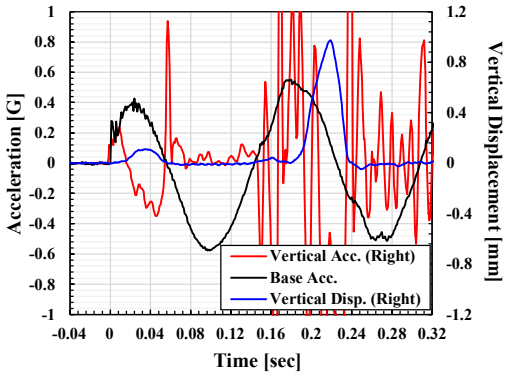

(b) Right Bottom Edge

Figure A4.10 Results of Shaking Table Test ($H/D = 0.30,\ A = 0.6$ G)

With Aspect Ratio = 0.35 (H = 29.8 cm)

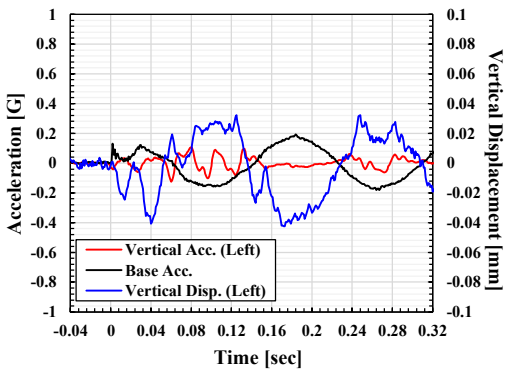

(a) Left Bottom Edge

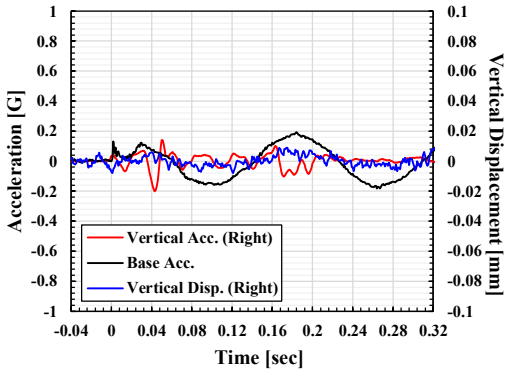

(b) Right Bottom Edge

Figure A4.11 Results of Shaking Table Test ($H/D = 0.35,\ A = 0.2$ G)

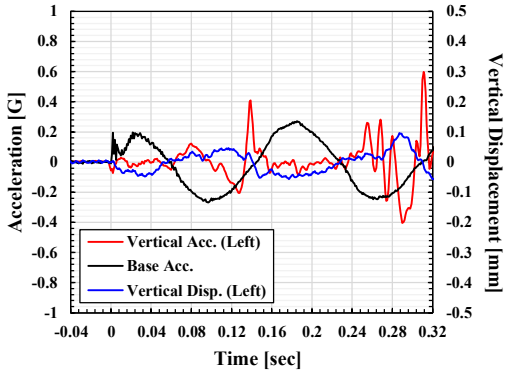

(a) Left Bottom Edge

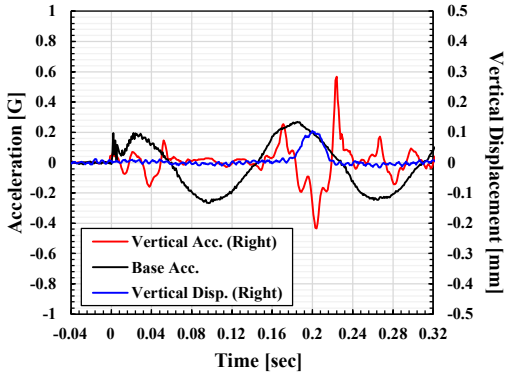

(b) Right Bottom Edge

Figure A4.12 Results of Shaking Table Test ($H/D = 0.35,\ A = 0.3$ G)

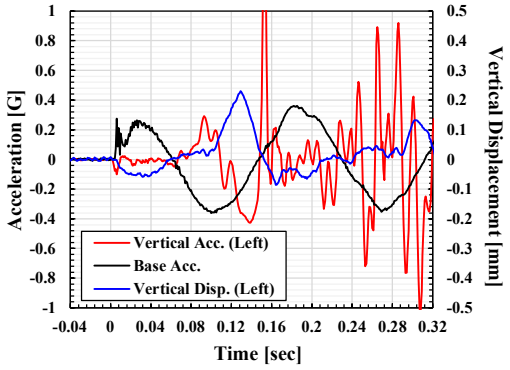

(a) Left Bottom Edge

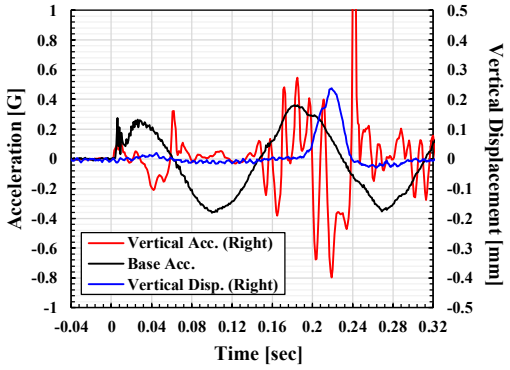

(b) Right Bottom Edge

Figure A4.13 Results of Shaking Table Test ($H/D = 0.35,\ A = 0.4$ G)

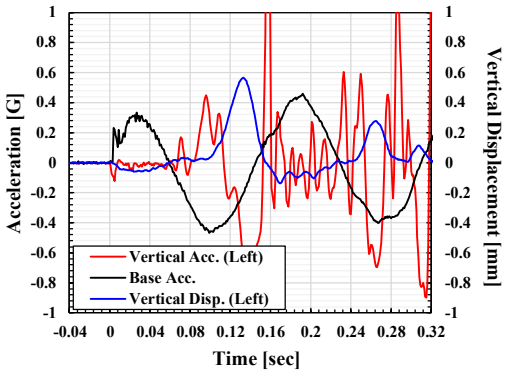

(a) Left Bottom Edge

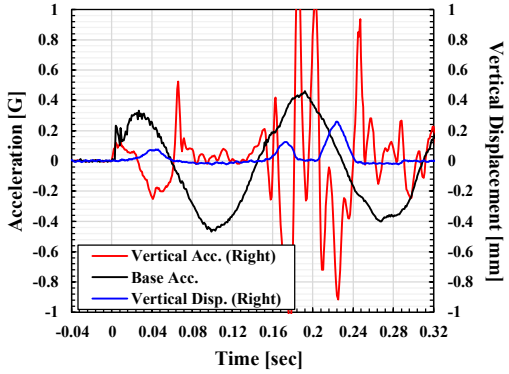

(b) Right Bottom Edge

Figure A4.14 Results of Shaking Table Test ($H/D = 0.35,\ A = 0.5$ G)

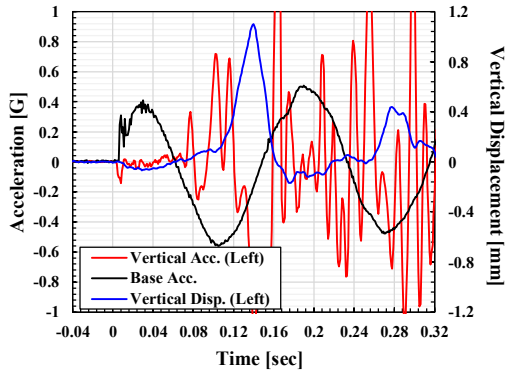

(a) Left Bottom Edge

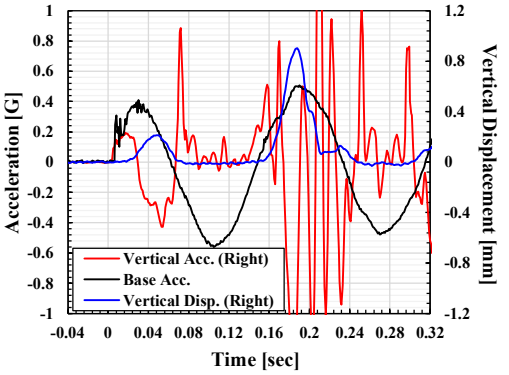

(b) Right Bottom Edge

Figure A4.15 Results of Shaking Table Test ($H/D = 0.35,\ A = 0.6$ G)

With Aspect Ratio = 0.40 (H = 34.0 cm)

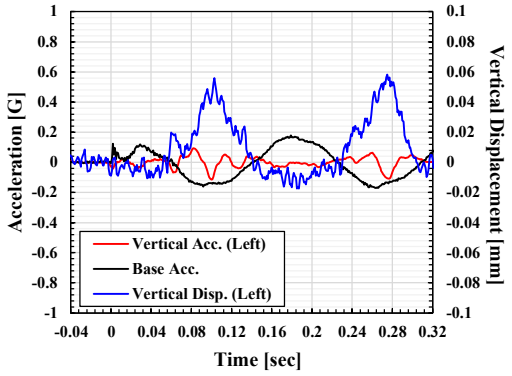

(a) Left Bottom Edge

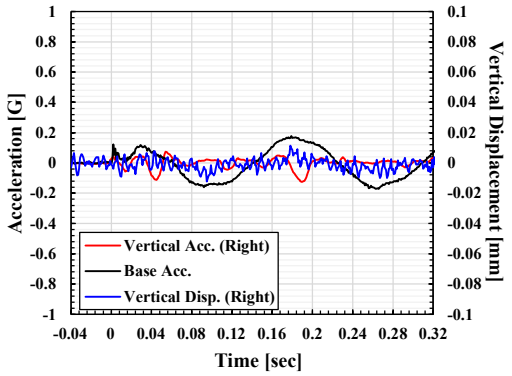

(b) Right Bottom Edge

Figure A4.16 Results of Shaking Table Test ($H/D = 0.40,\ A = 0.1$ G)

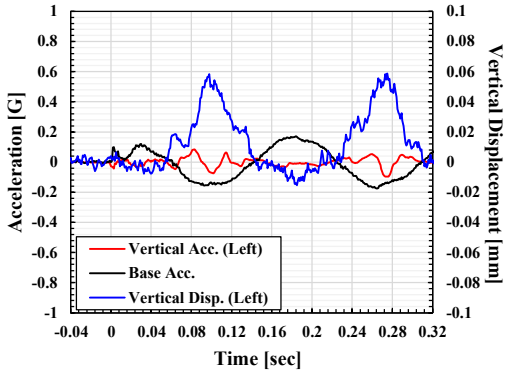

(a) Left Bottom Edge

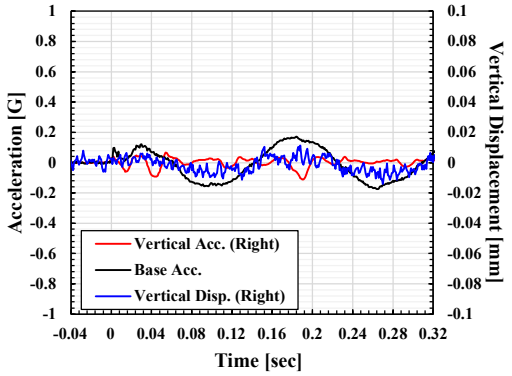

(b) Right Bottom Edge

Figure A4.17 Results of Shaking Table Test ($H/D = 0.40,\ A = 0.2$ G)

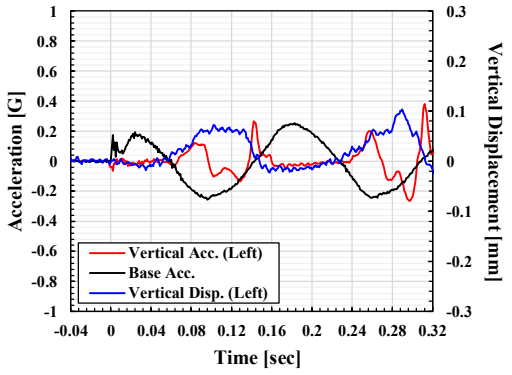

(a) Left Bottom Edge

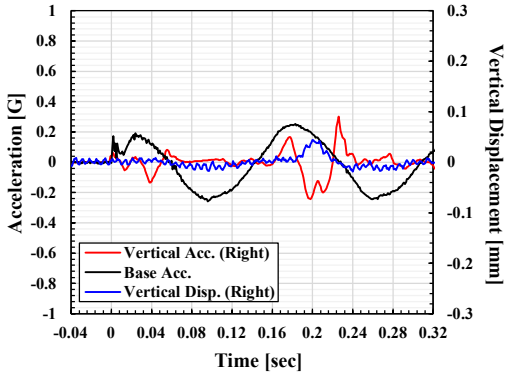

(b) Right Bottom Edge

Figure A4.18 Results of Shaking Table Test ($H/D = 0.40,\ A = 0.3$ G)

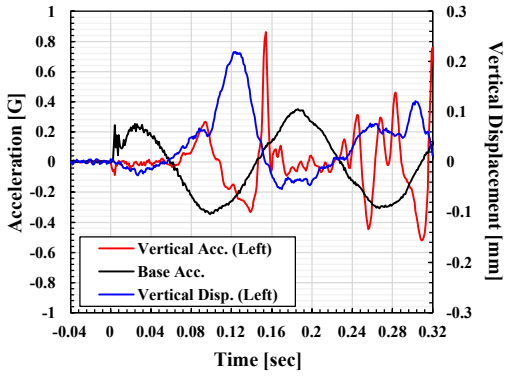

(a) Left Bottom Edge

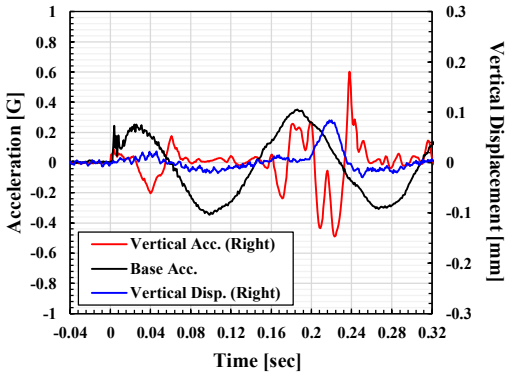

(b) Right Bottom Edge

Figure A4.19 Results of Shaking Table Test ($H/D = 0.40,\ A = 0.4$ G)

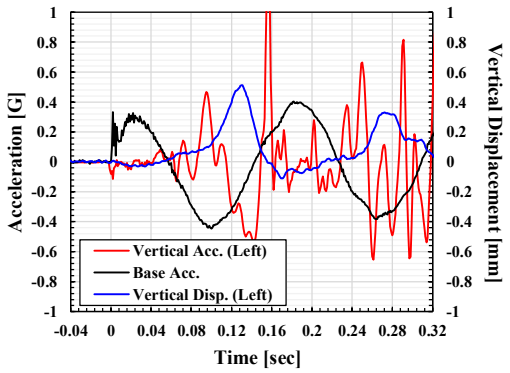

(a) Left Bottom Edge

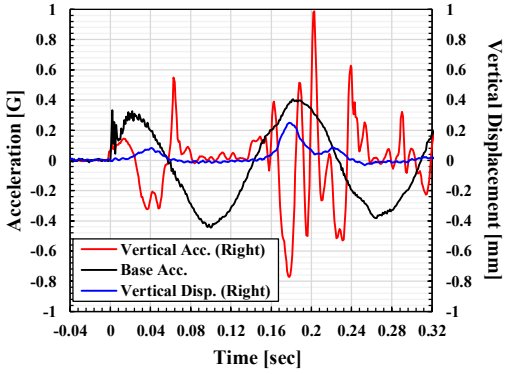

(b) Right Bottom Edge

Figure A4.20 Results of Shaking Table Test ($H/D = 0.40,\ A = 0.5$ G)

There are slits in the tank stand at both left and right sides for the sensors (see Figure 2.20), which causes an initial downward displacement of the tank bottom. Therefore, the initial position for the measurement of vertical displacement is set as shown in Figure A4.21. For this reason, even if an upward vertical displacement is recorded, it does not necessarily indicate an uplift of the tank bottom.

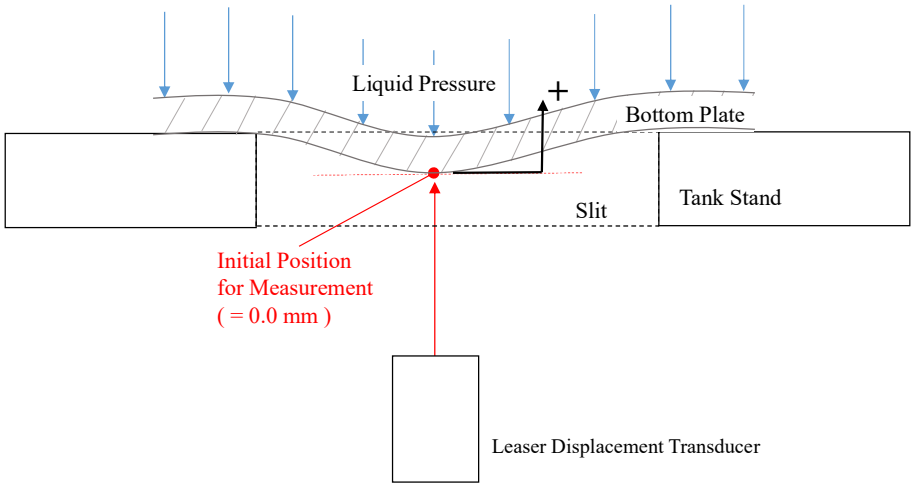

Figure A4.21 Initial Downward Displacement Caused by Slits

The method of estimating the values of acceleration required for uplift is explained below. The first step is to determine if the bottom has uplifted. In each test case, if the vertical acceleration record confirms the presence of a landing impact, it is taken that the tank bottom uplift has occurred (see Figure A4.22).

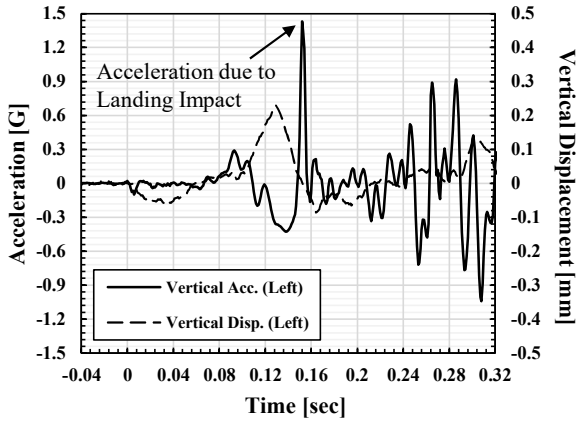

Figure A4.22 Typical Time History of Uplift Displacement and Vertical Acceleration When Tank Model Uplifts (e.g., $H/D = 0.35$, $A = 0.4$ G)

Next, the value of the initial vertical displacement is determined from the test results when no uplift of the tank bottom has occurred. For example, Figure A4.23 (a) shows that the initial vertical displacement at the left bottom edge is about 0.03 mm under the conditions of $H/D = 0.35$ and $A = 0.2$ G. In contrast, the initial vertical displacement at the right bottom edge is about 0.008 mm under the same condition as in Figure A4.23 (b). Since the left and right slits have different widths, the initial displacement values are also different between the left and right tank bottoms.

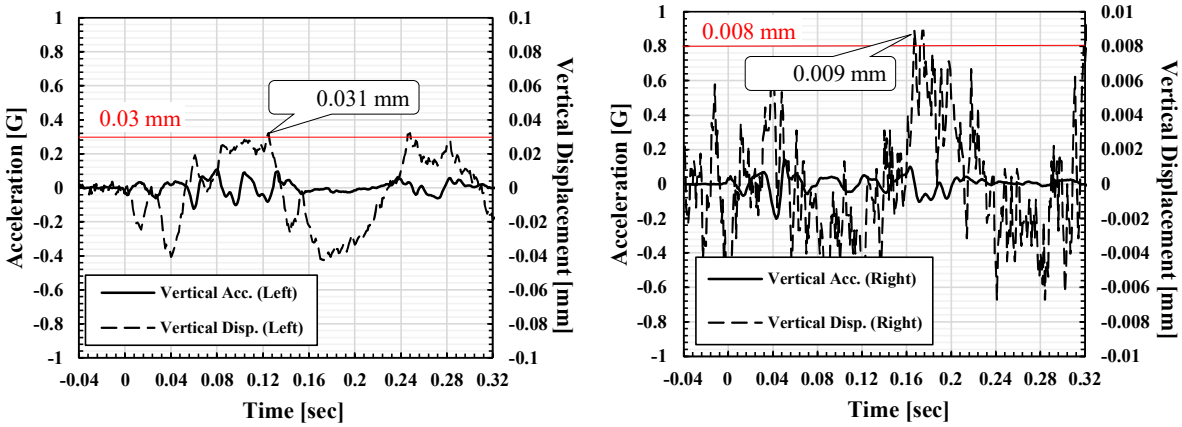

(a) Left Bottom Edge (b) Right Bottom Edge

Figure A4.23 Initial Vertical Displacement ($H/D = 0.35$, $A = 0.2$ G)

Finally, the values of the acceleration required for uplifting are estimated. The acceleration required for uplifting of the tank bottom is determined by using the initial displacement as the threshold for determination of the uplift. For example, Figure A4.24 shows that the required acceleration is $0.241 - 0.243$ G at $t = 0.176 - 0.177$ sec. At this moment, the uplift displacement at the right bottom edge exceeds the initial displacement ($= 0.008$ mm).

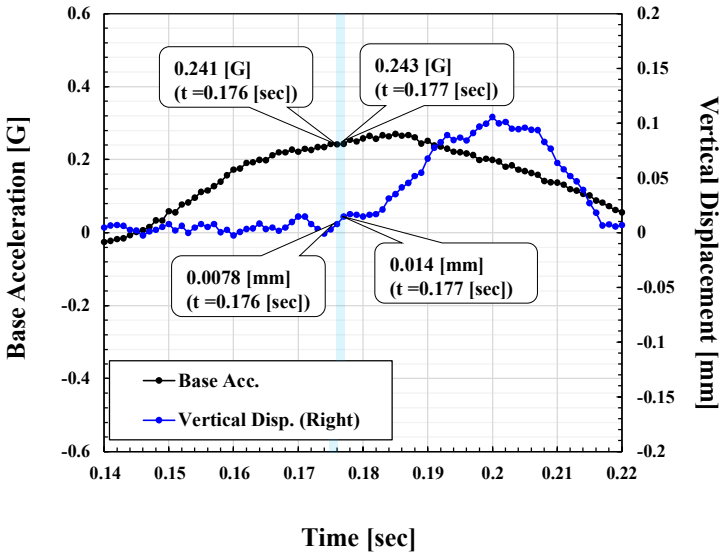

Figure A4.24 Estimation of Acceleration Required for Uplifting of Tank Bottom Edge (Right Bottom, $H/D = 0.35$, $A = 0.3$ G)

The accelerations required for uplifting of the tank bottom under each experimental condition are shown below.

With Aspect Ratio = 0.25 (H = 21.3 cm)

$A = 0.2$ g $- 0.4$ g: The tank bottom does not uplift.

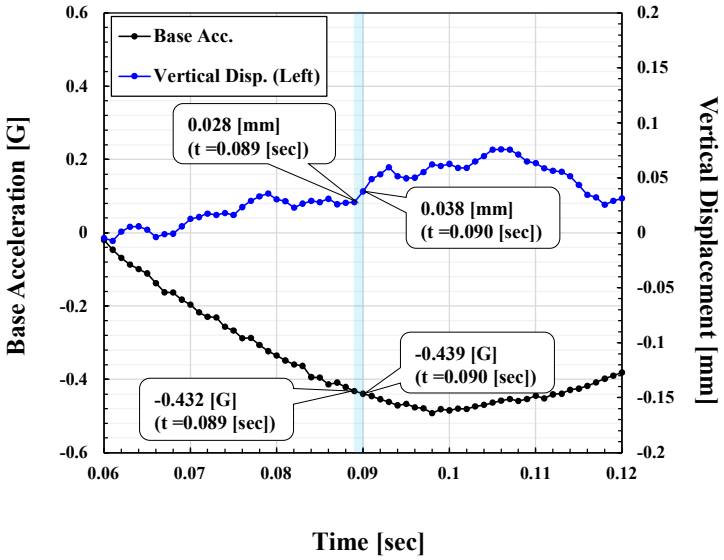

Figure A4.25 Estimation of Acceleration Required for Uplifting of Tank Bottom Edge (Left Bottom, $H/D = 0.25$, $A = 0.5$ G)

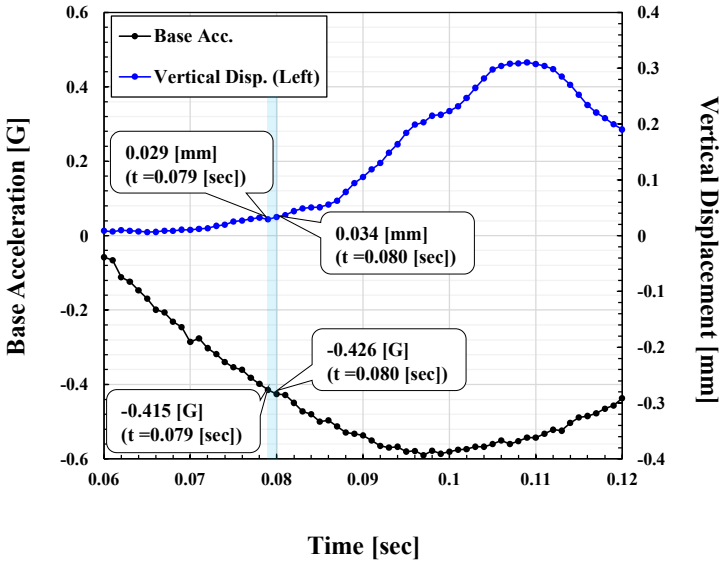

Figure A4.26 Estimation of Acceleration Required for Uplifting of Tank Bottom Edge (Left Bottom, $H/D = 0.25$, $A = 0.6$ G)

With Aspect Ratio = 0.30 (H = 25.5 cm)

$A = 0.2$ g $- 0.3$ g: The tank bottom does not uplift.

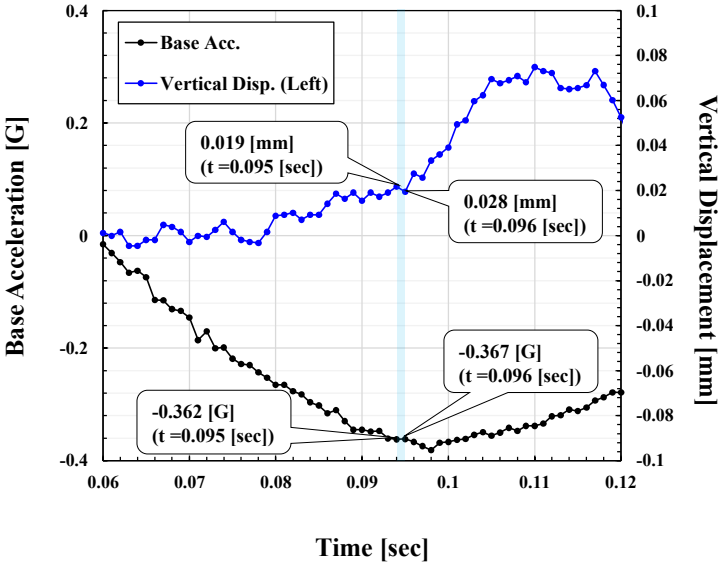

Figure A4.27 Estimation of Acceleration Required for Uplifting of Tank Bottom Edge (Left Bottom, $H/D = 0.30$, $A = 0.4$ G)

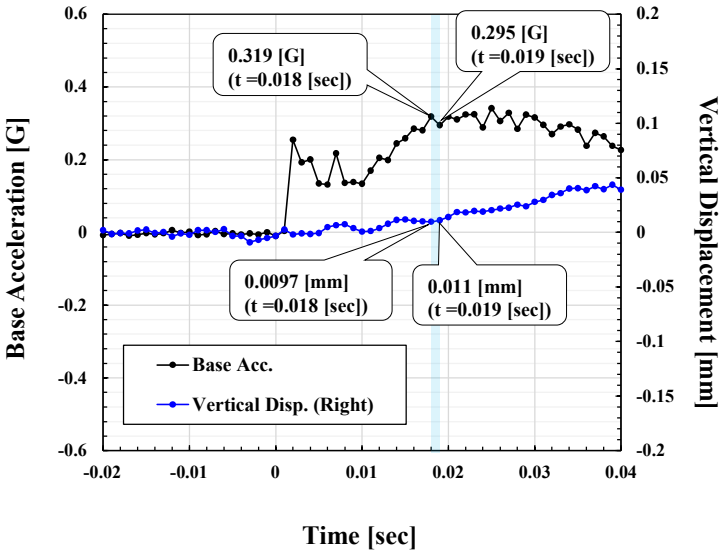

Figure A4.28 Estimation of Acceleration Required for Uplifting of Tank Bottom Edge (Right Bottom, $H/D = 0.30$, $A = 0.5$ G)

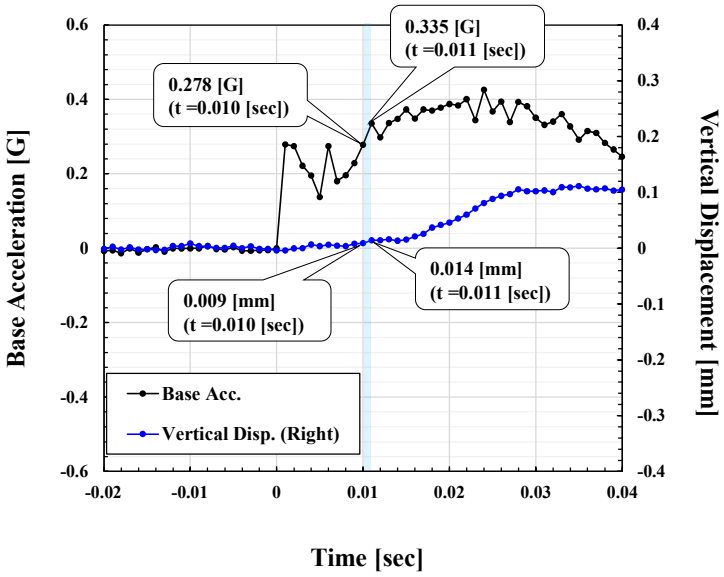

Figure A4.29 Estimation of Acceleration Required for Uplifting of Tank Bottom Edge (Right Bottom, $H/D = 0.30$, $A = 0.6$ G)

With Aspect Ratio = 0.35 (H = 29.8 cm)

$A = 0.2$ g: The tank bottom does not uplift. Test results for the case of $A = 0.3$ g are shown in Figure A4.24.

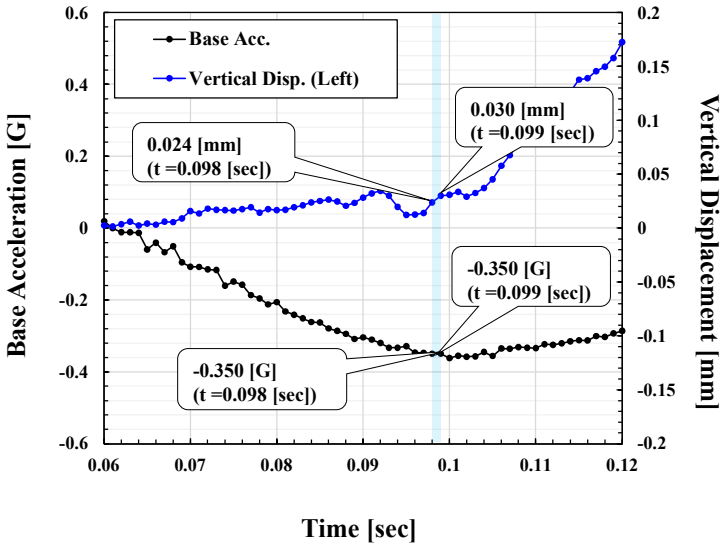

Figure A4.30 Estimation of Acceleration Required for Uplifting of Tank Bottom Edge (Left Bottom, $H/D = 0.35$, $A = 0.4$ G)

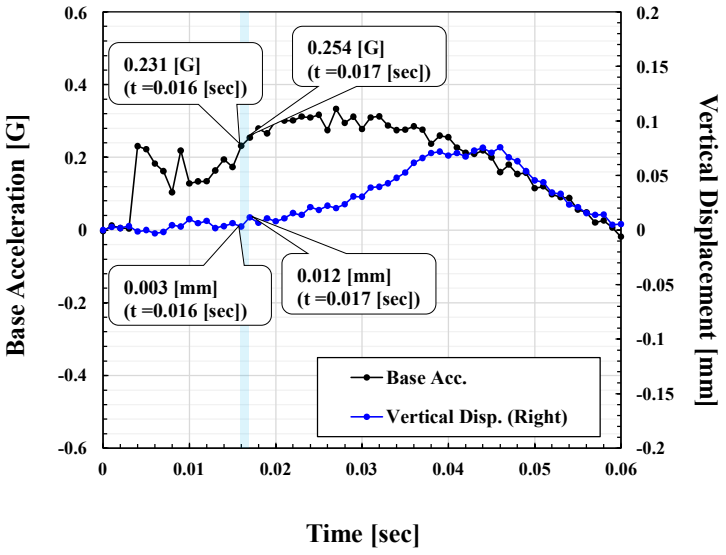

Figure A4.31 Estimation of Acceleration Required for Uplifting of Tank Bottom Edge (Right Bottom, $H/D = 0.35,\ A = 0.5$ G)

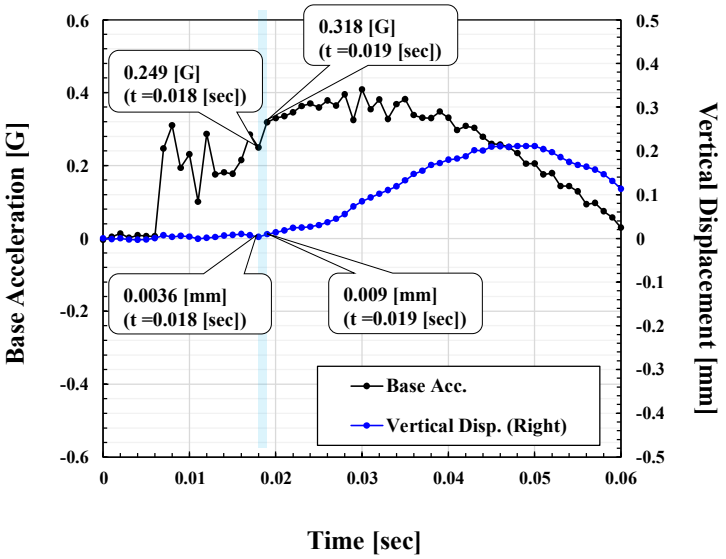

Figure A4.32 Estimation of Acceleration Required for Uplifting of Tank Bottom Edge (Right Bottom, $H/D = 0.35,\ A = 0.6$ G)

With Aspect Ratio = 0.40 (H = 34.0 cm)

$A = 0.1$ g $- 0.2$ g: The tank bottom does not uplift.

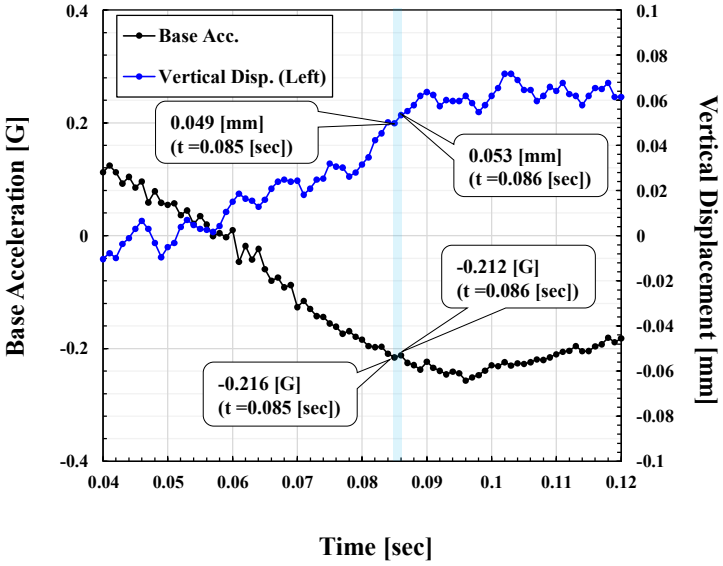

Figure A4.33 Estimation of Acceleration Required for Uplifting of Tank Bottom Edge (Left Bottom, $H/D = 0.40$, $A = 0.3$ G)

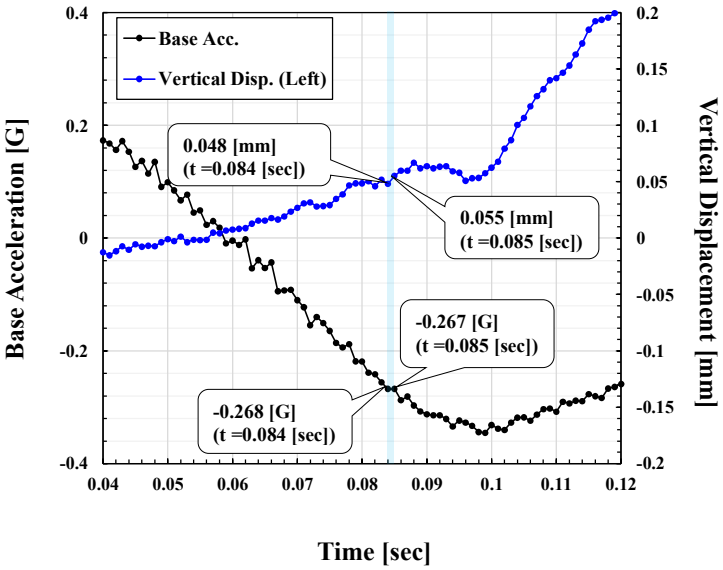

Figure A4.34 Estimation of Acceleration Required for Uplifting of Tank Bottom Edge (Left Bottom, $H/D = 0.40$, $A = 0.4$ G)

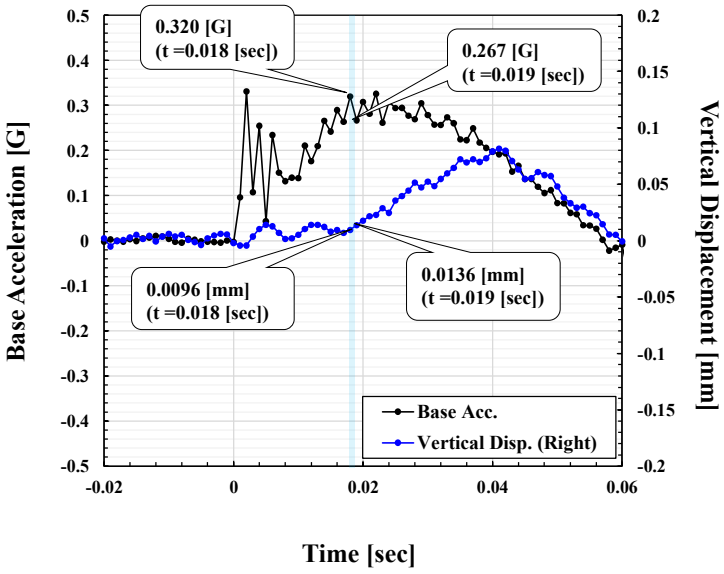

Figure A4.35 Estimation of Acceleration Required for Uplifting of Tank Bottom Edge (Left Bottom, $H/D = 0.40$, $A = 0.5$ G)

The results are summarized in Table A4.2.

Table A4.2 Acceleration Required for Uplifting (Results of Shaking Table Test) [G]

		Aspect ratio *H/D*							
		0.25		**0.30**		**0.35**		**0.40**	
Amplitude of Base Acceleration *A* [G]	**0.1**	-	-	-	-	-	-	No Uplift	
	0.2	No Uplift		No Uplift		No Uplift		No Uplift	
	0.3	No Uplift		No Uplift		0.241	0.243	0.216	0.212
	0.4	No Uplift		0.362	0.367	0.350	0.350	0.268	0.267
	0.5	0.432	0.439	0.319	0.295	0.231	0.254	0.320	0.267
	0.6	0.415	0.426	0.278	0.355	0.249	0.318	-	-
Average		0.43		0.33		0.28		0.26	

Appendix 5 Effective Quantities of Content Liquid for Tank Responses

The values of effective quantities of content liquid related to tank rocking motion are re-evaluated based on the theory of Taniguchi and Katayama (2016) [6], and these values are summarized in Tables A5.1 to A5.5. Where, δ is the uplift ratio ($\delta = \text{uplift width } L/\text{tank diameter } D$). Each table has been updated by the following additions.

- Values for $\delta = 0.00$ were added to the tables, because the time history response analysis requires the effective mass of content liquid for the tank rocking motion immediately after starting uplift of the tank bottom. Moreover, values for $\delta = 0.11$ to 0.15 were also added to the tables because of a design standard that assumes that the limit value of the uplift width is about 7% of the tank radius [7,8].
- Values for $H/D = 0.2$ were added to the tables, because a broad tank with $H/D = 0.25$ is used in this study. The values given in the original paper are in the range of $0.3 \leq H/D \leq 1.5$ [6].

Table A5.1 Values of Ratio of Effective Mass of Content Liquid for Rocking Motion to Total Mass of Fluid Filling Tank: f_r

δ	H/D													
	0.2	**0.3**	**0.4**	**0.5**	**0.6**	**0.7**	**0.8**	**0.9**	**1.0**	**1.1**	**1.2**	**1.3**	**1.4**	**1.5**
0.00	0.0144	0.0361	0.0686	0.1082	0.1503	0.1919	0.2316	0.2687	0.3029	0.3341	0.3625	0.3881	0.4116	0.4327
0.01	0.0248	0.0460	0.0783	0.1175	0.1589	0.1999	0.2390	0.2756	0.3093	0.3400	0.3680	0.3933	0.4163	0.4371
0.02	0.0365	0.0574	0.0899	0.1283	0.1688	0.2089	0.2473	0.2832	0.3163	0.3465	0.3740	0.3988	0.4215	0.4420
0.03	0.0484	0.0691	0.1016	0.1396	0.1792	0.2184	0.2560	0.2912	0.3237	0.3533	0.3803	0.4046	0.4269	0.4470
0.04	0.0604	0.0810	0.1134	0.1510	0.1899	0.2282	0.2649	0.2994	0.3312	0.3603	0.3867	0.4106	0.4325	0.4522
0.05	0.0724	0.0928	0.1251	0.1624	0.2007	0.2382	0.2741	0.3078	0.3390	0.3674	0.3933	0.4167	0.4381	0.4575
0.06	0.0843	0.1047	0.1369	0.1737	0.2114	0.2482	0.2833	0.3163	0.3468	0.3746	0.3999	0.4229	0.4438	0.4628
0.07	0.0961	0.1164	0.1485	0.1850	0.2221	0.2583	0.2926	0.3248	0.3546	0.3818	0.4066	0.4290	0.4496	0.4682
0.08	0.1078	0.1281	0.1601	0.1962	0.2328	0.2683	0.3018	0.3334	0.3625	0.3891	0.4133	0.4352	0.4553	0.4735
0.09	0.1194	0.1397	0.1717	0.2073	0.2434	0.2782	0.3111	0.3419	0.3704	0.3963	0.4200	0.4414	0.4611	0.4789
0.10	0.1308	0.1513	0.1831	0.2184	0.2539	0.2881	0.3203	0.3504	0.3782	0.4036	0.4266	0.4475	0.4668	0.4842
0.11	0.1421	0.1627	0.1945	0.2294	0.2644	0.2979	0.3295	0.3589	0.3860	0.4107	0.4332	0.4536	0.4725	0.4896
0.12	0.1532	0.1741	0.2059	0.2404	0.2747	0.3077	0.3386	0.3674	0.3938	0.4179	0.4398	0.4597	0.4781	0.4948
0.13	0.1643	0.1855	0.2172	0.2513	0.2851	0.3173	0.3477	0.3758	0.4016	0.4250	0.4463	0.4657	0.4837	0.5001
0.14	0.1752	0.1967	0.2284	0.2621	0.2953	0.3270	0.3566	0.3841	0.4092	0.4320	0.4528	0.4717	0.4893	0.5053
0.15	0.1860	0.2079	0.2395	0.2729	0.3055	0.3365	0.3655	0.3924	0.4168	0.4390	0.4592	0.4776	0.4948	0.5105
1.00	0.9261	0.8881	0.8530	0.8227	0.7980	0.7785	0.7637	0.7529	0.7453	0.7404	0.7375	0.7362	0.7362	0.7369

Table A5.2 Values of Ratio of Effective Mass of Content Liquid for Rocking-Bulging Interaction Motion to Total Mass of Fluid Filling Tank: f_{rb}

δ	H/D													
	0.2	**0.3**	**0.4**	**0.5**	**0.6**	**0.7**	**0.8**	**0.9**	**1.0**	**1.1**	**1.2**	**1.3**	**1.4**	**1.5**
0.00	0.0054	0.0176	0.0386	0.0672	0.1005	0.1359	0.1718	0.2067	0.2400	0.2711	0.3002	0.3269	0.3517	0.3743
0.01	0.0112	0.0235	0.0447	0.0733	0.1066	0.1420	0.1777	0.2124	0.2454	0.2764	0.3051	0.3316	0.3561	0.3785
0.02	0.0174	0.0304	0.0521	0.0808	0.1138	0.1490	0.1843	0.2188	0.2515	0.2821	0.3105	0.3367	0.3609	0.3830
0.03	0.0235	0.0372	0.0596	0.0886	0.1215	0.1564	0.1914	0.2255	0.2579	0.2881	0.3162	0.3420	0.3660	0.3878
0.04	0.0295	0.0439	0.0670	0.0965	0.1295	0.1640	0.1987	0.2325	0.2645	0.2944	0.3221	0.3476	0.3711	0.3927
0.05	0.0353	0.0505	0.0744	0.1043	0.1374	0.1718	0.2062	0.2396	0.2712	0.3007	0.3281	0.3532	0.3764	0.3977
0.06	0.0410	0.0570	0.0816	0.1120	0.1453	0.1796	0.2137	0.2468	0.2780	0.3071	0.3341	0.3588	0.3817	0.4027
0.07	0.0465	0.0634	0.0888	0.1196	0.1532	0.1875	0.2213	0.2540	0.2849	0.3136	0.3402	0.3645	0.3871	0.4077
0.08	0.0517	0.0696	0.0958	0.1271	0.1609	0.1952	0.2288	0.2612	0.2917	0.3201	0.3462	0.3702	0.3925	0.4128
0.09	0.0568	0.0757	0.1027	0.1346	0.1686	0.2030	0.2364	0.2684	0.2986	0.3265	0.3523	0.3759	0.3978	0.4178
0.10	0.0617	0.0817	0.1096	0.1420	0.1762	0.2106	0.2439	0.2756	0.3054	0.3329	0.3583	0.3815	0.4031	0.4229
0.11	0.0664	0.0876	0.1163	0.1492	0.1838	0.2181	0.2513	0.2828	0.3122	0.3393	0.3643	0.3872	0.4084	0.4279
0.12	0.0710	0.0933	0.1229	0.1564	0.1912	0.2256	0.2587	0.2899	0.3189	0.3457	0.3702	0.3927	0.4137	0.4329
0.13	0.0753	0.0988	0.1294	0.1635	0.1986	0.2330	0.2660	0.2969	0.3256	0.3519	0.3761	0.3983	0.4189	0.4378
0.14	0.0795	0.1043	0.1358	0.1705	0.2058	0.2403	0.2732	0.3039	0.3323	0.3582	0.3820	0.4038	0.4241	0.4427
0.15	0.0835	0.1096	0.1421	0.1774	0.2130	0.2476	0.2803	0.3108	0.3388	0.3643	0.3877	0.4092	0.4292	0.4475
1.00	0.2471	0.3470	0.4258	0.4841	0.5260	0.5563	0.5785	0.5955	0.6092	0.6206	0.6306	0.6395	0.6479	0.6555

Table A5.3 Values of Ratio of Effective Moment of Inertia of Content Liquid (around Centroid of m_r) to Moment of Inertia of Rigid Cylinder (around Centroid of m_t): s

δ	H/D													
	0.2	**0.3**	**0.4**	**0.5**	**0.6**	**0.7**	**0.8**	**0.9**	**1.0**	**1.1**	**1.2**	**1.3**	**1.4**	**1.5**
0.00	0.0199	0.0541	0.0906	0.1234	0.1526	0.1793	0.2040	0.2271	0.2484	0.2681	0.2862	0.3027	0.3182	0.3323
0.01	0.0282	0.0640	0.1007	0.1324	0.1605	0.1862	0.2102	0.2327	0.2537	0.2730	0.2909	0.3072	0.3225	0.3365
0.02	0.0374	0.0739	0.1126	0.1438	0.1704	0.1948	0.2179	0.2396	0.2600	0.2789	0.2964	0.3125	0.3276	0.3415
0.03	0.0469	0.0836	0.1240	0.1557	0.1813	0.2044	0.2264	0.2473	0.2670	0.2854	0.3025	0.3183	0.3331	0.3468
0.04	0.0566	0.0931	0.1350	0.1673	0.1925	0.2144	0.2353	0.2554	0.2744	0.2923	0.3090	0.3244	0.3390	0.3525
0.05	0.0662	0.1025	0.1456	0.1785	0.2036	0.2246	0.2445	0.2638	0.2821	0.2994	0.3156	0.3308	0.3451	0.3583
0.06	0.0757	0.1117	0.1560	0.1895	0.2144	0.2349	0.2538	0.2723	0.2899	0.3067	0.3225	0.3372	0.3513	0.3643
0.07	0.0849	0.1208	0.1661	0.2001	0.2250	0.2451	0.2632	0.2808	0.2978	0.3140	0.3294	0.3438	0.3575	0.3703
0.08	0.0940	0.1298	0.1760	0.2105	0.2354	0.2551	0.2725	0.2894	0.3057	0.3214	0.3363	0.3503	0.3638	0.3763
0.09	0.1028	0.1388	0.1858	0.2207	0.2455	0.2649	0.2818	0.2979	0.3136	0.3287	0.3432	0.3569	0.3701	0.3824
0.10	0.1113	0.1476	0.1955	0.2307	0.2555	0.2745	0.2909	0.3064	0.3214	0.3360	0.3501	0.3634	0.3763	0.3884
0.11	0.1196	0.1563	0.2050	0.2406	0.2653	0.2839	0.2999	0.3148	0.3292	0.3433	0.3569	0.3699	0.3825	0.3944
0.12	0.1276	0.1649	0.2144	0.2503	0.2749	0.2932	0.3088	0.3231	0.3369	0.3504	0.3636	0.3763	0.3887	0.4003
0.13	0.1354	0.1735	0.2237	0.2598	0.2843	0.3024	0.3175	0.3313	0.3446	0.3576	0.3703	0.3827	0.3948	0.4062
0.14	0.1430	0.1820	0.2329	0.2693	0.2937	0.3114	0.3261	0.3394	0.3521	0.3646	0.3770	0.3890	0.4008	0.4120
0.15	0.1503	0.1905	0.2420	0.2786	0.3029	0.3203	0.3345	0.3474	0.3596	0.3715	0.3835	0.3952	0.4067	0.4177
1.00	0.8732	0.8300	0.7938	0.7625	0.7354	0.7125	0.6939	0.6794	0.6687	0.6611	0.6563	0.6535	0.6527	0.6529

Table A5.4 Values of Ratio of Horizontal Distance toward Centroid of Effective Mass of Content Liquid for Rocking Motion to Diameter of Tank: $d_{r,x}$

δ	H / D													
	0.2	**0.3**	**0.4**	**0.5**	**0.6**	**0.7**	**0.8**	**0.9**	**1.0**	**1.1**	**1.2**	**1.3**	**1.4**	**1.5**
0.00	0.6187	0.5155	0.4570	0.4279	0.4140	0.4078	0.4057	0.4059	0.4077	0.4104	0.4136	0.4171	0.4207	0.4242
0.01	0.6531	0.5481	0.4758	0.4388	0.4211	0.4126	0.4092	0.4087	0.4099	0.4122	0.4151	0.4184	0.4218	0.4252
0.02	0.6606	0.5696	0.4944	0.4517	0.4295	0.4185	0.4136	0.4120	0.4126	0.4144	0.4170	0.4200	0.4232	0.4264
0.03	0.6627	0.5831	0.5088	0.4636	0.4382	0.4248	0.4182	0.4156	0.4155	0.4168	0.4190	0.4217	0.4247	0.4278
0.04	0.6635	0.5923	0.5201	0.4739	0.4465	0.4311	0.4230	0.4194	0.4185	0.4193	0.4211	0.4236	0.4263	0.4292
0.05	0.6639	0.5989	0.5292	0.4826	0.4541	0.4371	0.4278	0.4232	0.4216	0.4219	0.4234	0.4255	0.4280	0.4307
0.06	0.6641	0.6039	0.5366	0.4902	0.4609	0.4429	0.4324	0.4270	0.4247	0.4245	0.4256	0.4275	0.4298	0.4323
0.07	0.6644	0.6078	0.5428	0.4967	0.4670	0.4482	0.4369	0.4306	0.4278	0.4271	0.4279	0.4295	0.4315	0.4339
0.08	0.6646	0.6108	0.5480	0.5024	0.4724	0.4532	0.4411	0.4342	0.4308	0.4297	0.4301	0.4315	0.4333	0.4354
0.09	0.6649	0.6132	0.5523	0.5074	0.4773	0.4577	0.4451	0.4376	0.4337	0.4323	0.4324	0.4334	0.4351	0.4370
0.10	0.6651	0.6152	0.5560	0.5119	0.4818	0.4619	0.4489	0.4409	0.4366	0.4347	0.4346	0.4354	0.4368	0.4386
0.11	0.6653	0.6167	0.5592	0.5158	0.4858	0.4657	0.4524	0.4440	0.4393	0.4372	0.4367	0.4373	0.4386	0.4402
0.12	0.6655	0.6180	0.5619	0.5192	0.4895	0.4692	0.4557	0.4470	0.4420	0.4395	0.4388	0.4392	0.4403	0.4417
0.13	0.6656	0.6189	0.5643	0.5223	0.4928	0.4725	0.4588	0.4498	0.4445	0.4418	0.4409	0.4411	0.4420	0.4433
0.14	0.6656	0.6196	0.5662	0.5250	0.4958	0.4755	0.4617	0.4525	0.4470	0.4441	0.4429	0.4429	0.4436	0.4448
0.15	0.6656	0.6201	0.5679	0.5275	0.4985	0.4783	0.4644	0.4551	0.4493	0.4462	0.4449	0.4447	0.4452	0.4462
1.00	0.5207	0.5222	0.5217	0.5199	0.5174	0.5144	0.5113	0.5082	0.5053	0.5028	0.5005	0.4986	0.4970	0.4957

Table A5.5 Values of Ratio of Vertical Distance toward Centroid of Effective Mass of Content Liquid for Rocking Motion to Liquid Height: $d_{r,z}$

δ	H / D													
	0.2	**0.3**	**0.4**	**0.5**	**0.6**	**0.7**	**0.8**	**0.9**	**1.0**	**1.1**	**1.2**	**1.3**	**1.4**	**1.5**
0.00	0.6223	0.5602	0.5403	0.5314	0.5268	0.5243	0.5228	0.5223	0.5225	0.5232	0.5243	0.5255	0.5269	0.5281
0.01	0.5602	0.5441	0.5341	0.5283	0.5245	0.5221	0.5207	0.5202	0.5204	0.5212	0.5224	0.5236	0.5251	0.5263
0.02	0.5300	0.5295	0.5250	0.5223	0.5202	0.5186	0.5177	0.5174	0.5179	0.5188	0.5201	0.5215	0.5230	0.5243
0.03	0.5146	0.5197	0.5180	0.5166	0.5156	0.5148	0.5143	0.5144	0.5151	0.5162	0.5176	0.5191	0.5208	0.5222
0.04	0.5059	0.5130	0.5126	0.5118	0.5112	0.5109	0.5108	0.5112	0.5122	0.5135	0.5151	0.5167	0.5185	0.5200
0.05	0.5006	0.5082	0.5084	0.5077	0.5073	0.5072	0.5075	0.5081	0.5093	0.5107	0.5125	0.5143	0.5162	0.5178
0.06	0.4973	0.5048	0.5049	0.5042	0.5038	0.5038	0.5042	0.5051	0.5064	0.5080	0.5100	0.5119	0.5138	0.5156
0.07	0.4953	0.5022	0.5022	0.5012	0.5006	0.5006	0.5011	0.5021	0.5036	0.5054	0.5075	0.5095	0.5116	0.5134
0.08	0.4942	0.5003	0.4999	0.4986	0.4978	0.4977	0.4982	0.4993	0.5009	0.5028	0.5050	0.5071	0.5093	0.5112
0.09	0.4936	0.4989	0.4980	0.4963	0.4953	0.4950	0.4955	0.4966	0.4983	0.5003	0.5026	0.5048	0.5071	0.5091
0.10	0.4934	0.4979	0.4964	0.4943	0.4930	0.4926	0.4930	0.4941	0.4958	0.4980	0.5003	0.5026	0.5050	0.5070
0.11	0.4935	0.4972	0.4951	0.4926	0.4909	0.4903	0.4906	0.4917	0.4935	0.4957	0.4981	0.5005	0.5029	0.5050
0.12	0.4938	0.4966	0.4940	0.4910	0.4890	0.4882	0.4883	0.4894	0.4912	0.4934	0.4959	0.4984	0.5009	0.5030
0.13	0.4943	0.4962	0.4930	0.4896	0.4873	0.4862	0.4862	0.4872	0.4890	0.4913	0.4939	0.4964	0.4989	0.5011
0.14	0.4949	0.4960	0.4922	0.4883	0.4856	0.4844	0.4842	0.4852	0.4870	0.4893	0.4919	0.4944	0.4970	0.4993
0.15	0.4955	0.4958	0.4914	0.4871	0.4841	0.4826	0.4824	0.4832	0.4850	0.4874	0.4900	0.4925	0.4952	0.4975
1.00	0.4898	0.4784	0.4681	0.4595	0.4530	0.4483	0.4453	0.4438	0.4433	0.4437	0.4446	0.4460	0.4477	0.4494

Bibliography

[1] Taniguchi, T., Nakashima, T. and Yoshida, Y. 2016, “Contribution of The Bending Stiffness of The Tank Bottom Plate and Out-of-Round Deformation of Cylindrical Shell to The Tank Rocking Motion,” Proc. ASME PVP Conference, Seismic Engineering, Paper No. PVP2016-63916.

[2] Hayashi, S. and Taniguchi, T., 2012, “A Study of Formularization of Uplift Behavior at The Bottom Plate of Large LNG Storage Tanks during Earthquake,” Proc. ASME PVP Conference, Seismic Engineering, Paper No. PVP2012-78784.

[3] Yoshida, Y., Taniguchi, T. and Nakashima, T., 2020, “Uplift Deformation of The Bottom Plate of The Cylindrical Shell Tanks Under Steady-State Response of Tank Rocking Motion,” Proc. ASME PVP Conference, Seismic Engineering, Paper No. PVP2020-21418.

[4] Malhotra, P.K. and Veletsos, A.S., 1994, “Beam Model for Base Uplifting Analysis of Cylindrical Tanks,” J. Struct. Div., ASCE, Vol. 120, Issue 12, pp. 3471–3488.

[5] Malhotra, P.K. and Veletsos, A.S., 1994, “Uplifting Analysis of Base Plates in Cylindrical Tanks,” J. Struct. Div., ASCE, Vol. 120, Issue 12, pp. 3489–3505.

[6] Taniguchi, T. and Katayama, Y., 2016, “Masses of Fluid for Cylindrical Tanks in Rock with Partial Uplift of Bottom Plate,” Journal of Pressure Vessel Technologies, ASME, doi:10.1115/1.4032784.

[7] Wozniak, R.S. and Mitchell, W.W., 1978, “Basis of Seismic Design Provisions for Welded Steel Oil Storage Tanks,” API Refining Dept., 43rd Midyear meeting, Toronto.

[8] API Standard 650, 2020, “Welded Tanks for Oil Storage, Annex E: Seismic Design of Storage Tanks,” Thirteenth Edition.